UNIVERSITY OF
BIRMINGHAM

AN INTEGRATED INFORMATION MODELLING SYSTEM FOR ASSESSING URBAN GEOHAZARD RISK

by

STYLIANOS PROVIDAKIS

A thesis submitted to the University of Birmingham

for the degree of

DOCTOR OF PHILOSOPHY

Department of Civil Engineering

School of Engineering

University of Birmingham

June 2020

ABSTRACT

Over the years, the continuous expansion of cities has drawn the attention of engineers and researchers to the need to support sustainable planning. As cities expand, they would be more prone to geohazard risk, which could cause severe costs. Therefore, a system to provide information of geohazard risk could support sustainable urban planning. A suggested application is proposed in this thesis to assess settlement risk caused by tunnelling.

A framework methodology is proposed to aid the assessment of urban geohazard risk. The settlement risk assessment analyses and the associated building damage and cost assessment form the structure of the framework. Building Information Modelling (BIM) provided and supported the information for the data processes used in the whole analysis and the 3D geology-tunnel-building model creation.

The resulting risk assessments are presented using 3D visualisations. From these visualisations, further investigations could be focused on the 'higher-risk' outcomes presented. This forms a preliminary assessment a tool.

The final oucome of this research is an integrated information system based on advanced analysis and 3D modelling tools for urban geohazard risk. The research also provides information which contributes to knowledge and understanding for relevant associated problems and supports sustainable decision-making.

ACKNOWLEDGEMENTS

Initially, I would like to give my special thanks to my supervisors for their belief in my ability to conduct research. I would like to thank my principal supervisor Professor Chris Rogers for his invaluable support and guidance without which the present work would have never been possible. I would also like to thank my co-supervisor Professor David Chapman for his exceptional help and advice throughout this research work.

This research was made possible with the financial support provided by the School of Engineering, University of Birmingham.

Thanks to all my friends and my colleagues in the School of Engineering for their support.

A special thank you to my family for their encouragement, understanding and support during this period, without which I wouldn't have made it this far in my studies and achieved any of my goals.

PUBLICATIONS

Providakis, S., Rogers, C.D.F and Chapman, D.N. (2019) Predictions of settlement risk induced by tunnelling using BIM and 3D visualization tools. *Tunnelling and Underground Space Technology,* 92, https://doi.org/10.1016/j.tust.2019.103049.

Providakis, S., Rogers, C. D. and Chapman, D. N. (2020) Assessing the Economic Risk of Building Damage due to the Tunneling-Induced Settlement Using Monte Carlo Simulations and BIM. *Sustainability*, 12(23), 10034, https://doi.org/10.3390/su122310034.

Co-authorship:

Chapman, D., Providakis, S. and Rogers, C. (2019) BIM for the Underground–An enabler of trenchless construction. *Underground Space*. https://doi.org/10.1016/j.undsp.2019.08.001.

LIST OF SYMBOLS

B_d	building length (m)
CI	Consistency Index
Cs	economic cost (£)
D	tunnel diameter (m)
E/G	ratio of Young's modulus and Shear modulus
F	distance from inflection point to perpendicular passing the tunnel axis (m)
Fs	Probability Density Function of damage
h	depth (m)
H_b	building height (m)
H_w	depth from the ground surface to the groundwater table (m)
I	section moment of area of the equivalent beam height of the building at sagging/hogging zone (m^3)
i	the point of inflection
k	coefficient of the resistance between the soil and the cutter
L	length of building span at respective zone (m)
L_h	length of building at hogging zone (m)
L_s	length of building at sagging zone (m)
m_v	vulnerability factor value
R	tunnel radius (m)
r	distance in x-z plane (m)
RI	Random Index

Rs	Settlement Economic Risk due to tunnelling (£/m^2)
S	surface ground settlement (empirical methods) (m)
Smax	maximum ground settlement (empirical methods) (m)
t	longest distance from neutral axis to the edge of an equivalent beam (sagging zone: t=H/2, hogging zone: t=H) (m)
U_x	horizontal ground movement (analytical methods) (m)
U_z	surface ground settlement (analytical methods) (m)
V_i	settlement vulnerability factor value
w_i	weightings to the factor
x	lateral distance from the tunnel centreline (m)
z	depth below ground-surface (m)
Z_0	overburden depth (m)
β	Limit angle (°)
δ	ground deformation due to ovalisation of tunnel lining
Δ	maximum settlement (deflection) at the considered span (m)
Δ/L	ratio between the maximum relative settlement at the considered span and the length of this span (deflection ratio)
Δ_h	differential horizontal movement at hogging zone (m)
Δ_s	differential horizontal movement at sagging zone (m)
ε	uniform radial ground loss ratio (%)
ε_0	average ground loss ratio (%)

$\varepsilon_{b,max}$	bending strain (%)
ε_{bs}	total bending strain (%)
ε_{crit}	critical tensile strain (%)
$\varepsilon_{d,max}$	diagonal strain (%)
ε_{ds}	total diagonal strain (%)
ε_{h}	horizontal strain (%)
μ	mean value
ν	Poisson's ratio of the soil
σ	standard deviation
σ^2	variance
φ	friction angle (°)

LIST OF ABBREVIATIONS

AHP	Analytical Hierarchy Process
ANN	Artificial Neural Networks
API	Application Programming Interface
ARX	AutoRegressive eXogenous model
BIM	Building Information Modelling
CAD	Computer-Aided Design
DEM	Digital Elevation Model
FEM	Finite Element Method
GIS	Geographic Information Systems
GUI	Graphical User Interface
IFC	Industry Foundation Classes
KML	Keyhole Markup Language
PDF	Probability Density Function
STL	STereoLithography model

TABLE OF CONTENTS

LIST OF FIGURES

LIST OF TABLES

1 INTRODUCTION

1.1 Introduction to the topic

Geological and geotechnical hazards have always impacted on humanity. Numerous catastrophes over the years in the ancient world are linked with such phenomena, inducing human and economic costs (de Rienzo et al., 2008; Gibson and Chowdhury, 2009). Clues for ancient cities around the world to have been seriously hit by such events as earthquakes, volcano eruptions and other disturbances. In addition, many aspects within civilisations throughout history are related to the understanding and interpretations of those geohazards, which in many cases led them to be associated with gods and legends or myths. Over the years, people tried to understand their origin and characteristics, which became easier in the last decades with the advent of current technologies. However, while technologies advance there has been another issue increasing the geohazard risk in urban areas: urbanisation (Griffiths, 2016).

Urbanisation has been a growing phenomenon. Approximately half of the Earth's population lives in towns and cities (Price et al., 2016). While cities expand, sustainable urban planning is required to avoid more severe costs associated with natural hazards when occurring within the cities' limits. This led to numerous sustainable applications to be created over the years, one of which aligned with the increasing use of urban underground space – the lack of space on the ground surface makes the underground useful for infrastructure and other construction developments, such as tunnels and underground car parks (Rogers, 2009; Hunt et al., 2016). As a result, underground structures are being constructed beneath cities to a great extent, globally. This increase in subsurface construction is enhancing the risk of geohazards and makes the need for a better information, understanding and knowledge of the subsurface even more important.

The current and future safety of cities from these causes has become an urgent focus for several research groups, industries and authorities (Bridge et al., 2005; Mielby et al., 2017). A need to

know, understand and demonstrate in detail the underground features and their interactions with the built environment has been gaining attention to assess urban geohazard risk effectively (Price et al., 2016). Among many methods and tools used to provide this information, Building Information Modelling (BIM) proved to be a powerful tool to deal with structural engineering problems to date (Zou et al., 2017; Zhang et al., 2018).

Therefore, an advanced system that could provide information for ground condition changes and the interactions of ground with adjacent buildings, to predict geohazard risk would be clearly valuable. This system could be used to indicate and demonstrate hazardous areas, and hence provide the understanding required for sustainable land-use planning and decision-making.

1.2 Problem statement

Geohazards pose an increasing risk for urban areas as they expand. As cities make more use of their underground space, the settlement risk to adjacent buildings caused by tunnel construction has become an important geohazard to consider along with many other factors. Hence, better understanding and knowledge of the ground and its potential response to geohazards, in this case to tunnelling, is required to support sustainable urban planning by enhancing underground information, data management and visualisations.

1.3 Research Hypothesis

As cities expand, sustainable urban planning is needed to avoid more costs related to geohazards. Therefore, geohazard risk needs to be clearly assessed to inform for urban planning

and decision-making. A framework providing urban geohazard information is required in cities that would contribute to a more sustainable future, which includes the following considerations:

- A better understanding of the urban subsurface and its interactions with the built environment is an important aspect for better decision-making in urban environments.
- Geohazards can be significant in certain urban areas and they need to be considered within sustainable urban land-use planning.
- A thorough assessment of geohazard risk, such as tunnelling-induced settlement risk, which would be based on integrated analysis methods and 3D visualisations, could provide a framework for an urban geohazard risk assessment tool.
- The development of a BIM-based method could provide a robust assessment of geohazard risk by extending investigation and visualisation aspects. BIM could provide the information 'platform' required, which is based on data integration/exchange, and clearly present the outcomes of a geohazard analysis. This would improve sustainable urban planning and decision-making in relation to urban geohazards.
- The principles of sustainability can be supported using the power of BIM, and the associated environment of advanced software and multidimensional visualisations. Open-source software, low cost computational and communication power and common and widely used formats will enable advanced analyses and data integration/exchange methods, where all aspects are linked together through BIM. Hence, an integrated and 'multi-applicable' information tool for assessing geohazards could be created. This tool could support global sustainable 'targets' and align with the UN sustainable development goals. These goals indicate that decision-making and urban planning for sustainable cities need urban geohazard resilience, which is closely associated with

developing methods of integrated information, such as the integrated information tool for urban geohazards (United Nations, 2015).

- A BIM-based interactive environment of information for geohazard risk could help planners, scientists and engineers, and other users who are involved in relevant assessments. It could be used as an early-stage tool for various urban planning applications, associated with knowing in real-time important information of subsurface and its risk. To be important for users, this information needs to include visualisations of certain 'areas' of geohazard (tunnel-induced settlement) and damage risk. In addition, costs due to the damage risk would also be important to be indicate via clear risk-based visualisations. This information could support the ground investigation, i.e. it could extend desk studies by a 'multi-applicable' tool for potential urban construction and provide further/more detailed digital modelling applications on targeted areas, if required. It could expand on subsurface information though aiming at specific areas of potential risk and accompany other tools for urban expansion or further research in urban development projects. In this way, decision-making that advances the principles of sustainability is enhanced.
- A preliminary assessment tool for geohazards such as tunnelling-induced settlement risk would provide the information (and understanding) required to support urban land-use planning.
- The area around the new construction of the National Buried Infrastructure Facility (NBIF) within the campus of the University of Birmingham provides a representative example of a built-up area, which could be used in demonstrating such a preliminary assessment tool. The area has several structures exhibiting the characteristics of a typical urban area (close to the city centre), in this case a university campus. As the city

expands, sustainable urban developments associated with a crowded area (i.e. the campus), such as the tunnel construction, could take place in the area. Hence, the scenario of a potential tunnel construction in the area, as part of, for example, the local transport system expansion, could provide an efficient case study for modelling the consequent (tunnelling-induced) settlement risk. In addition, the known and commonly UK-wide found ground conditions of the site and its geological data, which is available from ground investigation, would play an important role in the selection of the specific area for the model. As a result, this case study could provide an interesting scenario for planners, users and engineers, to easily adapt their own models for assessing the settlement risk due to tunnel construction.

1.4 Aim & Objectives

The aim of this PhD project is to provide an integrated computer-based system that has all the required information to assess the risk due to geological hazards in an urban area to support decision-making for sustainable and resilient urban planning.

The objectives of this PhD are, to:

- study the ground conditions in an urban area and interpret them in 3D, using borehole data;
- establish a risk assessment for any given geohazard;
- select a geohazard (tunnelling-induced settlement risk) that would enable the application of an information system to clearly model and assess the risk;
- understand the (3D) ground condition changes and interactions with the built environment, with respect to the construction of a tunnel;

- provide a 3D geological model including the tunnel and adjacent buildings to generate and demonstrate clearly all the geological/geotechnical/structural information required for a risk assessment;
- integrate within the 3D model the geological, geotechnical and structural modelling information required to align with an urban assessment;
- establish a basic tunnelling-induced settlement risk assessment and define its components by advanced analyses based on developing a custom-made code (and adapting/integrating tools) to produce a framework tool;
- estimate the tunnelling-induced settlement hazard of adjacent buildings damage;
- provide the tunnelling-induced settlement vulnerability of an urban area by investigating impact factors;
- explore the probability of building damage costs caused by the tunnelling-induced settlement (hazard);
- provide the resulting integrated 3D visualisations of the tunnelling-induced settlement risk assessment;
- discuss the outcomes and the potential of this geohazard assessment tool within a geohazard information system for supporting better decision-making in sustainable planning of urban areas.

1.5 Introduction to the Chapters

The structure of the thesis provides a clear understanding of the integrated system for the geohazard risk assessment that has been developed during this study. Initially, the literature review describes the relevant state-of-the-art literature in the field – associated with the characteristics of this system. Then, the methodology chapter is provided, indicating how this

framework will be developed. This will be based on the reported geohazard risk assessment and detailed data management and integration processes. A flow chart is presented to show clearly the overall concept this study used. Then the methodology is applied in the three following chapters to build and demonstrate this integrated information system. Chapter 4 explores the Settlement Hazard using analytical models and Building Information Modelling (BIM), and presents its results. The settlement vulnerability using 3D spatiotemporal analyses and BIM, with its results then follows (Chapter 5). Finally, the settlement economic risk of buildings using uncertainty analysis and BIM and its results are described in Chapter 6. The discussion of the Chapters (4, 5 and 6) results combined, follows in a discussion chapter to expand on the outcomes, analysis resultants and resulting (3D) visualisations of the analyses. The conclusions of this PhD study, including a future work section, indicate the importance and describe the substantial contributions of this study. Then, after the references, the appendices follow with details such as further visualisations of the analyses used and other modelling aspects. The detailed description and specifications of the MATLAB scripts developed are included in the appendices.

2 LITERATURE REVIEW

2.1 Introduction

As urbanisation grows, the sustainable future of urban areas is important to be considered (United Nations, 2015). This has drawn the attention of scientists and engineers, who focused on the effects and the measures that need to be taken to ensure the sustainable urban expansion. Hence, sustainable urban planning plays an important role, and therefore relevant (contributing) methods have been considered. Among many, an increasingly adopted method is the use of the urban underground space, which requires ground-related information (Hunt et al., 2016). In addition, previous research demonstrates that information for ground-related or geological hazards risk needs to be accounted for when planning for construction developments within an urban area (Hunt et al., 2016). Therefore, knowledge and understanding of the subsurface is an important aspect for sustainable urban planning, as presented in the current literature review. More specifically, geohazard risk to the (adjacent) built environment due to ground movements and instability, would be crucial. These could be caused by natural phenomena and ground-structure interactions or interactions with underground structures, such as tunnels. As a result, geohazard-related decision-making is important for sustainable urban planning, to avoid economic and human costs (de Rienzo et al., 2008).

Tools to provide geohazard information to be used in decision-making in relation to urban planning have been provided (Griffiths, 2016). This was carried out by conducting geohazard risk assessments, which have been extensively used in the field (de Rienzo et al., 2008; Griffiths et al., 2012). These assessments were based on various risk assessment analysis techniques. Successful and widely used methods are provided from past research to demonstrate their characteristics and advantage. Multi-criteria analyses considered the ground-related parameters and provided efficient outcomes for relevant decision-making (Rozos et al., 2011; Nezarat et

al., 2015). In addition, geostatistical analyses were also widely used (Sun and Kim, 2016). Interpolation methods have been also widely employed in relevant geohazard assessments (Kim et al., 2019; Qi et al., 2019). Likewise, probabilistic analyses had also extended the relevant research with successful and useful outcomes. This specifically supported geological uncertainty estimations, which are important to be considered for accurate resultants in ground-related (geological) analyses (Phoon and Tang, 2019).

To provide an efficient geohazard risk assessment, the results of the analyses need to be presented effectively using digital tools. Therefore, 2D maps (using Geographic Information Systems (GIS)) have been widely used in relevant geoengineering applications, and hence important examples for decision-making are provided in the present literature review (Bathrellos et al., 2017; Weidman et al., 2019). However, due to their limitations, the 3D ground (geological) models have been employed in relevant assessments. These provide a principal tool of geoengineering in relation to ground characteristics (investigation), which enhanced ground representations significantly. The wider use of 3D geological modelling supported geohazard assessments and provided a robust knowledge and understanding of subsurface using many methods (Gakis et al., 2016; Burke et al., 2017). Previous research using 3D modelling applications is presented, demonstrating key data limitations. Building Information Modelling (BIM) has been a concept with a wider utilisation, due to its efficient performance in numerous construction data applications. As shown in prior research, this provided successful applications in other fields, including the use in geotechnics where it is shown to be promising (Chang and Lin, 2016; Zhang et al., 2018).

2.2 Literature Review

2.2.1 Urban sustainability

In recent years, there has been a rapid expansion of cities, globally. This significant expansion drew the attention of scientists and engineers to the sustainability of cities (Owens and Cowell, 2011; Rogers et al., 2012). There are many direct effects accompanying urbanisation, such as the transportation management, water and resources supply, and waste disposal and pipeline systems demands. Other or indirect accompanying effects could be due to the impact of natural/manmade hazards that may have on urban areas (Dai et al., 2001).

The problems arising from the expansion of cities in combination with climate change made people and civil authorities to take measures (Grimm et al. 2008; Owens and Cowell, 2011; Rogers et al., 2012). As described in the report of the Institution of Civil Engineers (ICE, 2009), there has been a demand for sustainability in urban areas in the UK to reduce these problems with the support of accompanying legislation. Sustainable development would be the initiative which is effective without affecting (negatively) potential aspects (Brundtland, 1987). Hence, sustainable measures are definitely needed for implementing a proper planning system for the future, where sustainability would be based on environmental, social and economic integration (Price et al., 2016). Therefore, it is evident that an emphasis has been given on urban planning, to align with sustainability and resilience (Giddings et al., 2002; Rogers, 2009; ICE, 2009).

An important aspect which aligns with sustainable planning in construction and infrastructure is related to the land use planning within an urban area. Consequently, urban land-use planning could successfully mitigate potential risks and costs (Delatte, 2008). More specifically, the land use refers to the suitability of an area for a potential construction by evaluating specific criteria (Dai et al., 2001). Those criteria would be factors which have an impact on the urban area. There has been a large amount of research that studies specific effects of social, economic and

environmental factors (Giddings et al., 2002). Among researchers, Dai et al. (2001) emphasised the importance of geoenvironmental factors in relation to their impact on land-suitability evaluation, and the need to be accounted for and for measures to be taken. This was important to be taken into consideration because these factors are associated with aspects of civil design, economics of proximity to resources or contamination and natural hazard impact (Dai et al., 2001).

It is important to be noted that sustainable planning is a complex task due to a combination of systems acting together, which has been challenging (Hall et al., 2014). In addition, Hall et al. (2014) noted that adapting different or custom scenarios could be useful for obtaining effective decisions while incorporating a planning strategy for multidisciplinary sustainable aspects. This is valid because, in this way, safe city developments (and expansion) could be ensured, as noted by Giddings et al. (2002). In the same fashion, a large amount of research has been done on investigating methods and tools to contribute to sustainable planning of urban areas by focusing on the previous factors and using specific applications (Giddings et al., 2002; Hunt et al., 2009; Rogers et al., 2012; Hall et al., 2014). Hence, robust methods or tools to ensure sustainable urban planning are needed.

One of these methods is related to urban underground space. This refers to the space below cities, which is capable of offering resources to the inhabitants (Hunt et al., 2016). Thus, there has been an increasing use of the underground space of urban areas (Rogers, 2009). In addition, there has also been a large amount of research in many fields of sustainable urban developments, which used the urban underground space and relevant applications (Hunt et al., 2016). By way of example, Hunt and Rogers (2005), Metje et al. (2007), Hunt et al. (2008) Rogers (2009), Hunt et al. (2016), Tengborg and Sturk (2016) and Hojjati et al. (2017) provided underground space applications and methods for sustainable development of urban areas

involving the underground. Hunt et al. (2016) demonstrated the past, the present and the potential opportunities for further use of the urban underground space, alongside the increasing demand for urban space and resources.

To align with sustainability, an appropriate urban (land-use) planning is required (Hunt et al., 2016). Nevertheless, underground space and urban planning aspects are closely connected, to ensure a sustainable future of cities, as implied by Giddings et al. (2002), Hunt et al. (2008), Rogers et al. (2012) and Admiraal and Cornaro (2016). More specifically, Hunt et al. (2016) presented the potential of using urban underground space to align with a sustainable and resilient future of cities via an accompanying planning and regulation framework.

The use of urban underground space provided an example to initially demonstrate a widely used method which supported sustainable cities. This is linked with sustainable urban planning. However, ground conditions and their characteristics play an important role in the underground space utilisation and related construction activities.

Beyond underground space, knowledge and understanding of ground-related information would be important for any (above-ground) sustainable construction within urban areas (Griffiths, 2016). A significant body of literature presented that subsurface information could be key in relation to the safe and sustainable future of an urban area (Price, 1971; de Rienzo et al., 2008; Gibson and Chowdhury, 2009; Dindarloo and Siami-Irdemoosa, 2015; Kim et al., 2015; Bathrellos et al., 2017). Hence, it was considered in urban (land-use) planning applications and in UK national planning process (de Rienzo et al., 2008; Culshaw and Price, 2011; UK National Ecosystem Assessment, 2011; Griffiths et al., 2012).

Therefore, a large amount of research aimed at advancing knowledge and understanding of ground conditions, to align with sustainable urban planning purposes, such as Thierry et al.

(2009), Culshaw and Price (2011), Kim et al. (2015) and Bathrellos et al. (2017). In fact, understanding and investigating ground conditions within an urban environment has always been a key objective in Engineering Geology, as noted by Price (1971) and Griffiths et al. (2012). More specifically, this is extensively studied in the field of 'Urban Geology' (Bridge et al., 2005; de Rienzo et al., 2008).

Hence, it is evident that changes of ground conditions can have an impact on the built environment (Griffiths et al., 2012). The importance of geological aspects due to ground condition changes alongside urban construction developments has been studied extensively by Griffiths et al. (2012) and Griffiths (2016). The need to incorporate a number of geohazards and their relevant severity is crucial. Price et al. (2016) have also correlated the changes of urban ground properties and interactions, and then showed the significance of investigating these changes in relation to a potential land use, which would align with sustainable planning. These changes are associated with natural or geological hazards, which need to be accounted for when planning (McCall, 1998; Gibson and Chowdhury, 2009).

2.2.2 Geohazards

Thus, key area of research within this thesis is the consideration of geological hazards or 'geohazards' that are caused by ground condition changes. These hazards and their subsequent considerations are important because they pose risk, inducing human, economic and environmental costs in urban areas, globally (McCall, 1998; Delatte, 2008; de Rienzo et al., 2008; Gibson and Chowdhury, 2009).

Geohazards occurring within an urban area pose a significant risk and should be considered in urban planning (McCall, 1998; Gibson and Chowdhury, 2009). There has been a large body of literature studying these geohazards in relation to their characteristics and effects. Geohazards

could be associated with both natural and manmade geological properties alterations, which are strongly caused by specific interactions with the built environment (Griffiths et al., 2012).

Among many geohazards, movements of the ground has been investigated as a common issue of building susceptibility in urban areas (Simons et al., 2002; Fedeski and Gwilliam, 2007; Amorosi et al., 2019). Ground movements have been considered more than other geohazards, such as floods, by construction regulations in the UK (Fedeski and Gwilliam, 2007).

More specifically, many research studies have focused on ground movement risk in urban areas, such as the examples by Thierry et al. (2009), Chakeri et al. (2013), Li et al. (2014) and Amorosi et al. (2019). Simons et al. (2002) described ground movements, as the movements induced by shear forces (due to earthquake events), loads of buildings or other sources, such as landslides. Pacheco-Martínez et al. (2013) indicated that ground movements, and especially urban subsidence in relation to the groundwater pumping and exploitations is regarded as a significant impact factor in urban regions in Mexico, where it has been causing human and economic costs due to poor geotechnical investigations. Rawlins et al. (2015) emphasised on the importance of clay properties and soil-structure interaction characteristics within urban soils. They indicated that these should be considered by geotechnical/environmental experts, as major causes of building susceptibility. More specifically, settlement and subsidence are related to the downward, and heave to the upward movement of foundations (in relation to buildings) (Simons et al., 2002). Thus, among urban geohazards, ground movements have been a major challenge for both scientists and engineers.

It is important to note that the increasing use of urban underground space has had an effect on ground movements (Hunt et al., 2016). Among urban geohazards, ground movements caused by underground construction, such as tunnels, have been considered significant, and has been

widely assessed, for example by Clarke and Laefer (2014), Giardina et al. (2018), Ding et al. (2019), Xie et al. (2016) and Providakis et al. (2019). Therefore, tunnel construction needs to align with safe settlement predictions (O'Reilly and New, 1982; Rankin 1988, Chapman et al., 2017; Avgerinos et al., 2017). Several examples were proposed, assessing potential damage from ground settlements on the built environment caused by tunnelling (Burland and Wroth, 1974; Burland, 1995; Mair et al., 1996; Schindler et al., 2016; Amorosi et al., 2019). In addition, important geotechnical criteria that affect building susceptibility and can cause considerable risk have been also widely assessed and are more likely to be found within 20m of depth from ground surface (Burland and Wroth, 1974; Mair et al., 1996; Bartolomey et al., 2003; Bauduin, 2003; Dindarloo and Siami-Irdemoosa, 2015). Hence, tunnel-induced ground movements have been considered a major urban geohazard, and consequent risk needs be taken into consideration in relevant decision-making.

Other types of geohazards have been also affecting urban areas, and hence need to be considered to support urban sustainability. For example, the framework developed by DCLG (2012) acknowledged a number of important urban geohazards apart from the ground movements, those of flood and land contamination risk, as well as the lack of potential for underground exploration and construction materials. These risks are increasingly accounted by European geo-industries to avoid costs (Baynes, 2010). Clayton (2002) provided a review on particular aspects related to rigorously assessing a geotechnical risk by focusing on challenges of ground conditions, their investigation problems to date and the potential approaches to handle them efficiently.

In addition, urban ground instability, for example, due to compressible soils or karst could also be critical. These issues (geohazards) in relevant susceptible areas have been extensively studied within urban environments. In fact, Gibson and Chowdhury (2009) proposed to account

them particularly when working within an urban area. By way of example, Papadopoulou-Vrynioti et al. (2013) provided the severity of geological factors causing a karst-induced collapse in an urban area. The findings showed the role of planning in mitigating such aspects (Papadopoulou-Vrynioti et al., 2013). Thus, risk due to karst collapse needs to be also considered in urban planning schemes due to the geology of the urban area investigated. This could accompany other types of geohazards.

In addition, flood risk has also been an important urban geohazard that would need consequent urban planning, as implied by a large amount of research in the field. Examples of studying the impact factors and causes of potential urban flooding events have been studied by Skilodimou et al. (2003), Ferrario et al. (2015). Among many examples, Lo et al. (2015) and Papaioannou et al. (2015) successfully revealed the risk by proposing applications to manage and predict this risk. They concluded that sustainability is clearly connected with a proper planning to tackle this risk and consequent planning should be adapted (Ferrario et al., 2015).

Hence, a large body of literature on urban geohazards revealed their severity, which needs to be accounted for when planning. However, they were more focused on providing a study of a specific geohazard effect than a tool aimed at assisting both scientists and engineers (i.e. ground investigation aspects) with sustainable decision-making. As a result, urban geohazard studies to date have a limited ('real-life') application, i.e. as sustainable urban planning tools.

In addition, to promote sustainable city applications, subsequent planning needs to consider various ground (geohazard) characteristics/criteria and manage their potential issues in decision-making (de Rienzo et al., 2008). Thus, relevant urban planning would need to consider a number of geohazards and their associated criteria, using specific methods that support decision-making.

2.2.3 Geohazard decision-making

Culshaw et al. (2006) proposed a method associated with sustainable urban planning to manage geohazards (and relevant issues), which have been increasingly drawing the attention of scientists and engineers in the UK. Thus, the Environmental Information System for Planners (EISP) was developed, which had a database focusing on geohazard applications for urban sustainability of many cities in the UK (Culshaw et al., 2006).

Geohazard consideration is key in decision-making for sustainable urban planning purposes (United Nations, 2015). This could provide the knowledge and understanding that is needed for decision-making, which aligns with sustainable urban planning. To ensure this, the proper geotechnical/geohazard information needs to be available (to be processed) (Price et al., 2016). This information could then indicate the potential geohazard risk posed to an urban setting. A system to demonstrate geohazard information in 'real-time' would be useful for accurate decision-making, which could be used in geotechnical applications.

Over the years, this has not caught the attention of planners, which led to issues. One recent issue affecting urban sustainability is related to the ignorance of the subsurface. In fact, Culshaw and Price (2011) mentioned that authorities tend to neglect the importance of the geological information within urban expansion and development planning. There has not been national legislation concerning underground aspects or changes, although the number of investigations for potential developments has been rising, as noted by Whitebread et al. (2016) in a Glasgow report for urban developments. An explanation could be the lack of communication to put the matter right within the geoengineering sector, which needs to be addressed (Culshaw and Price, 2011). However, as Price et al. (2016) proposed, understanding geohazard behaviour is significant for sustainability, and therefore this needs to be incorporated within planning and decision-making regimes.

Insufficient understanding due to limited geological data also led authorities/engineers to neglect subsurface characteristics in urban planning and developments across Europe, while the communication has been often skipped until mistakes were evident. (Mielby et al., 2017). Price et al. (2016) revealed the importance of collating information on subsurface conditions, because they have a great impact on the buildings, which made it important to for the ground suitability information planning. Likewise, Marker (1998) emphasised on the importance of geological and geotechnical factors information within the area for development, which was neglected in planning and led to many problems caused by geohazards within urban areas.

Therefore, obtaining information of geohazard risk is key in geohazard decision-making. In this way one can manage geohazards in an urban area properly. Relevant methods for providing information that can be used for decision-making have been created and used. These incorporated advanced applications to manage or assess various geohazard risks. Technological developments and applications to reduce human and financial costs have been extensively accompanying the geohazard risk assessment process (Price et al., 2016). This process, by definition, is based on the fundamental concepts for assessing a risk.

2.2.4 Geohazard risk assessments

To manage effectively ground conditions and minimise cost risk, the thorough prior knowledge and understanding is needed, as noted by Aldiss et al. (2012). This would involve a risk assessment, to produce all the required information for decision-making (and planning). There has been extensive research on numerous aspects of geohazard risk assessments, providing numerous applications, as for example these by Kazakis et al. (2015), Papaioannou et al. (2015) and Hyun et al. (2015).

A risk assessment process has been a useful tool for engineers/authorities to provide a thorough urban planning assessment, after realising its importance to avoid costs. As cities expand, sustainable urban planning and decision-making has incorporated geohazard risk assessments to prepare for costly consequences with time (Price et al., 2016). Rawlins et al. (2013) named such an assessment as a 'Platform of cities' Ecosystem', which served for above and below ground surface (Corvalan et al., 2005; UK National Ecosystem Assessment, 2011; Price et al., 2016). This is closely associated with geological and geotechnical knowledge to provide efficient evaluation of risk with accurate interpretations and estimations (Huber et al., 2015). Culshaw et al. (2006) indicated that a geohazard risk assessment is needed for sustainable civil design and urban planning. In addition, a key point was noted by Lee and Jones (2004) and Griffiths et al. (2012), who considered geohazards as natural alterations of geological/geotechnical parameters, which pose no risk until they have a direct impact on the built environment. These key findings explain the link of a geohazard risk assessment with the built environment.

In addition, Sigtryggsdóttir et al. (2015) indicated that construction problems could be predicted in advance by a risk assessment implementing various parameters. Huber et al. (2015) added that the geohazard risk management is complex due to the ground variability, and hence analysis may be needed for efficiency. This is common in urban geological studies that combines environmental, geotechnical and social aspects (Dai et al., 2001). Such interdisciplinary studies have been provided, as for instance building damage costs information in relation to geohazards, which was introduced by Blong (2003).

Previous research revealed that the selection and use of a particular geohazard risk assessment is typically based on using basic risk 'components', such as hazard, vulnerability and risk (Fedeski and Gwilliam, 2007). Further integration could be provided, as required by the aim of

the assessment. This would be defined by the assessment per se, which would be crucial for the prediction of the risk in an urban area. In addition, there has been a lack of geohazard risk assessments that could be rapidly employed within geotechnical applications. Their multi-applicability that could benefit ground investigation is also limited. Hence, a tool (system) of assessing the risk that could directly integrate a large amount of geohazard/geotechnical information could be useful, and advance sustainable urban decision-making.

Geohazard risk assessments within urban areas have used various analysis methods (before using 2D maps or 3D models to demonstrate their outcomes) (Papadopoulou-Vrynioti et al., 2013; Griffiths, 2016).

2.2.5 Geohazard risk assessments analysis

Geohazard risk assessment analyses are required to complete a risk assessment and produce the desired outcomes. The accuracy of the risk predictions (results) depends on the selection of the appropriate analysis method. They have been selected based on the aim of research, limitations, and available data. Numerous analysis methods have been used in the past and representative and widespread examples follow.

Due to the very nature of a geohazard study, the associated parameters provide important features, upon which complex models are based (Dindarloo and Siami-Irdemoossa, 2015; Yang et al., 2016). To provide accurate urban geohazard risk assessments, different types of parameters were correlated to support decision-making (Papaioannou et al., 2015). Among analysis methods, the methods that provide the severity between different factors (criteria) have been popular (Papaioannou et al., 2015; Kazakis et al., 2015; Kim et al., 2019). These methods have been useful for providing successful predictions for accurate urban ground-related decision making. Such approaches are known as multi-criteria decision-making analyses, such

as the Analytical Hierarchy Process (AHP) by Saaty (1977), which has been widely and successfully employed. In this type of analysis, a system of hierarchy is being developed between those geo-parameters, which has been extensively used to estimate geohazard risk, such as in the studies of Neaupane and Adhikari (2006) and Rozos et al. (2011). In addition, this type of decision-making analysis has been widely adopted using borehole data. More specifically, examples of such a system have been used successfully in correlating geotechnical (Kolat et al., 2012; Hyun et al., 2015; Nezarat et al., 2015; Taheri et al., 2015; Yang et al., 2016) and hydrogeological parameters (Fernández and Lutz, 2010; Papaioannou et al., 2015) provided effective (and successful) geohazard risk predictions. An example correlating several factors to assess related geo-information for flood susceptibility of an area has been also adapted by Kazakis et al. (2015). The risk of slope instability has been studied by Yoshimatsu and Abe (2006), Yalcin and Bulut (2007), Ayalew et al., (2005), Liu and Chen (2007) and Kayastha et al. (2013). Among numerous studies presenting the environmental impact within urban planning, such analytical risk assessments have been successfully produced for contaminated land management (Bello-Dambatta et al., 2009) and land-suitability aspects (Marinoni, 2004; Lee and Chan, 2008; Ersoy et al., 2013). Similar examples of analysis estimations have also been employed by correlating factors to assess underground risk, such as by Benardos and Kaliampakos (2004) and Chakeri et al. (2013). Bottero and Peila (2005) applied similar techniques to select across micro-tunnelling and trench excavation in an urban setting. Finally, Hyun et al. (2015) effectively assessed the safety of a tunnel using Tunnel Boring Machines (TBM).

Geohazard risk assessments have also used analysis approaches to deal with ground condition changes with time successfully (Yun and Reddi, 2011; Mercado et al., 2015; Varouchakis, 2017). Their results advance geological/geotechnical risk assessments, aligning with

sustainable decision-making (Chetouani, 2008; Berendrecht and van Geer, 2016). For example, the AutoRegressive eXogenous (ARX) analysis has been used in providing successful time-dependent estimations (Chetouani, 2008; Oskay and Zeghal, 2011). Similar applications of dynamic analysis have been used extensively for groundwater, and related successful examples are presented from Bierkens et al. (2001), Knotters and Bierkens (2001), Berendrecht and van Geer (2016) and Varouchakis (2017). Likewise, earthquake assessment risk analyses were also provided by Glaser and Baise (2000) and Oskay and Zeghal (2011).

Other analysis methods have also been proposed to solve ground-related problems by correlating parameters. For example, the Artificial Neural Networks (ANN) method has been successfully used in geotechnical (Suwansawat and Einstein, 2006; Santos Jr. and Celestino, 2008; Costalago Meruelo et al. 2016; Kim et al., 2019) and groundwater analysis (Daliakopoulos et al. 2005). Shahin et al. (2004) and Costalago Meruelo et al. (2016) noted the potential of ANN for use in non-linear and dynamic systems, although they depend much on available data. This was an important limitation for ground-related problems.

In addition, numerical methods such as the Finite Element Method (FEM), have been widely applied in relevant analysis. FEM analysis has become one of the most common technique in engineering, which has also been successfully used in solving relevant ground-related problems (Potts et al., 2001; Xie et al., 2016; Amorosi et al., 2019). Hence, a huge body of research used such numerical analyses to analyse soil-structure interactions and other (dynamic) geotechnical aspects in detail (Xie et al., 2016; Avgerinos et al., 2017; Amorosi et al., 2019 and Ding et al., 2019). Efficient ground estimations that used FEM analysis for the urban geotechnical risk assessment were performed by Marache et al. (2009), Amorosi et al. (2019) and Ding et al. (2019). The seismic hazard tool for an urban area by Sun (2012) is another such example. The past research using FEM analysis provided successful individual outcomes, however their use

within a framework for an urban geohazard risk assessment is limited due to software and data incompatibility. In addition, FEM analyses depend on available (geotechnical) parameter data (Potts et al., 2001). This could be critical when dealing with scarce data (such as in frequent geotechnical/geological problems dealing with complex ground conditions). A subsequent demand for computational power (and costs) would be needed, which is shown to be particularly challenging, and hence makes decision-making difficult. These limitations would imply that a post-analysis or more targeted assessment using FEM could be useful.

In addition, geostatistical analyses (and spatial analysis tools) have been widely used in similar assessments to provide successful outcomes and distribution of the geohazard-inducing factors (Khakestar et al., 2016; Sun and Kim, 2016; Pinheiro et al., 2018; Fisonga et al., 2018; Rahimi et al. 2019). Probabilistic analyses, for example, by González-Garcia and Jessell (2016) and Mashhadian et al. (2018) broadened the horizons in the field. Successful statistical outcomes showed useful predictions about geohazards and ground interactions.

Over the years, other techniques have supported geohazard risk predictions. For example, the interpolation methods have been a widely used tool in geological and geotechnical modelling (He et al., 2008; Qi et al., 2019; Kim et al., 2019; Rahimi et al., 2019). This provided a reliable way of estimating information between known points (Thierry et al., 2009). Among research examples, Marache et al (2009) and Al-Bittar et al. (2019) have used kriging interpolation successfully to provide geotechnical risk assessments in relation to urban planning. In addition, geostatistical analyses using borehole values and kriging have been widely adopted within a Geographical Information System (GIS) environment (Masoud, 2014; Rahimi et al., 2019).

In the same context, a key point to carry out a robust relevant assessment is related to the uncertainties involved. This is due to the nature of ground problems, which is associated with the variability of the ground.

2.2.6 Uncertainty analysis

Uncertainties have been widely considered in geological and geotechnical analyses (Zhang, et al., 2009; Wang et al., 2016; Phoon and Tang, 2019). Uncertainty analyses (and evaluations) have been used to provide more accurate predictions by quantifying a risk as shown for example by Gilbert and Tang (1995), Zhang, et al. (2009), Zhang, et al. (2012), Wang et al. (2016), Sun and Kim (2017) and Phoon and Tang (2019). However, most of relevant past research consists of individual studies, which tends not to provide useful information for sustainable planning, i.e. uncertainty information as a part of a complete assessment is missing. The geotechnical factors used are important to carry out uncertainty analyses. These depend on ground variability, which makes such an analysis complex, and hence needing further evaluation to model the uncertainty (Zhang et al., 2012; Mashhadian et al., 2018). The efficient input of these factors is related to geotechnical expertise or available data (Tang, 1984; Phoon and Kulhawy, 1999; Wang et al., 2016; Phoon and Tang, 2019). Phoon and Kulhawy (1999) also explained that limitations have been always an issue in this input in this type of analyses.

Applications using geostatistical and probability analyses, such as Probability functions, have been widely employed in geohazard uncertainty estimations to analyse geotechnical/geological processes (Juang et al., 2005; Cheung and Tang, 2005; Zhang et al., 2009; González-Garcia and Jessell, 2016; Mashhadian et al., 2018). They have been successfully used, although they tend to limit to individual research results, again. However, by way of example, Nguyen and Chowdhury (1985) noted that geotechnical risk assessments associated with design and cost analyses involve uncertainty, and hence its evaluation would enhance those processes. This could be carried out successfully by combining (closed-form) analytical methods, and probabilistic methods, such as the Monte Carlo method, which is commonly employed in geotechnics (Nguyen and Chowdhury, 1985).

Monte Carlo simulations have been widely used to analyse geotechnical problems via random-sampling tests to define the parameters needed, as shown by Peng et al. (2017) and Cao et al. (2019). These simulations have also been used to analyse uncertainties successfully, with relative literature employing them in geotechnical risk assessments, such as by Rowe and Fraser (1995) and Zhang et al. (2012). This has also supported assessing slope stability and landslide hazards (Hammond et al., 1992; Wang et al., 2010; Cao et al., 2017). For example, a risk assessment to the use a TBM was provided successfully by Benardos and Kaliampakos (2004), who indicated potential hazards successfully by using Monte Carlo analyses for uncertainty evaluations. Their results could be extended using structural factors within the analysis. Then, Marache et al. (2009) provided an integrated parametric modelling for geotechnical hazards, where the Finite Element Method (FEM) analysis and the Monte Carlo method were successfully used in forming uncertainty analyses to provide a geotechnical risk assessment. According to Marache et al (2009), these demonstrated the efficiency of the geostatistical approaches and the Monte Carlo method for ground uncertainty estimations, aligning with evaluating ground variability.

However, it is important to note that a relevant assessment analysis needs to be presented to model the resulting geotechnical risk assessment information (data). This aligns with sustainable applications (Rogers, 2009). Initially, this was performed using maps. Representative examples of geohazard assessments using 2D maps to promote sustainable urban aspects follow.

2.2.7 Geohazard maps

2D Maps provide an efficient and widely used way of presenting a geohazard risk assessment (Bathrellos et al., 2017). Geohazard maps use several tools and each one of those tools provide a different demonstration of the analysis outcomes (depending on the assessor and its focus)

(Bathrellos et al., 2009; Papadopoulou-Vrynioti et al., 2013; Bathrellos et al., 2017). However, it is evident that the interpretation of results would focus only in 2D aspects and could lack in data and attribute information (such as geological features information) aspects, which is key as technology and urban planning needs advance.

A widespread tool that has been extensively used in geoscience (and geohazards) and relevant mapping is the Geographic Information Systems (GIS), which could present any type of (thematic) map data to show the geographical (spatial) extent of a (risk) factor (Bathrellos et al., 2017; Weidman et al., 2019). El May et al. (2010) and Weidman et al. (2019) used various criteria to provide urban geological/geotechnical risk-based zones using GIS and integrated them with the urban area aspects (factors) successfully. GIS is an important tool for geoscientific applications, having successfully been used in demonstrating outcomes from numerous research studies (Busby et al., 2012; Sun and Kim, 2016; Weidman et al., 2019; Freeborough et al., 2019). Resulting maps have been very significant for assessing risks which can be used by planners (Entwisle et al., 2008; Bathrellos et al, 2017). This could be done by integrating different hazards into a map, providing tangible outcomes for a research study. The urban geohazard risk assessments using 2D maps (GIS) have been widely used over the years and led to important findings to support land-use planning. By way of example representative past research follows. Entwisle et al. (2016) provided a GIS tool to be used in informing for urban area developments using geological and geotechnical data from ground investigations of a study area (Glasgow). This successfully provided effective outcomes for decision-making, although data communication and the corresponding visualisations could be extended.

An application for informing the user of the earthquake hazard by a relevant assessment in an urban area in South Korea has been conducted using GIS and the Finite Element Method (FEM) (Sun, 2012). It revealed its efficacy for providing information on earthquake risk of an area,

although the need for integration with further data would be needed. Likewise, Sun and Kim (2016) provided a framework using GIS for seismic zones, which showed the same limitations. The significance of combining earthquake risk with land use planning was indicated by Sengezer and Koç (2005), who included in their research parameters such as the construction time, the building height and geology. Then, Berhane and Walraevens (2012) indicated the land suitability through assessing the risk of geological parameters of an expanding urban area in a region of Ethiopia with high seismicity. This is important revealing the common use of 2D mapping to present geohazard risk assessments used for planning, although the need for data compatibility and communication to form a geohazard framework remains challenging.

Papadopoulou-Vrynioti et al. (2013) demonstrated the importance of karst within land-use planning due to the ground instability during an earthquake. GIS maps evaluating geological factors inducing karstic collapsibility, were also developed (Papadopoulou-Vrynioti et al., 2013). Hence, it is shown that several parameters could be presented by risk assessment maps, such as the instability due to karstic environments (rocks).

Masoud (2014) has also used GIS to assess alluvial soils in Egypt, using geotechnical factors with their spatial likelihood to occur and hence provide zones of urban land-use. Lamelas et al. (2009) have also provided a platform to provide similar information in relation to geomorphological hazards using GIS. This has been done providing an integrated model using several ground-related and other factors used in sustainable decision-making predictions Lamelas et al. (2009). Hence, a key point of urban land-use planning is the suitability of an area according to factors, in this case, geological and geotechnical factors are considered. A relevant example is provided by Bathrellos et al. (2012) who proposed a sustainable urban planning approach using geohazard maps conducted by GIS and multi-criteria decision analyses to develop suitability maps for industrial developments. These maps used

geological/geomorphological (geohazard) parameter data apart from the typically used socioeconomic for an urban area in Central Greece (Bathrellos et al., 2012). Bathrellos et al. (2017) also expanded on earlier research, using the same methods (GIS) although applying a large amount of information to an enhanced thematic map to provide the land suitability for urban developments. The example of the seismic hazard map is provided in Figure 2.1 (Bathrellos et al., 2017). Youssef et al. (2014) studied geological and geomorphological characteristics/parameters of an area to provide land suitability maps from several natural hazards, using GIS and decision-making techniques. However, urban planning aspects would need to combine parameter (data) information to extend the understanding in geohazards, and hence align with sustainability. This is due to the different types of relevant information involved. Therefore, an integrated system which could integrate this information could be suitable.

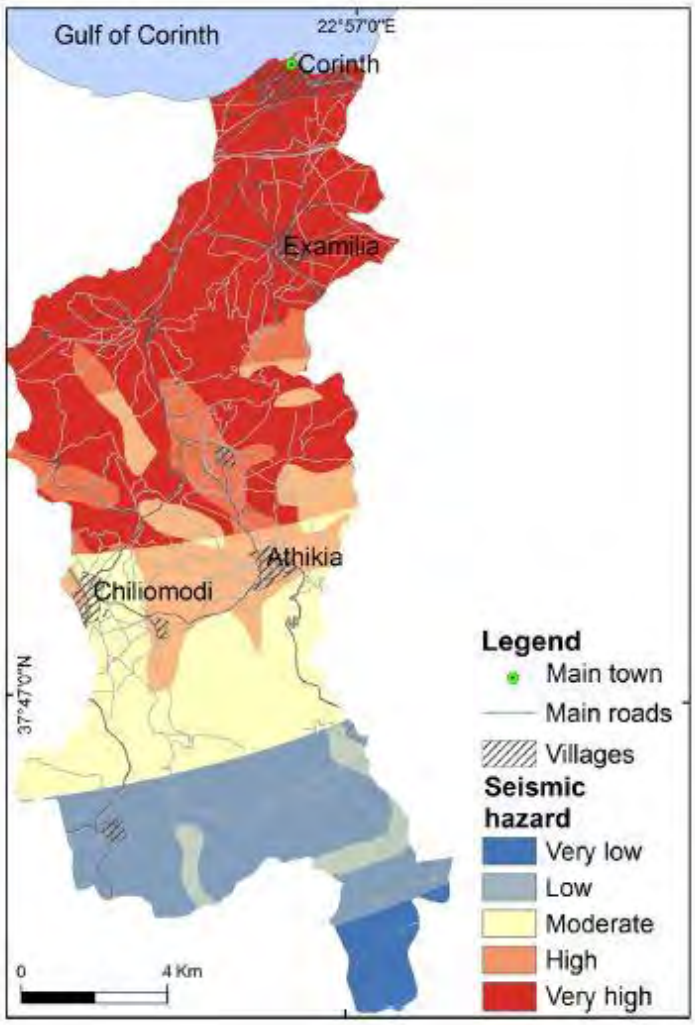

Figure 2.1: A seismic hazard map of an area in Greece (Bathrellos et al., 2017).

Coutinho-Rodrigues et al. (2011) included social and economic factors via a user-friendly decision support system for urban planning using a multi-criteria analysis. However, more factors would be needed for a complete decision support system. Weber (2003) demonstrated the importance of providing potential urban expansion zones to align with sustainability. They provided information for decision-making process using an interaction model supported by GIS and remote sensing, and hence established a database system to assess this information which could advance relevant decisions (Weber, 2003). Likewise, Marinoni (2004) provided an

automated land use risk assessment using a criteria decision system tool, which was presented using 2D maps (Marinoni, 2004). These examples of land suitability assessments provided the geotechnical risk, which demonstrated useful information for urban planning. However, their assessment was only focused on certain impact factors, and hence they lack in accurate assessment outcomes due to the complexity of the ground. An integrated framework that could combine and link different type of data together, would be capable of providing a robust risk assessment and align with sustainable decision-making.

Another geohazard that affects urban areas which needs to be considered by planners is landslide risk. A landslide risk map can be achieved contributing to the landslide analysis and producing results useful for sustainable planning (Dijkstra et al., 2015). The landslide-inducing factors have been studied extensively by incorporating factors and provided susceptibility maps showing corresponding risk zones (Yoshimatsu and Abe, 2006; Bathrellos et al., 2009; Kayastha et al., 2013; Prashad Bhatt et al., 2013). Risk of urban slope instability has been also indicated by combining ground investigation methods with geostatistics to model similar potential risk zones in Lisbon (Guillard and Zezere, 2012). In addition, a GIS-based tool using a rock quality index known as Rock Engineering System (RES) integrated with a multi-criteria assessment analysis using landslide-inducing risk factors successfully produced landslide susceptibility maps (Rozos et al., 2011). This showed the successful integration of multi-criteria analysis methods with 2D mapping tools. A rockfall analysis using ground investigation data demonstrated the associated vulnerable areas to provide efficient urban planning by Guzzetti et al. (2002) and Lacroix and Helmstetter (2011). Yalcin and Bulut (2007) also integrated successfully photogrammetric images with other factors to obtain earthquake-induced rockfall risk assessment using 2D maps. However, this application was again focused only on a particular assessment and not providing a common framework for geohazard information.

Besides, past research demonstrated a successful combination of geotechnical risk (such as landslide risk) factors with 2D mapping, providing accurate outcomes.

Flood risk has also been presented extensively using 2D maps. Skilodimou et al. (2003) and Chen et al. (2015) produced flood risk maps including events with related geological indications and groundwater table level fluctuations in the long term. They pointed out that manmade changes had been an important factor to increase this problem (Skilodimou et al., 2003). Lo et al. (2015) followed on using real-time evaluations for visual sensing of groundwater table fluctuation, which is an efficient tool for predicting flood risk. Ferrario et al. (2015) made a tool assessing geotechnical features in association with flooding in Como area in Italy, using a detailed geological and geotechnical data (boreholes), to provide a risk management to be used in urban planning. GIS and 2D risk-based mapping has been done using hydrogeological factors by Papaioannou et al. (2015). They classified flood-inducing factors using historical data as well, to provide areas of flood vulnerability to support infrastructure and authorities (Papaioannou et al., 2015). The susceptibility to flooding for an area in Greece was also assessed by Kazakis et al. (2015), who used (flood) impact parameters to develop a system for estimating the vulnerability and produced maps. However, this was limited to 2D.

The urban groundwater risk modelling has also been studied over the years to support urban planning aspects. Dai et al. (2001) also conducted a suitability map using GIS and multi-criteria analyses of geological groundwater and land-use factors with respect to the type of a potential building development. Urban planning data in relation to manmade changes was successfully used to evaluate hydrogeological risk and became available by combining GIS with post-processing analyses data (Morelli et al., 2012; Wang et al., 2017). However, the data communication aspects were limited.

Contaminated land and groundwater have been additional aspects which affect urban risk. By way of example, Fordyce et al. (2005) provided 2D maps of risk assessment data concerning water quality and contamination information for the UK, to support urban sustainability and environmental aspects in industrial and research applications.

Geohazard risk outcomes based on maps have been successfully used in producing suitability assessments by assessing the geohazard risks. These 2D maps indicated critical zones based on geohazard risk analysis, which can be used in urban planning and decision-making. However, data integration is shown to be challenging due to the nature of urban geohazards (and the variability of the ground), which requires more parameters to be included. By way of example, this would be more evident in ground-building interaction problems (and relevant risk assessment analyses information), where 3D ground models could be more efficient. In addition, 2D visualisations mainly incorporate assessments using risk-based zones, whereas a 3D ground model would be more indicative (i.e. preferable) (Rosenbaum, 2003; Culshaw, 2005; Wycisk et al., 2009). Therefore, to obtain better knowledge and understanding with more efficient findings, the 3D (conceptual) ground models had been increasingly used.

2.2.8 3D ground models

Conceptual ground models have been a widespread method to accompany analyses to produce geotechnical/geological risk assessments in 3D (Culshaw, 2005). Thus, ground modelling plays an important role in a geological study (Turner, 2005). Representative examples of relevant urban geohazard risk assessments that employed 3D ground models have been developed by Gakis et al. (2016), González-Garcia and Jessell (2016), Burke et al. (2017) and Thornton et al. (2018). A 3D ground model provides the whole information on the geological/geotechnical characteristics of an area, which is more detailed than the 2D maps (Kessler et al., 2008; Griffiths, 2016). Thus, it supports relevant assessments by totally demonstrating the desired

features and modelling dynamic changes with respect to available data and the natural processes (Rosenbaum, 2003; Culshaw, 2005; Wycisk et al., 2009). Hence, it contributes to the better identification and understanding of geoenvironmental information (Parry et al., 2014). This is because a 3D geological (ground) model could provide an effective way for the geometrical, lithological, spatial input of data for a specific geological layer (Dong et al., 2014). As Parry et al. (2014) stated, Commission 25 noted the importance of 3D ground models, being key in geological applications. Geological and geotechnical engineering applications have been using conceptual ground modelling, which supports ground investigations efficiently (Griffiths, 2016). Turner (2005) also noted that 3D modelling advanced geotechnology to align with ground investigations. In fact, it has been established as a key in Engineering Geology research and formed the basic design tool (Culshaw, 2005; Turner, 2005). This is due to its use as a tool for the better hazard management in constructions (Griffiths et al., 2012). Therefore, it has been widespread in geological/geohazard assessments in relation to urban planning (Culshaw, 2005; Entwisle et al., 2008).

The advance in utilisation, the potential for communicating the data and the development of risk assessment techniques for decision-making (using scenarios and advancing geological expertise) using 3D modelling were indicated by Gibson and Chowdhury (2009). Turner (2005) and Gakis et al. (2016) added that a more robust understanding of the underground could be obtained by integrating 3D modelling with analytical applications. Advances in 3D geological models to support construction projects, along with their limitations in relation to uncertainty, scaling and ground variability have been noted by Hack et al. (2005). A review of (representative) past research that used 3D ground models to accompany their assessments, which are associated with sustainable planning of cities follows.

Howard et al. (2009) provided an information exchange between organisations responsible for the geo-analyses that had been an issue, and the introduction of 3D modelling provided an environment to deal with it regarding geoscientific purposes in the UK. Geological survey organisations have already developed an international database framework to provide knowledge in the geological/geohazard context based on using 3D models (Howard et al., 2009). 3D geological modelling and simulations have been established in geotechnical research in Norway and globally, providing thorough resultants in many fields (Jarna et al., 2015). An example is the 3D geological model of Phnom Penh, Cambodia has been conducted by Touch et al. (2014). This included geotechnical and other engineering properties data, which have been analysed to provide results to support the understanding of the subsurface of an urban setting (Touch et al., 2014).

A 3D model was developed using geostatistical analyses and interpolation to define the geological strata boundaries, with a property assigned for all the stratum either by discretisation or variability analyses (Dong et al., 2014). This has provided successful visualisations to carry out geological investigations (Dong et al., 2014).

Royse et al. (2008) produced another example of a 3D geological model, which was used in combination with geological records and GIS, as shown in Figure 2.2. This was employed to provide visual information for the construction of London Thames Gateway in a geologically complex area (Royse et al., 2008). These evaluations of the geotechnical parameters of the site were done successfully by the 3D model developed by the British Geological Survey (BGS) (Royse et al., 2008). However, it focused more on displaying the hydrogeological/groundwater information of the study area in 3D (using 2D datasets), and hence not on providing a risk assessment framework for involving complex interactions or other integrated risk assessments. Likewise, the geoenvironmental assessment used in the 3D ground model of the developments

in Sheepcote Valley, Brighton, is another 3D modelling tool developed in the UK (Tame et al., 2013). A similar study has been conducted for the Farringdon underground railway station by Gakis et al. (2016).

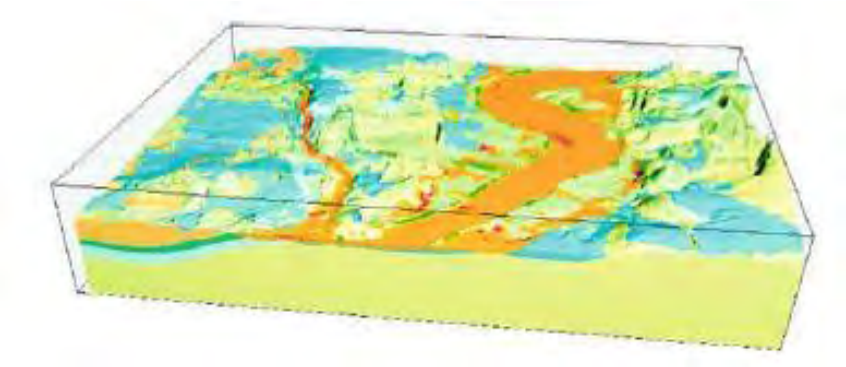

Figure 2.2: An example of a 3D geological model (near Thurrock) (after Royse et al., 2008).

Jørgensen et al. (2015) combined different techniques to provide a fully informed 3D geological model of Denmark to handle scarce borehole data. More specifically, remote (visual) sensing was integrated with probabilistic modelling to provide successful results, which demonstrated the importance of combining several methods to obtain geological data (Jørgensen et al., 2015). However, the use of this approach is limited due to the lack of data by utilising the particular technique. In addition, Wu et al. (2005) provided a method for 3D geological modelling when the borehole data is scarce using integrated data from several sources. This resulted in advancing geological thinking through a new geo-related information management and had successfully implemented in a complex area in China by Wu et al. (2005). The lack of borehole data alongside the alluvial changes made to the creation of 3D models challenging, as shown

by de Rienzo et al. (2008). Methods for borehole data integrations in relation to a model and consequent simulations were also developed (de Rienzo et al., 2008).

The 3D geological model of sedimentary strata using an automated approach that tackled data limitations via interpolation and 'discretisation' of borehole information in specific spots in the model has been developed by Zhu et al. (2011). The application of this information in several projects improved automation, and enhanced the 3D geological models (Zhu et al., 2011).

Another technique of 3D modelling was provided by Zhu et al. (2013), who noted that engineering-geological value may comprise of two types of data, that is the geological structure and the attribute of a parameter. They combined them to develop a 3D model of properly assigned spatial and geological data using interpolation (Zhu et al., 2013). A technique of error correction was then applied which provided information to the resulting 3D model combined with geological information (Zhu et al., 2013). However, communicating this information and assigning assessment data would enhance this 3D model.

Vanneschi et al. (2014) provided a 3D geological model of a quarry in the Italian Alps, using laser scanning photos data and combining the results for supporting excavation projects. Vatcher et al. (2016) built a 3D model of a mine focusing on geomechanical and relevant aspects, using rock quality indices in combination with geostatistics and geological information. It was applied successfully in Kiirunavaara, Sweden, providing the geological interactions within the 3D model, which could be useful for mining technology (Vatcher et al., 2016).

Kessler et al. (2008) focused on two different methods to provide the 3D geological modelling, to assign a bulk volume to a layer (Thames Gateway project in London), or to use spatial analysis such as interpolation when extra detail is needed (a construction project in Boston). Lázaro et al. (2014) presented 3D geological structures by developing an application that

described their information using 2D surfaces that could be located or Digital Terrain Models (DTMs). This could be done by a Graphics Processing Unit (GPU) increasing the efficiency (Lázaro et al, 2014). The tool by Maesano and D'Ambrogi (2017) is also a very good example of using a detailed 3D model to reach important conclusions.

Available database to create a 3D model of the subsurface to investigate the geotechnics of an urban soil and potential geohazards have been provided using geostatistical methods, a 3D geological model and 2D maps by Marache et al. (2009). Another urban geological tool was developed by Devleeschouwer and Pouriel (2006) to provide a thorough understanding of the subsurface of Brussels based on 2D/3D GIS models for decision-making. Olde Scholtenhuis et al. (2015) focussed on assigning geo-property data within 3D models and presented the potential of those integrations to enhance urban land-use planning and decision-making. Djamaluddin et al. (2012) produced a 3D model capable to comply with time indications alongside mining explorations, to conduct a subsidence risk for an urban area through combining GIS with geostatistical methods.

Huang et al. (2012) provided important and successful findings for planning using 3D underground models for an urban development in China. Similarly, a 3D ground modelling approach for a subsurface model of Turin in Italy provided the land suitability regarding alluvial soils (de Rienzo et al., 2008). Likewise, the Selby area's superficial deposits have been extensively studied by Burke et al. (2017).

Velasco et al. (2013) developed an advanced urban hydrogeological/groundwater modelling, using 3D geological models via GIS. Statistical modelling alongside spatial distribution analyses were combined to create the surfaces needed for the model (Velasco et al., 2013). The results indicated the importance of the layer integration, as shown in the 3D model used

(Velasco et al., 2013). This research was based on sediment analyses, where the data sharing and communication problems still existed. The geothermal potential using 3D geological modelling using a FEM mesh, borehole data along with temperature flow measurements has been adapted by Calcagno et al. (2014), advancing geothermal exploration.

Another aspect of ground modelling is the knowledge of groundwater flow that can be demonstrated in 3D (Wycisk et al., 2009). 3D modelling enhanced Environmental Impact Assessments (EIA), as specific geological and contaminant data could be easily drawn, as explained by Wycisk et al. (2009). In addition, unpredictable features that can affect groundwater, which can improve ground investigation and risk management practice, were provided by Aldiss et al. (2012). More specifically, the application for an underground station in London has been adapted to support ground investigations (Aldiss et al., 2012).

The gypsum dissolution susceptibility in Paris has been extensively assessed using a 3D modelling approach by Thierry et al. (2009). This was carried out by adding geological strata based on borehole data, which is taken from piezometer records (Thierry et al., 2009). These proved a groundwater risk to exist and 2D maps demonstrated the outcomes by risk-based areas taken from the 3D modelling analysis to support decision-making (Thierry et al., 2009).

Chakeri et al. (2013) studied tunnel induced settlement parameters for tunnels, using numerical methods in 3D in their analysis. The results showed the importance of this hazard and confirmed the implementation of 3D numerical methods (Chakeri et al., 2013).

In addition, research examples were based on adding more dimensions to 3D models by employing similar processes. This advanced 3D modelling using extra indications or tools, regarding aspects that are important in construction projects. More specifically, Kim et al. (2013) have indicated the advantages of a 4D CAD model of a bridge construction, which could

be updated and could be used in scheduling phase to inform about construction aspects, and hence improve decision-making. They provided a method of image-processing using the same multidimensional modelling method to build a 3D CAD model and then adding the 4th dimension, as shown in Figure 2.3 (Kim et al., 2013). Likewise, an expansion of 3D to 4D (CAD) modelling was studied by olde Scholtenhuis et al. (2016) to show its capabilities and efficacy on design processes and utilities' management. This was generated as a multidimensional subsurface model that could advance construction information management and scheduling (olde Scholtenhuis et al., 2016).

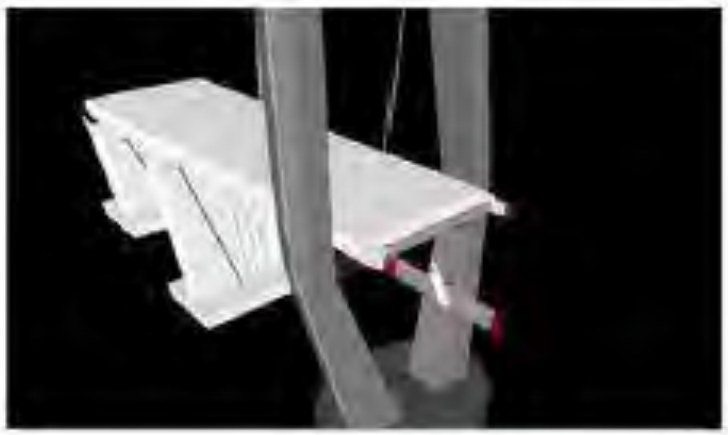

Figure 2.3: An example of a 4D (CAD) model of a bridge construction (Kim et al., 2013).

Previous research demonstrated that a wide use of 3D ground models has taken place to provide geohazard risk assessment outcomes. They have also been widely used in ground investigation. However, 3D models showed a lack in demonstrating all the (risk assessment) information required to be effectively used in urban planning. This was due to the variability of the ground (data) and the complexity of information associated with ground-building interaction problems

(which are commonly related to urban geohazard risk predictions). As a result, a geohazard risk assessment that could be used in decision-making would be challenging. Hence, an integrated system (based on 3D modelling) using different types of data and being capable of processing this data, could provide a useful framework for ground investigation by providing all the relevant information needed, which aligns with sustainable urban planning.

Until recently, geohazard risk assessments which have used analyses and 2D and 3D models lack in geological uncertainty due to the complexity of the ground. Problems consisting of ground-building interaction needing the use of integrated data and sustainable systems also remained challenging in terms of the information required. Therefore, subsurface information in relation to the previous limitations (of past applications), which have caught the attention of scientists and engineers follows.

2.2.9 Subsurface information modelling

Beyond 3D ground models, the previous research demonstrated the data sharing and management limitations, and the subsequent need for relevant geotechnical information applications. Such an application was provided, for example, via a 3D modelling tool to inform infrastructure projects by Tegtmeier et al. (2014). This showed the importance and the wider application of aspects of geological/geotechnical information.

Mielby et al. (2017) noted that there is a need for geological and geotechnical data utilisation, which could be managed by any user, while being widely available and avoiding computer-power limitations (Mielby et al., 2017). The Association of Geotechnical & Geoenvironmental Specialists (AGS) has provided geotechnical data formats in the UK (AGS, 2019). Thus, geotechnical data management and sharing has been important among researchers and engineers in the field, to improve tools, analyses and functions in planning and decision-making

applications, as indicated by Luo (2014). Construction and development projects need to be associated with these types of modelling tools, as Harding (2004) explained. However, they are sometimes neglected, and this has resulted in information transfer and communication issues within the project teams (Harding, 2004). This is due to the lack of understanding of the significance of geohazards in those projects which could then affect costs (Parry et al., 2014).

Turner (2000) and Parry et al. (2014) noted that developing a system, which is capable of providing geological information through multidimensional modelling processes, would be important for construction/infrastructure understanding. The related data mining, management and communication has always been of importance, which is associated with these processes (Parry et al., 2014). Hence, as Miettinen and Paavola (2014) stated, these could evolve recent (ground) modelling methods.

It is evident that there is a lack of data integration among tools used for geotechnical problems. Thus, the data processes required in a corresponding geohazard/geotechnical assessment, i.e. processing and managing/storing of, for example, the geohazard risk assessment analysis data, is limited. This is critical for supporting ground investigation and sustainable urban planning applications, where data integration is needed (Bridge et al., 2005). The previous examples demonstrate the need for an information system, which could be used in geohazard assessments that would be capable of handling all these data aspects effectively to provide an 'automated modelling' tool that can improve knowledge and understanding for geohazards (and ground-building interactions), and advance ground investigation and sustainable decision-making. This could be based on an advanced modelling concept that can support these data processes.

2.2.10 Building Information Modelling (BIM)

Building Information Modelling (BIM) is a concept that is capable of storing, sharing and visualising in 3D all the structural features, such as the geometrical, spatial and

properties/semantics information, used through all the phases of a (building) construction project (Eastman et al., 2011). The use of BIM throughout the lifecycle of a construction is shown in Figure 2.4. There have been many definitions of BIM and everyone has its own importance. It is defined by the Royal Institute of British Architects (RIBA), the Construction Project Information Committee (CPIC) and buildingSmart as 'digitally representing the information for all the characteristics relating to all stages of a construction'. As Miettinen and Paavola (2014) stated, it is the "digital representation of a building, an object-oriented 3D model, or a repository of project information to facilitate interoperability and exchange of information with related software application".

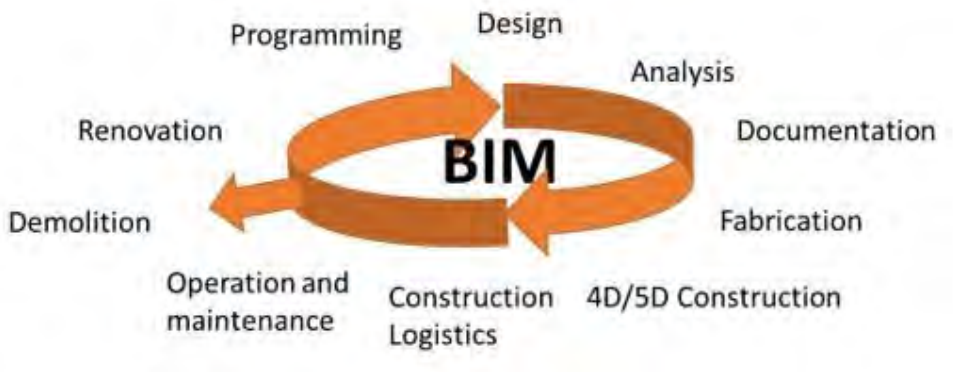

Figure 2.4: The use of BIM for the lifecycle of a building construction (Chapman et al., 2019).

According to Eastman et al. (2011), it is utilised for generating information for all building assets that could be used by any user, transforming conventional ways of delivering a construction project. Liu et al. (2015) implied that the communication of data (interoperability) in relation to the use in whole lifecycle of a project is key in its broader implementation in construction and civil engineering industry, which aligns with sustainable technologies. This is

confirmed by the tools developed within BIM, handling building models with relevant information and demonstrations (Miettinen and Paavola, 2014). In addition, BIM is regularly updated by adopting up-to-date design standards to provide an efficient tool for structural information management (Silva et al., 2016). In fact, BIM's advantages are mainly related to the interoperability of all the semantic information that BIM stores and uses for a construction project. This is provided by the Industry Foundation Classes (IFC) (buildingSMART, 2017). This has been a widespread format in BIM used in construction projects across the world, which advanced interoperability, such as Abanda et al. (2015), Zou et al. (2017), Liu et al. (2017) and Zhang et al. (2018). In this way, data management through BIM has achieved high levels of efficacy and productivity within construction management (Miettinen and Paavola, 2014). These are main reasons why it has been considered to advance sustainability, and therefore being widely used in application development.

More specifically, Alwan et al. (2016) stated that BIM has a potential of being used in producing applications which advance sustainability. This could be done through data integration and sustainable, design, using digital methods, which could improve decision-making (Alwan et al., 2016). As already mentioned, BIM owes much of its wider use to its integrated data(-related) advantages. The advent of technology and the need for sustainable buildings made construction management aspects to advance from 2D sketches to 2D/3D CAD (Georgiadou, 2016). BIM provided the next level of CAD by introducing an environment capable of storing and communicating information for all stages of a construction, including cost and asset management (Georgiadou, 2016). Hence, BIM combines successfully structural data related to visualisations, asset information and geometry, and building functions (NBS, 2014; Georgiadou, 2016). Therefore, BIM could accommodate not only the (semantic) information of a project, but also the functions that accompany a building (Succar, 2009; NBS, 2014). In

addition, it combines different sectors together, such as those handling the computer/modelling, and the engineers and institutes involved (Georgiadou, 2016). In addition, Liu et al. (2015) proposed a method for improving sustainable buildings using a BIM optimisation method for costs and carbon emissions for building in Hong Kong. They demonstrated that BIM could support such efficient sustainable applications (Liu et al., 2015). Likewise, Ladenhauf et al. (2016) have developed a method to improve sustainability through energy efficiency of a building. In their study this is done by integrating thermal properties with the geometrical information using BIM (Ladenhauf et al., 2016).

Kim et al. (2015) employed BIM in providing an automated evaluation and visualisation of the outcomes of a sustainable planning strategy for large-scale construction developments. This has been developed by considering, evaluating and visualising different design scenarios of these constructions to support sustainable decision-making (Kim et al., 2015). A similar example was provided by Lee et al. (2015) who produced an efficient warning-based system using a rule-checking in BIM. Such systems have been useful and could be adopted to improve decision-making (Lee et al., 2015).

In terms of its implementation in the UK, the research from Eadie et al. (2013) demonstrated that process-related aspects were considered important, whereas collaboration was shown as its most favourable characteristic. Bryde et al. (2013) also found that cost and time savings, along with general management aspects were also considered important. In addition, Miettinen and Paavola (2014) demonstrated that BIM could be widely used as an urban development tool. Its data management and visualisation capabilities which combines several engineering disciplines together has a potential for urban construction developments (Miettinen and Paavola, 2014). These are key reasons behind its wider utilisation in engineering, supporting sustainable decision-making applications. Chi et al. (2015) studied the impact and future of BIM-based

structural design and demonstrated the significance of the all the advantages of this technology (collaboration, information, visualisations, evaluations and relevant potential for further research).

Until recently, BIM has been significant in the design processes for (risk) management information throughout a construction (Zou et al., 2017). However, it is found that it can also serve efficiently as a centralised data platform to support other modelling tools and integrations and provide other/further risk assessments or analyses (Zou et al., 2017). Kang and Hong (2015) also studied the efficient BIM-GIS integration, and hence presented an advanced system for data management of a facility, which confirmed the advances of data integrations associated with BIM. GIS was combined successfully, although its limitations using 2D maps remained a challenge. In addition, Rafiee et al. (2014) employed BIM in combination with GIS to generate an environmental analysis application for the sunlight exposure of a building. The example of the BIM-building investigated is shown in Figure 2.5 (Rafiee et al., 2014). The semantic and geometry information was provided using BIM by a georeferenced model. It demonstrated important aspects regarding geo-environmental problems for decision making (Rafiee et al., 2014). However, a broader assessment (using for example an advanced analysis) combining additional criteria could provide further understanding. Deng et al. (2016) provided a framework for the providing the traffic noise using a noise mapping and evaluation by integrating BIM with GIS 2D maps, to obtain outcomes for the built environment. Noise estimations have been conducted in several level of detail, using parameters adapted from BIM to provide the resulting model and support urban planning (Deng et al., 2016).

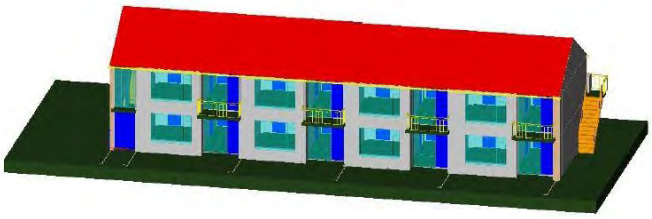

Figure 2.5: An example of an IFC model using BIM of a building (after Rafiee et al., 2014).

The flood risk to buildings was studied by Amirebrahimi et al. (2016). They integrated BIM with GIS to provide the potential risk, using a 3D model with spatial indications (Amirebrahimi et al., 2016). This advance was generated by combining BIM with the widely used Unified Markup Language (UML) (in geo-related studies), to provide a 3D building damage assessment due to flooding (Amirebrahimi et al., 2016). This showed the data integration aspects of BIM, enhancing flood assessments (Amirebrahimi et al., 2016). Another data application was produced by combining the Geographic Markup Language (GML) and BIM for geological modelling associated with large infrastructure developments (Tegtmeier et al., 2014).

Eleftheriadis et al. (2015) developed an early-stage design concept based on BIM that incorporates the lifecycle information of a building. In particular, it involved an Application Programming Interface (API) and program development tools of BIM software to provide a method to present solutions on materials and structural assets design. This example improved BIM's sustainable application in a construction project (Eleftheriadis et al., 2015). It also showed the advantages of combining it with API tools.

The application in deconstruction management using BIM was explored by Akbarnezhad et al. (2014), who developed a framework that can handle all information required for this task. Physical/material properties were needed to be combined with the functional and the processes

of deconstruction to carry out this task, while potential developments using this technique could be adapted (Akbarnezhad et al., 2014).

The previous literature provided examples of applications where BIM could be effectively used and increase the productivity and efficacy of projects. Hence, it is evident that other fields relating to construction and infrastructure could also benefit from using BIM's advantages (and provide their own objectives). This could be carried out by enhancing BIM through sustainable applications where new concepts could be based upon, exploring sustainable tools and methods in other sectors, such as geotechnics.

2.2.11 BIM in geotechnics

Migilinskas et al. (2013) proved that the communication between users, the various applications methods and the conventional methods of the geotechnical industry have been causing issues in construction developments. In particular, sharing could have been improved if visualisation could enable a better understanding of ground condition information for ground investigations (Migilinskas et al., 2013).

Until recently, BIM was mainly adopted for structural design and related applications. However, relevant research suggested that it was promising in handling geotechnical information (projects) (Morin et al., 2014; Wu et al., 2015; Kessler et al., 2015; Tawelian and Mickovski, 2016; Zhang et al., 2017; Wang et al., 2019). More specifically, Tawelian and Mickovski (2016) showed that BIM applications in this sector would be advantageous, aligning with industry demands. In addition, Borrmann et al. (2014) and Kim et al. (2015) considered the data integration and advances that could take place within a BIM environment applied in underground aspects. Svensson (2016) focused on subsurface modelling applications, where ground data would benefit by BIM's data communication advances, although uncertainties

should be accounted for while providing a study (Svensson, 2016). Its potential to enhance ground investigation aspects was also noted (Svensson, 2016). However, this concept among many others, focused more on demonstrating the visualisations and data processes using BIM, and not on a complete application, for example, by assessing (geotechnical) parameters involved. its study was focused more on demonstrating. In addition, Kessler et al. (2015) emphasised on the increasing direct use of BIM, which was approved by geotechnical engineers. This is rather due to the data communication and visualisation advantages that can advance ground modelling. Then, Zhang et al. (2017) investigated a data management strategy using BIM for geotechnical information. This used BIM as a centralised database by collecting and managing the geotechnical data throughout a construction project (Zhang et al., 2017). This could be a key aspect in using BIM in geotechnical engineering applications.

In addition, Chandler et al. (2011) considered examples of ongoing highway projects to point out that BIM's advantages in data processes and tools could contribute to the geotechnical industry/sector via efficient design applications (Chandler et al., 2011). Chandler et al. (2012) provided a review of the BIM potential in infrastructure projects and showed how geotechnical data implementation in BIM could support and improve the relevant decisions-making. Likewise, Morin et al. (2014) demonstrated the same potential, using recent case studies, which showed that the use of BIM in design could avoid future costs from issues from, for example, geotechnical hazards. This could be carried out in designs that could support ground investigation by a type of 'interactive' modelling (Morin et al., 2014). Specific points on the effort utilising BIM within geotechnical industry were drawn with respect to the curve of MacLeamy (2010), as shown in Figure 2.6 (Morin et al., 2014).

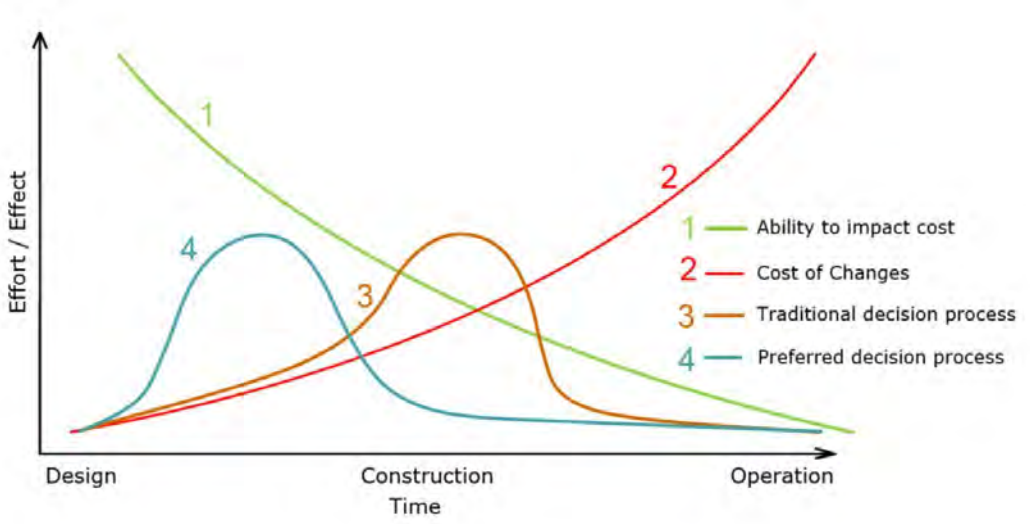

Figure 2.6: The MacLeamy effort curve (MacLeamy, 2010; Morin et al., 2014).

The demands of the construction industry for geotechnical (parameter) data selection and the potential for a strategy to be integrated within BIM were noted by Tawelian and Mickovski (2016). More specifically, after reviewing BIM applications in construction projects, they presented the importance of this process to geotechnical engineers, and the need for their support due to its cost and time-saving advances (Tawelian and Mickovski, 2016).

The potential of geotechnical data models was also demonstrated by Breunig and Zlatanova (2011) and Wang et al. (2019), who demonstrated that integrating BIM with GIS could provide efficient assessment systems, owing much to the visualisation power of BIM. However, the issues associated with 2D maps still existed, without a proper study of development of the ground condition changes (using for example an analysis). Similarly, geotechnical data was integrated with GIS in a city scale by Luo (2014), to provide a ground investigation database. Wang et al. (2019) provided a system to manage the underground utility network maintenance.

There have been many examples using BIM to provide various geotechnical applications. By way of example, Kim et al. (2015) showed the underground visualisation capabilities of BIM using another application. They developed a cadastral (surveying) system in South Korea using BIM successfully, where cost and time dimensions were also involved, and provided efficient outcomes for underground indications (Kim et al., 2015). Xie and Xie (2015) studied the maintenance management of a metro station using BIM, showing its effective application with managing all the information required for this task electronically and not conventionally. The application for underground infrastructure developments in Taiwan was successful, and future enhancements in pipelines and pipeline management could be promising and effective (Chang and Lin, 2016). Chang and Lin (2016) showed engineers, consultants and authorities that the use of BIM in geotechnics is efficient. However, this example focused again only on the (geotechnical) information management capabilities of BIM.

Likewise, Liu and Issa (2012) provided a framework based on 3D visualisations (information), which combined GIS maps of underground (mechanical, electrical and plumbing) pipeline systems with BIM for operation and maintenance information. Although, BIM was only used for storing information, as an asset management. In addition, more tools would be needed to be integrated with BIM to study underground data completely.

Zhang et al. (2018) provided a workflow on managing geotechnical data using BIM, for the whole life of a hydropower station construction, showing the potential of applying a complete geotechnical data repository (Zhang et al, 2018). However, again the focus was on geotechnical data management aspects. Zhang et al. (2016) proposed a workflow for using BIM in ground investigation to improve the indications and data management and confirm the findings of complex geotechnical data. The outcomes showed that there is a potential using the proposed framework, which could be adapted for ground investigations easily (Zhang et al, 2016).

Another geotechnical application in BIM was presented by Svensson (2016), who incorporated relevant data to accompany large infrastructure projects in Sweden. 3D geotechnical modelling tools within BIM were developed, and provided relevant information needed for data and visualisations to communicate design information across users (Svensson, 2016). However, a complete risk assessment was not clearly presented to obtain outcomes for utilisation in decision-making.

BIM has also been used in tunnelling applications. Among many, the construction of a subway station by Li et al. (2013) is another example of a geotechnical-BIM application, as shown in the pipelines BIM model used in Figure 2.7. They proved that construction time was reduced by nearly 15% by using it throughout the design stage (Li et al., 2013). It is important to be noted that an integrated analysis could confirm the detection results in this study using BIM.

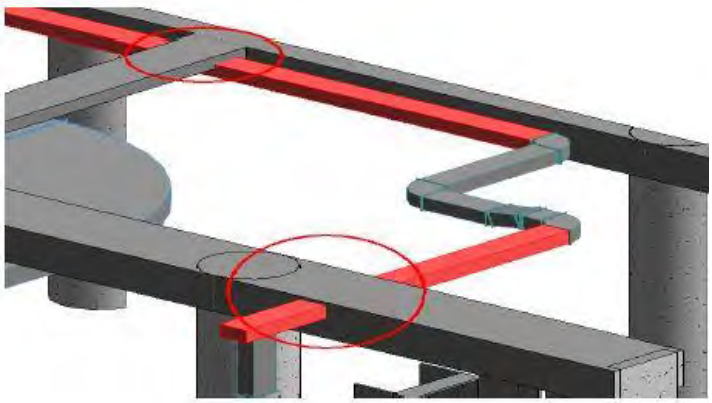

Figure 2.7: An example of the geotechnical application of the pipelines (collision detection) model using BIM (after Li et al., 2013).

Likewise, Lu et al. (2012) provided the environmental impact of an urban deep excavation project alongside the construction of an ongoing retaining wall, the groundwater pumping and the excavations. The corresponding geotechnical information for the safety of the excavation and adjacent buildings was modelled with respect to a case study of a metro station construction in Taiwan using BIM (Lu et al., 2012). This enabled risk-based visualisations using BIM of the geotechnical (input) data, which provided effective design and construction management (Lu et al., 2012). However, the information using BIM was only focused on geotechnical aspects for the analytical part (and not including structural information) with limited outcomes, which would need a further integration. Borrmann et al. (2014) used the BIM combined with GIS to provide a 'multiscale' tunnel-line geometry representation, using different Level of Details (LoDs). This was achieved by enhancing UML to form a framework for further data integrations (Borrmann et al., 2014). They suggested that it would be promising for further utilisations within geotechnics (Borrmann et al., 2014).

Wang et al. (2015) used BIM for the safety checking, which was included as an application for the risk assessment while investigating the geology of a site (Wang et al., 2015). The 3D visualisations supported the potential safety, geometrical and geotechnical indications, and suggested the selection of a proper equipment for the excavations (Wang et al., 2015). It is important to be noted that this was based on safety checking (using rules within BIM) and not a relevant risk assessment.

Finally, previous research demonstrated the successful use of BIM in various geotechnical applications to date. BIM was used as an advanced tool, which used geotechnical data and provided visualisations by improving geotechnical projects. However, it was found that BIM was mainly used for storing information, as an asset management tool. Hence, its use to robustly support a geohazard/geotechnical risk assessment, using all relevant information needed, is

lacking. Thus, such a BIM-based 'system' does not exist. It could be based on integrating BIM with a relevant risk assessment analysis, producing the resulting visualisations and link all aspects. Finally, this system could provide useful information required to compete an assessment and support ground investigation and sustainable decision-making.

2.3 Summary of Key Findings

As cities expand, sustainable urban planning tools are becoming essential. Hence, alongside the increasing use of the urban underground space, which aligns with sustainable development, the need to avoid ground-related or geohazard risk, should be clearly considered. This could be handled by the efficient understanding of the urban subsurface, to assure safe and sustainable decision-making. In this case, the information taken from geohazard risk assessments has been widely used, as they indicated methods to solve such problems in specified areas caused by specific geohazards. In terms of geohazards, these have been examined in detail using corresponding risk assessment analyses combined with the use of 2D maps and the widely used 3D ground modelling. However, due to the very nature of the ground associated with its complexity and uncertainty, and the ground-building interactions, which need integrated systems, limitations in current systems always remain a challenge.

Hence, an integrated information system that could provide an urban geohazard risk assessment 'tool' for sustainable decision-making, is to date missing. An important aspect that risk assessments to date do not meet is to align with sustainability, due to the lack of the direct or rapid use and multi-applicability caused by the very nature of the ground (and geohazards). Hence, a risk assessment tool that could be directly used in any type of geohazard would support

ground investigation and enhance geohazard knowledge and understanding. The gap for an integrated system of advanced analyses and 3D ground modelling applications was evident.

In terms of the risk assessment analysis information, the limitations were initially linked with the integration of criteria (such as ground parameters), which were insufficient to build a complete geohazard risk assessment (analysis), as required in a robust system. Although multicriteria analyses have been conducted, a (geohazard risk assessment) analysis 'platform', which would be capable of incorporating the relevant criteria into a system to successfully combine ground-building interactions with 'real-life' applications (such as vulnerability, building damage and costs) for decision-making, still using conventional borehole data, was identified as lacking, and hence needs to be developed. Likewise, data processes and integration of this information, including the communication, analysis and modelling, and visualisation aspects were particularly limited, negatively affecting decision-making.

3D ground models have already become an essential part of geological/geotechnical risk assessments. However, their use so far has been limited to demonstrations of 3D ground models, which have been insufficient to produce a robust geohazard risk assessment in an urban area. This could be explained by the fact that the lack of efficient 3D visualisations could lead to the lack of understanding of the underground, and therefore the geohazard effects on adjacent buildings. Hence, a 'real-time' tool presenting geohazard risk assessment information within the 3D models, which would produce efficient results of ground-building interactions for decision-making, was missing. A system combining 3D ground modelling, which could store (extract) and visualise multidimensionally the information (data) of an integrated geotechnical/geohazard risk assessment analysis, did not exist. Likewise, a lack of managing and sharing the data of such risk assessments, was also found to exist, which caused problems in decision-making. In terms of data criteria, BIM has been found promising to combine them

successfully, although it has not been applied in an integration within a geotechnical risk assessment (framework). However, a system integrating the previous aspects, which could be applied to a broad range of applications, would be important for sustainable decision-making.

3 METHODOLOGY

3.1 Introduction

While cities expand, people need to focus on providing sustainable urban land-use planning methods and digital applications to ensure safety of urban areas (Price et al., 2016). An increasingly used way, which aligns with sustainable planning, is the use of urban underground space (Hunt et al., 2016). This use is closely associated with the interactions between the ground and the built environment. Hence, understanding better ground characteristics that lead to geohazards is important in sustainable urban planning. This makes ground information to be crucial. There has also been a growing need for knowledge and understanding of the urban subsurface, which aligns with sustainable land-use planning. In addition, efficient decision-making in an urban area requires (constant) ground condition monitoring to provide information on geohazards (Thierry et al., 2009; Kim et al., 2015). The cost and limitations of such equipment is an addition to the variability of the ground, and make this challenging. A large body of literature proposed sustainable tools that can be adopted for geohazard risk assessment, such as by Chakeri et al. (2013), Giardina et al. (2018) and Amorosi et al. (2019). However, one that would enable a robust information system of the (geohazard) risk and its (geohazard risk) effects with time, still does not exist. The impact on adjacent buildings would also be important in producing such a system (Griffiths et al., 2012). Such a system could then assess urban geohazard risk, and effectively support a wide range of applications, such as saving cost and time in ground investigation. This could be handled by an automated framework that could directly model changing ground condition that could produce any urban geohazard, considering the ground-building interactions. However, to achieve such a system, advanced risk assessment methods and digital tools are required.

An advanced risk assessment framework based on the previous aspects could provide a robust understanding and knowledge of urban geohazard risk. In addition, due to the nature of the ground in relation to ground variability/inhomogeneity, this framework would need to be adjusted to handle a range of geohazards and locations (de Rienzo et al., 2008). The development of this tool would be enabled by an advanced geohazard risk assessment analysis, using relevant borehole data (to align with conventional data). In addition, the nature of this assessment would need low computational power to align with sustainable outcomes. The rapid advance in speed and memory processes of low-budget computers led to various advanced computational tools to be adopted, to handle related geo-engineering problems (Price et al., 2016). However, the complex nature of ground conditions and their interactions with the built environment would need a system, in which ground variability could be considered throughout (de Rienzo et al., 2008).

Examples of analyses undertaken to support risk assessments for subsurface and geohazard applications were achieved by adopting (different) criteria or factors to provide decision-making analyses, such as the analyses by Kazakis et al. (2015), Papaioannou et al. (2015) and Kim et al. (2019). Advanced analytical techniques, which could work with different types of information by correlating the severity of the criteria, were suggested. For example, Papaioannou et al. (2015) provided a way of investigating flood-prone areas using multicriteria decision-making analysis techniques, which involved a number of hydrogeological factors. More specifically, this combined advanced analysis and geographic data mapping, and showed the potential of these techniques for geohazard applications (Papaioannou et al., 2015). Advanced numerical simulation techniques, such as the FEM, have also been widely used in ground-related analyses (Potts et al., 2001; Avgerinos et al., 2017; Amorosi et al., 2019 and Ding et al., 2019). Among a large body of relevant applications, for example, Amorosi et al.

(2019) and Ding et al. (2019) focused on providing efficient numerical analysis methods to solve problems associated with tunnels. FEM has been used to assess issues on structures via 3D soil-structure interactions analyses (Amorosi et al., 2019; Ding et al., 2019). A combination with advanced geostatistical or other tools to provide integrated analyses for real-life applications of complex tasks could also have potential. However, due to the very nature of the ground, a subsequent analysis using relevant ground parameters to solve geotechnical/geological problems, would need a reasonable computational power by handling complex equations, which needs to be considered.

In addition, the results of the geohazard risk assessment analysis need to be presented clearly (Price et al., 2016). This task has been successfully performed by 2D maps in the past, although more detail would be needed to create such a system (Griffiths, 2016). Among many relevant examples of geohazard risk assessment applications which used GIS, Bathrellos et al. (2017) provided 2D maps which included different geohazards. These 2D maps successfully provided the land suitability for investigating zones for development, using GIS combined with advanced multi-criteria decision analyses (Bathrellos et al., 2017). This application exhibited that 2D-map tools (and GIS) could be used for relevant geohazard risk (assessment) applications, in this case associated with urban planning (Bathrellos et al., 2017). 3D ground models have also been widely used, providing clear visualisations, and examples are presented by Gakis et al. (2016), Burke et al. (2017) and Thornton et al. (2018). These visualisations help to indicate potential geohazard locations and improve the understanding of the subsurface, and therefore ground-related problems could be addressed more effectively (Culshaw, 2005; Wycisk et al., 2009). More specifically, Gakis et al. (2016) used 3D geological modelling to provide a risk assessment related to tunnelling for building an underground railway station. This application created a 3D ground model which could effectively provide the information needed for

understanding the subsurface characteristics of the area investigated throughout the project Gakis et al. (2016). This showed the importance of the use of 3D ground models in relevant applications. However, information from conventional 3D geological modelling has been mainly limited to 3D demonstrations of the subsurface. Therefore, there is a reasonable need for 3D geological modelling to be enhanced to manage more complex underground data (applications and investigations). Hence, a tool incorporating underground and other features within a geohazard risk assessment analysis, would be efficient, such as the one presented by Velasco et al. (2013). This would provide a better understanding and more advanced models, but also deal with more complex problems, using integrated data applications. In addition, integration with other software and sharing of data, is limited. Hence, a key point of the development of an information system is associated with the need for digital data integration with advanced digital tools, including a geohazard analysis.

An advanced tool that can easily manage, share and visualise (in 3D) the digital data would be efficient (Mielby et al., 2017). For example, Tegtmeier et al. (2014) provided a method for creating such a modelling tool which uses geotechnical data. In this way, different data formats could be employed, providing the geo-information, which is a key aspect for geotechnical investigations and construction projects (Tegtmeier et al., 2014). This would allow important information to be automatically included in the (3D) model. Hence, a framework of an 'automated modelling platform', which could be integrated with an advanced geohazard analysis, could be built. In addition, a combination of different type of information would be important to be integrated, such as geotechnical/geological factors with structural, to align with a rigorous geotechnical/geohazard modelling. Therefore, an advanced (digital) platform, which could successfully manage and share data, could be adopted. The utilisation of such an advanced modelling platform could also be enhanced, if this allowed for clear multidimensional

visualisations of the whole data, which would include detailed 3D models in combination with the results of the geohazard analysis. It is evident that a digital tool, which has previously managed successfully integrated information and produced advanced applications in constructions, could be applied in geohazard risk predictions (Parry et al., 2014). This tool could advance geohazard-based studies and investigations, which are based on rigorously managing and sharing 3D geotechnical/geological modelling information.

In addition, potential geohazard-induced risk from damage to the built environment is important to be assessed. Many relevant methodologies have been widely used, however a way to integrate (and store) and visualise their analysis results in an advanced 3D environment, is lacking. Due to the lack of such integrated 'geohazard information systems', including clear 3D visualizations, engineers/scientists and authorities often fail to realize the actual performance of their buildings due to geohazards, and/or the difference between design alternatives (Tawelian and Mickovski, 2016). Likewise, relevant tools which combine different methods or providing potential targets for further investigations could be also helpful. An integrated framework for combining modelling tools to obtain ground-related information, which is needed by ground investigation, would be useful. In this way, knowledge and understanding for the urban underground could be formed, and hence support sustainable decision-making.

The previous research showed the need to develop a framework to build a system capable of modelling geohazards that could have an impact within an urban setting, and hence support better decision-making (Gibson and Chowdhury, 2009). An integrated information system for assessing geohazard risk in an urban area was proposed for this research. The aim was to use advanced (3D) modelling tools and an integrated analysis with a BIM framework.

The aim was to develop a framework to provide a geohazard information system for urban areas using a 'preliminary' assessment tool. This would fill the technological gap to be used prior to a more detailed investigation/analysis, e.g. using Finite Element Method (FEM) analysis tools or further ground investigation. This required an integrated multi-applicable tool for ground-structure interactions. The idea was to ensure compatibility to any location and geohazard being investigated, and hence useful resultants in engineering projects, when a preliminary assessment is required.

To establish the framework, this research considered the 'basic' risk assessment components (such as risk, hazard, vulnerability and exposure) to ensure the compatibility of the proposed tool with the current approaches (UNISDR, 2009). Details about the proposed risk assessment follow in the next sections of the Methodology.

It was proposed to set up the tool to use 'simple' deterministic analyses to obtain initial outcomes and estimations on the potential risk of the area caused by geohazards. This was to be done by a risk assessment approach using a dynamic analysis of geohazard-inducing factors. This aligns with the recent demand for a digital tool that can support ground investigations (easily/rapidly) (Parry et al., 2014). This would be done through advanced geological analyses that can handle geological data and computational power limitations. The use of a preliminary assessment tool, which is based on such deterministic analysis methods, could be also justified by its benefits compared to other methods. Hence, key advantages over other computer-aided techniques used for analysis of similar (ground-related) problems (such as the FEM-based techniques) were considered. These would be:

- only low computing capacity needed;
- straightforward to use;

- relatively fast analysis;
- widely adopted (open-source) formats can be used;
- low economic cost;
- potential for easier data integration;
- further tools can be easily integrated;
- easy to change/adjust the model parameters in case of an error or a change.

In addition, an important aspect in ground-related problems is associated with the uncertainties involved. Hence, uncertainties in relation to the ground parameters involved also need to be taken into consideration, here (Sun and Kim, 2017; Phoon and Tang, 2019). By way of example, Wang et al. (2010) provided an uncertainty analysis to explore the probability of risk for slope instability. This analysis was conducted using Monte Carlo simulations, which tested the effect of various factors and obtained important outcomes for slope stability (Wang et al., 2010). Therefore, a method to incorporate a relevant uncertainty analysis within the assessment was needed to be developed, to enhance (underground) risk assessment considerations. A cost analysis has been included to complete the advantages of this tool, and to present tangible outcomes of the proposed framework. In this way, robust information could be provided, which would be useful for relevant decision-making that accounts for ground variability. A key outcome of the research was to provide 3D visualisations of the information, and particularly the results of the risk analyses. The approach adopted for the geohazard risk assessment framework is described in a following section.

3.1.1 Scenario-based approach

A focus should be given on the variability (inhomogeneity) of the ground, which is crucial when conducting similar studies (de Rienzo et al., 2008; Huber et al., 2015). This implies that the ground conditions and characteristics change when moving towards another area. As a result,

multi-applicability and compatibility are important. In this research, this is provided by an information tool whose built-in framework could be used within a range of applications of geohazards and locations. This would be useful for decision-making and sustainable urban planning applications.

Building a successful ground-related risk assessment framework is associated with the adaptability and compatibility in different ground conditions. An approach based on proposing a representative methodology via exploring a possible 'scenario' of risk due to a specific type of hazard, such as geohazard, has been widely employed to draw useful conclusions (for example, as demonstrated by Lu et al. (2012), Hall et al. (2014) and Whang et al (2015)). In the present research, this is handled by a 'scenario-based' approach, which would provide a robust example to conduct a number of similar cases. This is applied here by assessing a representative example of a geohazard. However, the focus here was more on demonstrating and integrating the proposed framework, rather than revealing detailed specifications of ground conditions of a particular area investigated (which could be indicated using this framework in further investigations). Therefore, the development of this framework has taken this into account by producing a framework that is able to work for a range of urban ground conditions (geohazards) and at different geographic locations, without the need to change the underlying basis of the framework.

Likewise, various locations were tried, to present the adopted framework. However, the final selection of the location of the study area was based on demonstrating a representative example of a subsurface (geological strata). This aligned with the current approach objectives, and provide a geohazard risk assessment which would demonstrate successfully the present framework.

Another important consideration was associated with the proposed factors and their subsequent values. Their selection was again based on providing a representative example of the important factors. The aim was to provide the best possible demonstration of the framework for the geohazard assessment tool being developed. Thus, there was a focus on a proof-of-concept approach to robustly demonstrate the resulting data integrations, visualisations and potential of this tool, rather than a very elaborate and detailed analysis taking into account all the involved factors, which was beyond the scope of this PhD study. The framework, however had to be sufficiently flexible that the ideas and concepts could be applied to other factors as required in the future. The idea was to provide a representative example to show the framework development, and ultimately to demonstrate how this could be used to provide clear risk indicators.

There are many examples of geohazards in urban areas that could have been chosen in this research to demonstrate the framework being developed, for example, ground movements and land contamination. In fact, during the development of the present method, the land contamination risk in combination with groundwater table fluctuation was initially examined. This was then followed by an initial analysis, and the resulting diagrams of contaminant concentration and move with time (at an initial stage) are shown in the Figure C.1 of Appendix C. The example of flood risk was also examined, but it was decided to be considered at a later stage, as an example focussing more on ground-building interaction would be more suitable. The ground movements were then considered to align more with the scope of this research. In particular, a scenario which was based on the settlements induced by tunnelling in an urban area, was chosen as an exemplar, as discussed in the next section. It is also important to realise that the framework being proposed could be applied to any urban geohazard.

3.1.2 Tunnelling–induced settlement

The ground settlement caused by tunnel construction in soft ground (defined here as soils or weathered soft rocks) is selected to explore the proposed methodology. This provided a representative framework for the development of a thorough geohazard information system for urban areas. The ground settlement risk assessments produced from this scenario would provide a tangible example in relation to an important urban geohazard. This is also associated with the increasing need for developing underground space and related developments, such as tunnel constructions (Rogers, 2009). Tunnelling-induced ground settlement is an important geotechnical problem (geohazard), which should be considered in sustainable urban planning and decision-making. It is strongly associated with safety and sustainability of urban areas and construction (Burland and Wroth, 1974; Mair et al., 1996).

A key point to solve this geotechnical problem is to assume green-field ground conditions. In those conditions, the ground settlements create a 'Gaussian' or 'bell-shaped' (inverted normal distribution) curve known as settlement trough with the maximum settlements above the tunnel centreline (Peck, 1969). Hence, in this way settlement estimations can be provided. This has been commonly used in past research, along the evolution of empirical (Peck, 1969; O'Reilly and New, 1982; Attewell et al., 1986; Mair et al., 1996) and analytical methods (Sagaseta, 1987; Verruijt and Booker, 1996; Loganathan and Poulos, 1998). These have been proven suitable for developing preliminary analysis estimations for assessing the associated tunnelling-induced settlement risk (Rankin, 1988; Attewell and Woodman, 1982; O'Reilly and New, 1982; Mair et al., 1996). In addition, during tunnel construction within urban areas, it is important for adjacent buildings to consider the surface and subsurface interactions in relation to adjacent buildings (Burland and Wroth, 1974; Attewell et al., 1986; Mair et al., 1996). An extensive methodology has been adopted by ITA/AITES (2007) to handle this matter (Chapman et al.,

2017). In terms of modelling, Mair et al. (2016) proposed the following phases to assess relevant building damage due to settlement risk.

A preliminary Phase 1 uses the empirical and/or analytical methods (described in detail in the following sections), using the settlement trough under greenfield conditions. The corresponding effect on building damage is assessed (Chapman et al., 2017). This was based on a classification for assessing settlement risk for adjacent buildings, which used the ground settlement and slope (Rankin, 1988).

In a Phase 2 assessment, to provide an understanding for solving this soil-structure interaction issue, the affected buildings needed to be integrated within a modelling analysis. This can be done using the location of the structure in relation to the settlement trough (inflection point) and the structural deformations that take place (Burland and Wroth, 1974; Burland et al., 1977; Attewell et al., 1986). Thus, Burland and Wroth (1974) assumed a building as a simple beam and developed a method for the damage risk estimation in terms of the critical strain known as the Limited Tensile Strain Method (LTSM). Boscardin and Cording (1989), Burland (1995) and Mair et al. (1996) provided a categorization of building damage (severity) risk, using structural damage and critical strains. Then, a more detailed evaluation phase would follow, for the buildings with a moderate and high risk from the previous stage (Phase 2), accounting further characteristics for a building damage assessment (such as structural condition/features, measures to be taken) (Chapman et al., 2017).

These damage criteria create an adequate initial assessment for indicating the tunnelling-induced settlement risk to adjacent structures caused by a tunnel construction. However, previous research in this (soil-structure interaction) problem indicated the importance of including a number of factors, for example, the Young's modulus and Shear modulus, which

affect the relevant building-damage risk (Burland and Wroth, 1974; Fedeski and Gwilliam, 2007; Dindarloo and Siami-Irdemoosa, 2015). Hence, to manage the many factors involved and completely assess (and understand) this problem, digital data techniques for analysing and visualising the whole problem, thoroughly, are required. In this way, an integrated assessment technique could align with urban geohazard modelling and decision-making. This could be supported by the development of new technologies and tools, which could advance risk predictions, and hence reduce efficiently human and economic costs. Such a (3D) modelling tool is reported in the current methodology.

As noted, conventional 3D geological (conceptual) modelling needs to be enhanced to handle more complex underground aspects and investigations. In this way such a conceptual ground model would progress to a new level, through a new platform integrating and providing more advanced underground information and enable visualisations of the risk assessment analysis. This is achieved in this study using the Building Information Modelling (BIM). In this research it is adjusted to a geotechnical-based risk assessment system to align with the associated requirements of the system. This is provided using a dynamic analysis combined with a digital framework to develop an integrated package. The resulting risk-based demonstrations for an urban area support the proposed methodology and demonstrate how it can be used for sustainable decision-making.

3.1.3 Building Information Modelling (BIM)

Building Information Modelling (BIM) is an emerged technology that overcomes previous limitations of digital modelling, by storing, sharing and visualising the information required for the whole life of a construction project (Eastman et al., 2011). The interoperability of this platform is advanced by the widespread use of Industry Foundation Classes - IFC (buildingSMART, 2017). This is due to IFC promoting interoperability (Abanda et al., 2015).

This communication of data (interoperability) in relation to the whole lifecycle of a construction project is significant for its broader use, aligning with sustainable technologies and applications (Eastman et al., 2011). Thus, BIM could be the next level of CAD systems, due to advancing data communication between users (Miettinen and Paavola, 2014).

BIM has been widely applied in many aspects of design, (risk) management and scheduling processes, whilst the proper use of a relative (BIM) software depends on the aim of a project (Abanda et al., 2015). In this way, using this new technology, productivity is improved through minimising design misconceptions, as stated by Abanda et al. (2015). Thus, BIM provides a method for improving efficiency, using digital tools and connecting all parties of a construction project together through shareable designs for the whole life of the project (Abanda et al., 2015).

In fact, the trend of using BIM showed an increase in the initial stages (design) and then a decrease through subsequent phases, according to Eadie et al. (2013). Likewise, a fluctuation is demonstrated for the data processes/demands and the need for smaller companies to implement and trust it more (Eadie et al., 2013). The integration of BIM within infrastructure projects has been extensively studied by Shou et al. (2015), who implied that it has been widely used, based on previous experience in building constructions, however a progress in construction management aspects was succeeded. After reviewing its potential, Eadie et al. (2013) and Abanda et al. (2015) also implied that it is a widely adopted digital technology, and has gained attention due to the efficacy and successful operation in construction and UK regulations.

BIM has been widely adopted in studies/applications through integrating several disciplines across projects. It has been providing knowledge and understanding using interoperable data, to create the proper environment for integration, and promote sustainability within construction

management. BIM has been promoting sustainability with building design, as stated by Liu et al. (2015), who demonstrated the power of BIM via its capability to generate environmental impact assessment through various simulation methods. Alwan et al. (2016) added that it provides an environment for integrating and generating frameworks for providing sustainable tools within construction developments (and management).

At the core of BIM lies the need to improve the multidimensional representation of a facility using various design and construction applications, after having already advanced the communication (shareability) between those involved within a relevant project. Hence, as already having been hugely adopted in advancing structural projects, it is evident that there is a potential for it to be extended to 'nearby' fields within construction design. Thus, as implied by Chandler et al. (2012), Kessler et al. (2015), Kim et al. (2015) and Mielby et al. (2017), geotechnical and geological engineering would be a promising application for this platform to implement within. BIM could store and visualise the information required in underground applications, design of earthworks, structures and geotechnical assessments.

In fact, BIM would progress 3D modelling, if used within geological/geotechnical 'assets'. It provides (modelling) data attribution, extraction, storage, management, sharing and thorough multidimensional visualisation, and enables modifications to the attributed features within a model, if required. Hence, using this technology there is a clear potential for more complex investigations and analysis such as in the ground-building-interaction context of this PhD study.

3.1.4 BIM for the underground

Therefore, BIM technology is chosen to be used here due to its potential in solving ground engineering problems concerning urban areas (Zhang et al., 2016). Svensson (2016) also exhibited this aspect via creating 3D models for infrastructure projects, which could

successfully share/communicate the ground information using BIM. It was also proved that this could be used effectively in ground investigations (Svensson, 2016). In particular, the objectives of this study could be supported by an integration of BIM with an analysis, and enables 3D visualisations. Data describing information of geological/geotechnical features could be combined with structural features using a BIM model, to be employed within a geotechnical analysis. The resulting 3D visualisations of the outcomes of this analysis could enhance geotechnical modelling.

In the proposed methodology, BIM plays the role of providing or 'implementing' the structural information and visualisation outcomes to present the current study. Hence, the concept of the current methodology aligns with BIM, and utilises available (BIM) model files to provide the detailed information required, such as characteristics of a building. In this case for instance, these characteristics (building assets) could be included within 3D building models in IFC format, which could be used, since they are commonly adopted in this platform.

The idea of the current research was based on using the structural data aspects and integrating them with a geohazard modelling, which includes time-dependent underground aspects. The system will use common formats in BIM, such as the IFC. This aspect of BIM is studied using the example of tunnel induced settlement to develop the geohazard modelling, and generate the mechanism (components) of the information system that is developed in this study.

Thus, an information modelling platform has been created, which integrates BIM with the underground. This aligns with using existing BIM data. However, the introduction of a concept of an underground-based BIM framework has been explored throughout the present methodology. The approach described provides a framework that this concept could be based

upon. Hence, the current approach could be used to enable a complete underground-based BIM framework.

In particular, the data integration processes (and formats) used could support assigning the resulting (analysis and other) data as attributes for this application in a following stage. In addition, methods that could create or use/edit (modelling) tools for an underground-based interface within BIM, which are based on the present methodology in a future work, are also investigated within the current study.

3.2 Geohazard risk assessment

Initially, to develop an information system for assessing risk, an approach where a risk assessment with 'basic' risk terms is handled, was considered. Establishing such a clear approach, enables the correlation and processing (analysis) of the geological/geotechnical information used, as this would describe the problem in detail. Thus, the following section introduces the risk assessment concept that the information system in this study is based. This concept provides the background that all the parts of the analyses and data integrations in the methodology use, and where their demonstrated resultants are built upon.

The aim of this research was to create a system for assessing geohazard risk in an urban area. The risk assessment in this research is provided by the 'basic' risk assessment components, as shown in Equation (3.1) (UNDHA, 1992; UNISDR, 2009; Roberts et al., 2009).

$$\text{Risk} = \text{Hazard} \times \text{Vulnerability} \times \text{Exposure} \quad (3.1)$$

The 'Risk' is the likelihood that a hazard will have a negative consequence, a measured chance or negative product of effect from a (natural/manmade) Hazard (van Staveren, 2009; UNISDR, 2009; HSE 2017). 'Hazard' is a dangerous threat that could cause a negative (health, social, economic environmental) change, which results in a potential harm that can be either physically

or manmade related or induced (Clayton, 2002; UNISDR, 2009). The probability, extent and severity indicate the subsequent damage caused by a Hazard (Fedeski and Gwilliam, 2007). The important and determining criteria (factors) which indicate that a hazard could have a negative impact provide the 'Vulnerability' to this risk (Clayton, 2002; UNISDR, 2009). 'Exposure' are the elements, such as buildings, infrastructure, agricultural land and people, which could have a negative impact within zones of risk due to this hazard (Clayton, 2002; UNISDR, 2009). Exposure and vulnerability are distinct terms and should not be confused, and if the elements are not located inside these risk zones, no risk occurs because there is no exposure to the risk (Cardona et al., 2012). To evaluate (assess) exposed elements, information about their location and characteristics is needed (Fedeski and Gwilliam, 2007; UNISDR, 2011). More specifically, common characteristics could be the geographical location/distribution or number, structural characteristics, and population density and social/economic characteristics (UNISDR, 2011). Another term, broadly used in risk assessments is the associated 'uncertainty', which occurs when there is a lack of information or knowledge for a specific aspect under investigation (Smallman, 2000; Willows et al., 2003). The probability of a specified risk to occur is also used to describe 'uncertainty' (Fedeski and Gwilliam, 2007).

The focus of this research is on urban Hazards associated with ground-related issues, referred to as geological, geotechnical or simply 'geohazards'. The approach uses BIM to manage data of a combined risk posed on buildings caused by geological hazards or 'geohazards'. This platform is capable of evaluating this (damage) risk, under current and future conditions, in the light of geological/geotechnical and building changes.

In the current research, the term 'Exposure' relates to the building elements which are negatively affected by a geohazard when these buildings lie within zones of risk caused by this

geohazard (Fedeski and Gwilliam, 2007). More specifically, the location and characteristics, such as the distribution/number and structural characteristics of the buildings in these zones, are required to provide an exposure assessment (Fedeski and Gwilliam, 2007; UNISDR, 2011). However, since the idea here was to demonstrate a risk assessment under different scenarios of potential geohazard risk, it is assumed that the location/number of the buildings would be constant and their distribution would be uniform. A complete assessment of the exposure could also depend on the detail of the (conducted) risk assessment and its available data (Merz et al., 2010). In the present study, it is assumed that the detail needed for analysis is solely associated with the detail of the geohazard risk assessment and size of the corresponding area investigated. The available data regarding structural characteristics is also limited. Hence, in the present research, to clearly demonstrate the adopted framework and its integration with BIM, rather than providing a detailed analysis of asset characteristics which were assumed to be beyond the scope of the geohazard risk assessment investigated, exposure is not a variable that was explored (i.e., Exposure=1). However, although exposure is a factor that must always be considered, it does not affect the geohazard risk assessment evaluations of this research. Future work based on the proposed methodology could include an exposure assessment, focusing more on detailed asset and structural characteristics and the spatial variation of the zones of risk associated with the geohazard that would result in differential degrees of exposure.

As already mentioned, the present research aims to demonstrate a method that uses, by way of example, data in relation to ground settlement. Hence, if it can be proven to work successfully for this scenario, then it will be feasible to develop the additional functions required to support further decision-making and sustainable planning in urban areas. The use of normalisation techniques also allowed the subsequent damage to be compared, correlated and integrated, as required by the current research objectives.

In order to establish an approach for an information system for geohazards and their consequences in an urban area, it should be initially based on a model of a risk assessment. This could describe a total risk caused by a number of geohazards, '*Total GeoRisk'*. For the scenario used in the current study, the 'components' constituting this risk could be divided in three subcategories, i.e. the risk due to ground settlements, $Risk_{SE}$, the risk due to contaminated land, $Risk_{CN}$ and the risk due to other (secondary) factors, $Risk_{SR}$. The resulting *Total GeoRisk* is provided as the following sum of risk subcategories in Equation (3.2).

$$\text{Total GeoRisk} = W_{se} * \text{Risk}_{SE} + W_{CN} * \text{Risk}_{CN} + W_{SR} * \text{Risk}_{SR} \quad (3.2)$$

$$\text{while } \sum_{k-1}^{n} w_{k_j} = 1 \quad (3.3)$$

where W_{SE}, W_{CN}, W_{SR} are the (importance) weights of each risk subcategory that can be estimated by the experience/expertise of the expert (author). For example, to demonstrate the approach, it is limited to the effect of tunnelling-induced ground settlement risk (W_{CN}=0, W_{SR}=0 and W_{SE}=1). Likewise, as already mentioned, exposure is not further explored (i.e., Exposure=1). Equation (3.1) therefore becomes Equation (3.4), as follows.

$$Risk_{SE} = Hazard_{SE} \times Vulnerability_{SE} \quad (3.4)$$

where $Hazard_{SE}$ is the tunnelling-induced settlement Hazard (investigated here by the probability, and subsequent Damage Extent and Severity), and $Vulnerability_{SE}$ the Vulnerability to tunnel induced settlements.

Key steps and subsequent parts of this methodology follow.

1) In Chapter 4, the tunnelling-induced settlement $Risk_{SE,}$ is assessed using Equation (3.4), where only the $Hazard_{SE}$ is explored, in this case using the (degree of) building damage likely to occur due to tunnelling-induced settlement (hazard). To reduce the computational limitations

of the problem, Empirical/Analytical models are employed within the (spatial) analysis of $Hazard_{SE}$, while available geotechnical data from boreholes and available BIM data of the adjacent buildings (building geometry and building material properties) are used. To carry out the current method for the tunnelling-induced settlement risk assessment and estimate the $Risk_{SE}$, the analysis (using custom-made scripts in MATLAB, described in the following section) consists of two Phases (steps). Phase 1 Building Damage Assessment (Damage extent) used analytical methods for estimating the ground settlement in the investigated area (Rankin, 1988). Phase 2 (Damage severity) used analytical methods based on the Limiting Tensile Strain Method (LTSM) to provide estimates of building damage as a function of critical tensile strains at the level of each building foundation and considering the building as a uniform beam (Burland and Wroth, 1974). This provided a damage classification for all the buildings investigated. Tools related to spatial modelling (interpolation) to create the 3D geology-tunnel-building model were also employed. BIM was used to collect the structural data to support the risk assessment analysis. The resulting risk-based 3D visualisations are produced from BIM.

2) Chapter 5 focuses on the Vulnerability 'component' of the risk assessment (in addition to $Hazard_{SE}$), which includes the settlement vulnerability factors to provide a clear tunnelling-induced settlement risk assessment. The settlement risk $Risk_{SE}$ due to a tunnel construction has been described using Equation (3.4) using the Settlement Hazard ($Hazard_{SE}$) and Settlement Vulnerability ($Vulnerability_{SE}$). The Settlement Hazard ($Hazard_{SE}$) is explored by the damage extent (considering the settlement and slopes) and damage severity (considering the structural interactions using critical tensile strains) for a building, using analytical approaches. $Vulnerability_{SE}$, is provided by a resulting index of a spatiotemporal analysis (MATLAB) involving factors having an impact on settlement vulnerability of the area. The spatial and associated modelling tools were adapted to develop a 3D geology-tunnel-building model. BIM

was adopted for importing the building characteristics into the model. The settlement risk assessments are demonstrated by producing visualisations of the risk distributions and 3D BIM visualisations.

3) Finally, Chapter 6 uses an uncertainty analysis to complete a full package for a settlement risk assessment framework, and hence describe all the 'components' of a risk assessment. An uncertainty analysis has been carried out using probabilistic simulations (MATLAB) to provide the probability for the economic (costs) risk in relation to the building damage. In this method, the $Hazard_{SE}$ is explored due to the available database of building damage costs. The analytical methods for the settlement estimations were used in combination with assessing the building damage extent and severity. Uncertain settlement-inducing geotechnical and structural factors (BIM) were used in the analysis. The resulting risk-based 3D visualisations (BIM) of the building damage costs were then produced.

To develop the geohazard risk assessment, subsequent data integration using digital tools took place. Therefore, the data integration and management used throughout the research is important to be presented.

3.3 Data integration and management used throughout the research

3.3.1 Approach used

The adopted approach involves the development of an automated process to create a complete geohazard risk assessment framework using 3D (geology-tunnel-buildings) modelling, by utilising BIM data and integrating it within the analysis in MATLAB (Mathworks Inc., 2016).

The data integration and management aspects used throughout the research are an integral part of the methodology. This is done using both the analysis and the BIM frameworks, with the modelling tools providing further options in the findings or supporting the previous

frameworks, as required. This section initially describes all these frameworks and data-formats in detail. Particular emphasis is given to providing all the data features and their characteristics used in the analysis, to provide the risk assessments as well as the integration processes adopted.

The present methodology used the following digital tools:

- MATLAB (Mathworks Inc., 2016) was used to develop the analysis and support the development of this research;
- BIM (model) data in Industry Foundation Classes (IFC) (buildingSMART, 2017) format were employed throughout;
- SketchUp (Trimble Inc., 2016) was used for 3D (solid) model visualisations aligned with the BIM framework.

Details about their selection and use are provided in the next subsections. However, to present a full picture of the background data integration adopted within this study, the particular data input/output mechanism is important to be described.

3.3.2 Data input/output steps

The key processes describing the data integration are:

1. Data input/output and format conversion processes.

These are the particular format conversions (data input/output) that have taken place in this study based on the concept of developing a framework for the integration of the data used within this information system. This process is shown in Figure 3.1. The key points used to provide an integrated BIM-based geohazard risk assessment tool follow (as presented by Providakis et al. (2019)):

- The borehole data used is interpolated to form the 3D geological and tunnel models and the topography of the area (ground surface);
- BIM building data used from available IFC model files (Graphisoft, 2018; SUPodium, 2018);
- Data is integrated using the adopted formats that SketchUp (BIM visualisations) and MATLAB can recognise and modify (Figure 3.1):
    - The BIM/IFC building data (file) (Graphisoft, 2018; SUPodium, 2018) used is imported to SketchUp;
    - SketchUp converts these IFC files to STL (3D Systems, 2017) that is a compatible format with MATLAB, and can be used for further analysis;
    - MATLAB reads the STL-building data to create a complete 3D geology-tunnel-buildings model using 3D solid elements;
    - MATLAB exports the interpolated data of the whole 3D model to SketchUp using the embedded API (in Ruby programming language (Ruby, 2017)).
- Georeferencing of the whole model into BIM, to provide an assessment in relation to the exact borehole locations.

2. Creation of the georeferenced 3D geology-tunnel-building model: The data integration used to provide the 3D models using BIM is used throughout this research study.

3. Mesh development: This section explores the data integration for creating the meshing requirements of this study.

4. Geospatial modelling tools integration: This describes advanced tools used to enhance the visualisations in this study.

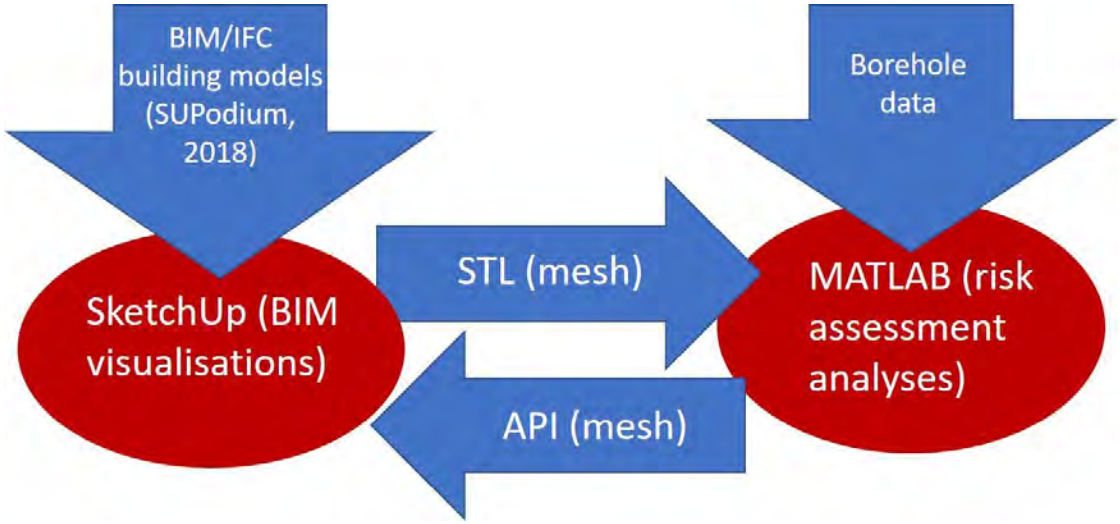

Figure 3.1: Diagram showing the main data processes in the present study.

Initially, each feature of the integration process used throughout this research is described in more detail in the following sections. This is carried out to provide the whole picture of all the data and interface interactions and processes involved in the research.

3.3.3 Utilising MATLAB

The analysis of the geohazard assessment in this study was undertaken using MATLAB (Mathworks Inc., 2016). This is a widely adopted software that generates a powerful environment for integrated (dynamic) analysis. The tools (and toolboxes/functions) that have been developed using this program make it capable of solving complex analytical problems. It is commonly utilised in geotechnical analyses, and it could efficiently support the analysis objectives in this research, such as a risk assessment tool. It could combine successfully complex problems such as soil-structure interactions or other advanced analytical processes with time. Its Graphical User Interface (GUI) with its many options and tools is another

advantage for its selection. The wide range of format that MATLAB supports, makes it an efficient tool for data integration.

The MATLAB analysis undertaken in this study was produced using predominantly custom-made scripts. These comprised of functions and tools to create the proposed modelling analysis, to support the current methodology. The MATLAB custom-made scripts were based on the proposed (geohazard) risk assessment approach, and their use is presented in the Appendix A, B, C and D. Where appropriate, MATLAB toolboxes and spatial modelling tools were also adapted, as required for the analysis. By way of example, the interpolation was such a method employed in the current modelling and geological data analysis regularly.

MATLAB (Mathworks Inc., 2016) produces the 'environment', which apart from performing the analyses, could fully support the data integration processes generated within this study. This is carried out by creating or using tools that can define all the basic procedures that work in the background. It also 'supplies' the spatial modelling, visualisation and data analysis tools that the framework is based upon, and which is required to develop the whole 3D ground modelling. It supports all the processes used, such as data conversions and integration (transfers). MATLAB can read the 3D model in the STL format from SketchUp. It should be noted that it is not limited to this format and depends on the (BIM) software used. It is also integrated with the Application Programming Interface (API) tool used, to export the resulting 3D modelling to SketchUp (Trimble Inc., 2016). The key points related to the use of MATLAB in the current research are:

- Interpolation tools for the 3D geological and tunnel models;
- Integration with Google Earth (Google Inc., 2018) tools;
- Generating the mesh;

- Conducting the risk assessment analyses;
- Integration with the API to extract the resulting 3D geological-tunnel-buildings model and the risk assessments;
- Visualisation (2D/3D) of the features investigated.

The scripts of the MATLAB analysis used are presented throughout the Appendices.

SketchUp (Trimble Inc., 2016) was then selected to support the 'BIM environment' in the research. This was all done using the IFC format (file import/export and edit), which was an important reason why this software was chosen. SketchUp can support the BIM framework characteristics and it can provide clear 3D modelling, designs and visualisations.

3.3.4 Utilising SketchUp

SketchUp (Trimble Inc., 2016) has been widely adopted in a range of Computer-Aided Design (CAD) applications. It could support advanced CAD characteristics by a straightforward interface for 'rapid-sketching', in this case for the 3D geology-tunnel-buildings models. SketchUp provides a straightforward Graphical User Interface (GUI), which enables the user to easily import/export BIM models (files), and further modify them using three dimensional options (e.g. via IFC format). Additionally, it is widely used among surveyors, engineers and designers in various integrated applications, enabling several data format conversions of the models. Any design of a model could be (easily/quickly) produced and present its details (attributes) in 3D and then be forwarded to clients directly, speeding up such processes. The client could then give feedback and request for alterations. Then, the engineer/user can review the models until the client is satisfied with the result.

The present methodology used SketchUp (Trimble Inc., 2016) as the BIM visualisation software. It was the tool used to collect the structural characteristics and integrate the data from

the analysis (MATLAB). This is based on the capability of SketchUp to hold and create or edit 'attributes' with information in relation to a specific 3D element (object). In this way the advanced characteristics of BIM are effectively implemented. It was used as the 3D visualisation software for demonstrating the resulting (3D) models using BIM. Hence, SketchUp (Trimble Inc., 2016) has been utilised in the current study as the tool for data integration processes and the 3D (BIM) visualisations. The advantages of using this design tool vary:

- The straightforward Graphical User Interface (GUI) makes it a widely adopted software within its field;
- The BIM environment and background options that it offers including: detail attributes, solid objects, groups and components;
- The interoperability and share-ability using the IFC standards, through importing, exporting and converting to this widely used format in BIM, providing full BIM framework capabilities;
- Supports conversions to other widely applied formats of a model, such as to STL;
- Capable to import/export using numerous broadly employed formats;
- Design preferences and options for easy 3D object design and manipulation;
- Compatibility to work with other programs, such as MATLAB;
- Embedded API version, ready to be used in data integration and further developments;
- Advanced geo-referencing capabilities if combined and integrated with an analysis software.

SketchUp provided an easy-to-use interface for the resulting multidimensional (BIM) visualisations of the analysis. Furthermore, it also enabled the use (and conversion to, if

required) of BIM (IFC) data and its conversion to a format capable for export (in this case to the STL format). Hence, SketchUp allowed the data transformations/processes in this research. The data used in these transformations and the associated processes are described in following sections. As a result, it provided the capability of the resulting 3D models to be used by any conventional BIM software. Any such software could easily implement and edit the resulting models and visualisations of the present study.

To clarify the digital background used to provide the analysis within this study, a thorough description of all the applications involved is required. A tool working within or in combination with SketchUp was also required to carry out the analysis of this research. This would provide the digital grounds (commands) for assigning and integrating all information between various frameworks through an automated method.

3.3.5 API and Ruby API integration

The use of an Application Programming Interface (API) tool was important to support the objectives of this study, and hence the required data integration. This is an environment that enables the capabilities of the software used to be developed or extended, using programming within the software. An API uses a particular programming language (and its characteristics) to provide the subsequent command lines as required. This varies across different types of software and applications used. Recently, the majority of design software has an accompanying version of an API to cover any 'needs for developing' of a user. This is done via an embedded API so as to automatically input more complex and rapid design information, i.e. it can provide an environment for transferring (import/export) digital data, and developing advanced options/properties and designs, automatically. Digital data management is a particularly important process in geoengineering and geoscience, (Parry et al., 2014). Therefore, the selection of SketchUp was significantly based on its compatibility with other software.

SketchUp provides an embedded API using the Ruby programming language (Trimble Inc., 2016; Ruby, 2017).

Ruby was developed by Y. Matsumoto in the late 90s and has been a widely accepted programming language (Ruby, 2017). As noted by the developer himself, Ruby reveals advance features and capabilities whilst performing, using processes which 'imitate a natural object' (Ruby, 2017). It offers a flexible object-oriented programming language, which is useful and convenient while programming (Ruby, 2017).

The use of this interface aligned with the development of an automated process. In particular, it provides the information that is required for the integration of the MATLAB analysis with SketchUp. This information needs to be integrated within the API, to be extracted to SketchUp. Thus, by employing it, the post-analysis risk assessment data in combination with all the 3D geology-tunnel-buildings model information could be exported to SketchUp, and presented clearly in 3D. Hence, it forms an important connection tool in this study, allowing the data to be easily exported so as to be visualised and provide the results of the risk assessment. It also has to be noted that by using the API, the automated process of developing the 3D models could be conducted, i.e. the geometry of the models is defined using the information adopted from MATLAB and BIM (SketchUp).

SketchUp uses a light version of Ruby within its main interface –which is called 'Ruby console' (Trimble Inc., 2016; Ruby, 2017). In the current research, the API was integrated within MATLAB. Further details of this approach are described in the relevant sections related to the creation of the 3D models and in the relevant sections in the Appendix A.

In addition, to provide a clear picture and the background for the data processes/integration within the present study, it is important to clearly describe the formats and their interface. The

main formats employed to support the integration processes are the IFC and the STL (3D systems, 2018), which are described in the following sections.

3.3.6 BIM-IFC

As previously mentioned, an important advantage of BIM is based on the communication and share-ability of a large amount of digital data between users involved in a construction project (Eastman, 2011). This process which is known as 'interoperability' describes this compatibility, share-ability and connectivity of data, and is easily adapted by any relevant user (Miettinen and Paavola, 2014). These aspects – which are accounted throughout the present study – made BIM to become an important information tool with numerous engineering applications.

The use of a standardised format was important for the development of BIM framework to support the previous indications. Such an open-source format that provides these advances of BIM is the Industry Foundation Classes (IFC) (buildingSMART, 2017). It is a widely adopted (accepted) standardised format in BIM across construction projects, globally (Steel et al., 2012). IFC are described as an object-oriented system of classes that effectively 'attribute' the BIM framework (Liebich, 2004). IFC have already been widely used within construction industry in numerous projects, and similarly within research applications using BIM. As a standardised format it advances communication between the engineers/users through interoperability, and the resulting efficiency, supporting BIM throughout all the engineering stages of a construction project (Fazio et al., 2007; Nour, 2009; Steel et al., 2012). Therefore, a categorisation in different layers or classes according to the position/role in BIM is adopted for a specific object (Liebich et al., 2013).

In the present methodology the IFC (buildingSMART, 2017) was employed due to the previous advantages progressing the compatibility with various modelling tools (interoperability). It provided the link between the ground data and the building data used in the present approach. It should be mentioned that BIM/IFC files are taken from available files, and not created from scratch, as this would be beyond the scope of this study. However, if required this could be carried out in future research (more details provided in Chapter 8.2 - Future Work).

In the present research, the BIM file in IFC format of an already built model of a building in Archicad (Graphisoft, 2018) was utilised, which was available from SUplugins (SUPodium, 2018). This provided a representative example of processing a (3D) BIM/IFC file that holds all the required (structural) information for this analysis. SketchUp supports the BIM framework advantages by enabling the use (and editing capabilities) of the IFC standards. As a result, this initial 'data process' of the methodology is related to importing this BIM/IFC file into SketchUp (BIM Framework). Hence, all the features required for the following analysis could similarly be imported, to support the current aim and methodology. Further details on the BIM/IFC files imported follow.

3.3.6.1 BIM/IFC building model

The initial conducted data transformation focuses on the building import to SketchUp. The representative example of a 3D building was used through the BIM file available from SUplugins (SUPodium, 2018) of a low-rise (residential) two-storey masonry structure. It was generated in Archicad (Graphisoft, 2018) and contained all the structural information required in the present study in IFC standards (buildingSMART, 2017). This building model is shown in Figure 3.2a. The structural information is related to the building geometry or dimensions information, e.g. size and type of the whole building (building width, building length and building height). Likewise, structural elements (slabs, columns, beams, walls etc.), information

related to the structure of the building's spaces (room limits, realised construction, building volume etc.) and structural characteristics, i.e. what the structural components are made of, are also included within the 3D building model. This is important for relevant integrated modelling applications. The BIM/IFC building model has 3D element categories comprising (objects):

- 22 walls;
- 14 slabs;
- 19 columns;
- 10 beams.

The building models have a gross plan area from 100 to 300m^2. The interior consists of four rooms on each floor, with two small outer balconies and a large internal balcony that has glass openings up to the ceiling.

This IFC-model file would represent a building in the campus of the University of Birmingham, UK, theoretically located in the southwest part of the campus, as shown in the satellite image demonstrated in Figure 3.3. To provide efficient results for decision-making and urban planning, a built-up area was required. This was formed by copying the initial BIM building model into ten buildings of various sizes, as presented in SketchUp in Figure 3.2b (Providakis et al., 2019). These are then superimposed onto the satellite image of the area of interest, as shown in Figure 3.3 (adapted from Providakis et al., 2019).

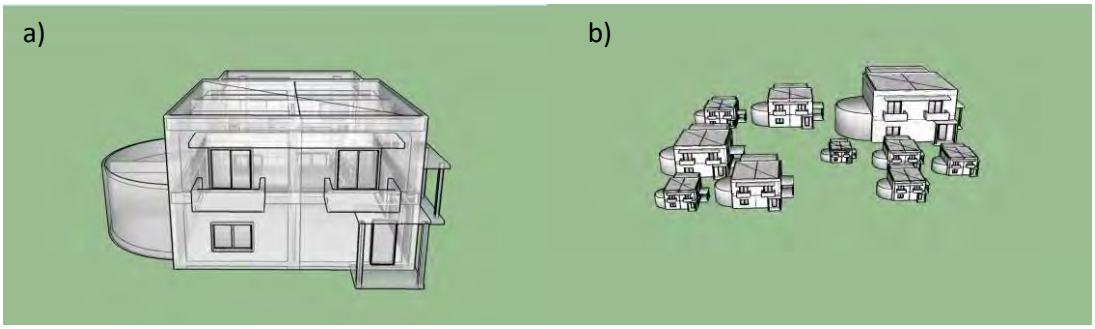

Figure 3.2: A view of the BIM/IFC building model (SUPodium, 2018; Graphisoft, 2018) as: (a) an individual building and (b) a building block, using SketchUp (Trimble Inc., 2018), adapted after Providakis et al. (2019).

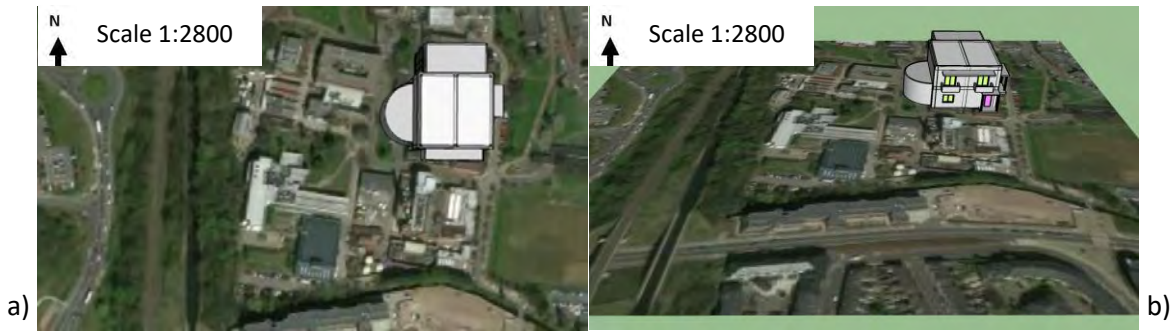

Figure 3.3: A BIM/IFC building model superimposed onto the satellite image of the area, shown (a) vertically and (b) with angle (Providakis et al., 2019).

Although beyond the focus of the present study, a level of detail depending on the detail of the BIM/IFC models, could be provided. Hence, due to the characteristics (details) of the 3D BIM/IFC building models used, technically a subsequent 'Level of Detail 2 (or LoD 2)' could be implied to have been adopted here (BCA, 2012; CanBIM AEC (CAN) Designers Committee, 2012; Fai, 2014).

The structural information (3D buildings model) could now be imported to SketchUp (BIM framework) to align with the objectives of this study. However, before describing the geometry of the 3D geology-tunnel model (with the corresponding mesh), a detailed description of the method (format) to transfer it between different frameworks is provided, while keeping all the 3D model characteristics. This is done due to the use of this format in specific processes, described later in detail. Hence, it is evident that apart from the IFC, a format capable to export the 3D geology-tunnel-buildings model would provide the link between BIM (visualisations; SketchUp) and the analysis framework, and successfully demonstrate this methodology. This is the STL format (3D systems, 2018) described in the following section.

3.3.7 STL model

The digital format used to provide the next link in the data integration processes within the current study is the 'STereoLithography' or STL format developed by 3D systems (2018). This was used in importing/exporting the information of the 3D models including the mesh, which is significant for developing the methodology.

This format is widely used in 3D printing and related applications. It has been also used successfully in producing and modifying 3D objects, and therefore it is suited to the aim of this study. Recently, it has been used as the interface for the data exchange from design or CAD to another object-oriented software (Kumar and Dutta, 1997; Jurrens, 1999; Hague and Reeves, 2000). It can successfully assign data and geometry for a 3D mesh without referring to any other kind of information (Chiu and Tan, 2000; Stroud and Xirouchakis, 2000). It carries the required information for producing a mesh for any triangulated 3D (solid) object geometry containing surface and vertex data. This is mainly done by dividing a surface into small

triangular pieces (facets), which are defined by a vertical direction as well as their three corners to align with the vertices -shown in Figure 3.4. STL could simply provide a feasible interface for transferring 3D object information between different software. This means that the georeferenced location information could be also stored using it, although it provides no initial coordinate information for 3D objects by itself. It is widely used due to the relative straightforward application and interface, having a simple syntax, using the ASCII or Binary type (Liu et al., 2017).

Among many, the selection of the STL format was based on its ability to hold the appropriate information for 3D objects, while being compatible with MATLAB. It was chosen because it is supported by SketchUp, which provides a direct conversion (transformation) of the 3D models (BIM/IFC models) within it, into this format. In particular, this format supports the data of the BIM/IFC building models in SketchUp (BIM) to be exported into MATLAB, for use in subsequent analysis. In addition, it could enable the re-transfer of data of 3D modelling data within a mesh at a later stage, if needed, as it could support the post-analysis undertaken in MATLAB to be imported back from SketchUp, and update the resulting 3D model data.

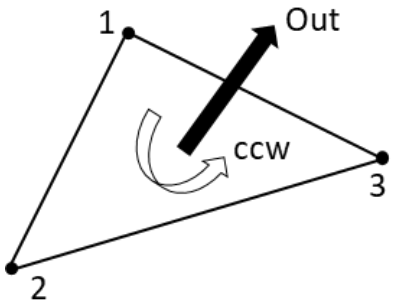

Figure 3.4: An STL facet triangulation through a Counter ClockWise (CCW) order.

Therefore, its compatibility and transferability between several frameworks makes this format efficient for the present modelling. The adopted approach moves on from the IFC-model file import into the BIM visualisation software (SketchUp), and then its conversion into the STL format. This takes place within the BIM visualisation software (SketchUp), to allow every aspect involved to be further analysed or modelled and modified, i.e. by exporting it to MATLAB in this study.

3.3.8 Georeferencing and spatial modelling tools

An important task required in the present method is the accurate (geo)location of features of a 3D model (Legat, 2006). A model, and its subsequent features, should be placed correctly to provide subsequent accurate and integrated 3D model and analysis resultants. This is achieved by their proper georeferenced position (e.g. in a 'map' or a 3D model), through a process known as georeferencing, which is a common process in geoscience (Li and Briggs, 2008). It allows the correct location of features and topological characteristics of a particular area to be integrated with different coordinate systems (used by different software).

This has to be considered in the present study, where the coordinate systems of the BIM/IFC building files (Graphisoft, 2018) and those of the rest of the 3D models, i.e. the 3D geology-tunnel model, which were used in the settlement risk assessment analyses, are different. The present approach focuses on 3D modelling of multiple ground-structure interactions. Therefore, georeferencing is important to be adapted to align the 3D models used, i.e. the 3D geological, 3D tunnel and 3D (BIM/IFC) buildings (and the resulting risk-based assessment indications), and therefore, yield an accurate modelling. In this case, the 3D BIM buildings were needed to be superimposed on the 3D geology-tunnel model to align with the accurate modelling of the

ground-building interactions. Therefore, the 3D models used need to align with a common (geo)reference system, i.e. the BIM/IFC building files need to have the same coordinate system with the rest of the 3D models used in this study. This is carried out in advance by acquiring all the digital information for the accurate location of all features. A subsequent method that could be used to handle the previous aspects could employ spatial modelling tools.

The process to define the actual position of a model is a complex task. An approach to achieve this would be to use a reference map and the IFC standards to incorporate all the (geo)referenced points in the BIM framework. A correlation between those used in the modelling and those used in the actual coordinates could be gained using this method. Thus, every feature included in the BIM/IFC models could be adapted to the coordinates system assigned and be accurately located.

This means that an integrated approach to set the successful position using the IFC of BIM file features could be developed. IFC has the classes of information to achieve it. In theory, longitude, latitude and altitude values in the *IfcSite* class with adapted offset and true North from *IfcGeometricRepresentationContext* class would achieve a proper georeferencing of a subsequent IFC file (buildingSMART, 2017). However, in practice, these classes are mostly null, unfilled or incorrectly located. Therefore, consequent classes need to be developed in IFC to accommodate this georeferenced position. Based on the previous details, an alternative method had to be implemented in the current methodology.

3.3.8.1 Georeference transformation

Initially, the actual position is described by a Geographic Coordinates System (GCS). In contrast, the BIM/IFC (building) files do not indicate a relevance to those systems and their

features are normally described using a Cartesian coordinate system. BIM/IFC models mainly align with the (default) Cartesian coordinates of the software used, originating in (0, 0, 0).

In the present approach, the conversion to a GCS has been employed to align with the actual (earth) coordinates using angular units, the prime meridian and the datum of the spheroid. Therefore, a coordinate transformation had to take place. The British National Grid 'OSG-36' system commonly used in the UK is selected, to provide the new system and a transformation to this GCS should be generated. This is done on the STL buildings exported from SketchUp, which are converted to the "OSG-36" and now align with the borehole data used in the study area.

A georeferenced position of the (3D) BIM/IFC building models was generated by a method of locating its features and adjusting their information, using the STL format. A coordinate transformation for the valid position of a 3D model was conducted, using the 3D affine transformation Equation (3.5), where (STL's) coordinates (x, y, z) was given, and the offset (w) represents the distance from the origin (0, 0, 0).

$$\begin{bmatrix} a\ b\ c\ d \\ e\ f\ g\ h \\ i\ j\ k\ l \\ m\ n\ o\ p \end{bmatrix} x \begin{bmatrix} x \\ y \\ z \\ w \end{bmatrix} = \begin{bmatrix} ax + by + cz + dw \\ ex + fy + gz + hw \\ ix + jy + kz + lw \\ mx + ny + oz + pw \end{bmatrix} \quad (3.5)$$

This was adopted by MATLAB through implementing related affine transformation functions to translate and set the (3D) STL model correctly. The current process keeps the lines or polygons in space, and allows the model to rotate, scale and be translated again.

This STL setup is presented in Figures 3.5 and 3.6. BIM/IFC building models could now be ready to be correctly placed onto the 3D geology-tunnel model. This process aligns with the borehole data records adopted from the study area. The buildings on their actual location after

the transformation took place are then shown in Figure 3.7 (using a satellite image for reference on SketchUp). Further detail about MATLAB tools used during this analysis is presented in the Appendix A.

The next section describes the creation of 3D geology and tunnel models, as well as the mesh generation. This would provide a robust understanding of the details for the 3D modelling used, completing a full description of each part of the data processes in this research.

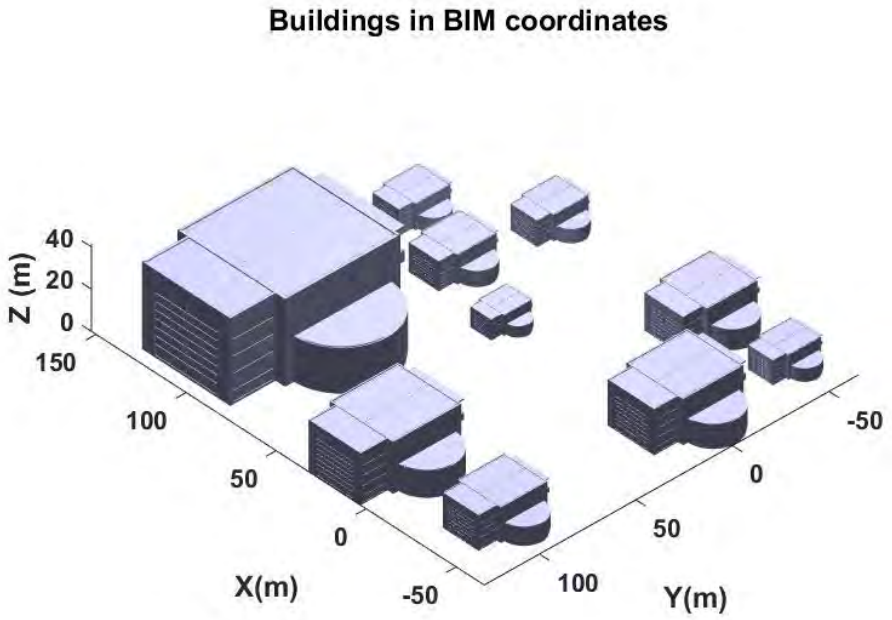

Figure 3.5: The STL buildings in the local coordinate system of the BIM framework, initially, demonstrated using MATLAB (Providakis et al., 2019).

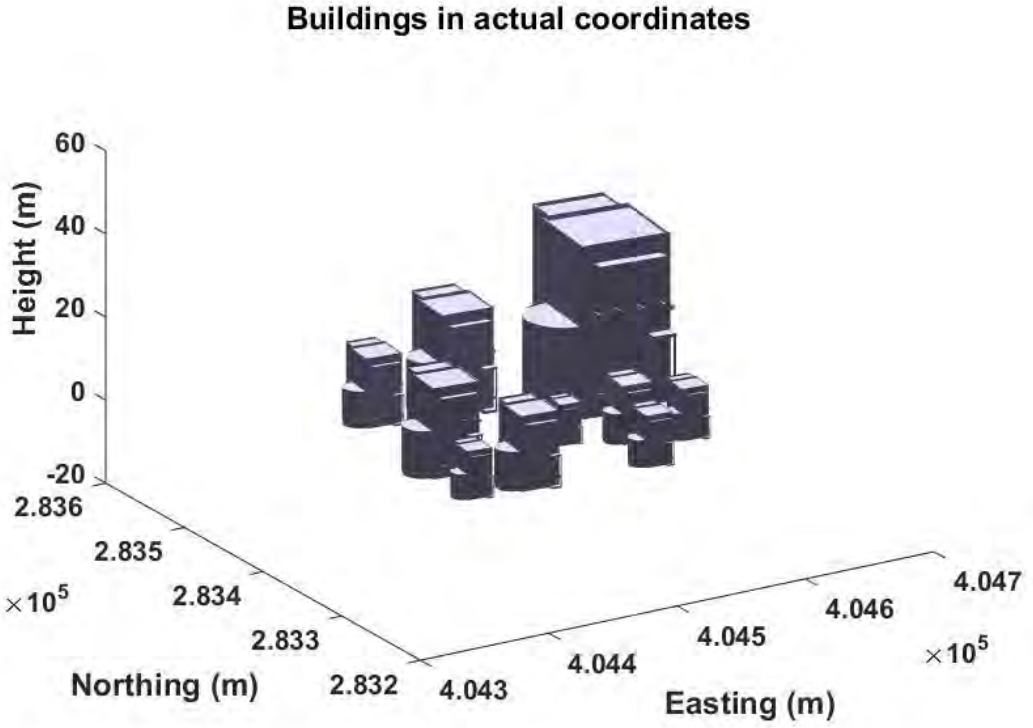

Figure 3.6: The STL buildings converted to the OSD-36 coordinate system, as shown in MATLAB (Providakis et al., 2019).

Figure 3.7: Buildings on their georeferenced position in actual topography using BIM (SketchUp) after Providakis et al. (2019).

3.3.9 3D modelling

The mesh generation is an important part of the 3D modelling processes. To understand the theoretical background of meshing, the geometry of 3D models had to be initially considered. 3D modelling introduces several elements connected together through several geometries, e.g. surfaces and faces. These create a 3D object existing within a 3D environment. This process consists of point data, which could be presented in various ways. 3D models could be: solids – which are specified by their volume, or boundaries – which are specified by their surface boundaries. Common graphical interfaces align with boundaries, through considering the exterior visualisation characteristics. A widely used example is the polygon mesh.

3.3.9.1 Polygon mesh

A polygon mesh brings together vertices, edges and faces to form a (3D) polyhedron. This is important in 3D modelling. More specifically, the triangulated mesh is widely used, although quadrilaterals, convex, and others (polygonal shapes of faces) may also be employed. A particular polygon mesh is utilised depending on the objectives of the 3D modelling process/application, and numerous methods have been proposed to adapt them.

Since there are various types of modelling elements, a particular polygon mesh could be associated with one. The selection also depends on the objectives. By way of example, a surface is commonly applied in graphical interfaces. Such (polygon) mesh elements, as shown in Figure 3.8a, and form 3D objects through corresponding information could be the:

- Vertex: A specified point of a data record;
- Edge: A union of vertices;
- Face: A closed group of edges;
- Polygon: Coplanar faces. Similar to a face, depending on the case and program;

- Surface: a closed group of faces.

There are various approaches to store such element information, which describe a resulting (Polygon) mesh (Xiaodong, 2002). Such an approach is the Face-Vertex mesh, which is broadly implemented in graphical interfaces – an example is demonstrated in Figure 3.8b. This approach was utilised in the current study, to store the element information of the 3D models that were developed.

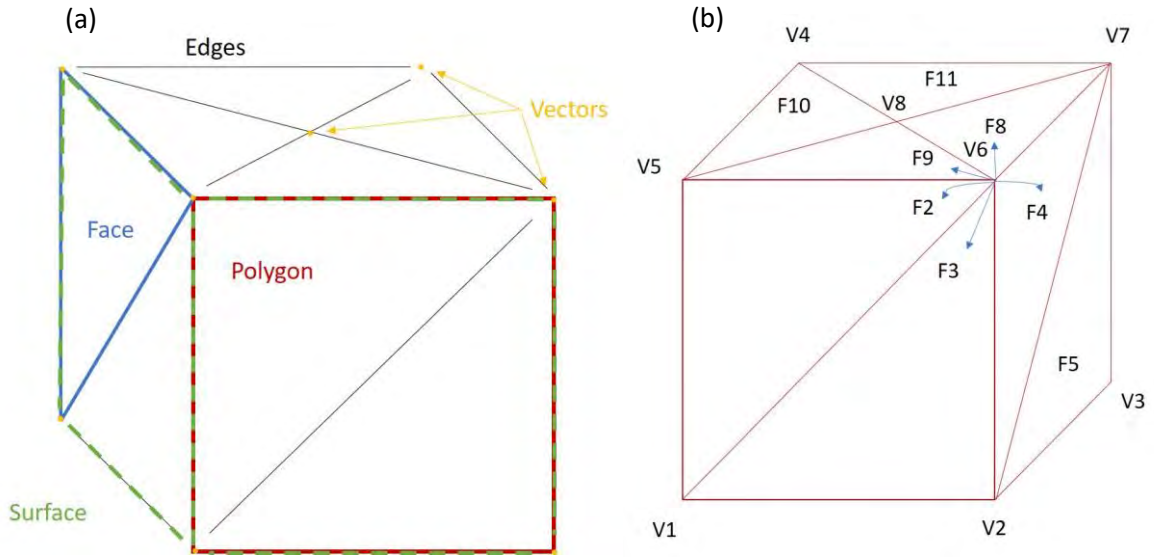

Figure 3.8: (a) Polygon mesh modelling elements represented by corresponding colours, and (b) an example of a Face-Vertex mesh approach through a specific vector, V6.

A 3D geological (ground) model is similarly developed. It comprises of 'interface' models, which use geometrical surfaces via a mesh generation through several methods, or 3D objects of various 3D geometries and boundaries, which use polygon meshes (Mei, 2014).

Therefore, the development of a mesh is crucial in Computer-Aided Design (CAD) modelling and geological modelling. In theory, mesh generation is the process of subdividing an object into a grid of cells of several geometries to simulate it. A 'Finite Element Method analysis'-type mesh is typically used in engineering simulation applications. Its role is to hold information to support the modelling (carry out the analysis).

3.3.9.2 Mesh generation

Meshing is therefore key to provide the proposed approach. It provides the environment for holding (and adapting) all the data used. To carry out the objectives in this study, a (polygon) mesh has been developed. It stored, and transferred between software, the required (geological/structural) data. A mesh that is integrated with BIM was used to store the geotechnical/geological analysis data.

In the present methodology, to generate the (polygon) mesh, the Delaunay Triangulation method (Delaunay, 1934) was used. This method assures that a 'circumcircle' provided to every triangle includes no other point within it (Rajan, 1994). A relevant demonstration of this method is given in Figure 3.9. As Mei (2014) states, this is a "straight-line dual structure" use of the Voronoi diagram (Dirichlet, 1850; Voronoi, 1908; Rajan, 1994). These diagrams are widely used in relevant applications to represent relationships for proximity of set of points (using the nearest-neighbour rule), and have been conducted by implementing several algorithms (Golias and Dutton, 1997; Mei, 2014). Delaunay Triangulation of 3D points is provided using tetrahedra. Delaunay triangulation is a very common approach for meshing, according to Mei (2014), with several algorithmic methods which have been developed to apply it, and the most common one to be the incremental algorithms of Lawson (1977) and the Bowyer-Watson (Bowyer, 1981; Watson, 1981). Delaunay triangulation operates by creating triangles using known points as vertices (Mei, 2014). However, when points and segments together need to be

also triangulated, a ‘constrained Delaunay triangulation’ (Lee and Lin, 1986; Chew, 1989), could be conducted as noted by Mei (2014). By way of example, a mesh using formed by Delaunay Triangulation is demonstrated in Figure 3.10, adapted after Shewchuk (2002).

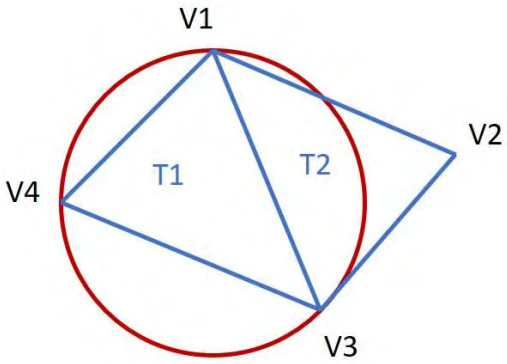

Figure 3.9: A simple example of the Delaunay triangulation method.

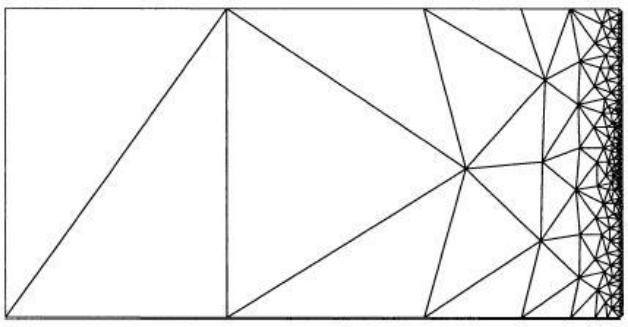

Figure 3.10: An example of a mesh by Delaunay triangulation (Shewchuk, 2002).

In more detail, a matrix representing a set of points for the triangulation is formed, the size of which depends on the number of triangles (or tetrahedra), while its rows specify those triangles through indices associated with the points (Mathworks Inc., 2016). Delaunay triangulation has

been extensively utilised in the present methodology to generate the mesh and for interpolation, and to create the 3D geology-tunnel models.

A process to connect triangulated surfaces, forming the intersections of a mesh, could be provided using Boolean operations. Boolean operation algorithms have been widely used in (3D) modelling (Mei, 2014). More specifically, a Boolean operation has been also adopted here for estimating the intersections, in combination with the Delaunay triangulation, to finalise the 3D tunnel mesh.

More specifically, the mesh is generated using a combination of custom-made scripts (functions) of Delaunay triangulation and Boolean operation, using MATLAB. Further details are provided in the Appendix A. In this research, a typical mesh grid (of the 3D models used) is generated, which is similar to the mesh used in FEM models. The generation of this type of mesh means that potentially an integration with a FEM software could be possible, and hence following assessments using, for example, a FEM analysis, could be made available.

3.3.9.3 Creation of the 3D models

The 3D modelling within this study follows on from the mesh generation, to create the (geometry of the) georeferenced 3D geological and tunnel models. The creation could now be individually described. This was mainly based on the data processes (which supported their development). An example demonstrating the MATLAB outcomes of these processes of 3D modelling is presented in Figure 3.11. It is important to note that they are generated performing interpolation in MATLAB.

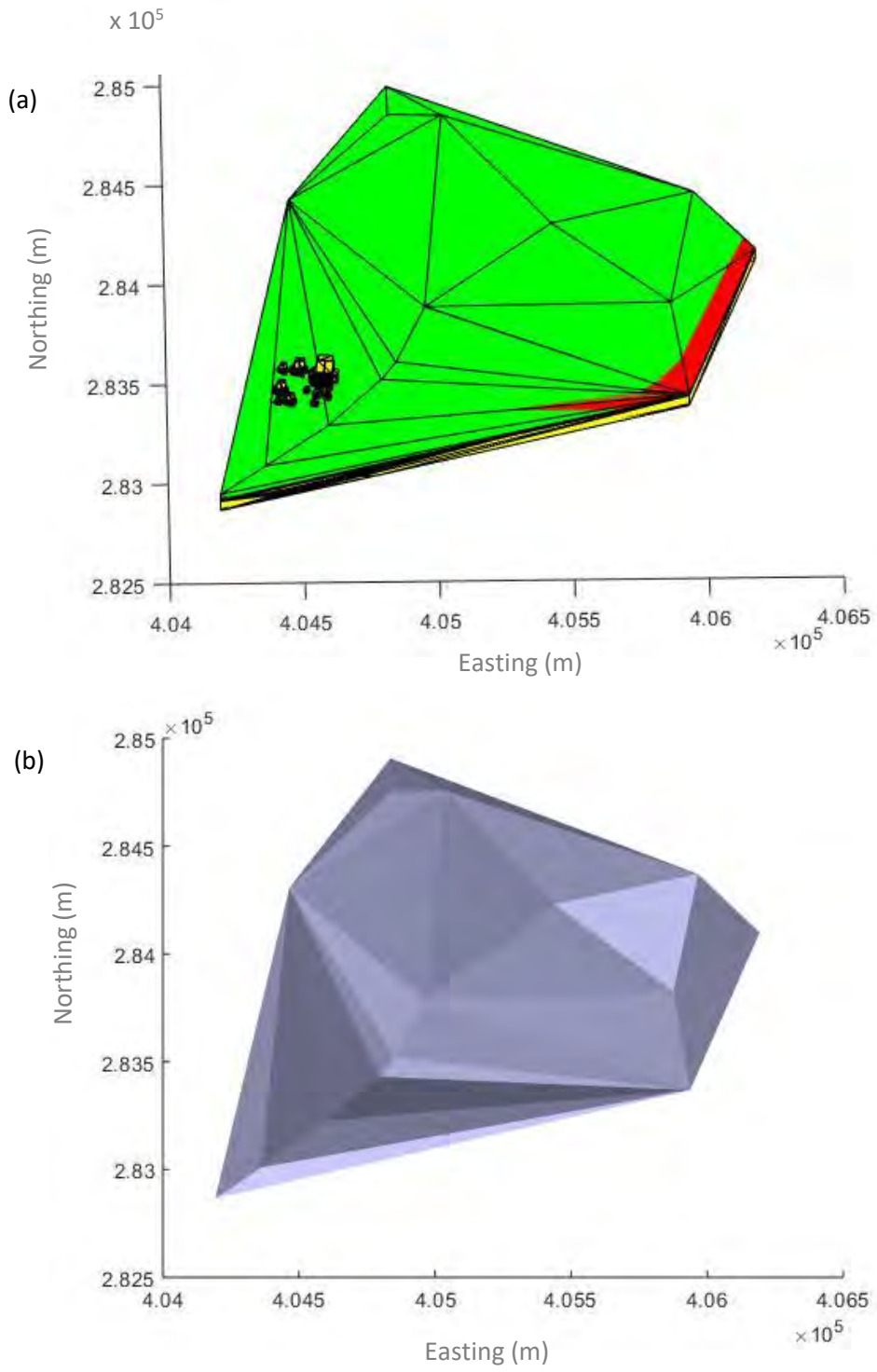

Figure 3.11: Demonstrations of the 3D modelling outcomes here using MATLAB (Mathworks Inc., 2016): (a) of the whole 3D model and (b) of the 3D geology.

Interpolation is a process associated with (geo)statistics, which is widely adapted in 3D (geological) modelling (He et al., 2008; Royse et al., 2009; Dong et al., 2014). This method is used to predict spatial distributions of a geological data in points that available records exist, as described by Thierry et al. (2009). This is done by assigning the data of the geological layers, their margins and their properties, around an available borehole (or other source) data, while considering the relevant uncertainties (Dong et al., 2014). To develop the 3D model, interpolation of properties at the locations of nodes of defined grid takes place, as noted by Chiles and Delfiner (2009). The level of the top and the thickness of the layer are obtained, and then the bottom could be easily estimated (by subtracting them) (Thierry et al., 2009).

In the present methodology, the (3D) spatial distribution of the points around the boreholes was obtained by interpolation from the borehole data. This provided the geometrical and geotechnical/geological information required for the whole 3D modelling, using MATLAB. As already noted, Delaunay triangulation for interpolation was used to provide the 3D geology-tunnel model, (acquiring information from the borehole data) to define the strata (geology) and the boundaries (tunnel).

Likewise, the resulting risk assessment visualisations (as described in the following chapters of this study, which were developed as 3D layers) are generated by interpolation. In particular, the settlement risk distributions (visualisations) were produced using kriging interpolation, as described in relevant sections in Chapter 5.

The topography of the ground surface of the area was developed by (Delaunay) interpolation, using the available borehole data. To demonstrate this interpolation process, an example is illustrated in Figure 3.12, where topographical (and the groundwater) data is processed. Information with respect to the specific model creation is given in the following sections.

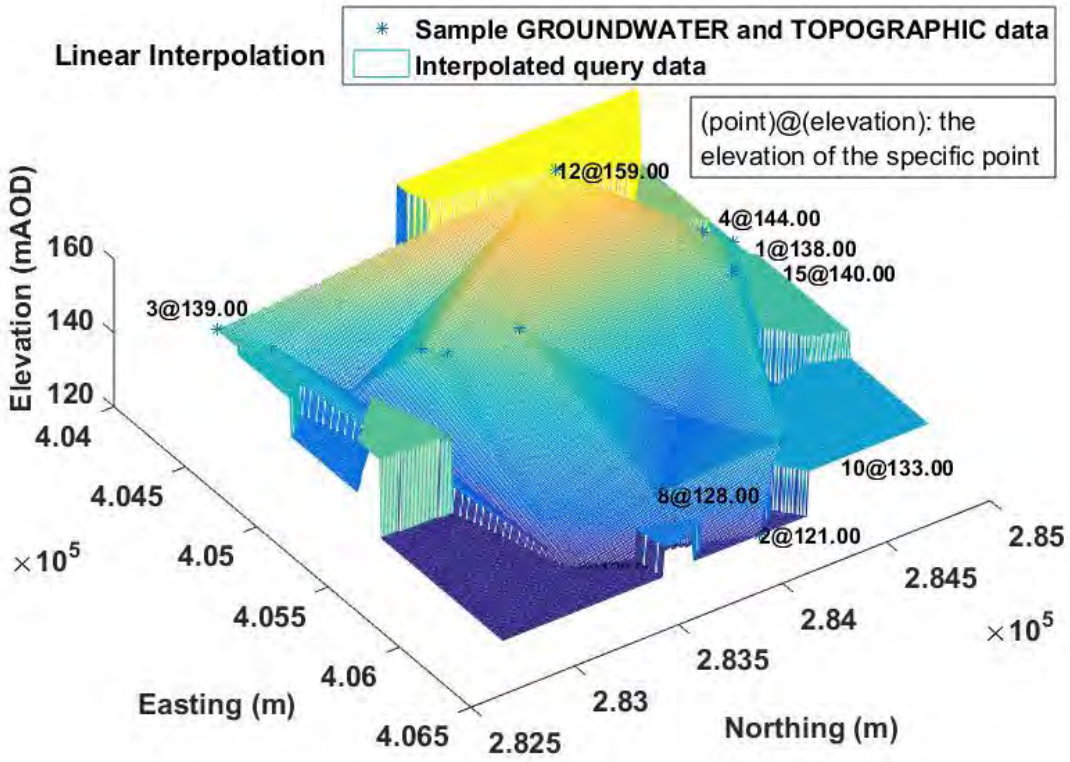

Figure 3.12: A demonstration of the interpolation of, for instance, the groundwater table fluctuation and the topography –using interpolated values taken from borehole data, which was adopted during the 3D modelling process (Chapter 5) from MATLAB.

The next sections provide details about an important aspect in the present methodology in relation to the data processes, i.e. the creation of the georeferenced 3D geological and tunnel models (geometry) using interpolation. These are presented individually in the following subsections.

3.3.9.3.1 3D geology model

The georeferenced 3D geology is developed using (Delaunay) triangulation for interpolation in MATLAB. This process generated the geological layers information for the 3D geology model, using borehole data (Providakis et al., 2019).

Interpolation (using Delaunay triangulation) was carried out, yielding the top and the bottom surface of the layer, using its thickness, and then joining them into a single layer (stratum). Boundaries of the geological strata could be provided by a Delaunay triangulation algorithm (MATLAB). This was an efficient approach, providing complex modelling outcomes for any type of geological layers. In particular, the estimation of the thickness of the topsoil is provided by subtracting the available Digital Elevation Model (DEM) data of the depth of the first layer boundary, which is taken from borehole data (with accurate borehole locations). In addition, the overlapping of geological layer surfaces is negligible. However, there is a limitation in a single-layer interpolation, in the case of large gaps between data points. In the present method, elevations of single-layer surfaces were adjusted to their full extent below the layer or when a gap exists. In addition, to ensure there were not any visible and non-visible gaps or overlapping, the bottom surface is made to be in alignment with the top surface of the layer below.

However, the process of producing the DEM of the study area was challenging, due to the lack of open-access DEM data for the specific area. Therefore, the elevation data was taken from Google Earth (Google Inc, 2018) by collating data for the elevation of 200 onsite spots on Google Earth Pro (Google Inc, 2015). This produced a DEM for the topography of the corresponding area investigated. This was sufficient to demonstrate the proposed framework. It also aligns with the objectives in this research, although more detailed approaches could be used in other studies, depending on their aim and the desired DEM specifications.

As noted, the transfer of the 3D geology model from MATLAB (as shown in Figure 3.11b), into SketchUp was made available using the integrated Ruby API (Ruby, 2017).

The resulting georeferenced 3D geology using this approach is illustrated using various views in Figure 3.13. The (georeferenced) 3D ground modelling task was achieved using borehole

data, and the geological information is taken from the corresponding logs. Other relevant data used was derived from available geological data and 2D maps of the study area. More details regarding the specifications and the data mining are provided in the following chapters. Further information is provided in the Appendix A.

3.3.9.3.2 3D tunnel model

The next stage was to produce the georeferenced 3D tunnel model and place it within the 3D geology model. This was generated by a cylindrical surface (Delaunay) triangulation. A cylindrical surface of a tunnel centreline was produced, using representative values of diameter and depth.

In addition, the reported methodology employed the differential Boolean operation function between the geological model mesh and the tunnel model's mesh, within MATLAB. In this way, an integrated 3D geology-tunnel model (mesh) was generated, as presented with different views in Figures 3.13(a, c) and 3.14. This model is provided using the Ruby API (Ruby, 2017), which exports the generated data needed from MATLAB to SketchUp. Technical information and custom-made scripts used are presented in the Appendix A.

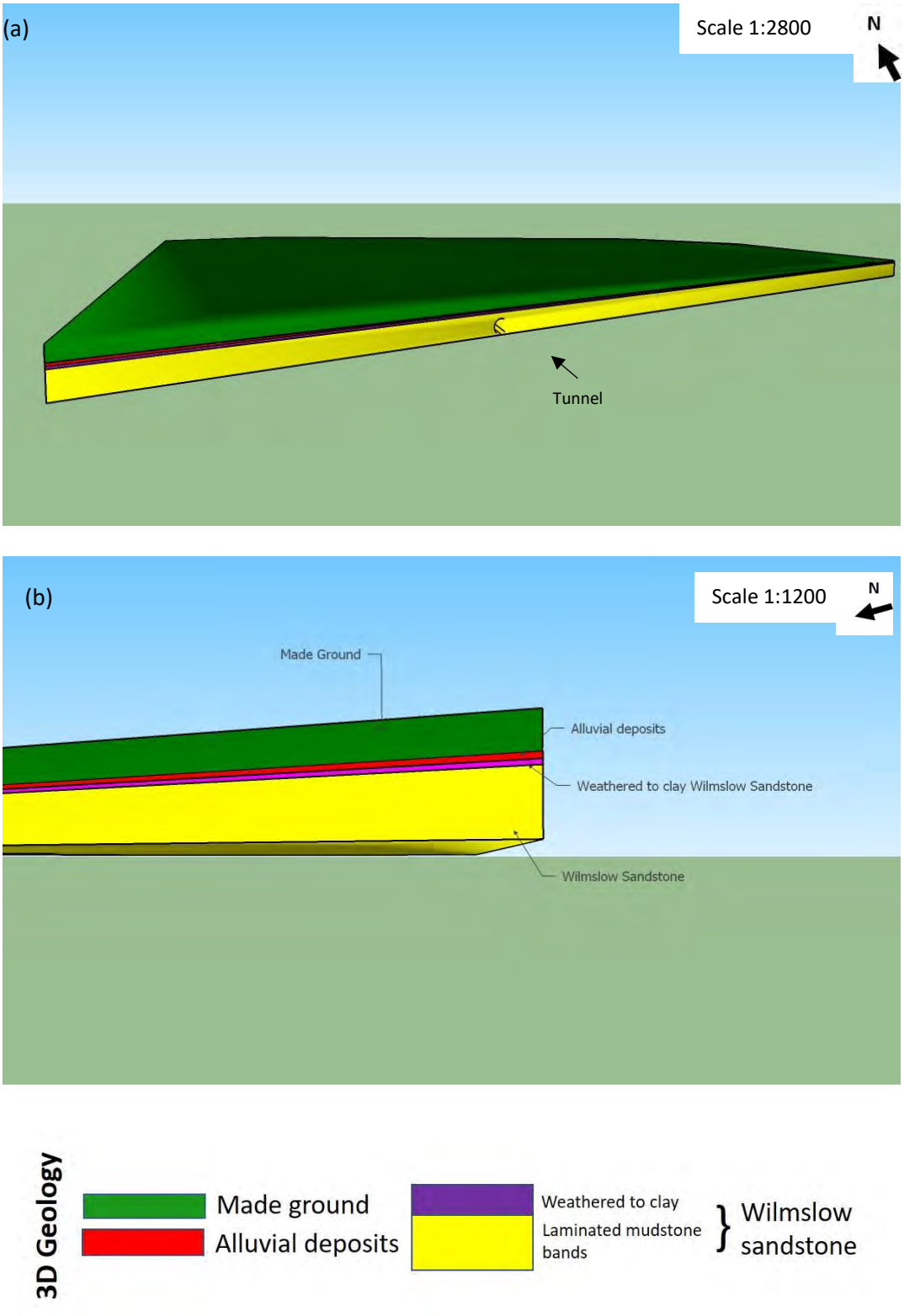

(Figure 3.13 continues in the following page)

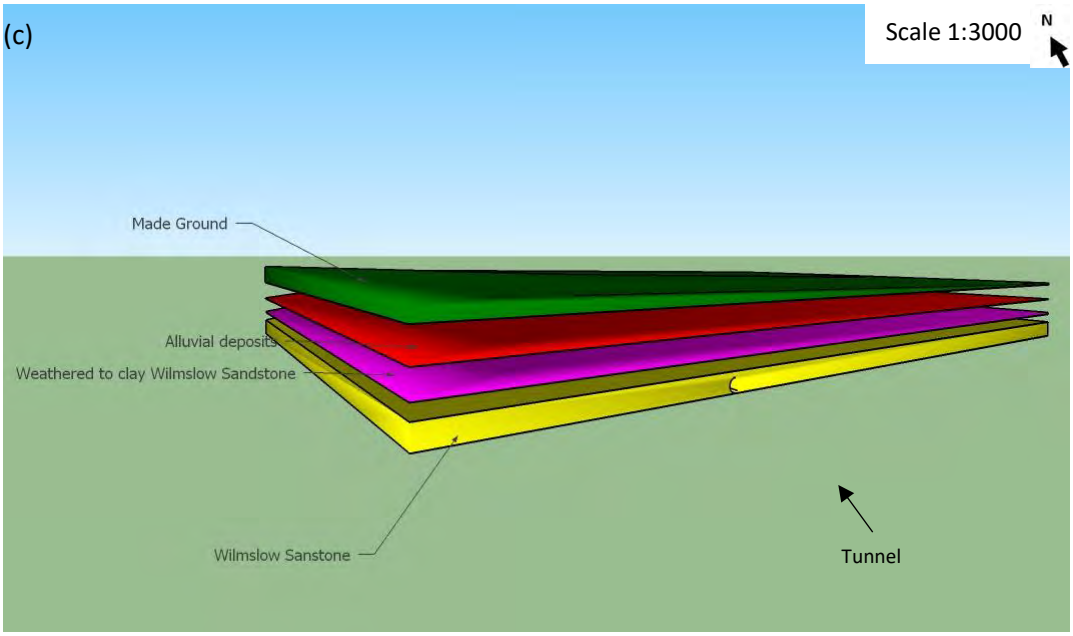

Figure 3.13: Alternative views (a, b) and an exploded view (c) of the resulting 3D geological and tunnel models, using SketchUp after the approach of Providakis et al. (2019).

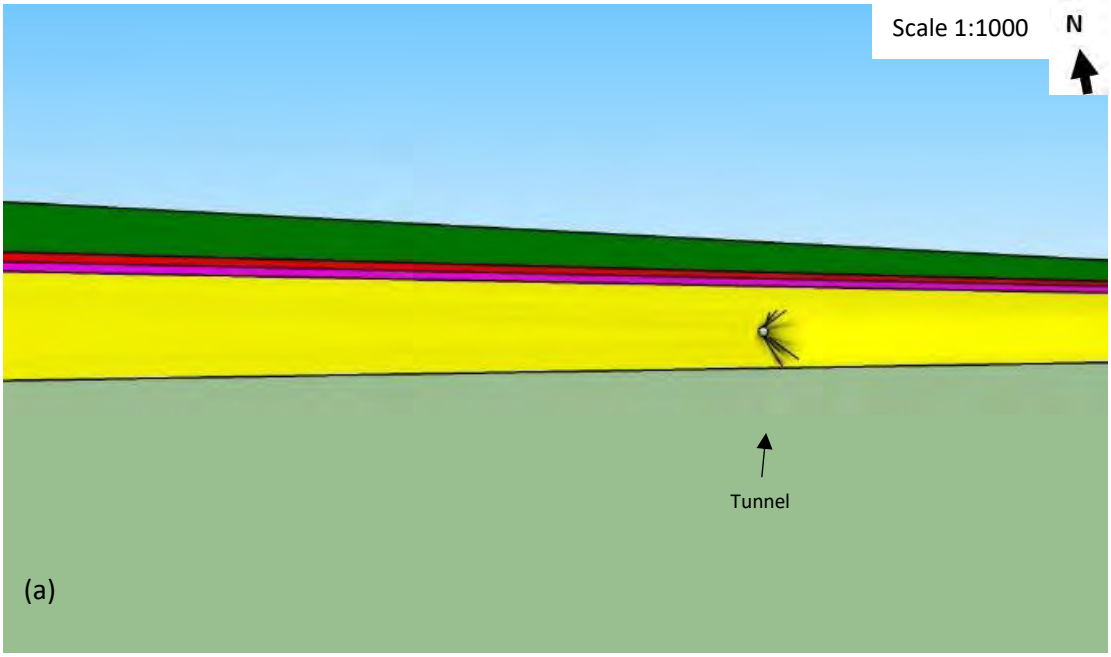

(Figure 3.14 continues in the following page)

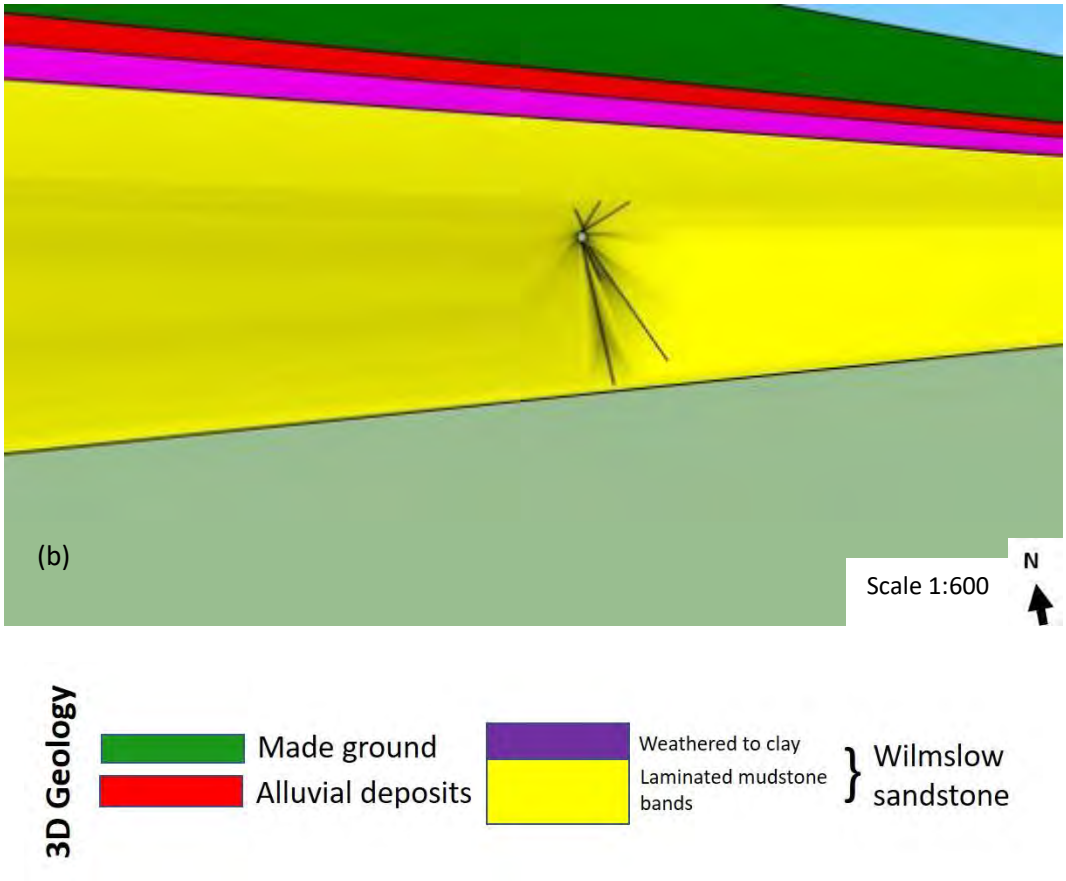

Figure 3.14: 3D Tunnel object by a (a) wider and (b) closer view in SketchUp.

In terms of the resulting BIM visualisations the tunnel was a 3D object placed within the 3D geology model. The idea was to generate ground-structure interactions caused by tunnelling, and hence several positions of the tunnel with respect to the adjacent buildings could be provided.

3.3.9.4 3D objects concept

Key in this methodology was that the BIM building information was converted using SketchUp to a compatible format with MATLAB so that the analysis could take place. This took place after importing those models into SketchUp using IFC. The resulting analysis could now include ground (adapted from MATLAB) and structural information (BIM) to be assessed

within MATLAB. This information could then be exported to SketchUp to visualise clearly the results (or to be extracted to other BIM software, if required), as presented in the previous section (Chapman et al., 2019; Providakis et al., 2019). The resulting geohazard risk assessment visualisations (described in the following chapters of this research) are provided as an extra layer (which is a 3D solid object (Chapman et al., 2019; Providakis et al., 2019)). Hence, all the geotechnical/geological and structural information required, which is taken from the prior analysis is then 'projected' onto this layer.

In the proposed approach, the data integration using the power of BIM provided the 3D geology-tunnel-building models. The idea was to use the data integration aspects of this research to provide a tool which could be compatible with other modelling/analysis and visualisation tools to align with sustainable decision-making.

3.3.10 Integration with geospatial and secondary assessment tools

Further modelling and visualisation tools have been used to achieve an adequate risk assessment that was integrated with BIM. This was done using, and integrating with, Google Earth Pro (Google Inc, 2015) and Google Earth (Google Inc., 2018) tools. In fact, Google Earth Pro (Google Inc, 2015), which is a widely used mapping tool, is regularly utilised for geo-related applications, such as the one described here. It can be used as a 'spatial modelling tool' or as a 3D modelling tool for detailed visualisation or support.

Visualisation applications using Google Earth (Google Inc, 2018) are provided in the following chapters. These included integrated views of satellite images/maps for the generated 3D models and assessments, such as the locations of boreholes. This could provide further understanding, and therefore support the analysis. Maps of the study areas have been imported from Google

Earth showing the actual site and area of investigations. These ‘maps’ are also marked with features to provide a better understanding of the processes used by showing:

- spots of the location of boreholes;
- 3D borehole log ‘tubes’ objects on those locations;
- analysis resultants, i.e. maps with contourlines, for enhanced visualisations of the distribution of parameters after the analysis.

An integration of the present analysis data with Google Earth (Google Inc., 2016) has been achieved. This used the Keyhole Markup Language (KML), which is currently incorporated into Google Earth (Google Inc., 2018). It is an accepted format for indicating geographic information visually, typically implemented in Google Earth (Google Inc., 2018) and Google Earth Pro (Google Inc., 2015). In this study, a conversion of the borehole and analysis information used was done to KML by producing subsequent custom scripts and adapting a toolbox using MATLAB (details in the Appendix A) (Mathworks Inc., 2016). These provided the geographic information for the borehole locations, the borehole logs as tubes placed on those locations and the contourlines from the present analysis data. In addition, the (Google Earth) spatial modelling tools allowed to generate topographic measurements, supporting the present methodology. As noted previously, this is generated by collating the elevations of on-site points in Google Earth Pro (Google Inc., 2015). Further details about this process given in Appendix A.

Finally, the idea was to create a preliminary assessment tool to advance ground investigation, and hence a more detailed or ‘secondary’ analysis software (tool) to be able to use the information (results) from the present framework. Therefore, the proposed approach makes all the information (data from the proposed tool) to be compatible with another analysis software

(tool). Hence, the information from this tool could be processed to another software, which could allow a more detailed analysis to follow, as required. By way of example, an integration with a FEM analysis software for a 'secondary' assessment analysis is made available.

3.4 Methodology structure

The relationship between Chapters 4, 5 and 6 is presented in Figure 3.15. In addition, the structure of the whole approach is presented in a flow chart in Figure 3.16. In this flow chart, the chapters (steps of the processes used) are presented using different colours (Figure 3.16). The data processes to create the 3D geology-tunnel-building model (black colour) produced the basis of the whole modelling, where the rest of the framework is built upon. The analysis and resulting visualisations steps of Chapter 4 are shown in blue. Likewise, the steps of Chapter 5 are shown in green. Chapter 6 follows on from (the initial analysis) stage of Chapter 4, and then proceeds along the orange (analysis) steps of the flow chart.

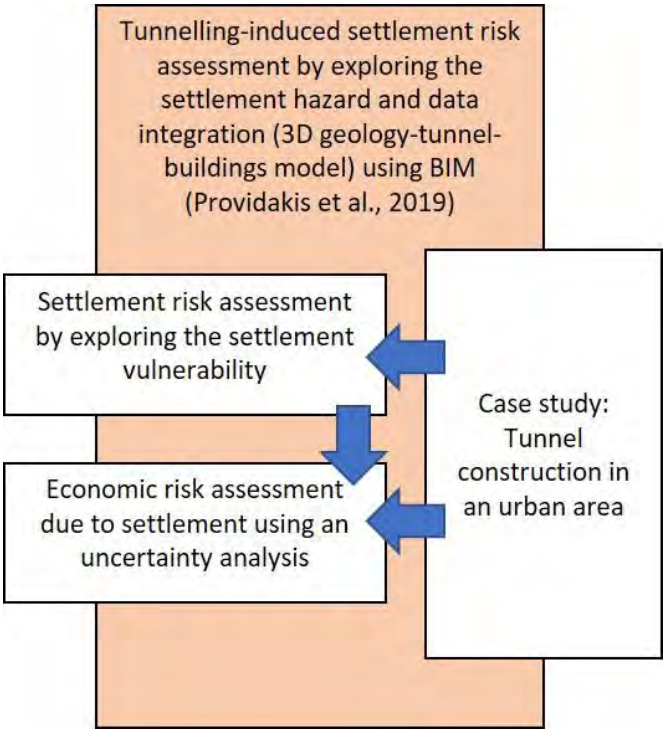

Figure 3.15: The relationship between Chapters 4, 5 and 6.

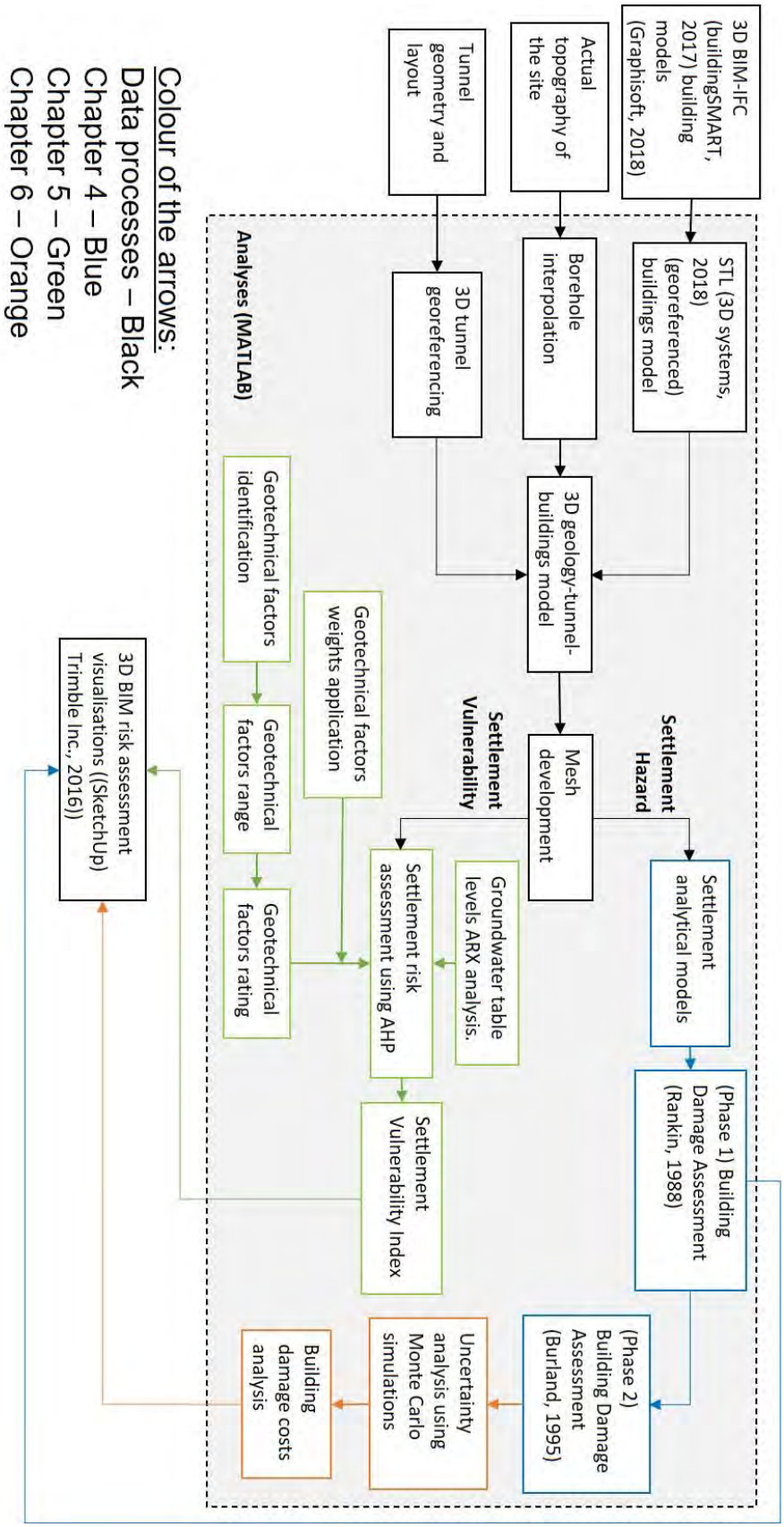

Figure 3.16: The research methodology.

4 TUNNELLING-INDUCED SETTLEMENT HAZARD ESTIMATION USING ANALYTICAL MODELS AND BIM

4.1 Overview

In this chapter, the previously described methodology (Chapter 3) is applied to develop a framework for assessing geohazard risk, in this case tunnel-induced ground settlement. In this chapter particularly, the risk is estimated by exploring the tunnelling-induced Settlement Hazard. This is done by employing Analytical methods and building damage assessments to identify the building damage. This is applied in this research, for example, for a tunnel construction in a soft ground. A tunnelling-induced ground settlement risk analysis is initially proposed using empirical/analytical models, under 'green-field' conditions, through the resulting settlement trough (Peck, 1969). Among many methods, a widely used analytical method is adopted here, as a representative example, to build this methodology proposed by Loganathan and Poulos (1998) and Loganathan (2011).

In addition, a robust settlement risk assessment analysis would be achieved by exploring the Settlement Hazard with respect to the building characteristics. Therefore, this takes place in two phases. A Phase 1 Building damage assessment, where the damage extent of this Hazard is provided through. Buildings with a higher (moderate to high) risk proceed to a Phase 2 Building Damage Assessment, which investigates the damage severity of this Hazard. This secondary Building Damage Assessment (Phase 2) provides detailed damage indications for every building using the critical tensile strains (Limiting Tensile Strain Method –LTSM) involving the 'hogging' or 'sagging' (from the settlement trough) states in relation to a building (Burland et al., 1977; Burland, 1995; Mair et al., 1996). Integration with BIM takes place to extract geotechnical and structural parameters from the available building models used (e.g. building

dimensions and structural component information), as described in Chapter 3 (Methodology) and presented by Providakis et al. (2019).

This would provide a 3D georeferenced 'map', using the Ordnance Survey's (OS) coordinate system that clearly models the investigated urban area via generating 3D geological-tunnel-buildings models, using BIM. In addition, 3D geohazard 'maps' with the boundaries of the zones affected, in this case due to the Settlement Hazard caused by a tunnel construction, using Phase 1 assessment, are provided. This is conducted by risk-based colourmaps of the ground surface and buildings. In Phase 2, the demonstrations finalise the current settlement risk assessment via showing each building damage risk caused by this Settlement Hazard. A flow chart showing the method used is demonstrated in Figure 4.1.

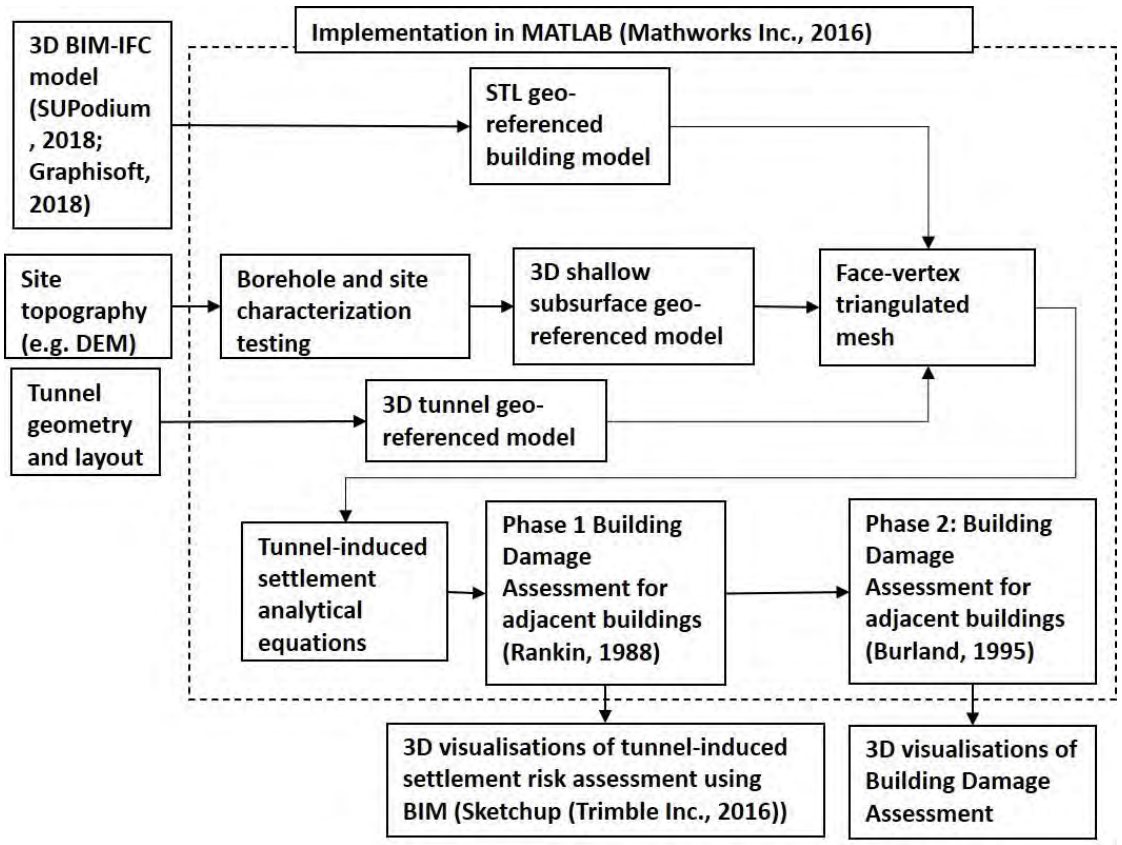

Figure 4.1: A flow chart showing the methodology adopted in Chapter 4 (after Providakis et al., 2019).

4.2 Previous studies to estimate ground movements due to tunnel construction

The methodology in this study uses the ground settlement caused by tunnel construction to provide a representative example of a geohazard. Hence, to provide a robust analysis for an information system using this geohazard, its detailed characteristics and estimation methods are required.

There has been a large amount of research on adapting methods to estimate ground settlements due to tunnelling (Giardina et al., 2018; Ding et al., 2019). These have been focused on soft ground –in this study soil to soft rocks are accounted. They have been categorised as empirical, analytical and numerical methodologies (models). A detailed description of the specifications/characteristics of their use in relevant applications is provided in the next section.

4.2.1 Settlement trough

Empirical/analytical methodologies have been widely used to estimate tunnelling-induced ground settlements, relating to soft grounds. They use an inverted Gaussian curve, known as 'settlement trough', to describe those settlements under greenfield conditions, as presented in Figure 4.2. This curve is formed (under green-field conditions) to provide the ground movement characteristics (Peck, 1969). This curve has the largest settlement depth directly above the tunnel centreline. The curve is divided into the hogging and sagging parts (which are described in a following section in this chapter). The settlement trough in relation to the tunnel is shown in Figure 4.2.

4.2.2 Empirical methods

The use of the settlement trough and its relevant characteristics are important in achieving the best possible results, using an empirical approach. The tunnelling induced settlement is

provided by estimating the maximum settlement. This is carried out along the sagging and hogging parts of the curve, created above the centreline of the tunnel, as shown in Figure 4.2.

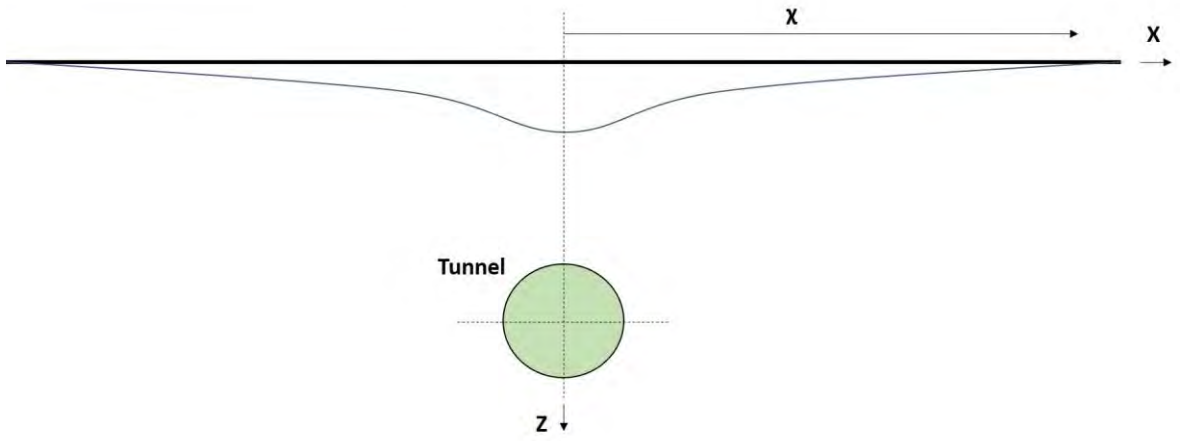

Figure 4.2: The settlement trough developed about a tunnel in soft ground, adapted from O'Reilly and New (1982), Rankin (1988), Clarke and Laefer (2014) and Providakis et al. (2019).

4.2.2.1 Surface settlement

Peck (1969) collated several in-situ data to provide an estimation of this settlement cause by tunnel construction, implementing the settlement trough, as shown in Equation (4.1).

$$S = S_{max} \cdot \exp\left(\frac{-x^2}{2i^2}\right) \quad (4.1)$$

where *S* is the transverse settlement with a distance x from the tunnel's centreline; *Smax is* the maximum settlement at x=0; *i* is the point of inflection with values depending on relevant ground parameters.

Table 4.1 lists i values, which are proposed by several studies on tunnelling-induced ground movements. This indicated the significant impact of the ground conditions and properties on the resulting i value.

Table 4.1: Recommended i values with respect to the ground (where H is the depth of the tunnel springline and R is the radius of the tunnel) (table adapted from Loganathan, 2011).

Name	i value	Comment
Peck (1969)	$\frac{i}{R} = (\frac{H}{2R})^n$: n=0.8 to 1.0	Based on field observations.
Atkinson and Potts (1979)	$i = 0.25(H + R)$ for loose sand $i = 0.25(1.5H + 0.5R)$ for dense over-consolidated clay	Based on field observations and model tests.
O'Reilly and New (1982)	$i = 0.43H + 1.1$ for cohesive soil $i = 0.28H - 0.1$ for granular soil	Based on field observations of tunnels in the UK.
Mair (1993)	$i = 0.5H$	Based on field observations worldwide and centrifuge test.
Attewell (1977)	$\frac{i}{R} = a(\frac{H}{2R})^n$: a=1 and n=1	Based on field observations on tunnels in the UK.
Clough and Schmidt (1981)	$\frac{i}{R} = a(\frac{H}{2R})^n$: a=1 and n=0.8	Based on field observations on tunnels in the US.

Among the parameters involved in the settlement estimations, the volume loss was important to be estimated. This parameter provides important information about the ground deformation

above the tunnel centreline. Hence, Mair (1993) provided Equation (4.2) for the maximum ground settlement due to tunnelling.

$$S_{max} = \frac{0.313\varepsilon_0 D^2}{i} \quad (4.2)$$

where ε_0 is the average ground loss; D the tunnel diameter; i is the inflection point.

However, there are some limitations when using empirical methods in relevant studies, which need to be considered, as implied by Chapman et al. (2017). Rankin (1988) and Chapman et al. (2017) noted that these could be associated with:

- subsurface and horizontal ground movement prediction inaccuracies, and
- limitations due to ground variability problems.

The next part of the empirical methods for the ground settlement concerns the subsurface movements. Typical estimations for this type of ground movements for different ground conditions were proposed by Atkinson and Potts (1979) and Mair (1993), in which a Gaussian curve is also produced alongside tunnelling excavations. More detailed aspects of these ground movements are provided by Chapman et al. (2017).

Empirical methods were broadly used for these tunnel-induced ground movements. However, ground variability and the need to use complex properties lead to the implementation of the analytical methods for ground movement estimations.

4.2.3 Analytical methods

Efficient findings have been obtained from the empirical approaches in estimating (correlating parameters inducing) the subsequent settlement due to tunnel construction developments.

However, they do not account for all the factors involved. Hence, analytical methodologies have been widely accepted and used for the estimation of the tunnelling-induced settlements. Advanced relevant approaches to assess related settlement risk, considering all the factors involved, have been generated.

Analytical methods used 'closed-form' equations to estimate efficiently tunnel induced settlements. In fact, their successful application involves carefully taking into consideration of (Loganathan, 2011; Giardina et al., 2018):

- construction approach used, such as Tunnel Boring Machine (TBM) specifications;
- tunnel geometrical characteristics;
- groundwater;
- initial stress-state;
- strains and stresses within the tunnelling soil layer.

Initially, tunnel induced ground settlements occurring in a homogeneous, isotropic and incompressible soil were estimated by Sagaseta (1987) via incorporating volume (ground) loss findings of the involved soil, which is indicated from the ground surface. This was enhanced to a homogeneous but elastic ground by Verruijt and Booker (1996). Extended settlement outcomes of incorporating the Poisson's ratio in addition to 'oval-shaped' deformations of the tunnel centreline were also obtained by Verruijt and Booker (1996). Thus, Equations (4.3) and (4.4) are provided, for ground settlement and horizontal movements, respectively (Verruijt and Booker, 1996).

$$U_z = -\varepsilon R^2\left(\frac{z_1}{r_1^2}+\frac{z_2}{r_2^2}\right)+\delta R^2\left(\frac{z_1\left(kx^2-z_1^2\right)}{r_1^4}+\frac{z_2\left(kx^2-z_2^2\right)}{r_2^4}\right)+\frac{2\varepsilon R^2}{m}\left(\frac{(m+1)z_2}{r_2^2}+\frac{mz\left(x^2-z_2^2\right)}{r_2^4}\right)-$$

$$2\delta R^2 h\left(\frac{x^2-z_2^2}{r_2^4}+\frac{m}{m+1}\frac{2zz_2\left(3x^2-z_2^2\right)}{r_2^6}\right) \quad (4.3)$$

$$U_x = -\varepsilon R^2 \left(\frac{x}{r_1^2} + \frac{x}{r_2^2}\right) + \delta R^2 \left(\frac{z_1\left(x^2 - kz_1^2\right)}{r_1^4} + \frac{x\left(x^2 - kz_2^2\right)}{r_2^4}\right) - \frac{2\varepsilon R^2}{m}\left(\frac{1}{r_2^2} + \frac{mzz_2}{r_2^4}\right) - \frac{4\delta R^2 xH}{m+1}\left(\frac{z_2}{r_2^4} + \frac{mz\left(x^2 - 3z_2^2\right)}{r_2^6}\right) \quad (4.4)$$

where *ε:* uniform radial ground loss; *δ:* ground deformation due to the ovalisation of tunnel lining (long term); $z_1 = z\text{-}H$; $z_2 = z+H$; $r_1^2 = x^2+z_1^2$; $r_2^2 = x^2+z_2^2$; *R:* tunnel radius; *H:* tunnel axis depth; $m = 1/(1\text{-}2v)$; $k = v/(1\text{-}v)$; *v:* Poisson's ratio of the soil.

The previous indications were revised by Loganathan and Poulos (1998), who specified boundary conditions accounting for the ground (volume) loss while tunnelling. Additionally, Loganathan and Poulos (1998) explained that ground deformation takes place along several construction phases, creating an oval-shaped vacuum around the tunnel with 75% within the crown area.

To provide the ground deformation characteristics, the subsequent ground loss characteristics should be defined, as mentioned by Loganathan and Poulos (1998), who enhanced the indications of Verruijt and Booker (1996). The wedge angle, known as limit angle (β), $\beta = 45° + \varphi/2$ (where φ is the friction angle), is drawn from the parallel line to the ground surface that passes through the tunnel centre (spring line) to the settlement trough width on the ground surface, as shown in Figure 4.3 (Loganathan, 2011). In addition, Loganathan (2011) explained that sandy soils have an angle of $\beta = 45° + \varphi/2$. For clays, this angle is assumed to be almost equal to β=45° (Cording and Hansmire, 1975). As a result, most of the ground movements are within this angle frame (wedge). Successful estimations have also been provided using the closed-form equations for each ground movement, which were adopted by Loganathan and Poulos (1998).

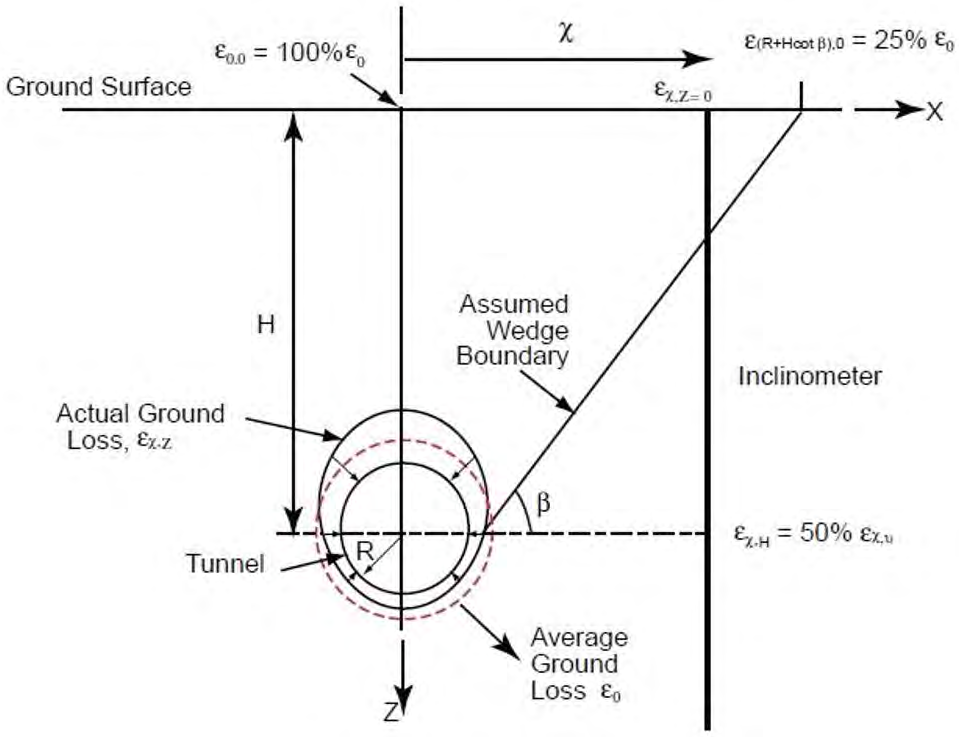

Figure 4.3: Ground deformations and ground loss characteristics (adapted from Loganathan and Poulos, 1998; Loganathan, 2011) (where $\varepsilon_{x,z}$ is the equivalent ground loss parameter).

4.2.3.1 Surface settlement

Hence, efficient estimations for the surface settlements could be obtained using the Equation (4.5) by Loganathan and Poulos (1998) and Loganathan (2011).

$$U_{z=0} = \varepsilon_0 R^2 \frac{4H(1-\nu)}{H^2+x^2} exp\left\{-\frac{1.38x^2}{(Hcot\beta+R)^2}\right\} \quad (4.5)$$

where R is the radius of the tunnel, z is the depth below ground-surface, H is the depth of tunnel axis level, ν is the Poisson's ratio of soil, ε_0 is the average ground loss ratio (not a displacement), x is the lateral distance from the tunnel centreline, and β is the Limit angle: β= 45 + φ/2 and φ is the friction angle.

Equation (4.5) (Loganathan and Poulos, 1998; Loganathan, 2011) provides a successful estimation of ground movements, accounting numerous factors in the relevant analysis (closed-form equation). Hence, it could be considered an applicable approach among analytical methods, and this explains its wider use in relevant research studies. Therefore, it is selected to provide the analysis parts in the present study.

Except the surface ground movements, analytical models have been conducted for the estimation of subsurface movements, such as by Loganathan and Poulos (1998) and Loganathan (2011). It is decided that this study will not focus on these ground movements, although future work based on the present framework, could be developed.

4.2.3.2 Horizontal movement

In addition, another important aspect is that the vertical is double the horizontal movement at spots on the tunnel's springline, as stated by Loganathan and Poulos (1998). The horizontal movements or lateral deformation is provided using the closed-form Equation (4.6) by Loganathan and Poulos (1998) and Loganathan (2011).

$$U_x = -\varepsilon_0 R^2 x\left[\frac{1}{x^2+(H-z)^2} + \frac{3-4\nu}{x^2+(H+z)^2} - \frac{4z(z+H)}{(x^2+(H+z)^2)^2}\right] \cdot \exp\left\{-\left[\frac{1.38x^2}{(Hcot\beta+R)^2} + \frac{0.69z^2}{H^2}\right]\right\} \quad (4.6)$$

where R is the tunnel radius; z is the depth below ground surface; H is the depth to tunnel axis; ν is the Poisson's ratio of the soil; ε_0 is the average ground loss ratio (no displacement); x is the lateral distance from tunnel centreline; β is the Limit angle of 45 + φ/2.

Apart from the empirical/analytical, the numerical models have been also studied thoroughly for estimating the settlements due to tunnelling. These advanced methods use more intensive computer-aided data and analyses.

4.2.4 Numerical methods

Numerical methods are widely employed in engineering analyses, including tunnelling analyses. Their wide use is based on their advanced analyses to handle complex and ground characteristics, their geometries, and on the large amount of ground data records, e.g. the borehole data. By way of example, Xie, et al. (2016), Giardina et al. (2017), Avgerinos et al. (2017), Amorosi et al., (2019) and Ding et al. (2019) achieved reasonable results on several case studies, however it was noted that limitations could occur.

The broad use of numerical analyses and consequently FEM modelling is also associated to complex ground estimations. Therefore, a substantial computer use and capacity would be required and accompanied with computer expertise. Relevant research is so far ambiguous, concerning an appropriate method for the estimation of tunnel-induced settlements, and although it could be based on the objectives of a study, attention needs to be given on (Loganathan, 2011):

- Soil-structure interactions alongside the tunnel centreline;
- The impact from the ground loss;
- The stress/strain characteristics of the soil along the tunnel centreline.

4.2.5 Summary of the methods

To sum up, the previously described methods have been adopted for the estimation of the settlement caused by a tunnel construction. As noted, Equation (4.5) after Loganathan and Poulos (1998) and Loganathan (2011) is employed here in combination with building damage assessments to provide a representative analysis for the ground-building interactions and elaborate the present methodology. These building damage assessments which were used

within this part of the methodology, are described in the following sections. But, initially, the study area that the current 3D modelling takes place has to be described.

4.3 Georeferenced 3D geology-tunnel-buildings model of the study area

A 3D model has been developed, using the data process and integration aspects, as described in the Methodology (Chapter 3). This is achieved by the use of a georeferenced 3D geological, tunnel and building model (which includes a typical mesh to assign and transfer the information (section 3.3.9)).

In this chapter, a study area was selected to provide the initial source of geological information (from borehole records), as shown in Figure 4.4 (Google Earth, 2018). This site was chosen to provide the 3D underground modelling and settlement risk assessment for this study due to the availability of ground investigation data in relation to the construction of the new National Buried Infrastructure Facility (NBIF). The ground investigations took place between 2016 and 2017 and consisted of 9 boreholes. Their locations are demonstrated in Figure 4.5 (Google Earth, 2018), in which two representative borehole (BH2, BH3) data examples used, were marked. The georeferenced 3D shallow subsurface model consists of 3D geological strata, and this section utilized the borehole records data from those ground investigations.

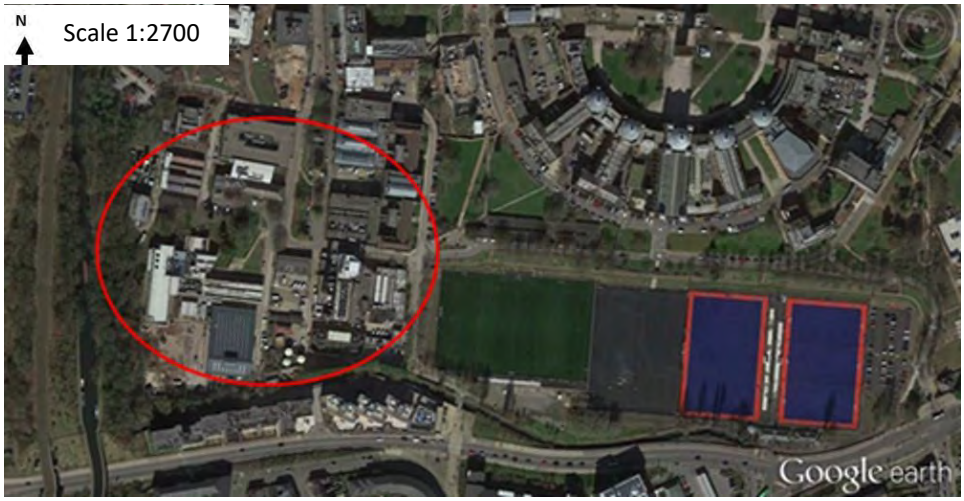

Figure 4.4: The location of the study area of this chapter using a satellite image by Google Earth (Google Inc., 2018) adapted from Providakis et al. (2019).

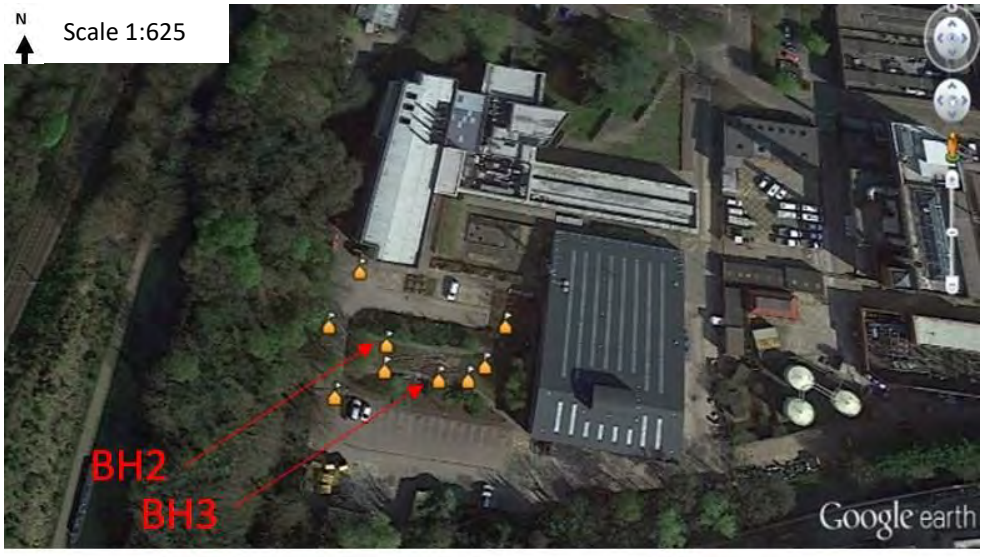

Figure 4.5: The location of the boreholes used, using a satellite image by Google Earth (2018) (Providakis et al., 2019). Boreholes BH2, BH3 are marked.

This study area is located in the southwestern corner of the campus of the University of Birmingham, approximately 4 km south-west of the city centre of Birmingham, UK (Figure 4.4). It has a National British Grid reference (OSG-36) of 404420, 283310 (approximation with British National Grid reference SP 044 832 UK). The area is mostly levelled, apart from an approximately 2m high mound of about 40m x 20m, in the centre. There is a slight southward fall of level towards Bourn Brook, while ascending towards the embankment of Worcester and Birmingham canal that runs along the western boundary. Bourn Brook has undergone straightening in the past, with one known in 1888, and hence brick wall banks are found adjacent to the setting.

The site has an area of approximately 2.5km^2. The ground investigation indicated a topsoil of made-ground that underlies the whole site, with superficial alluvial deposits below it. The Wilmslow Sandstone is underlying the bedrock, which has a weathered to clay top and mudstone bands, below.

Tables 4.2 and 4.3 provide representative data from the borehole logs of BH2 and BH3, adapted from the ground investigation for the site. These are representative examples of the information used to create the 3D geological strata for the 3D geology model. Their locations in relation to the other seven boreholes drilled as part of the ground investigations, are shown in Figure 4.5. The nine borehole logs and the geological maps taken from the British Geological Survey (UKRI NERC, 2018a, b; maps available online and provide geological information of the wider area), consists the information used in forming the 3D model of the examined area.

Table 4.2: A borehole log summary for BH2 (Providakis et al., 2019).

Geological stratum – BH2	**Depth (m)**
Made ground (brown sand, sandy gravel, red-brick gravel and concrete)	0-3.3
Gravel (dense brown sandy clayey)	3.3-6.3
Clay (stiff brown)	6.3-6.5
Sandstone (very to extremely weak and thinly bedded / horizontal discontinuities, with very thin mudstone bands)	6.5-20.5 (borehole completed)

Table 4.3: A borehole log summary for BH3 (Providakis et al., 2019).

Geological Stratum – BH3	**Depth (m)**
Made ground (gravel, red-brick gravel, cobbles with concrete)	0-5.0
Clay (stiff brown sandy)	5.0-6.0
Sandstone (very weak brown / sub-horizontal discontinuities, with a 30mm band of brown sandy clay)	6.0-6.85
Clay (stiff brown locally grey gravelly slightly sandy)	6.85-7.6
Sandstone (very weak brown / horizontal to sub-horizontal discontinuities, with thin mudstone bands)	7.6-20.5 (borehole completed)

To demonstrate the methodology and how it can be used to assess hazards, and in this case the effect of tunnel-induced ground movements, a cylindrical 3D model of a 'fictional' tunnel with a diameter of 12m was included at approximately 20m depth to the tunnel centreline (Providakis et al., 2019).

BIM/IFC building models taken from SUPodium (2018) have been superimposed on the rest of the 3D model, using the method described in the previous chapter. As presented in the Methodology (section 3.3), this is based on the capabilities of the BIM visualisation software of SketchUp, which is used here to import IFC files and export the information using the STL format. After the superimposition of the buildings on the 3D model, the assessment analysis adopted in this chapter, could be conducted. The final 3D geology-tunnel-building model in this chapter is illustrated in Figure 4.6.

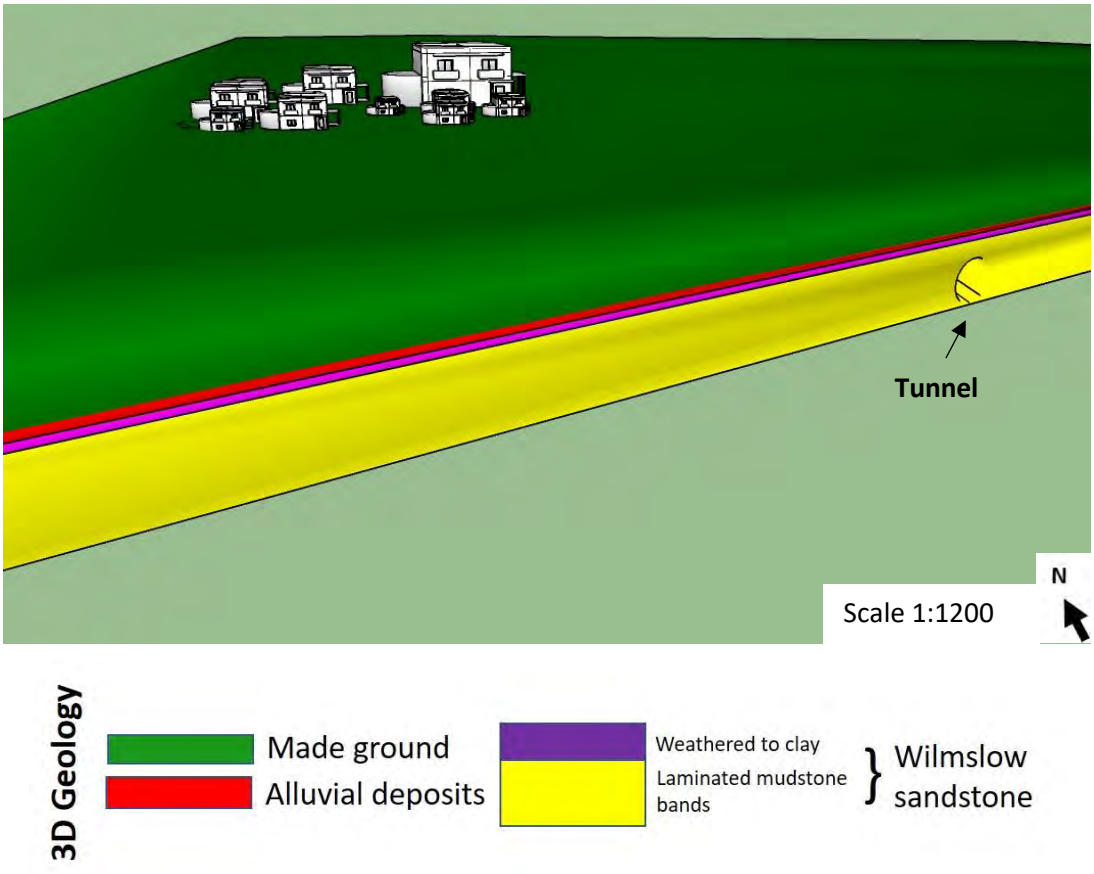

Figure 4.6: A view of the 3D geology-tunnel-buildings model using BIM on SketchUp after Providakis et al. (2019).

4.4 3D tunnel induced settlement risk: Building Damage Assessment

4.4.1 Introduction

Building damage for buildings on shallow foundations affected by ground movements could affect the following (Loganathan, 2011):

- Aesthetical – indicating exterior changes on buildings;
- Services – indicating cracking/damaging of particular building parts (affects the weather performance);

- Stability – indicating that a building is unstable or at risk of collapse, and measures should be taken.

The related building damage risk assessment is broadly studied in geotechnical research and applied in industry (Loganathan, 2011). An integrated process with an application aligning with the objectives of this study is presented in the following sections.

The analytical model proposed by Loganathan and Poulos (1998) and Loganathan (2011) has been employed in combination with the BIM-building file information. This was carried out to provide a system for analysing and demonstrating thoroughly the settlement damage due to tunnel constructions to adjacent structures. Among many approaches from relevant literature for the assessing building (damage) risk due to tunnel construction, the reported methodology presents one, as an example of the process. Emphasis has been given on its integration within a BIM-based framework presented in this study, rather than suggesting that this is the only/best option to use. This approach is provided by two Phases of the Building Damage Assessment in the present chapter.

4.4.2 Phase 1 Building Damage Assessment (Damage extent)

After integrating all the 3D BIM/IFC building models in the case area with the 3D geology-tunnel-buildings modelling process, a Phase 1 Building damage assessment was conducted (Figure 4.1). Building damage risk categories were estimated using Table 4.4, adapted by Rankin (1988) and CIRIA (1996), which implemented the maximum settlement of ground beneath each building (footprint) and the maximum slope below those buildings. This indicated the (building) damage extent. The analysis was undertaken in MATLAB, and the details of the codes are presented in the Appendix B.

The maximum slope of every building was estimated by the ratio of the differential settlement between the predicted maximum and minimum settlement in every building footprint, divided by the distance between the meshing (settlement) points. In addition, to estimate the maximum and the minimum settlement within a building footprint, the ground settlement was obtained (in 3D) using Equation (4.5) in MATLAB. Resulting settlement risk 'maps' using SketchUp, have been developed.

Table 4.4: Damage risk categories with common values of maximum slope and settlement of a building, adapted from Rankin (1988), CIRIA (1996) and Chapman et al. (2017).

Damage Risk Category	**Maximum slope of building**	**Maximum settlement of building (mm)**	**Risk description**
1	< 1/500	< 10	Negligible: superficial damage unlikely
2	1/500 to 1/200	10 to 50	Slight: possible superficial damage that is unlikely to have structural significance
3	1/200 to 1/50	50 to 75	Moderate: expected superficial damage and possible structural damage to building, possible damage to relatively rigid pipelines
4	> 1/50	> 75	High: expected structural damage to buildings and rigid pipelines or possible damage to other pipelines

4.4.2.1 Phase 1 building damage assessment visualisations

To obtain the maximum and minimum settlement within a building's footprint, the ground movements were provided in 3D visualisations, using Equation (4.5) in MATLAB, and generating ground settlement susceptibility maps on SketchUp (Trimble Inc., 2016). Using the previous analysis information, two risk-based colour maps were generated: a map for the settlement –on the ground surface, and another map for the slope of the buildings –on the building faces. Three representative and different locations of the tunnel centreline are presented to clearly demonstrate the explored methodology; at 30m and at 10m away from the first (closest) building, and finally below the build-up area. Hence, Figures 4.7-4.9 demonstrate the impact of settlement on adjacent buildings with a decreasing distance to them, caused by tunnel constructions (Providakis et al., 2019).

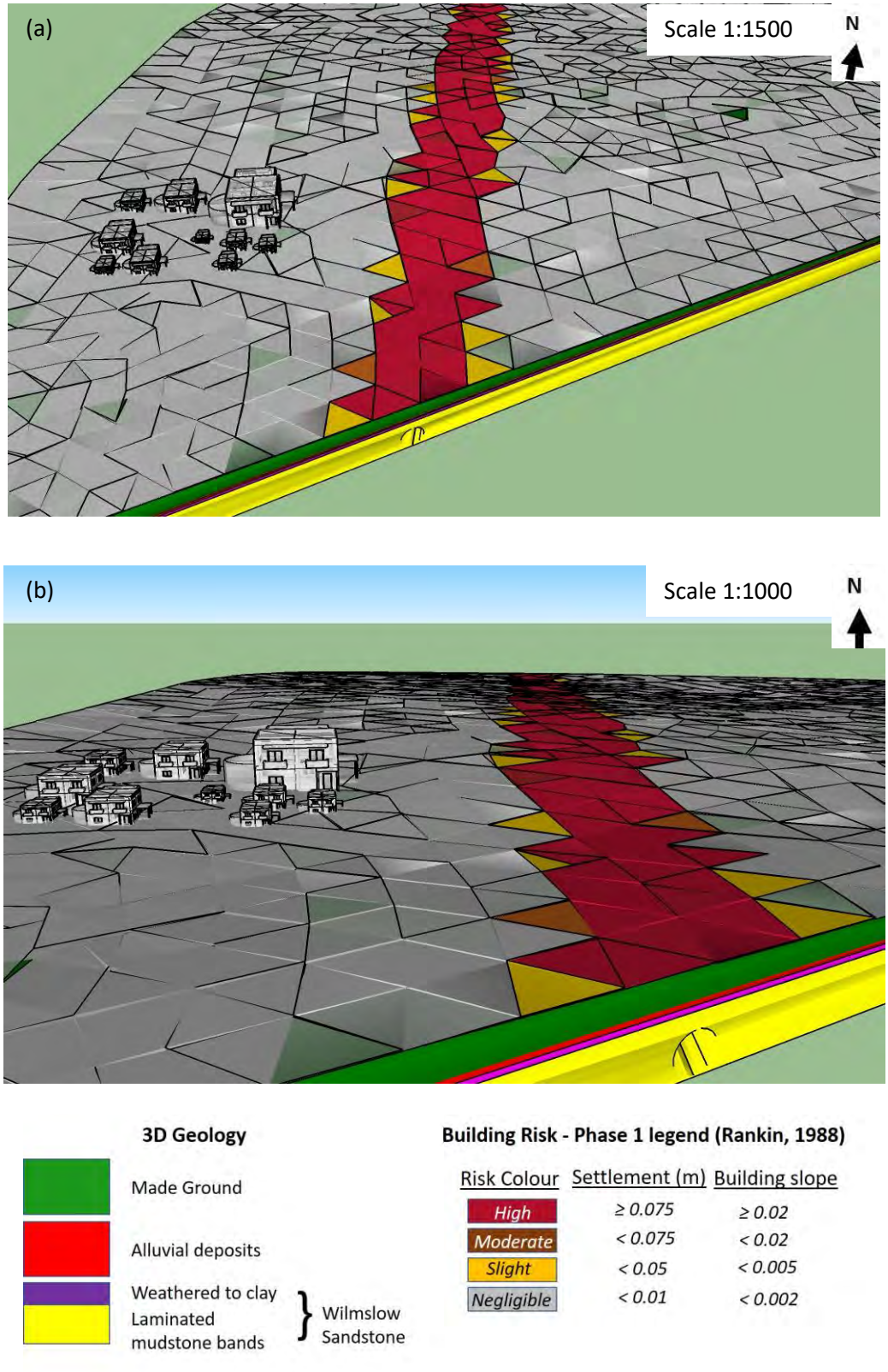

Figure 4.7: The settlement risk assessment for a tunnel 30m away: (a) wide view and (b) close view (Providakis et al., 2019).

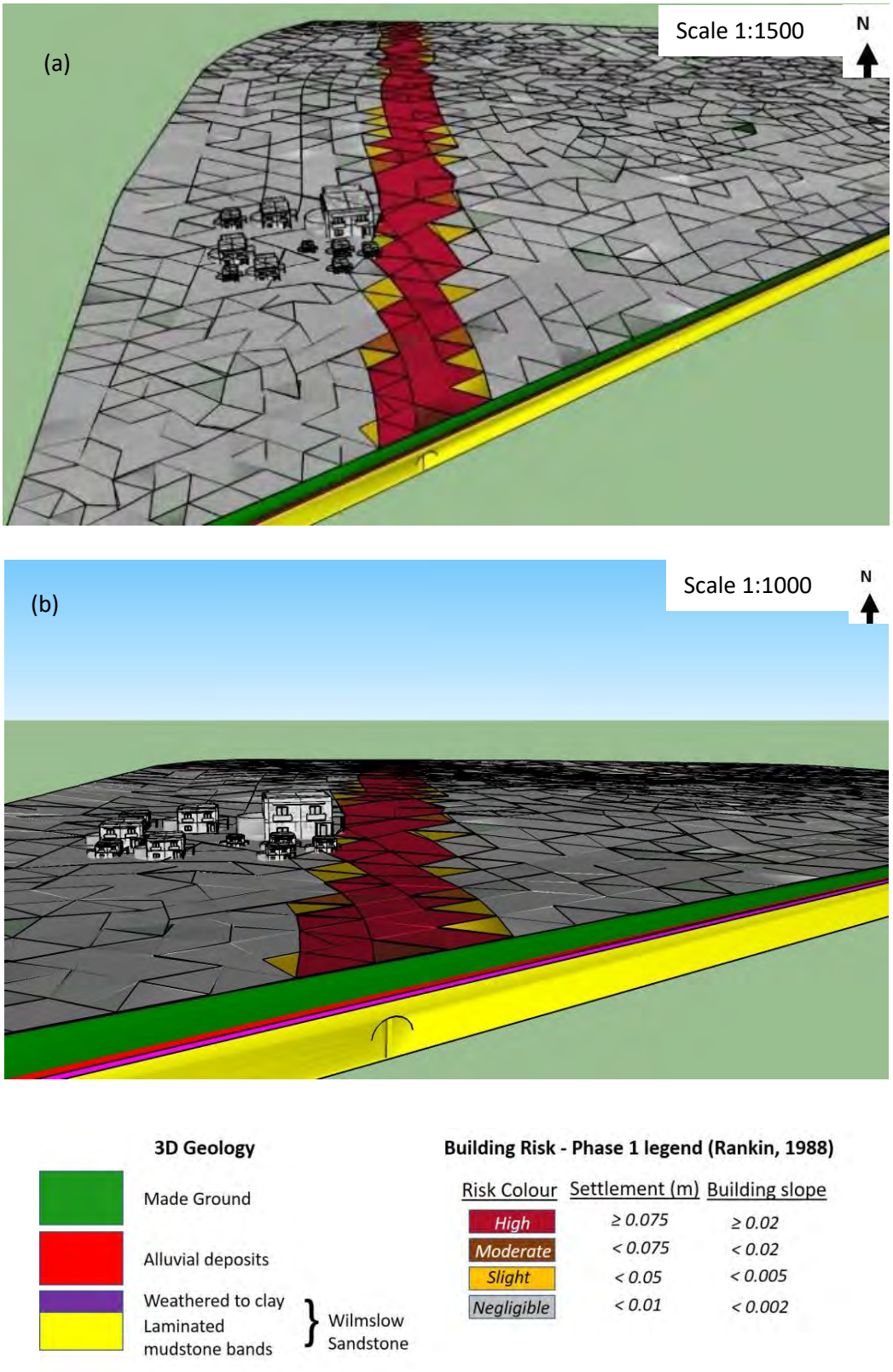

Figure 4.8: The settlement risk assessment for a tunnel 10m away: (a) wide and (b) close views (Providakis et al., 2019).

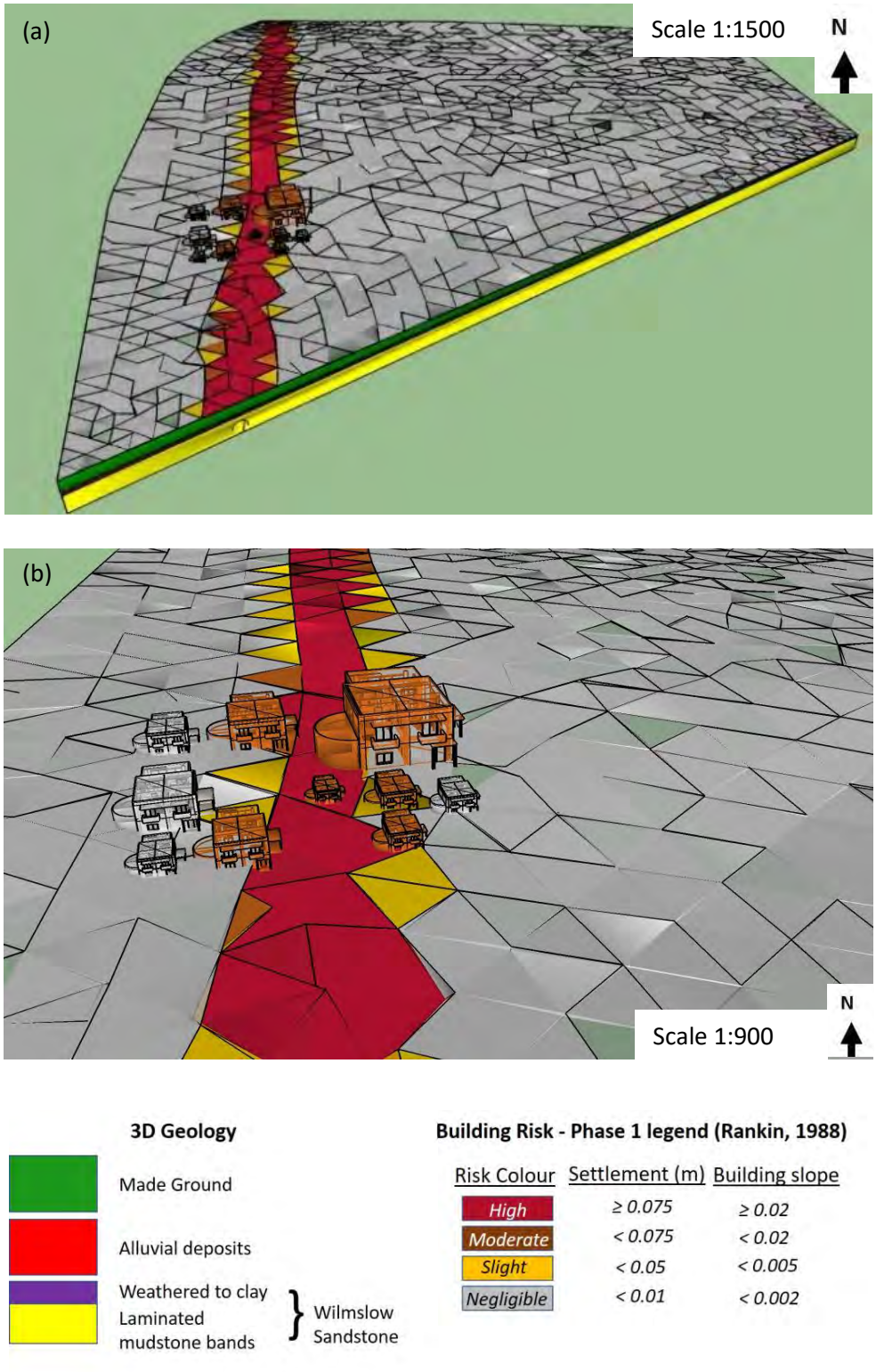

Figure 4.9: The settlement risk assessment for a tunnel below the buildings: (a) wide view and (b) close view (Providakis et al., 2019).

A similar 3D modelling application extended to trenchless operations, which was based on the same framework and risk assessment analysis, in this case for predicting the settlement risk caused by pipes in an urban area, has been provided by Chapman et al. (2019).

4.4.3 Phase 2 Building Damage Assessment (Damage severity)

The buildings which have a 'Moderate' or 'High' rating in relation to their preliminary damage assessment, using Phase 1 risk assessment, were taken forward to Phase 2. The Phase 2 assesses in more detail the potential damage severity to each building. This could be achieved using empirical, analytical or numerical modelling approaches, however by way of demonstration, an analytical method is adopted, in this case.

This approach considered the strains associated with the 'hogging' or 'sagging' areas, using the settlement trough below the buildings, as demonstrated in Figure 4.10. The Critical or Limiting Tensile Strain Method (LTSM) simplifies a building as a (simple) beam that creates visible damages or cracking due to bending or shearing (Burland and Wroth, 1974; Boscardin and Cording, 1989; Mair et al., 1996). The resulting assessment emphasises on estimations of building risk. Equations (4.7)-(4.9) show the maximum bending ($\varepsilon_{b,max}$), maximum diagonal ($\varepsilon_{d,max}$) and horizontal (ε_h) strains (Burland and Wroth, 1974):

$$\frac{\Delta}{L} = \left(\frac{L}{12t} + \frac{3IE}{2tLH_bG}\right)\varepsilon_{b,max} \quad (4.7)$$

$$\frac{\Delta}{L} = \left(\frac{H_bL^2G}{18IE} + 1\right)\varepsilon_{d,max} \quad (4.8)$$

$$\varepsilon_h = \frac{\Delta_h}{B_d} \quad (4.9)$$

where H_b: building height; E/G: ratio of the Young's modulus and shear modulus of the building; L: length of building span at respective zone; I: section moment of area of the equivalent beam height of the building at the respective zone (sagging zone: $I=H_b^3/12$ and hogging zone: $I=H_b^3/3$); t = longest distance from neutral axis to the edge of an equivalent beam

(sagging zone: $t=H_b/2$ and hogging zone: $t=H_b$); Δ: maximum settlement (deflection) at the considered span; Δ_h: differential horizontal movement at hogging zone (using Equation 4.6); Δ/L: ratio between the maximum relative settlement at the considered span and the length of this span (deflection ratio); B_d: building length.

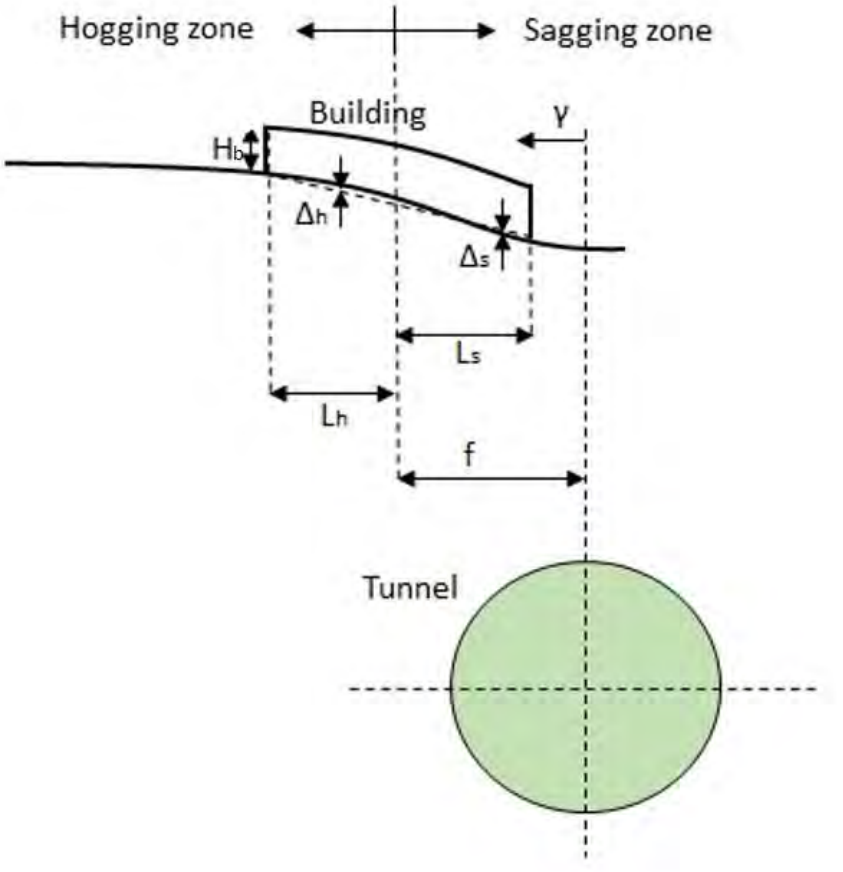

Figure 4.10: The hogging and sagging zones of a settlement trough in relation to a building, due to tunnel-induced settlements (where H_b: building height; Δ_s: differential horizontal movement at sagging zone; Δ_h: differential horizontal movement at hogging zone; L_s: length of building at sagging zone; L_h: length of building at hogging zone; f: distance from inflection point to the perpendicular axis passing the tunnel centre) (after Burland and Wroth, 1974; Boscardin and Cording, 1989; Providakis et al., 2019).

The total bending (ε_{bs}), diagonal (ε_{ds}) and critical (ε_{crit}) strains, based on the 3D building footprints, could then be estimated, respectively, from Equations (4.10)-(4.12) (Burland and Wroth, 1974; Boscardin and Cording, 1989).

$$\varepsilon_{bs} = \varepsilon_{b,max} + \varepsilon_h \quad (4.10)$$

$$\varepsilon_{ds} = \varepsilon_h \left(\frac{1-\nu}{2}\right) + \sqrt{\varepsilon_h^2 \left(\frac{1-\nu}{2}\right)^2 + \varepsilon_{d,max}^2} \quad (4.11)$$

$$\varepsilon_{crit} = \max\left(\varepsilon_{bs}, \varepsilon_{ds}\right) \quad (4.12)$$

where v is the Poisson's ratio.

The critical strain was then correlated to a damage category using Table 4.5 (Burland et al., 1977; Boscardin and Cording, 1989; Burland, 1995; Mair et al., 1996). To carry out the Phase 2 - Building Damage Assessment, several parameters had to be examined. The subsequent analysis is conducted in MATLAB and is integrated with BIM. The MATLAB codes used are provided in Appendix B. This integration is carried out to collect structural parameters from the available BIM/IFC building models, i.e. building plan/height/length and the structural component data, e.g. the ratio of Young's modulus to shear modulus (E/G) (Providakis et al., 2019). Likewise, the sagging and hogging zones, at a distance from a building (beam) and the maximum settlement, were also provided. A ratio E/G = 2.6 of a masonry building, and a Poisson's ratio, v=0.3, were adopted (Burland and Wroth, 1974; Boscardin and Cording, 1989).

Table 4.5: The building damage categories due to tunnel construction (Burland et al., 1977; Boscardin and Cording, 1989; Burland, 1995; Mair et al., 1996).

Damage Category	**Normal degree of Severity**	**Critical (Limiting Tensile) Strain (%)**
1	Negligible	0-0.05
2	Very Slight	0.05-0.075
3	Slight	0.075-0.15
4	Moderate	0.15-0.3
5	Severe to very severe	> 0.3

The building damage assessment resultants are provided using a planar approach. This is done to describe in detail the settlement risk and demonstrate it properly. Therefore, an approach to extract planes from a building is considered in the following sections.

4.4.3.1 Phase 2 Building Damage Assessment visualisations

All the buildings examined are two-storey low rise masonry structures, (gross plan area of 100-300m^2). Each building is supported on strip foundations. The geometrical features of each building are obtained from the georeferenced STL building model and the resulting triangulated mesh, as shown in Figure 4.11, and described in the following points (Providakis et al, 2019):

1. A horizontal plane through the building, together with two vertical planes, were chosen to pass through the centroid of the building. An adequate number of intersection points with their georeferenced 3D coordinates were extracted along the building shape envelope.

2. The maximum distances in relation to the horizontal section plane provided both the width and the length of each building being assessed, while the maximum distance in the vertical plane provided the height of each building.

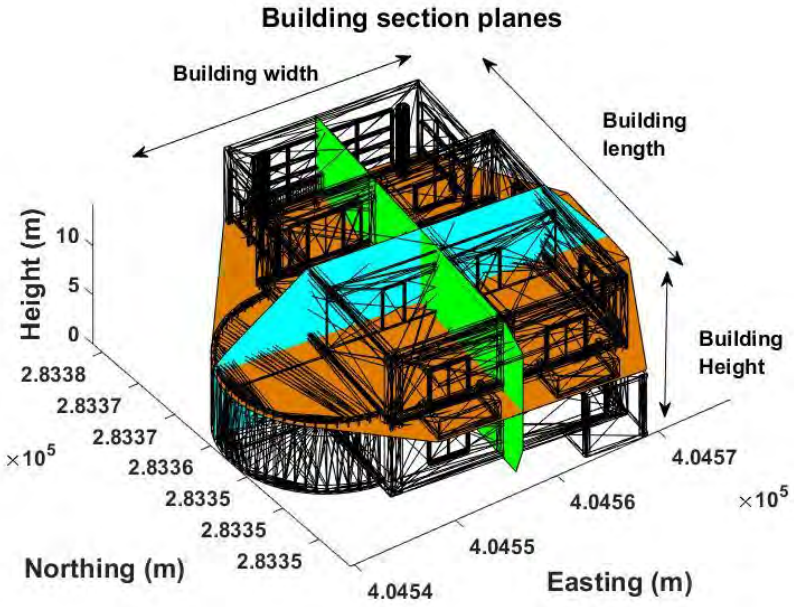

Figure 4.11: The adopted approach of estimating the various building parameters for the adopted Phase 2 building damage assessment (alongside the generated mesh). Orange: horizontal plane; cyan and green: vertical planes (Providakis et al., 2019).

After evaluating the critical strain using Equation (4.12) for each building, a colourmap could be made for the background colour of building faces. The settlement trough is also provided, below each building. A map of the buildings used is presented in Figure 4.12. Figures 4.13-4.16 show representative 3D examples of the Phase 2 risk assessment, as investigated along the longest vertical plane and along the other vertical plane (from Figure 4.11), which was generated in MATLAB, using the approach of Providakis et al. (2019). The settlement trough

is demonstrated as a blue curve below the buildings, and is compared with the horizontal level (green line). The selection of the buildings was based on providing a robust understanding of the risk assessment, through demonstrating various risk levels.

The rest of the coloured dots in the demonstrations show the section planes. More specifically, the blue, red and pink/purple dots define the outer shape of each investigated building, and they are represented by planes, which pass through the centroid of the building and are parallel to the length (vertical plane of Figure 4.11 in green), the width (vertical plane of Figure 4.11 in cyan) and the footprint plan area (horizontal plane of Figure 4.11 in orange) of the building, respectively.

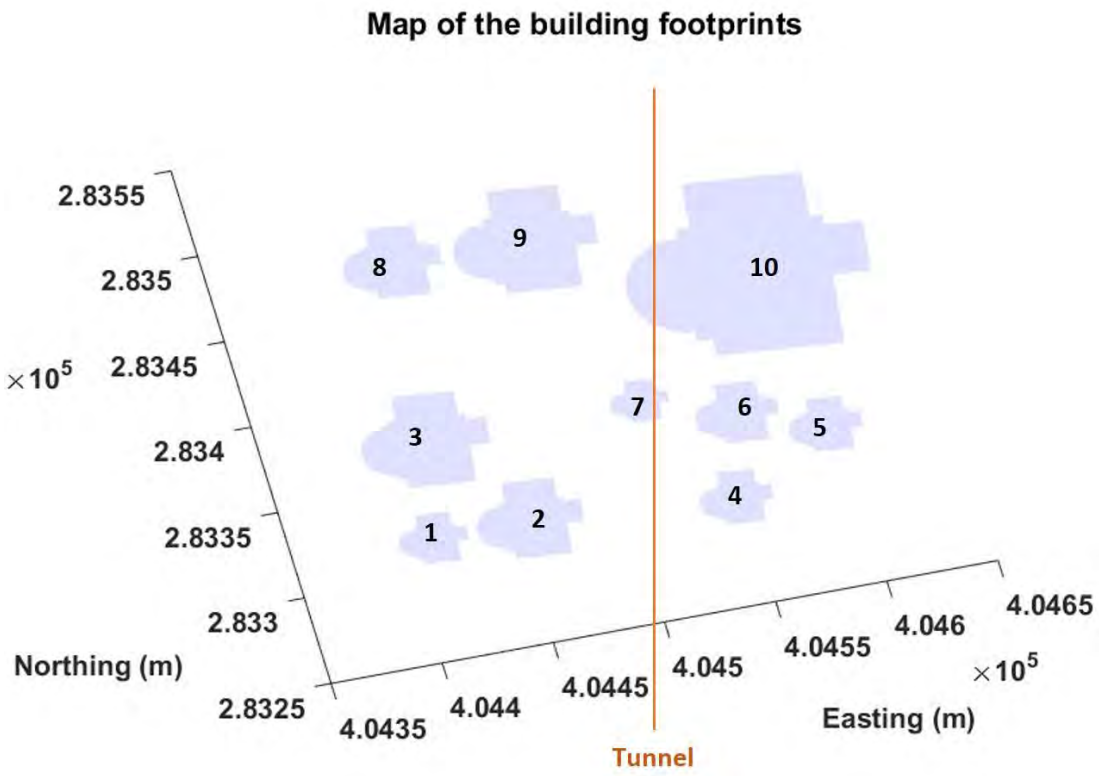

Figure 4.12: A building-footprint map including the Building Nos and the tunnel centreline, adapted from MATLAB (Providakis et al, 2019).

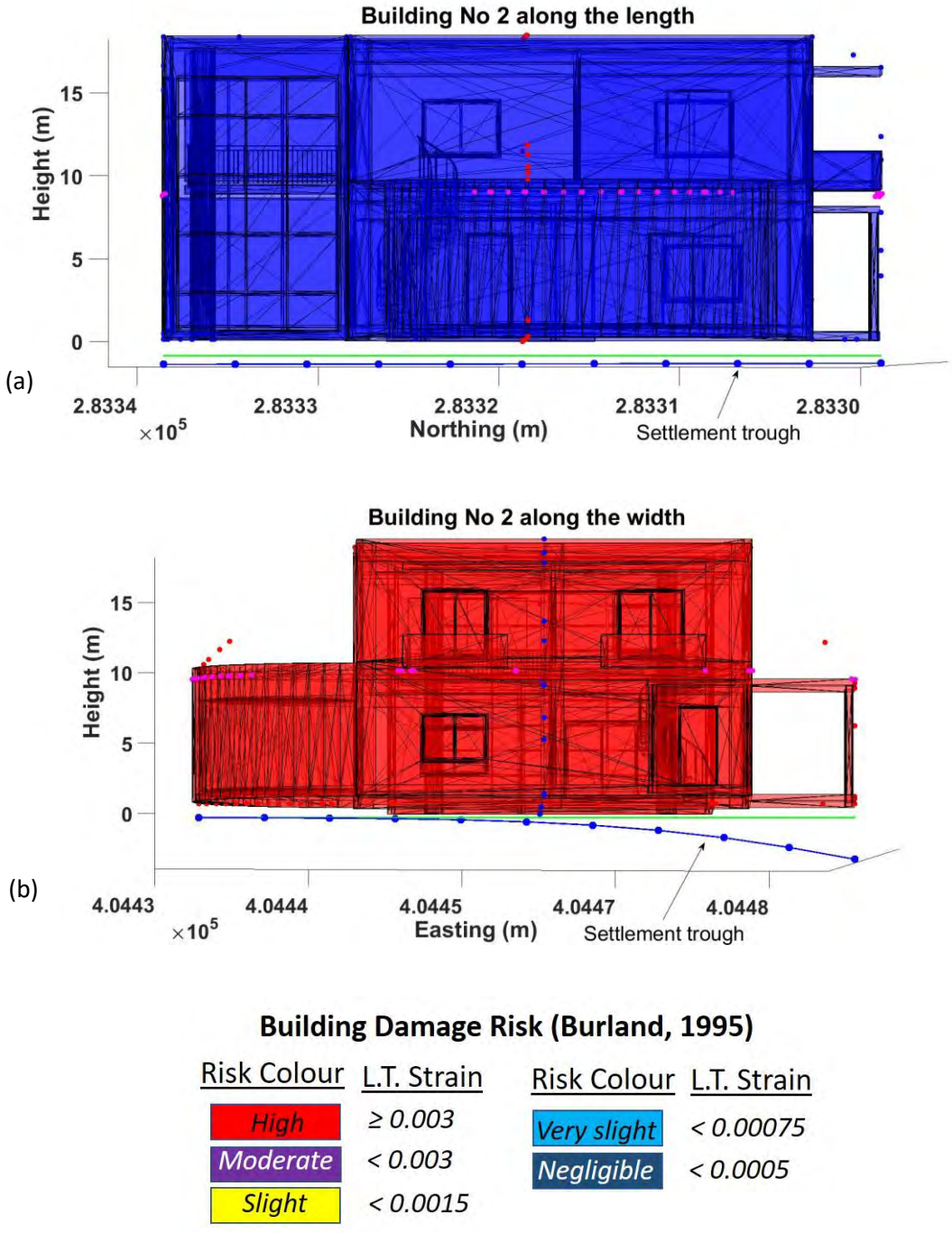

Figure 4.13: Resulting Phase 2 damage risk assessment for Building No 2, (a) along the longest plane and (b) along the vertical plane (Providakis et al, 2019).

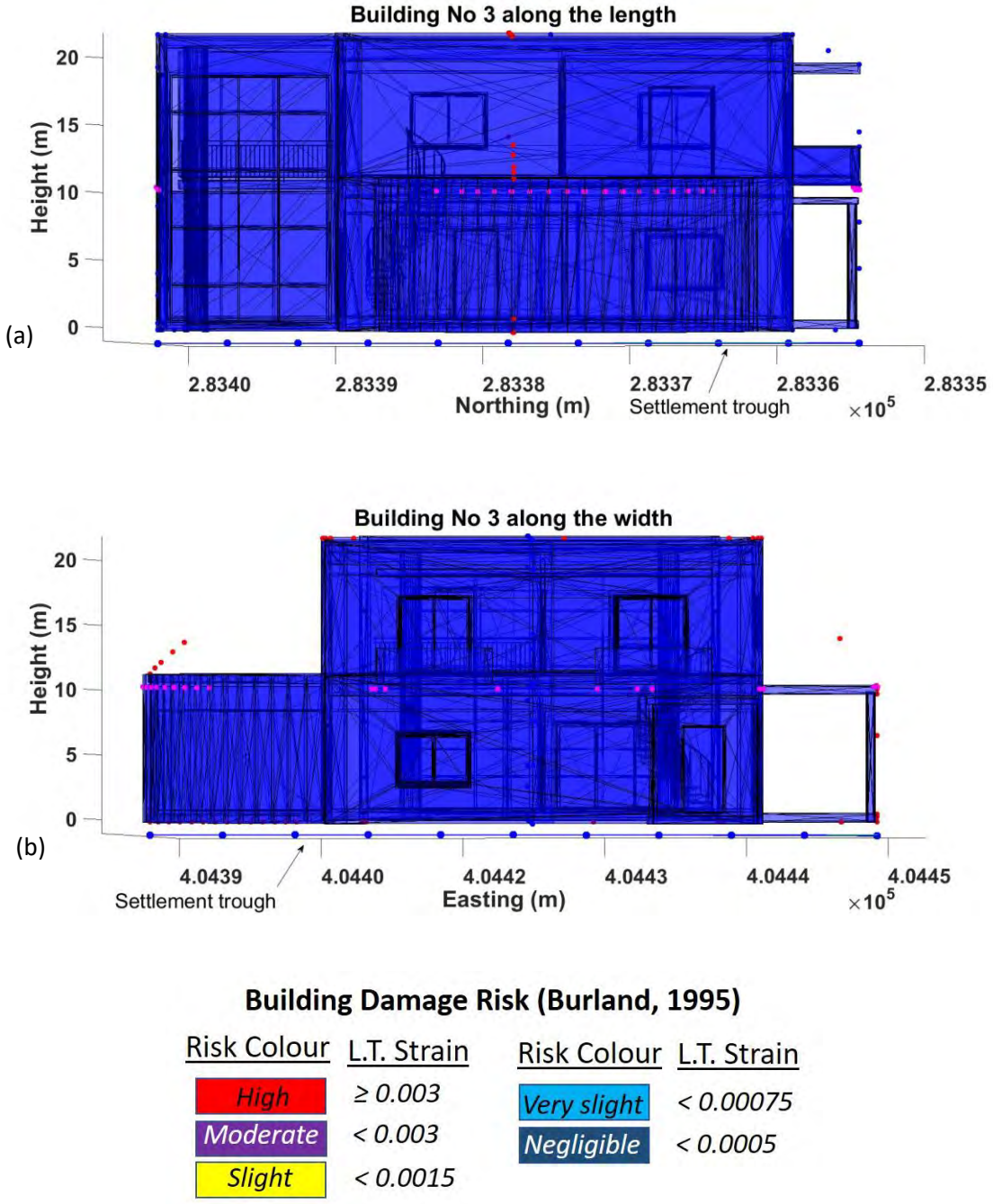

Figure 4.14: Resulting Phase 2 damage risk assessment Building No 3, (a) along the longest plane and (b) along the vertical plane (Providakis et al, 2019).

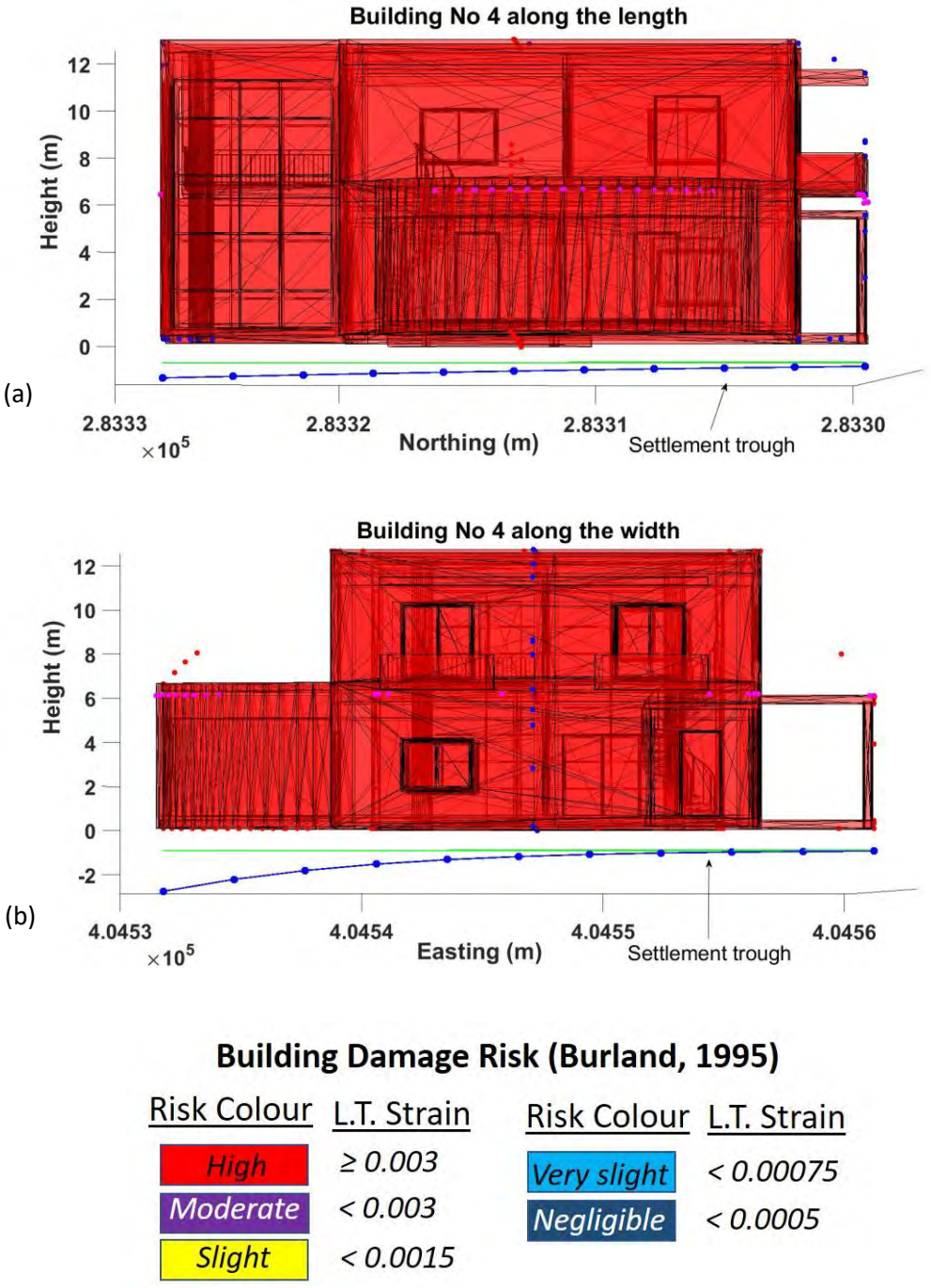

Figure 4.15: Resulting Phase 2 damage risk assessment for Building No 4, (a) along the longest plane and (b) along the vertical plane (Providakis et al, 2019).

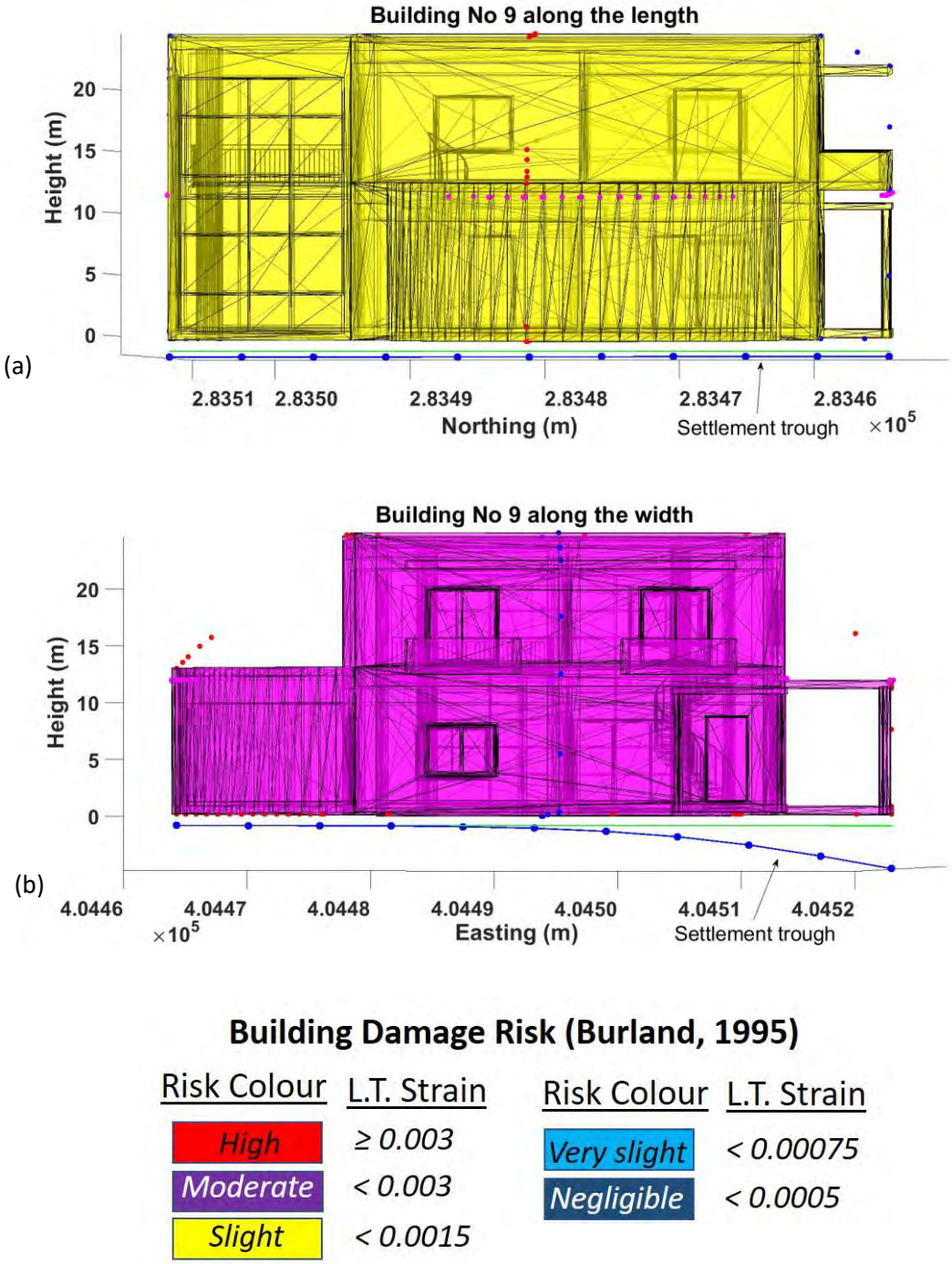

Figure 4.16: Resulting Phase 2 damage risk assessment for Building No 9, (a) along the longest plane and (b) along the vertical plane (Providakis et al, 2019).

4.5 Discussion of the results

4.5.1 Phase 1 Building Damage Assessment visualisations

Initially, the resulting visualisations in Chapter 4 were developed by employing the Building damage assessment Phase 1 (Damage Extent), using Equation (4.5). These are visualisations of the settlement risk caused by tunnelling in 3D, using BIM (SketchUp). Three visualisation cases of alternative locations of the tunnel centreline were investigated. It is evident that the higher risk-based colours were found (on the ground surface) along the direction of the tunnel, because of the creation of the settlement trough. Risk-based colours also demonstrate an increasing risk towards the tunnel centreline, again caused by the trough.

Figure 4.7 showed the tunnel centreline at 30m away from the first (closest) building of the built-up area. Risk-based colours indicate higher risk in the area above the tunnel centreline (settlement trough). However, the tunnel was away enough not to pose a risk on buildings – as shown on risk-based colours on buildings faces.

Figure 4.8 demonstrated a tunnel centreline at 10m away from the closest building. Similar to the previous example, the area directly above the tunnel centreline would indicate the greatest risk. The risk on the buildings is again shown as negligible.

However, in Figure 4.9, which demonstrated the tunnel being located directly below the area of the buildings, the risk-based colours of the buildings changed. The buildings falling within the area of higher (slight to high) risk due the tunnel centreline construction – caused by the settlement trough, exhibit a moderate risk. These buildings had a brown risk-based colour, whilst the rest that were not affected by the settlement trough exhibit a negligible risk (in grey).

Hence, Figures 4.7-4.9 clearly indicated the effect of ground settlements caused by tunnelling on adjacent buildings due to a potential tunnel construction, as the distance to them was decreasing. Colours of moderate to high risk indicate that further investigation is required.

The present method of 3D visualisations enhances demonstrations of multidimensional risk assessments, and therefore allows for better understanding of the settlement risk in relation to construction of alternative tunnelling routes.

4.5.2 Phase 2 Building Damage Assessment visualisations

In this section, the detailed 3D visualisations of the investigated buildings were presented, using MATLAB. These were generated from the critical strains for each building, using Equation (4.12) (and Table 4.5), to provide a background colour of building faces. The settlement curve below every building investigated, was also presented below each building. Thus, Figures 4.13-4.16 presented examples of the Phase 2 assessment with risk-based colours, depending on the settlement trough. The settlement trough was demonstrated as a blue curve below the buildings, which was compared with the horizontal level (green) line used to evaluate the slope angle (inclination) of the settlement trough. The visualisations presented here each building along (a) the longest and (b) the vertical dimensions (planes), to provide a thorough view of the risk assessment being conducted.

Figure 4.13a presented the Building No 2 risk assessment-Phase 2 visualisations, in which the risk is negligible with blue risk-based colour due to a smooth to horizontal slope (gentle angle) of the settlement trough (judging by comparing with the horizontal level line shown), as shown along the longest plane. However, in Figure 4.13b the same building exhibited a high risk along the vertical plane, caused by a large angle of the slope (steep) of the settlement curve below the building – in comparison with the horizontal (green) line.

Figures 4.14a and 4.14b indicated a negligible risk with very small angle of the slopes of the settlement curve, along the longest and the vertical planes, respectively, for Building No 3.

Then, Building No 4 as shown in Figures 4.15a and 4.15b exhibited a high risk (red colour), due to a large angle of the settlement trough's slope (below the buildings), which are presented in the lower part of both of these figures.

Finally, for the Building No 9, a slight risk was demonstrated in Figure 4.16a due to a slight settlement curve slope angle, which is shown (in the same figure) along the longest plane. However, a moderate risk was found in Figure 4.16b due to a steeper (greater angle of) corresponding slope of the settlement trough (shown within the figure), along the vertical plane.

The resulting visualisations showed the effect of ground settlements in each building successfully. They were found to align with the settlement trough indications and their (expected) location on the map (Figure 4.12). Hence, the impact of a new tunnel construction on existing buildings has been explored here, as a geohazard example. In particular, the power to integrate estimations – using empirical, analytical or numerical methods – and create multidimensional visualisations in the BIM environment, was a special characteristic of this method. This was presented using a relatively simple example, but this could be extended to provide a powerful tool for planning and decision-making.

4.6 Summary

The research in Chapter 4 provided an integrated framework of a preliminary risk assessment tool for geohazard risk in an urban area (e.g. the tunnel-induced settlement risk). 3D ground modelling is advanced by the creation of an integrated 3D model of the area to base the assessment, using BIM. A risk assessment was provided, using an advanced integration of BIM with a risk assessment analysis. The process of the integration of advanced (spatial) modelling

tools and an analysis with BIM was demonstrated. A framework was developed, based on the power of BIM to manage and process, and then visualise the results of the relevant information, as required. This provided a robust indication of the geohazard risk using several 3D (BIM) visualisations for the urban area investigated. This information would be important for sustainable decision-making and urban planning.

5 TUNNELLING-INDUCED SETTLEMENT VULNERABILITY ESTIMATION USING A 3D SPATIOTEMPORAL ANALYSIS AND BIM

5.1 Overview

As the risk assessment Equation (3.4) shows, Risk is a function of Hazard and Vulnerability. As already stated, these can be noted as Hazard and Vulnerability 'components'. The Hazard could be considered by an extent and severity degree (and probability) in relation to damage (Fedeski and Gwilliam, 2007). In this case, these form the tunnelling-induced Settlement Hazard (probability is explored in the following chapter). Vulnerability is the susceptibility of the investigated objects (buildings) to the same hazard. In the present methodology, to obtain the risk, these three elements are separately assessed.

In the previous chapter, the extent and the severity of this Hazard ($HAZARD_{SE}$) are thoroughly investigated by a 3D geology-tunnel-building modelling scheme. Hence, the evaluation of the Vulnerability to the tunnel-induced settlement geohazard ($Vulnerability_{SE,}$) is explored, here. This is provided by exploring it through a number of impact factors. These are referred to as settlement vulnerability factors, with values taken from boreholes. These factors were then combined to create an 'index' that represented the Vulnerability of the buildings to tunnel-induced settlements within the risk assessment.

To provide the resulting damage, it is not efficient to assess those factors only by combining them using an Analytical model. This is due to the data limitations and diversity of those factors. Instead, to enhance the approach with a combination of quantitative and qualitative factors, the use of an efficient approach, which dealt with a wide range of social, economic, environmental and geological aspects, was chosen. In this system, severity – here, as 'priorities' – had to be assigned to the system through a combination of quantitative and qualitative factors (Papaioannou et al., 2015). This is provided by a multi-criteria analysis technique, the

Analytical Hierarchy Process (AHP) (Saaty, 1977). This is employed to indicate the severity of the particular geohazard vulnerability factors, providing the spatial part of the analysis. The AutoRegressive eXogenous (ARX) modelling was also employed, to provide the temporal changes of risk for settlement vulnerability factors, in this case for groundwater head fluctuations. This produces the temporal part of the analysis, respectively. Hence, to analyse those factors, a spatiotemporal analysis was undertaken. Then, using this analysis, an index, providing the Settlement Vulnerability of an area could be genereated, which could be extracted withn a risk assessment.

As already mentioned, to provide the tunnelling-induced settlement risk ($Risk_{SE}$), the resulting Settlement Vulnerability ($Vulnerability_{SE,}$) should be combined with the Settlement Hazard ($Hazard_{SE}$). The latter is provided in the present part using the Analytical methods in combination with the Damage extent and severity of the Settlement Hazard. Finally, the tunnelling-induced settlement risk ($Risk_{SE}$) is estimated, using Equation (3.4).

The use of 3D georeferenced maps simplifies this process via overlaying layers of vulnerability maps and identifying buildings at risk, implementing the approach described in section 3.3 (Methodology). Integrated modelling is also enhanced, using advanced spatial modelling and visualization tools on Google Earth (Google Inc., 2018). To provide clear settlement risk assessment outcomes, Settlement risk distributions for the settlement vulnerability factors and the damage extent, are demonstrated. The resulting settlement risk assessment visualisations with time, including 3D geology-tunnel-buildings models through BIM, which were provided as described in section 3.3.9 (Methodology).

A flow chart of the proposed methodology in this chapter is presented in Figure 5.1.

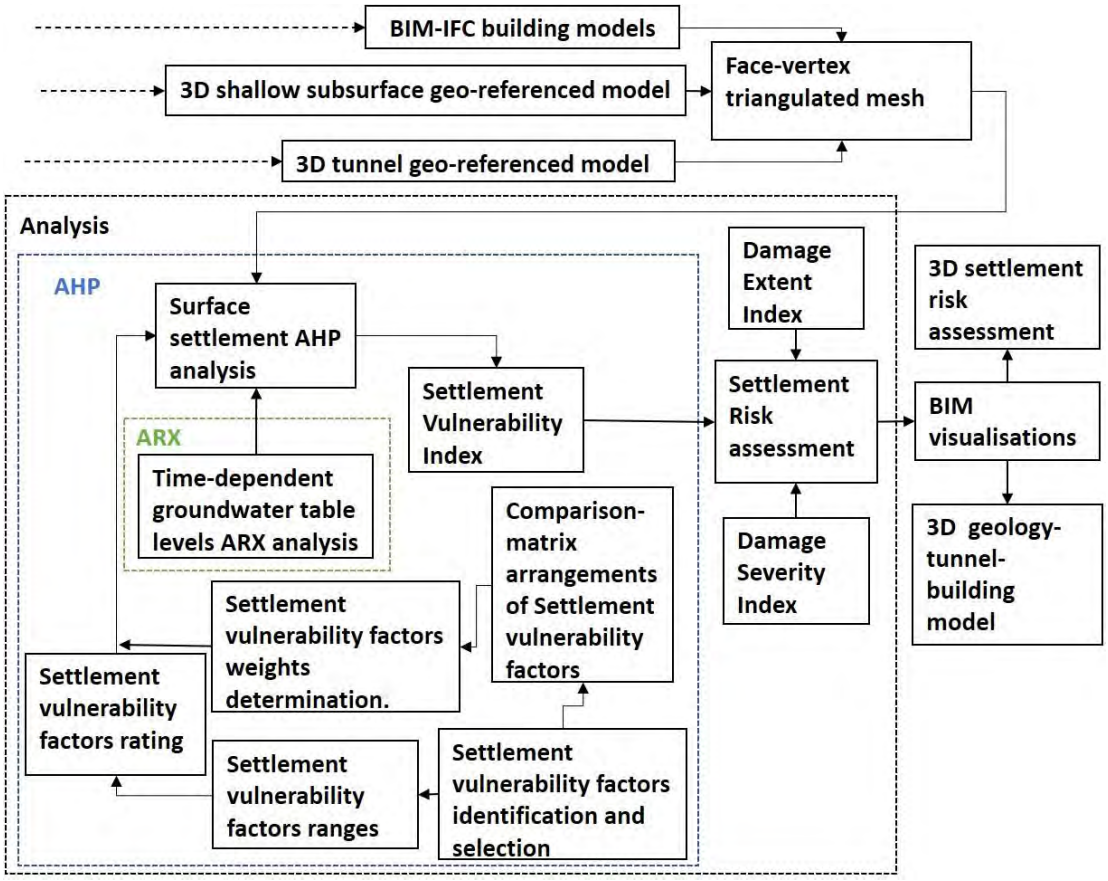

Figure 5.1: The flow chart of the methods used following on from Providakis et al. (2019).

5.2 Georeferenced 3D geology-tunnel-building model of the study area

To demonstrate the methodology, an area had to be chosen. The area surrounding the University of Birmingham, UK, was selected, as demonstrated in Figure 5.2. The geological strata which were considered to build the 3D model, comprised of made ground above alluvial deposits that overlie the sandstone, which has a weathered to clay top (and mudstone bands below). The actual topography of this area was implemented. The method that was used in this chapter employed the approach described in Chapter 3, which provided the layers of the 3D geology model using interpolation in MATLAB. The resulting model is shown in Figure 5.3, which is presented in the BIM visualisation software SketchUp (Trimble Inc., 2016). This model was made by data, which is taken from fifteen designated boreholes (monitoring sources), to

demonstrate the approach used. These are illustrated in Figure 5.2 (Google Earth, 2018), where these boreholes are represented by 3D (borehole-log) tube models on Google Earth (Google Inc., 2018).

By way of example, a representative 3D tunnel model was generated using (Delaunay) interpolation within the 3D geology model of this study area. A view of the 3D geological model that is generated, which showed the potential tunnel location, is demonstrated in Figure 5.3. By way of example, the tunnel was built using a diameter of 10m at a depth of 20m.

The BIM building models (Graphisoft, 2018; SUpodium, 2018) were superimposed on their actual position on this 3D model, employing the approach of Providakis et al. (2019) to build the present analysis (described in Chapter 3).

Figure 5.2: The borehole locations around the University of Birmingham, UK, utilised in the modelling demonstrated on Google Earth (Google Inc., 2018). The adopted tunnel is marked with a red dotted line.

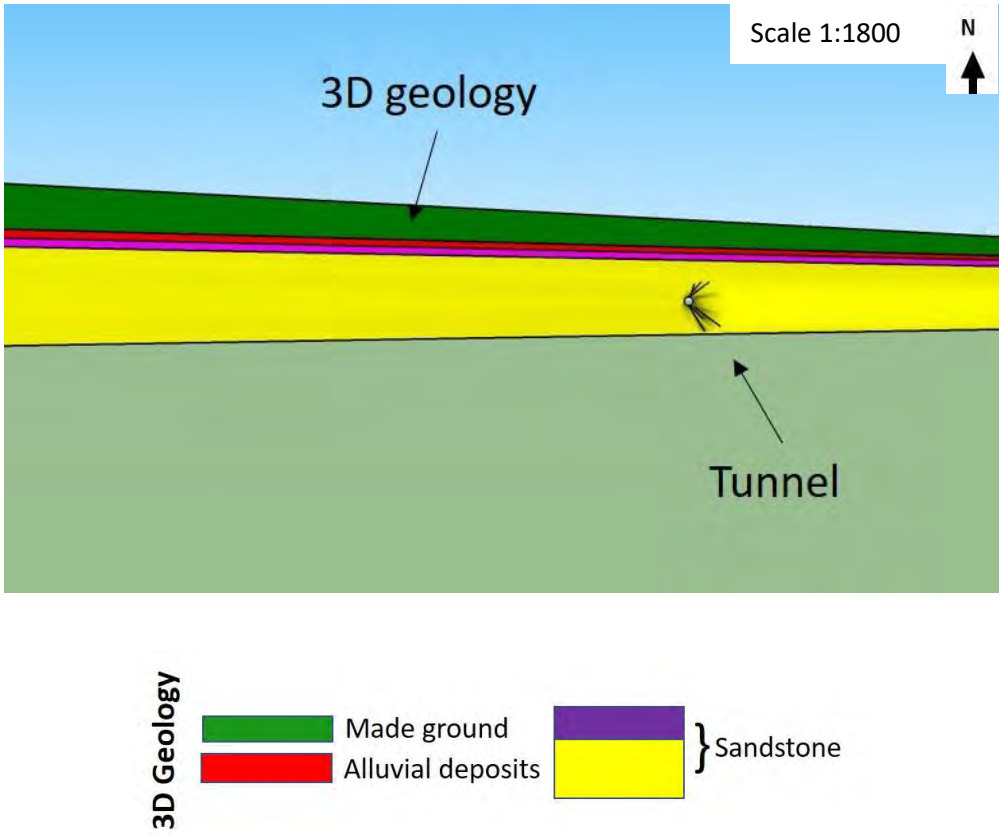

Figure 5.3: The 3D geology-tunnel model using the BIM visualisation software of SketchUp. The geological strata used were made ground (green), alluvial deposits (red) and the sandstone (purple/yellow).

5.3 Tunnelling-induced settlement risk assessment analysis

The settlement risk due to a tunnel construction can be obtained by an integrated form of the basic settlement risk assessment Equation (3.4). However, here an index that presents the Settlement Vulnerability will be provided in addition to the index which indicates the Settlement Hazard. This would enable a settlement risk assessment to be set.

5.3.1 Tunnelling-induced Settlement Vulnerability analysis

In this chapter, the analysis is developed using a spatial analysis of involved factors through the Analytical Hierarchy Process (AHP) (Saaty, 1977), and then using a temporal analysis of factors through the AutoRegressive eXogenous (ARX) model. Their combination produces the Settlement Vulnerability of the area ($Vulnerability_{SE}$) using a Settlement Vulnerability Index, through a 'spatiotemporal' analysis, as shown in Figure 5.4. (here, the settlement vulnerability factors were involved). In this way the settlement risk assessment is provided.

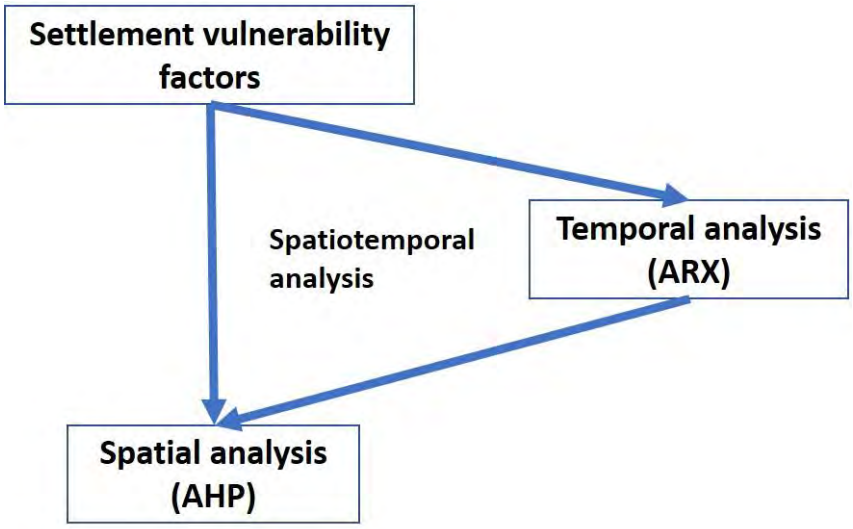

Figure 5.4: The spatiotemporal analysis scheme adopted.

5.3.1.1 Spatial analysis using the Analytical Hierarchy Process (AHP)

Multicriteria analysis methods, as already stated in the Literature Review Chapter 2, have been commonly used in similar assessments. A widely used technique is the Analytical Hierarchy Process (AHP), which was introduced by Saaty (1977, 1990a). Its hierarchical and structured aspects made it preferable for analyses of many complex tasks in past research, where

interconnected (multi-objective) criteria were occurring (Kazakis et al., 2015). Hence a ranking was made available using this method, through a pairwise matrix following criteria adopted by Saaty (1977). These are described later in this chapter, and an example of the concept of this method is shown in Figure 5.5. There have been numerous examples of geotechnical risk assessments implementing this method to provide a correlation by 'weighting' various different factors, by way of example, among them are Ayalew et al., (2005), Yalcin and Bulut (2007), Kayastha et al. (2013), Hyun et al. (2015), Nezarat et al. (2015), Taheri et al. (2015) and Yang et al. (2016).

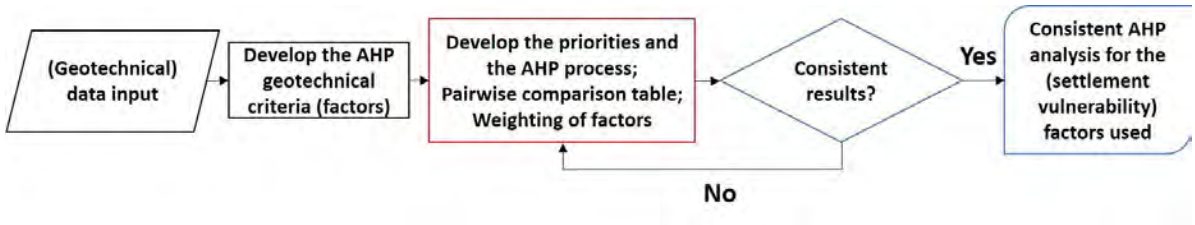

Figure 5.5: The AHP methodology.

The principal aim of the AHP is depicted within the current analysis, which is the correlation of different factors involved. A pairwise table is produced to compare every factor against each other and indicate their corresponding severity of risk through their weightings. Finally, all aspects are linked together to support the overall risk assessment (Bottero and Peila, 2005). The main phases of the AHP used are provided in the next section.

5.3.1.1.1 Settlement vulnerability factors

The significant geotechnical criteria to provide the AHP analysis are the settlement vulnerability factors (V_i) (where i is the total number of factors involved). Initially, their selection is important, made before their comparisons and the rest of the AHP stages. As Rozos et al. (2011) implied this could stem from:

- A review of the state-of-the-art literature of similar research;
- The background and experience on the research field.

In the present representative example, the selection of the vulnerability factors is based on previous research and the expertise of the author in the specific field. This selection was more based on demonstrating the adopted framework, and its integration within BIM, rather than providing a detailed analysis of all the factors involved in the tunnel-induced settlement vulnerability. With respect to the requirements of the users, these could be edited or added to according to the analysis that is carried out. This also provided no further need for ground investigation or laboratory tests and could be applied when there is a limitation of geological data. Interrelationships or interactions between factors could occur, for example, when one or more factors interact with each other, due to the nature of the ground. However, this did not have any effect on the current analysis, because each factor was examined individually with any other factor, employing the AHP. In the current example, settlement analyses and settlement vulnerability factors were selected for soft ground conditions (Figure 5.6a). Specifications and details of these factors follow.

The groundwater characteristics are associated with the groundwater table level factor (V_1). The groundwater table level is significant in the settlement susceptibility, and is a common (impact) factor in relevant literature (Terzaghi, 1950; Santos Jr. and Celestino, 2008; Wongsaroj

et al., 2013). Its interaction with other ground factors (such as cohesion, shear strength) could make the ground unstable. Potential changes of ground conditions along tunnelling could be linked with this parameter, as implied by Wongsaroj et al. (2013). Suwansawat and Einstein (2006) showed that the settlement risk is connected with the depth of the groundwater table in relation to the invert of the tunnel. An example of the generated groundwater table levels using interpolation, which was taken from the analysis of this chapter, were presented in Figure 3.12 of the Methodology (Chapter 3). A normalised factor $(Z_0+D)/H_w$ (Shin et al., 2009), with the parameters shown in Figure 5.6b, has been used to describe it in the present analysis. The corresponding settlement risk that was posed, was categorised, as shown in Table 1.

The hydraulic conductivity (V_2) was also chosen because it causes surface settlements, when it falls within dangerous levels. This could be explained as, 'the more groundwater that is let to pass through a soil, the less stable this soil would then be', and has been commonly employed in similar underground assessments.

The ground strength is a factor that controls the development of ground displacements linked with tunnelling. In fine-grained soils, the short-term or undrained shear strength Cu (V_3) were used because of the geology of the area. This was widely used, such as in the analysis by Neaupane and Adhikari (2006) and Dindarloo and Siami-Irdemoosa (2015).

Young's modulus (V_5) was also considered here as an important factor for the stiffness of the ground because this is closely connected with ground movements. Other selected ground characteristics of importance were the soil density (V_4) and the unit weight (V_6).

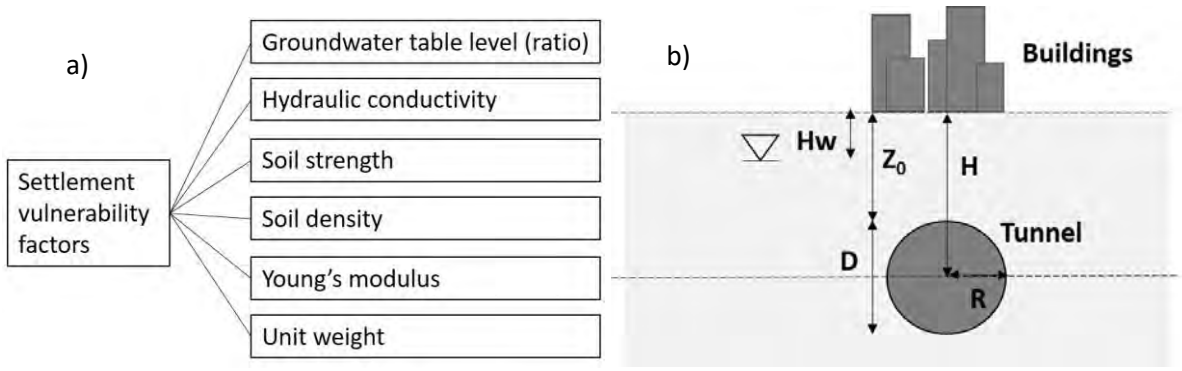

Figure 5.6: (a) The settlement vulnerability factors used, and (b) the geometrical criteria used in the present analysis (where Z_0 is the overburden depth also known as 'cover depth', D is the diameter, R is the radius of the tunnel, H_w is the depth from the ground surface to the groundwater table and the tunnel depth, H, defined from ground surface to the tunnel axis).

5.3.1.1.2 Risk ranges and ratings of the settlement vulnerability factors (AHP)

To carry out the AHP, risk ranges needed to be assigned. These were selected from their effect or severity of risk to produce surface settlements. A subsequent rating for this severity of risk (with a high value being unfavourable) was then assigned to each range. It should be noted here that the values of the ranges and ratings were representative, which were adopted from previous research and the author's expertise to demonstrate the efficiency of this tool. The range values reflected the actual values, being able to change, if required. Thus, every settlement vulnerability factor was classified into different ranges of risk. These had corresponding rating values that varied from the most favourable (low value) to the most unfavourable (high value). The final classification, which was used in the analysis (in MATLAB; as shown in Appendix C), is shown in Table 5.1.

The ranges of the groundwater table level were produced by the relation of the groundwater head (H_w) to the tunnel invert (Suwansawat and Einstein, 2006). Their ratio of their depths from the surface was employed in the analysis using a normalised factor $(Z_0 + D)/Hw$ (Shin et al., 2009). Unfavourable values, i.e. a higher risk of settlement, are expected with increasing groundwater table level above the tunnel invert (Benardos and Kaliampakos, 2004; Santos Jr. and Celestino, 2008), while hazardous conditions were represented by values of 10 or more (Shin et al., 2009). Hydraulic conductivity was divided into four ranges, with higher risk associated with increasing values and reaching a critical level at 10^{-2} m/s. The undrained shear strength, covering a range of typical values drawn from literature, is obviously inversely proportional to the risk for the example of a fine-grained soil used in this analysis. Young's modulus was likewise assigned a typical range drawn from the literature, with risk increasing as the value of Young's modulus decreases and values below 100MPa would commanding extra caution. The soil density and unit weight are primary ground parameters with typical ranges shown in Table 5.1 and settlement risk increasing as they reduce.

Table 5.1: The risk ranges and ratings of the settlement vulnerability factors used, and their corresponding weights adopted using the AHP.

Settlement vulnerability factor V_i	**Range**	**Rating**	**Weight (w_i %)**
Groundwater table: $(Z_0+D)/H_w$	>20	10	24.5
(V_1)	10-20	8	
	5-10	6	
	1-5	4	
	0-1	2	
Hydraulic conductivity (m/s)	$>10^{-2}$	3	5.2
(V_2)	10^{-4}-10^{-2}	2	
	10^{-8}-10^{-4}	1	
	$<10^{-8}$	0	
Undrained shear strength (kN/m^2)	<50	3	24.5
(V_3)	50-100	2	
	100-150	1	
	>150	0	
Soil density (kg/m^3)	<1800	3	13.2
(V_4)	2000-1800	2	
	2100-2000	1	
	>2100	0	
Young's modulus (MPa)	<10	3	24.5
(V_5)	100-10	2	
	200-100	1	
	>200	0	
Unit weight (kN/m^3)	<18	3	8.2
(V_6)	20-18	2	
	24-20	1	
	>24	0	

Table 5.2: The AHP scaling system proposed by Saaty (1977).

Preference factor	**Preference Degree**	**Explanation**
1	Equal	Equal participation of both factors.
3	Moderate	Slightly to moderately favour a factor over another.
5	Strong	Strongly favour one factor over another.
7	Very strong	Very strongly one factor favour over another.
9	Extreme	Extremely favour a factor over another.
2, 4, 6, 8	Intermediate	Compromises between the 1, 3, 5, 7 weights.
Reciprocals	Opposites	Inverse comparison.

Table 5.3: The pairwise comparison table of the settlement vulnerability factors using the AHP.

Factors	Groundwater Table	Hydraulic Conductivity	Shear Strength	Density	Young's modulus	Unit weight
Groundwater Table	1	4	1	3	1	3
Hydraulic Conductivity	1/4	1	1/4	1/2	1/4	1/2
Shear Strength	1	4	1	3	1	3
Density	1/3	2	1/3	1	1/3	3
Young's modulus	1	4	1	3	1	3
Unit Weight	1/3	2	1/3	1/3	1/3	1

5.3.1.1.3 Weightings of the settlement vulnerability factors (AHP)

The weighting process is very important in multi-criteria decision analyses. Thus, assigning weightings to the factors (w_i) is significant in the AHP. A pairwise comparison table had to be produced following the AHP method, implementing the scales given in Table 5.2, which are introduced by Saaty (1977, 1980). Hence, Table 5.3 was then generated, in alignment with the literature and the expertise of the author. Subsequently, a weighting value was assigned to each factor to characterise its severity (in relation to the other factors) in terms of its effect on settlement risk, as demonstrated in the last column of Table 5.1.

More specifically, the AHP processes, which were carried out to provide the weightings, are given in Appendix C.

5.3.1.1.4 Consistency of the settlement vulnerability factors (AHP)

To finalise the AHP method, a consistency check is required. This is done to validate the resulting values and to confirm the accuracy of the AHP used (Saaty, 1980). This process that utilises the Consistency Ratio (CR), which should be *CR<0.1* to achieve accurate resultants, is described using Equation (5.1) (Saaty, 1980; Kazakis et al., 2015).

$$CR = \frac{CI}{RI} \tag{5.1}$$

where the Consistency Index is $CI = (\lambda max - n)/(n - 1)$, n is the number of criteria and λ_{max} the maximum eigenvalue of the comparison matrix, and RI is the Random Index.

Using the pairwise comparison Table 5.3 and Equation (5.1), the consistency check in the present analysis gave: $n=6$, $\lambda_{max}=6.20$, $CI=0.04$ and $RI=1.24$. As a result, $CR=0.03$, which indicates that the present AHP analysis is accurate (valid).

5.3.1.2 Temporal analysis using ARX

As mentioned previously, the AHP produces the spatial part of the proposed analysis. However, to complete a robust settlement risk modelling, a time variation parameter of the groundwater table level $H_w(t)$ is needed because of the local climate changes, such as from wet to dry periods. Therefore, to produce the temporal part of the analysis, AutoRegressive eXogenous (ARX) analysis has been used (Oskay and Zeghal, 2011), in combination with the AHP. ARX is a dynamic model that predicts groundwater head level values, y(t), depending not only on the current actual groundwater table level $H_w(t)$ taken from the boreholes by input u(t), but also on the input/output at previous times, u(t-1)…u(t-1-n_k) and y(t-1)…y(t-n_a), respectively. The ARX method requires a time delay, while validation is provided by testing of the input impact, u(t), on the output y(t), estimated from Equations (5.2)-(5.6) (Chetouani, 2008):

$$y(t) = -a_1 y(t-1) - \cdots - a_{n_a} y(t-n_a) + b_1 u(t-1-n_k) + \cdots + b_{n_b} u(t-n_b-n_k) + e(t) \quad (5.2)$$

where, e(t) is the "Gaussian" noise, a_{n_a} and b_{n_b} are the parameters examined, n_a and n_b the polynomial order of the output A(q) and the input B(q) from the least-squares identification, n_k is the y(t) to u(t) time delay, and the polynomial is given by Equation (5.2):

$$\mathrm{A(q)y(q)} = \mathrm{B(q)u(t} - n_k) + \mathrm{e(t)} \quad (5.3)$$

where: $A(Q) = 1 + a_1 q^{-1} + \cdots a_{n_a} q^{-n_a}$ (5.4)

$$B(Q) = b_1 q^{-1-n_k} + \cdots b_{n_b} q^{-n_b-n_k} \quad (5.5)$$

$$u(t-1) = q^{-1} u(t) \quad (5.6)$$

A demonstrator of the temporal changes of this time-dependent factor, which was monitored at one of the designated boreholes used, is provided in Figure 5.7. These alterations are based on

actual ranges taken from hydrographic examples for a nearby area with similar characteristics, which show small fluctuations within a period of months (BGS, 2018; NERC UKCEH, 2018). By way of example, the time-points of t_1: 25.08.2017 and t_2: 15.10.2017, as shown in Figure 5.7, were chosen to provide representative examples of different (and near-extreme changes in) groundwater table levels using the ARX. The groundwater table levels for each borehole were adopted at these two time-points (using custom-made KML scripts on MATLAB, as shown in Appendix A). Their resulting different groundwater table levels at t_1 and t_2 are demonstrated, using an integrated risk-based contour map in Figure 5.8 (Google Earth, 2018). Details of the MATLAB codes used, are presented in the Appendix C.

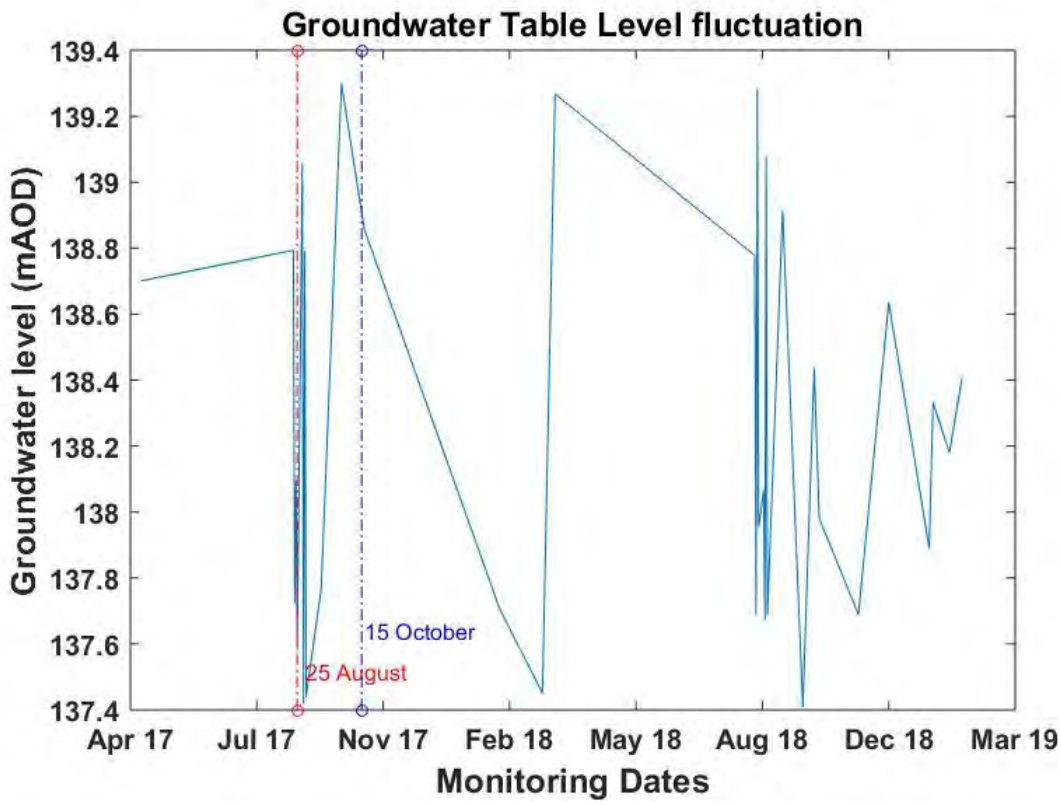

Figure 5.7: The groundwater table fluctuations adopted from the ARX analysis, which were monitored in one of the boreholes used (two times are employed in the subsequent settlement analysis at t1: 25.08.2017 – red and t2: 15.10.2017 – blue).

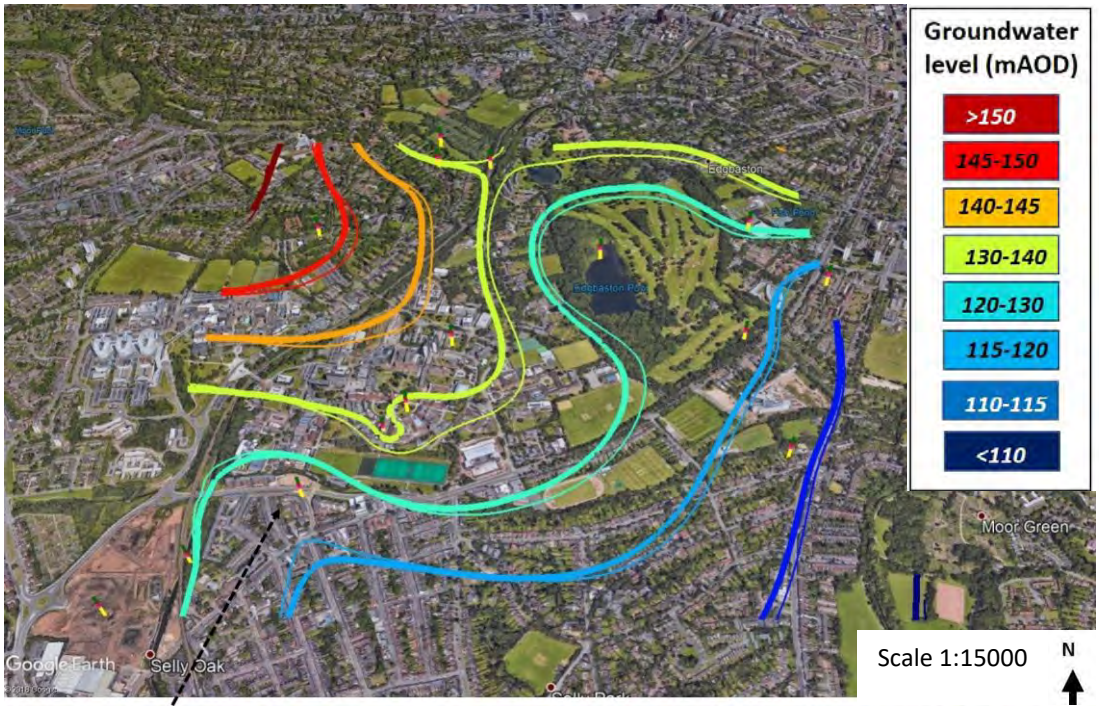

Figure 5.8: The integrated groundwater table level fluctuations, shown with (risk-based) contours at the two times (at t1: 25.08.2017 with a thicker line; t2: 15.10.2017), on Google Earth (Google Inc., 2018). A black dotted arrow marks the borehole used (where groundwater table levels were monitored) to provide Figure 5.7.

5.3.1.3 Normalisation

To provide dimensionless values which are used in the values of risk-assessments (indices), the data was standardised in advance, using the maximum difference normalisation method (Wang et al., 2017). This method is employed to correlate different ranges (categories) of several variables into a combined classification, before a major analysis takes place. This process is made via using tools on MATLAB (scripts shown in Appendix C), allowing the resulting damage to be compared, correlated and integrated, aligning with the current objectives. As a result, the data was readjusted to fit in the same range (0, 1). In this way, dimensional and magnitude information for a variable were considered within the actual data, although their

impact is diminished. The correlation of coefficient did not change and pre-processing of the data was needed for the analyses (due to the weighted values that have an effect on the outcomes) (Yu et al., 2009). This was adapted by Wang et al. (2017), using Equation (5.7).

$$X_i^n = \frac{X_i - min(X_i)}{max(X_i) - min(X_i)} \quad (5.7)$$

where X_i is the actual data and X_i^n is the normalised data within a range of [0-1].

5.3.1.4 Settlement Vulnerability Index

The Settlement Vulnerability can now be provided. An index providing the geohazard Vulnerability Index of an area (VI) could be produced, which could be extracted in a risk assessment, as shown in Equation (5.8) (Fedeski and Gwilliam, 2007).

$$VI = w_{v1} \times m_{v1} + w_{v2} \times m_{v2} + \cdots + w_{vx} \times m_{vx} \quad (5.8)$$

where $v1$, $v2$, . . ., vx are subscripts to differentiate individual vulnerability factors; w is the weight given to a vulnerability factor in the AHP in which $w_{v1} + w_{v2} + \cdots + w_{vx} = 1$ and m_v is the vulnerability factor value.

Hence, the settlement vulnerability of the area, $Vulnerability_{SE}$, would be generated by forming a Settlement Vulnerability Index. This is created from the already defined settlement vulnerability factors (V_i) as well as their severity from their corresponding weights (w_i), using the AHP combined with the ARX. Hence, an index indicating these correlations was generated at a monitored time, using Equation (5.8), as presented in Equation (5.9):

$$Settlement\ Vulnerability\ Index = w_1V_1 + w_2V_2 + w_3V_3 + w_4V_4 + w_5V_5 + w_6V_6 \quad (5.9)$$

where V_i is the spatially distributed (normalised) vulnerability values. The six V_i factors provided in Table 5.1 were used, which values at any point within the area examined can be gained from values adopted from the boreholes. The boreholes in the examined area using interpolation at t_1 and t_2 were also used; w_i is the weighting adopted from the AHP analysis.

The adopted algorithm used for the Settlement Vulnerability Index estimation in MATLAB scripts is presented in Appendix C. To provide a complete tunnel-induced settlement risk assessment, the Hazard 'component' had to be defined as well. This is carried out here implementing the analytical methods.

5.3.2 Settlement Hazard using Analytical methods

The Settlement Hazard ($Hazard_{SE}$) is formed by a settlement damage extent and a settlement damage severity. There have been various methods (Empirical/Analytical methods) to provide the surface settlements above a tunnel development. By way of example, the Analytical method introduced by Loganathan and Poulos (1998), provided a representative approach to predict surface settlements successfully through Equation (4.5).

However, this has to be combined with building damage assessments to generate efficient resultants in relation to adjacent structures risk. Here, these assessments align with elaborating an integrated risk assessment process through forming relative indices.

5.3.2.1 Damage Extent Index

A building damage assessment was generated to provide the damage due to settlement and slope of the ground surface. Table 4.4 (Rankin, 1988; CIRIA, 1996) demonstrates the corresponding risk (damage) categories. This is adopted in this analysis using Equation (4.5) in MATLAB (details in Appendix C) to provide the damage extent on the ground surface, through a relative index, named here as Damage Extent Index. The damage classes are generated from the maximum ground settlement and ground slope in relation to the footprints of the buildings, using BIM.

5.3.2.2 Damage Severity Index

The building damage assessment provided by Burland et al. (1977), Burland (1995) and Mair et al. (1996) has been also conducted, here. This has been carried out to provide the damage severity of buildings due tunnel-induced settlements considering structural interactions, utilising the critical tensile strain (ε_{crit}). The analysis was undertaken in MATLAB with the details presented in Appendix B. It was integrated with BIM – to combine geotechnical with structural parameters, as structural parameters (and building locations from sagging/hogging zones and maximum settlements) were extracted here from BIM/IFC buildings. The integrated damage categories employed, as proposed by Burland (1995) and Mair et al. (1996), are presented in Table 5.4. The ratio of Young's modulus to Shear modulus of a masonry building, E/G = 2.6, was also employed, along with a Poisson's ratio of v=0.3 (Burland and Wroth, 1974; Boscardin and Cording, 1989). Total bending strain (ε_{bs}), total diagonal strain (ε_{ds}) and finally Critical tensile strain (ε_{crit}) were estimated from Equations (4.10)-(4.12) (Chapter 4) (Burland and Wroth, 1974; Boscardin and Cording, 1989; Burland, 1995).

Table 5.4: The building damage categories adapted (Burland, 1995; Mair et al., 1996).

Damage Category	**Severity**	**Limiting (Critical) Tensile Strain (%)**
0-1	Negligible to Very slight	0-0.075
2	Slight	0.075-0.15
3	Moderate	0.15-0.3
4-5	Severe to very severe	> 0.3

5.3.2.3 Settlement Hazard estimation

Finally, the estimation of the Settlement Hazard ($Hazard_{SE}$) can now be provided, to obtain a complete risk assessment. This is carried out as a multiple regression function of the Damage Extent Index, using Equation (4.5) and Table 4.4, as well as the Damage Severity Index, using Equation (4.12) combined with Table 5.4. The resulting Settlement Hazard ($Hazard_{SE}$) component is presented in the integrated Equation (5.10).

$$Hazard_{SE} = Damage\ Extent\ Index \times Damage\ Severity\ Index \quad (5.10)$$

5.3.3 Settlement Risk assessment estimation

Finally, a more 'comprehensive' Settlement Risk assessment is now possible. This could be estimated by combining all the previous 'components' (indices) adopted from Equation (5.9) and (5.10), which could provide a basic risk assessment using the initial Equation (3.4). The resulting integrated Settlement Risk is drawn from Equation (5.11).

$$Settlement\ Risk = Damage\ Extent\ Index \times Damage\ Severity\ Index \times Settlement\ Vulnerability\ Index \quad (5.11)$$

where the dimensionless Damage Extent Index and Damage Severity Index are defined as a multiple regression function of damage extent on a scale from 0 to 1 (or percentage values 0-100%), corresponding to a particular building damage category, as shown in Table 5.4. The Settlement Vulnerability Index (which is also dimensionless) varies similarly from 0 (fully resilient) to 1 (highest vulnerability). The dimensionless values for the above indices are obtained after the entire data was standardised, using the maximum difference normalisation approach (Wang et al., 2017), before the AHP analysis, as described in a previous section.

5.4 3D risk assessment using interpolation

5.4.1 Processing the borehole data

A key to the assessment analysis generated was the interpolated geological/geotechnical information (data). The values of this information (data) is taken from boreholes, which were the monitoring sources. The process involves interpolated values for each geotechnical/geological factor at a specific location, which is represented by variables that have three-dimensional coordinates. The process of this 3D factor-value conversion to a mean value on the 2D surface, in this case from four layers, is demonstrated in Figure 5.9. These mean values of factors were then used in generating the final risk assessment ‘map’.

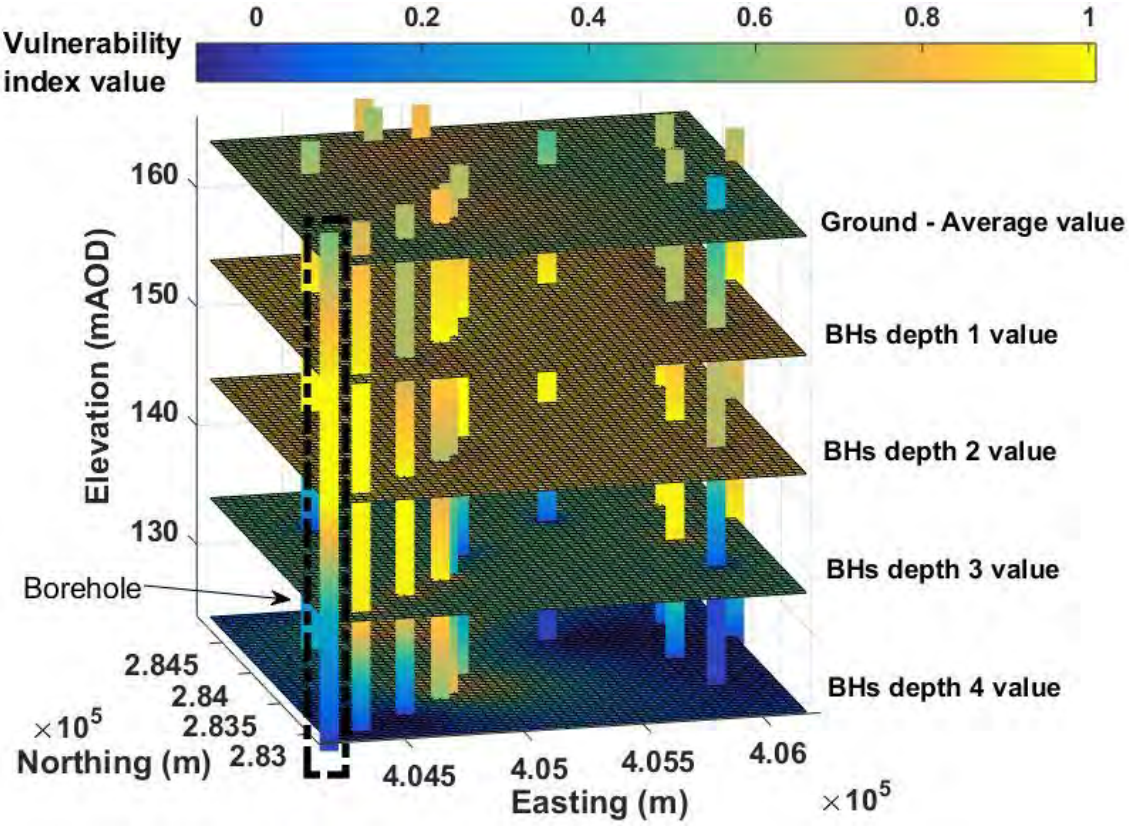

Figure 5.9: The process used in assigning values to factors, taken from boreholes' (BHs) interpolated data, to provide the 3D settlement risk assessment layers (MATLAB). A borehole example is marked.

5.4.2 Kriging interpolation

Kriging interpolation was employed here for the settlement risk distribution of factors. Kriging which was introduced by Krige (1951) and extended by Matheron (1963) has been a commonly used interpolation method. For example, Marache et al. (2009) and Thierry et al. (2009) have used it successfully to solve geotechnical problems, while Masoud (2014) utilised it in geo-environmental problems. Among many interpolation methods, this has the ability to provide 'deterioration' information in the resulting modelling, using a precision parameter in relation to the uncertainty (Thierry et al., 2009). Hence, interpolation errors are reduced using this

method (Marache et al., 2009). Oliver and Webster (1990) noted that this method could be employed for local variables (within a frame) using the variogram and covariance methods (Mei, 2014). Therefore, it could provide precise results of the current risk assessment. Kriging interpolation is closely related to the original data not interfering with any mesh, which is important in 3D geological models (Mei, 2014). For regionalised variables Z(x), at location x_0 it would be $Z(x_0)$, for no linear weighted sum of $Z(x_1)$, $Z(x_2)$, …, $Z(x_n)$ at $x_1, x_2, \ldots, x_n$, as shown in Equation (5.12) (Mei, 2014).

$$Z(x_0) = \sum_{i=1}^{n} \lambda_i \times z(x_i) \qquad (5.12)$$

where $\sum_{i=1}^{n} \lambda_i = 1$ and λ_i is the weightings at x_i using kriging interpolation.

Hence, being an estimation of a weighted linear sum, it could then be estimated using the weights λ_i (i=0, 1, …, n) (Mei, 2014). Kriging was used to estimate λ_i using a constant mean value (Mei, 2014).

5.5 Results - Settlement risk assessment visualisations

To demonstrate the outcomes of the present chapter, settlement risk distributions have been presented in the subsequent sections. These are provided to show how the background method used in the MATLAB analysis can be used to obtain 3D settlement-building risk-assessment visualisations in BIM.

5.5.1 Settlement risk distributions

The settlement vulnerability of the demonstration area was assessed by average values projected to the ground surface, using individual risk distributions for the settlement vulnerability factors and the Damage Extent Index. These distributions are formed using kriging interpolation for

each factor individually from the adopted boreholes (at a specified time). This is based on the process demonstrated in Figure 5.9, using a scale from low (blue) to high (yellow) risk-based colours, on MATLAB. The normalised results are shown in Figures 5.10-5.13.

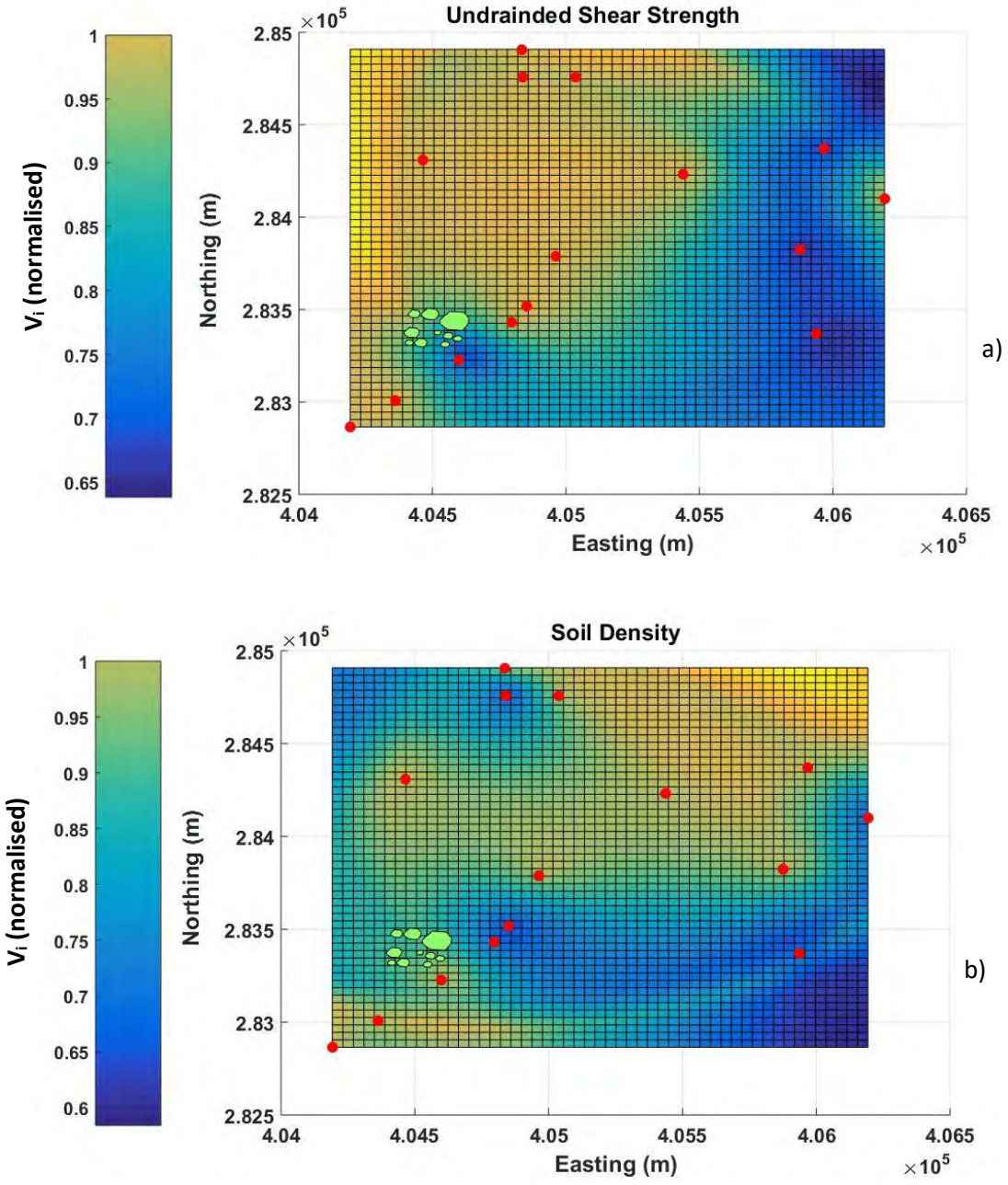

Figure 5.10: The settlement risk distributions due to (a) undrained shear strength and (b) density of the soil (red spots: borehole locations; green spots: building locations).

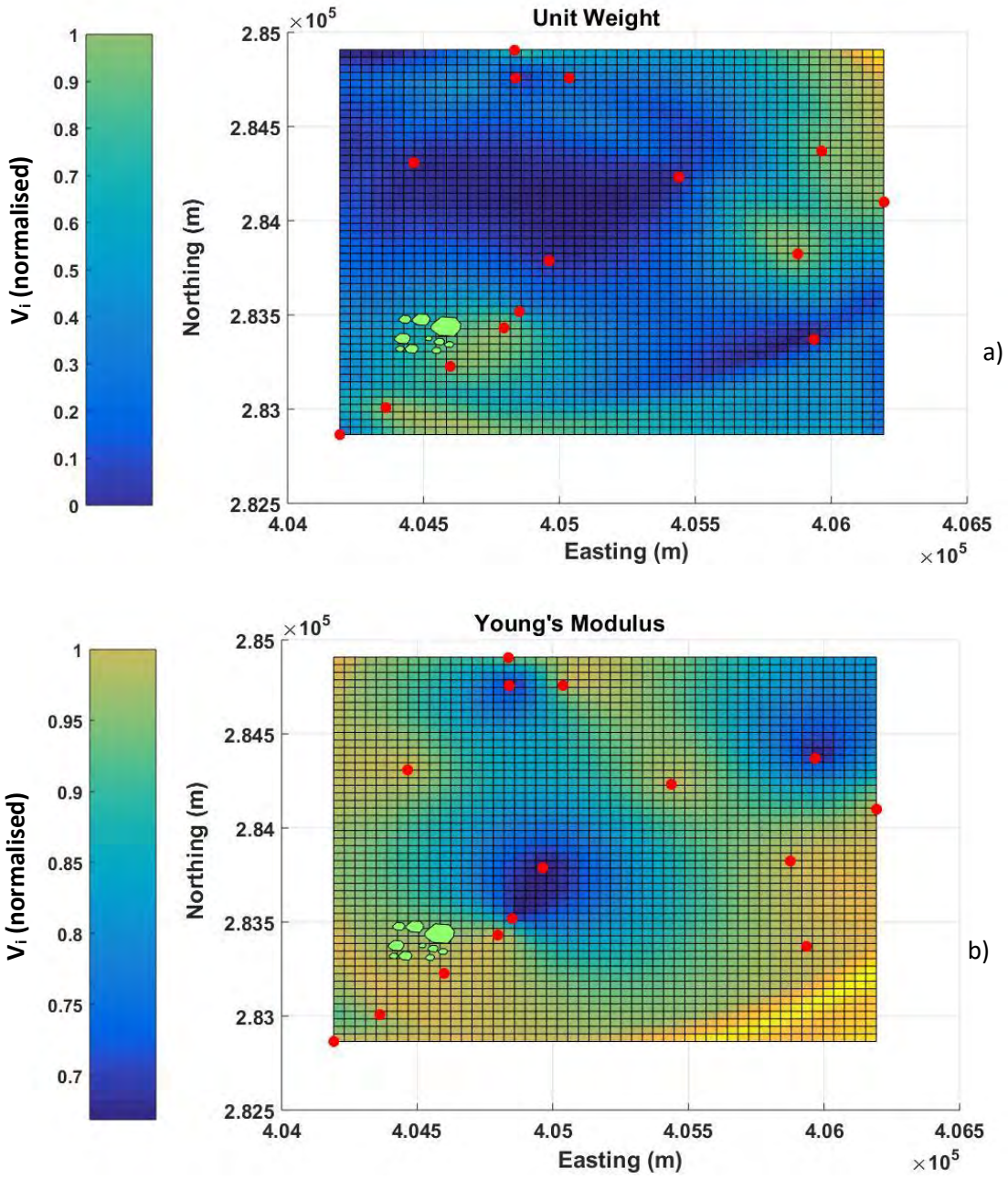

Figure 5.11: The settlement risk distributions due to (a) unit weight and (b) the Young's modulus (red spots: borehole locations; green spots: building locations).

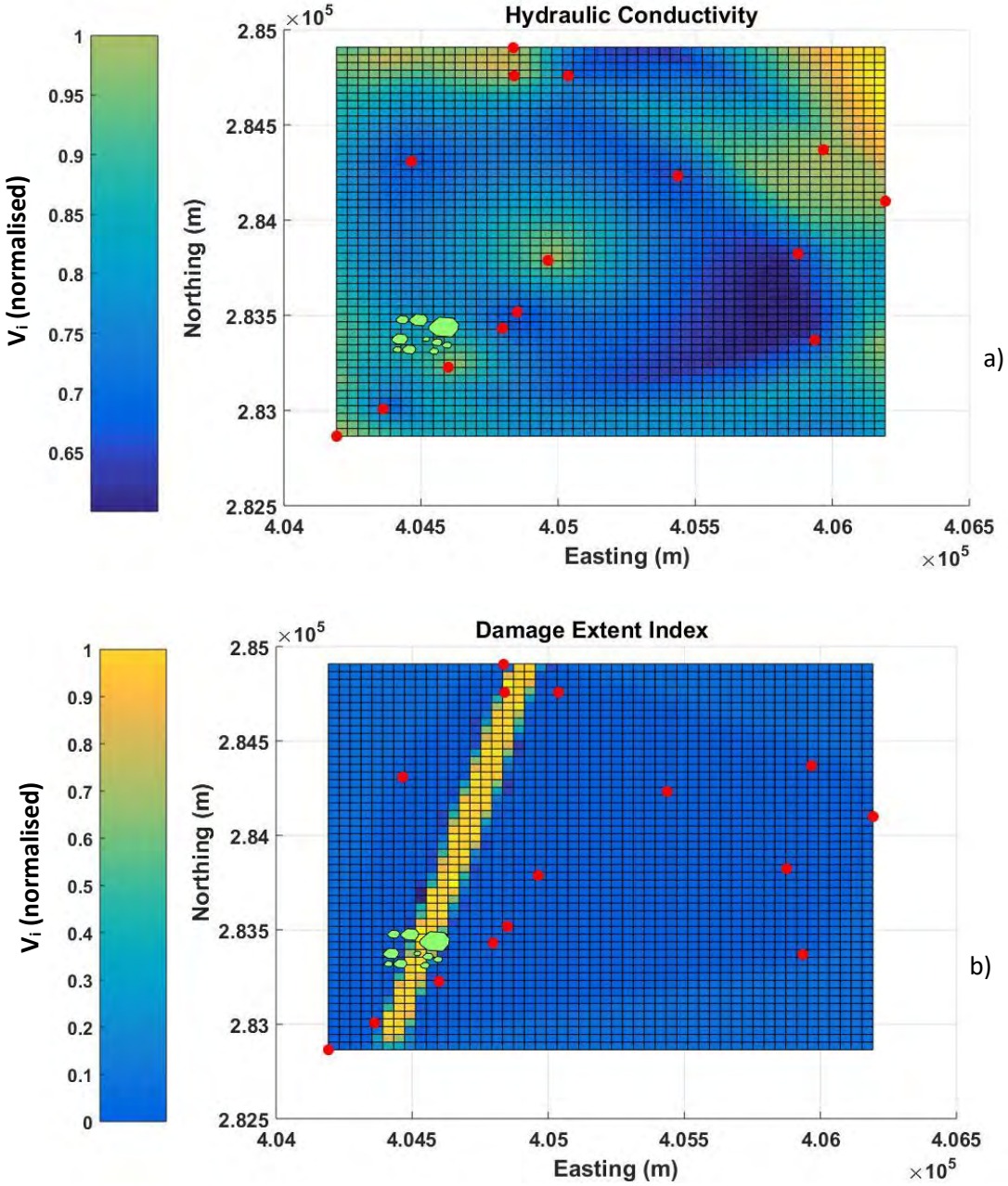

Figure 5.12: The settlement risk distributions due to (a) hydraulic conductivity and (b) the Damage Extent Index (as a factor) (red spots: borehole locations; green spots: building locations).

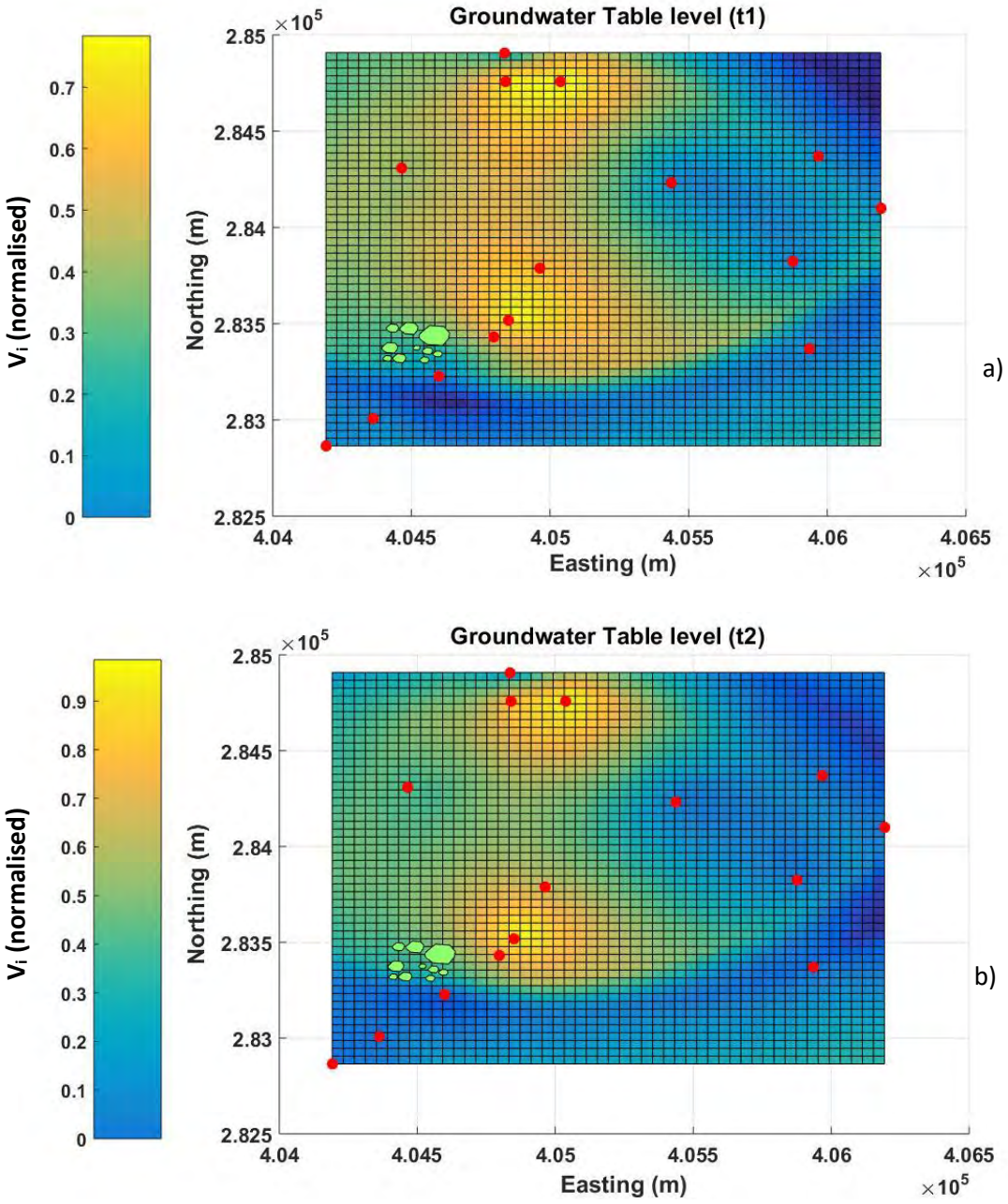

Figure 5.13: Settlement risk distributions from the groundwater table level changes, at the time-points of (a) t1: 25.08.2017 and (b) t2: 15.10.2017 (red spots: borehole locations; green spots: building locations).

5.5.2 Settlement risk assessment using BIM

To present a robust risk assessment, all the relevant criteria had to be integrated and demonstrated within the same visualisations. Therefore, the Settlement Vulnerability (Index) and the Settlement Hazard (Damage Extent Index and Damage Severity Index) were combined to provide a multidimensional settlement risk assessment using the BIM framework. This was conducted using the Settlement Risk assessment from Equation (5.11). It is presented using a risk-based colour-map layer on the ground surface, presenting areas of risk (which is superimposed on the 3D geology-tunnel model). In addition, risk-based colours on buildings were also provided. Further or more detailed investigations could be conducted in areas indicating moderate to high risk.

Figures 5.14 and 5.15 present these integrated visualisations of the Settlement Risk assessment, at the time-points t_1 and t_2, with full and close-up views, respectively (using SketchUp). The times t_1: 25.08.2017 and t_2: 15.10.2017 were chosen to provide representative examples of different Settlement Risk (from different results of Settlement Vulnerability Index) using ARX, which would demonstrate the differences in the resulting 3D visualisations. To provide more comprehensive visualisations and present clearly the impact on the buildings, the Damage Severity Index is not accounted in Figure 5.14, whereas it is accounted in Figure 5.15 (Equation (5.11)). Additional views of the 3D visualisations of the Settlement Risk using BIM are provided in Appendix C, Figure C3 (including the Damage Severity Index).

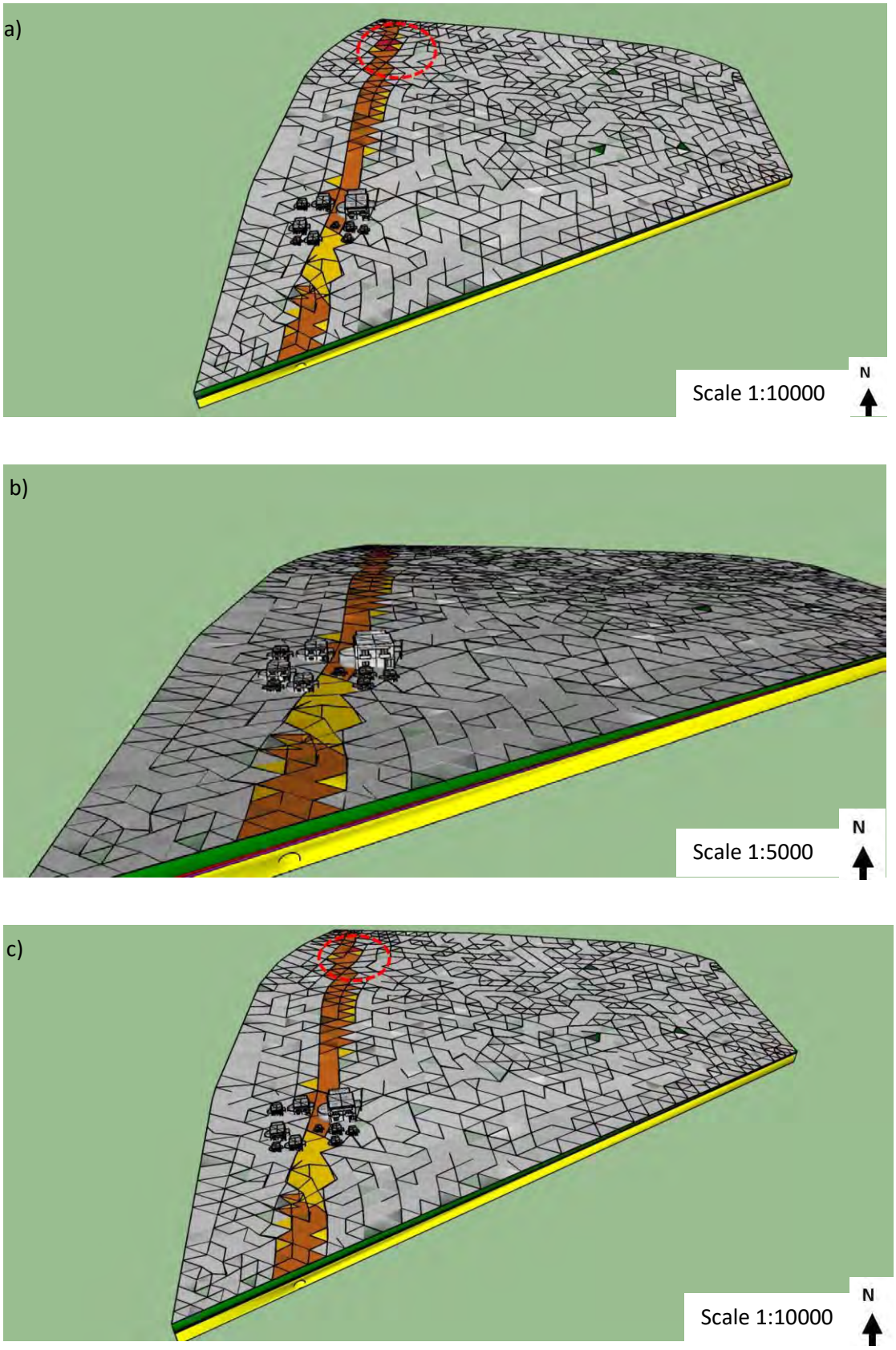

(Figure 5.14 continues in the following page)

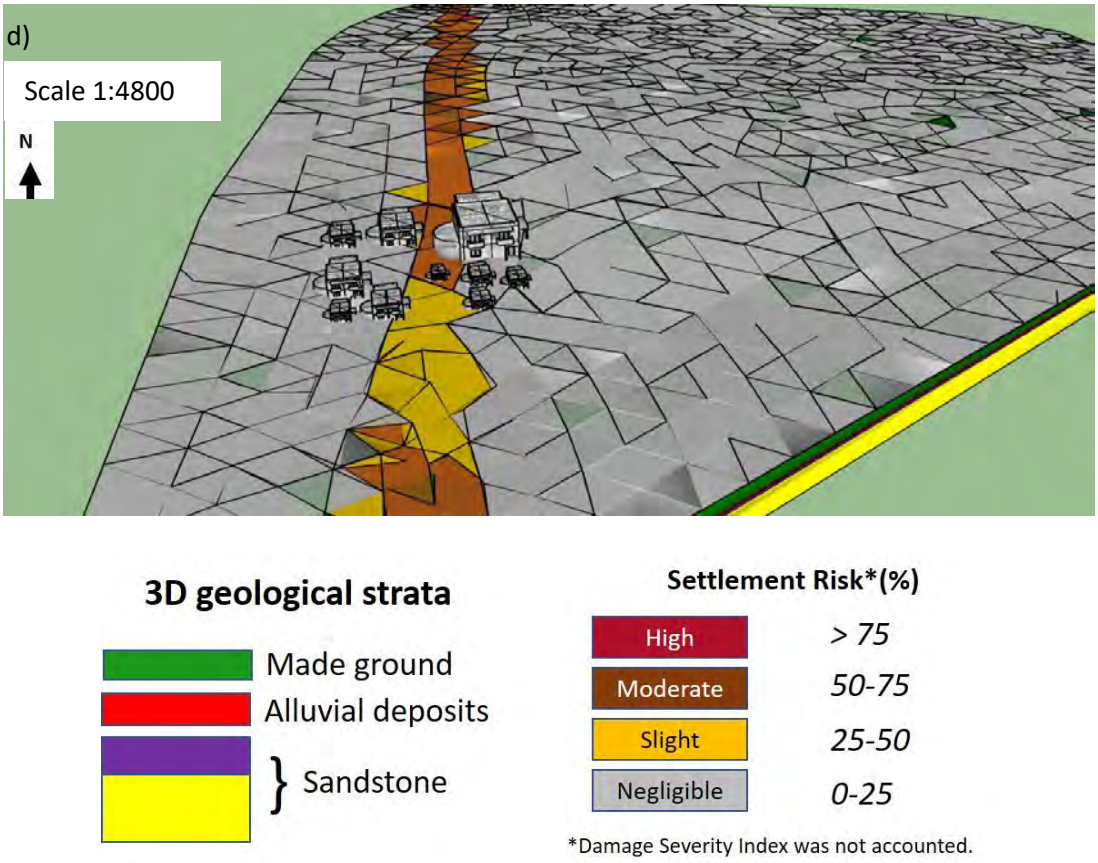

Figure 5.14: BIM visualisations of the temporal changes of the Settlement Risk assessment superimposed onto the 3D geology-tunnel, estimated at two different monitored time-points, (a), (b) at t1: 25.08.2017, and (c), (d) at t2: 15.10.2017.Areas of high risk are shown within the red circle. [NB. This figure does not include the Damage Severity Index, and buildings were not risk-based coloured.]

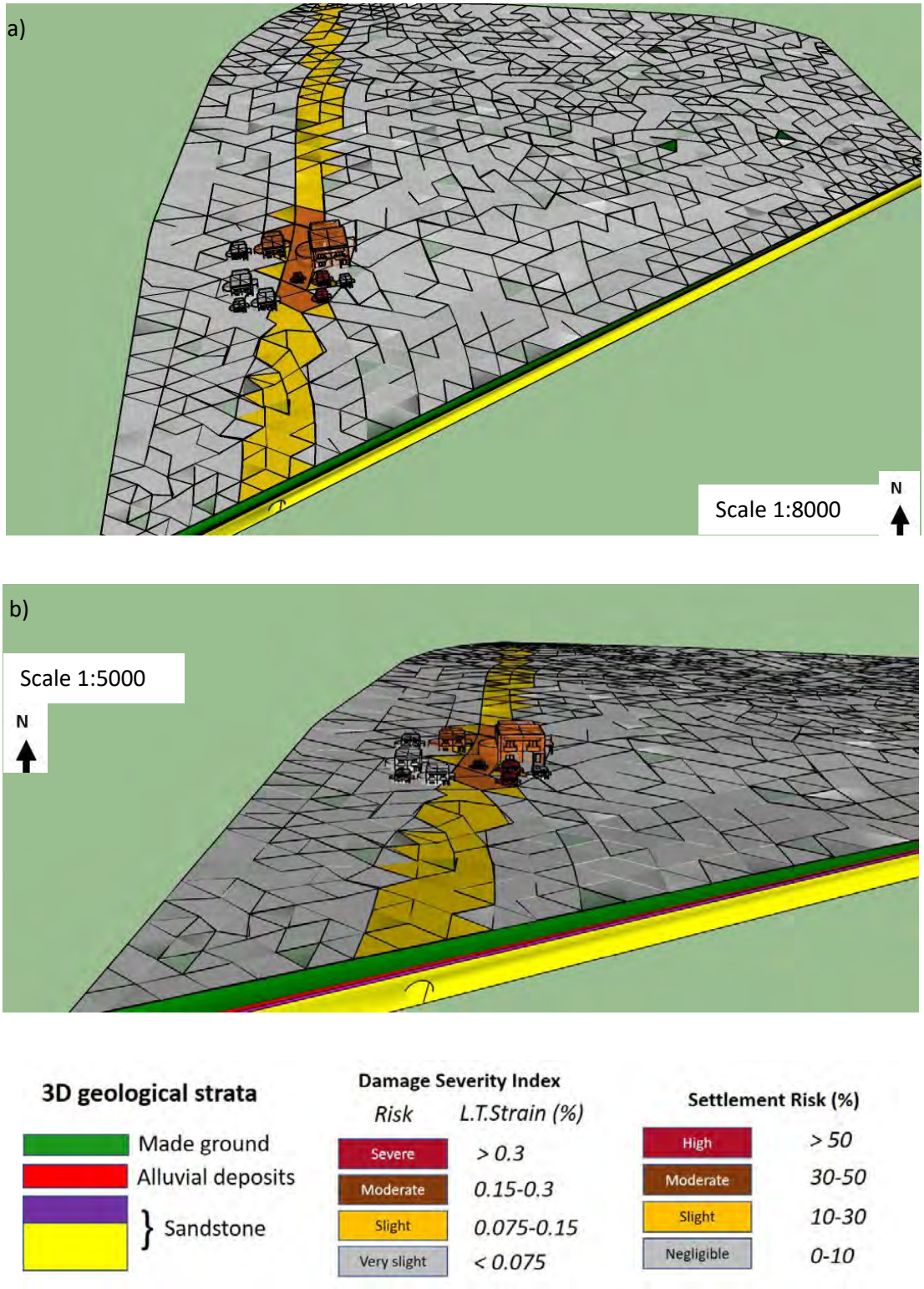

(Figure 5.15 continues in the following page)

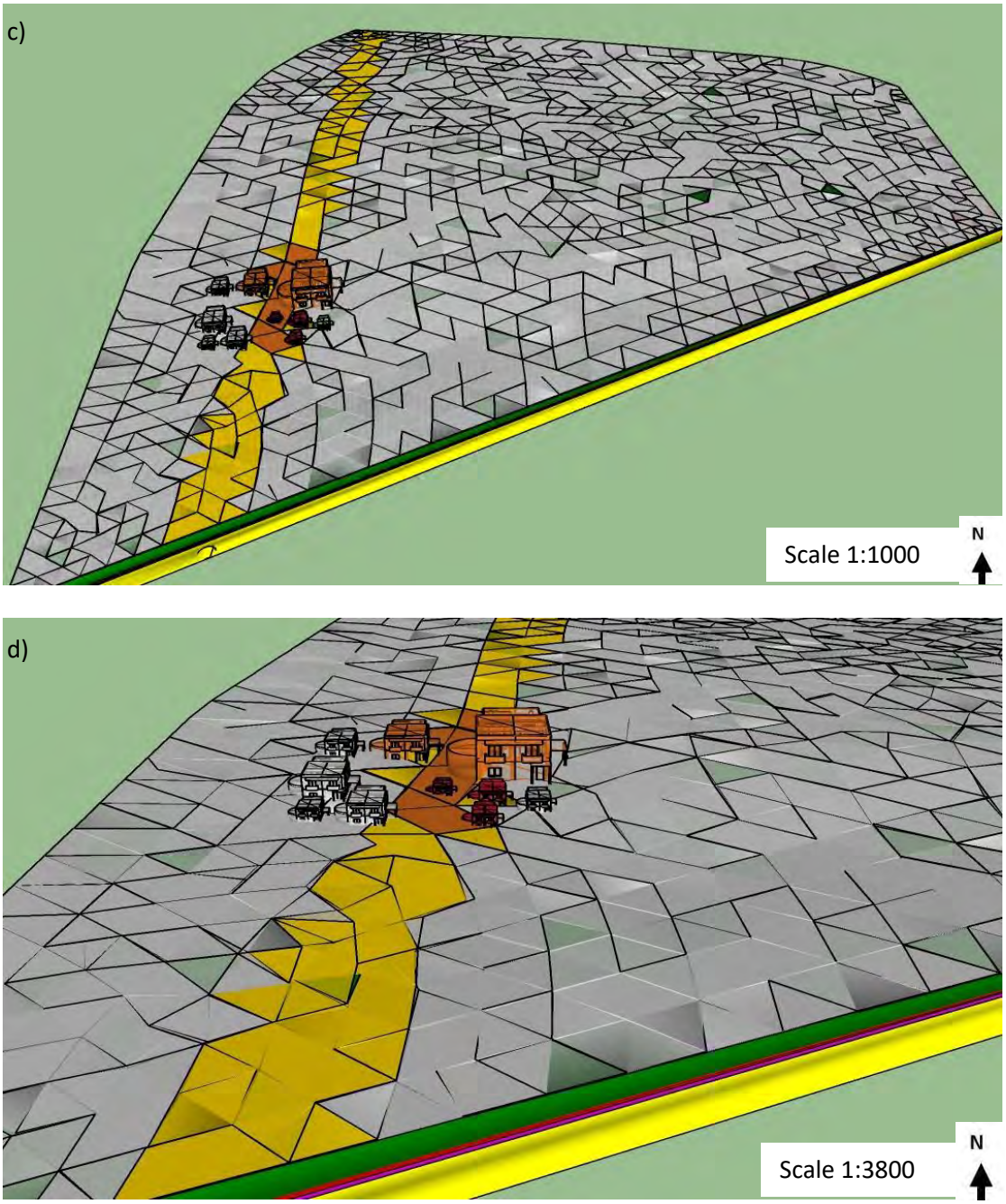

Figure 5.15: 3D visualisations (BIM) of the temporal changes of the Settlement Risk assessment superimposed onto the 3D geology-tunnel model, estimated at two different time-points, (a), (b) t1: 25.08.2017, and (c), (d) t2: 15.10.2017, from a normal and a closer view, respectively.

5.6 Discussion of the results

5.6.1 Settlement risk distributions

In this section, the settlement vulnerability of the area investigated was assessed in Figures 5.10-5.13. This was carried out using average values through kriging interpolation, providing the settlement risk distributions on ground surface. This was performed for each settlement vulnerability factor, as well as the Damage Extent Index (as a factor here), individually. The resulting settlement risk distributions were presented in Figures 5.10-5.13, using MATLAB, and demonstrated a rage of low (blue) to high (yellow) risk-based colours (interpolation).

The assessment analysis was conducted in MATLAB, for the timepoint t_1: 25.08.2017. Figure 5.12b demonstrated the settlement risk distribution due to the Damage Extent Index. This was successfully shown via a higher settlement risk along the resulting settlement trough, as expected. This could also confirm this approach.

In addition, in the case of the groundwater head level fluctuation, the ARX approach was additionally used to provide the changes with time at another timepoint, t_2: 15.10.2017, as well, as shown in Figure 5.13. The resulting slight changes between Figure 5.13a and 5.13b were expected, aligning with a normal groundwater-table level fluctuation within months (BGS, 2018; NERC UKCEH, 2018). The footprints of the georeferenced buildings were also included in the demonstrations to provide a relative view of all the components of the model. The areas where a considerable risk (in yellow) was shown, imply hazardous conditions due to settlements with respect to an investigated settlement vulnerability factor (Figures 5.10-5.13).

5.6.2 Settlement risk assessment using BIM

This section provided the resulting 3D settlement risk assessment visualisations using BIM. In the multidimensional settlement risk assessment visualisations of Figures 5.14 and 5.15 of this

chapter using BIM (SketchUp), the Settlement Vulnerability Index and the Settlement Hazard (Damage Extent Index and Damage Severity Index) were accordingly combined using Equation (5.11). It was presented by a risk-based colour-map layer on the ground surface and colour on the building faces, indicating zones of risk and damage risk, respectively.

More specifically, in Figure 5.14, only Damage Extent Index was combined with Settlement Vulnerability Index (Equation (5.11)), presented along the direction of the tunnel centreline and projected on the ground surface. In particular, Equation (4.5) (Chapter 4) was employed to provide the visualisations. This demonstrated risk-based colours with a range of 25% to greater than 75%. In the same Figure 5.14, higher risk-based colours were exhibited along the direction of the tunnel centreline, 'implying' the resulting settlement curve. Higher risk levels were shown to extent along the whole length of the tunnel centreline – demonstrated on the ground surface. A settlement area of high risk is marked, by way of example, with red circles in Figures 5.14a and 5.14c (for both time-points). The changes of risk areas in these visualisations (between Figures 5.14a and 5.14b), which were mainly shown in high-risk areas, were due to the groundwater head level fluctuations, analysed previously using the ARX. These are found to be of slight magnitude due to the slight fluctuations within the specific (small) time period of the groundwater head levels described in Chapter 5. Here, damage severity of buildings was not considered, and therefore buildings are shown with negligible risk.

In Figure 5.15, the Damage Extent Index and Damage Severity Index were integrated with the Settlement Vulnerability Index (through Equation (5.11)). In particular, Equation (4.12) (and Table 5.4) was employed for generating the visualisations. Higher risk-based colours on the ground surface were shown again along the direction of the tunnel, caused by the settlement trough. In contrast to the previous case in Figure 5.14, the highest risk here was found next to the buildings, directly below the built-up area, as shown in Figure 5.15. In this case, this was

caused by the incorporation of the Damage Severity (Index) of buildings data into the settlement risk assessment, using Equations (5.10) and (5.11). Further or more detailed investigation would be needed at these locations close to buildings that presented a moderate risk, and mainly in areas that demonstrated a moderate to high risk. The tunnelling-induced settlement risk was analysed with time as time-dependent factors, such as the groundwater table level here, were involved. This was exhibited by two different time-points due to the groundwater table level fluctuations, demonstrated in Figures 5.15a,b and Figures 5.15c,d. Due to the small groundwater table level fluctuation range, slight changes between the previous resulting figures in terms of Settlement Risk levels were expected and presented. Figures 5.15b and 5.15d provide a closer view of the buildings investigated – the Damage Severity Index is included, here – with risk-based colours to provide a clear understanding.

The vulnerability of an area (through the example of the settlement vulnerability factors) was explored in the previous example of this chapter, and was included in the settlement risk assessment, through clear 3D visualisations. Hence, it clearly revealed the impact that geotechnical/structural and time-dependent factors have on the related risk, here caused by tunnelling. Areas of risk for further investigation were shown. Hence, a tool was provided to support urban land use planning.

The resulting visualisations in this chapter presented the Settlement Risk by the addition of the Settlement Vulnerability. This used settlement vulnerability factors which had an impact to the resulting settlements as demonstrated in the previous visualisations. This risk assessment could be extended with other/additional vulnerability factors –dependent on the geohazard, if required.

5.7 Summary

Chapter 5 provided a framework for the development of a geohazard information system in an urban area. This followed on from the previous chapter, using the similar data integration using BIM, although a larger 3D model was developed. The aim here was to develop a geohazard risk assessment (in this case the tunnelling-induced ground settlement risk) using a multi-criteria decision analysis integrated with BIM, based on borehole data. All the aspects of this integration linked together, enhancing 3D ground modelling, were demonstrated. This integration produced several detailed 3D geohazard risk assessment visualisations (including further supporting visualisations) to provide a complete preliminary assessment tool for ground investigations. This tool could obtain important information to be used identifying vulnerable areas for assisting for sustainable urban planning. It could also be employed for advising for alternative tunnelling routes, if required.

6 ESTIMATION OF THE TUNNELLING-INDUCED SETTLEMENT ECONOMIC RISK OF BUILDING DAMAGE USING AN UNCERTAINTY ANALYSIS AND BIM

6.1 Overview

In this chapter, a tool to predict the tunnelling-induced settlement costs caused by adjacent building damages was generated. This is conducted by creating a 'layer' that will demonstrate these costs using a 'Settlement Economic Risk' assessment. This is combined with the georeferenced 3D geological-tunnel-building model, which was developed using the method described in Chapter 3 and presented by Providakis et al. (2019).

Indications and estimations of uncertainty are crucial for assessing geohazard risk and impact (such as damage costs) and reducing the danger. As an example of the approach that can be used within the context of the integrated geohazard assessment proposed in this thesis, this chapter aims to provide an integrated computer-based approach to estimate and visualise the economic risk (costs) associated with building damage caused by tunnelling-induced settlements, using Building Information Modelling (BIM).

A risk is explored with respect to the probability, extent and the severity of the hazard (Fedeski and Gwilliam, 2007). Therefore, this chapter utilised Monte Carlo simulations to provide a probabilistic approach. In addition, analytical models were employed to provide the surface settlement caused by tunnelling (Loganathan and Poulos, 1998). These were combined with building damage assessments methods (Burland, 1995). This used geotechnical factors, while the structural factors required for the analysis were adopted using BIM structural models.

Damage Categories have been adapted for use in the simulations. These categories are correlated with corresponding repair costs due to the ground settlement for each investigated

building. The data used was based on relevant building damage survey records and research for England and Wales from the Office for National Statistics (2017). Subsequent probabilistic diagrams were developed to assess the risk for the building-damage costs. A resulting Settlement Economic Risk (Rs) (£/m^2) due to ground settlement for each building was estimated. This is carried out using the diagrams developed, for the adopted damage criteria for a corresponding Damage category.

This study provides an example method that has explored the probability of the Settlement Hazard ($HAZARD_{SE}$) to occur using basic risk assessment assumptions (Equation 3.1). In this case it was performed by a building-damage cost analysis caused by tunnel-induced settlements in an urban area. A cost analysis of the settlement risk assessment of building damage is proposed. This was integrated with an uncertainty analysis, to estimate the risk, efficiently. In addition, the creation of the 3D geology-tunnel-building model was provided using the data integrations with BIM, as described in section 3.3.9 (Methodology). The resulting Settlement Economic risk assessment visualisations using this 3D model were then generated.

The flow chart of the approach adopted in this chapter is presented in Figure 6.1. This follows on from the data integration to create the 3D models, using the approach proposed by Providakis et al. (2019), as described in Chapter 3, and expands it to an uncertainty analysis of building-damage costs, using the Monte Carlo analysis (Figure 6.1). The results of this analysis are then demonstrated by 3D visualisations of the Settlement Economic Risk assessment using BIM.

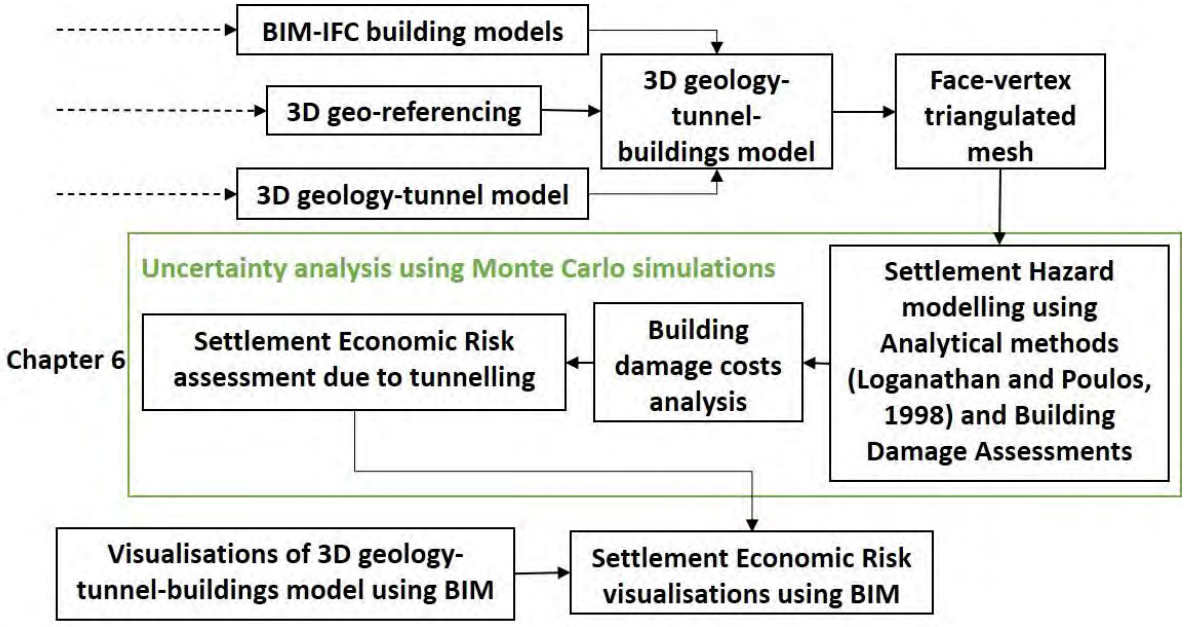

Figure 6.1: A flow chart of the method for this chapter following on the BIM integration approach proposed by Providakis et al. (2019).

6.2 Georeferenced 3D geology-tunnel-buildings model of the simulated urban area

In this chapter, the simulated urban area used the same set-up as Chapter 5. In particular, the wider urban area around the campus of the University of Birmingham, UK, was employed as a representative example of a study area. Its geology was extracted using fifteen boreholes, the locations of which are shown in Figure 6.2 (Google Earth, 2018). These boreholes provided the data for interpolation (MATLAB) to form the 3D geological model, as described in Chapter 3. The geology of the area consisted of soft ground, and a 3D geology model was developed as shown in Figure 6.3. A representative 3D tunnel model having a 10m diameter was placed within this model at a depth of 20m (Figure 6.3). More specifically, the MATLAB scripts used are presented in the Appendix D.

Ten low-rise masonry BIM/IFC building models taken from SUPodium (2018) were placed on the resulting 3D model of the simulated urban area, as described in Chapter 3 (and proposed by Providakis et al. (2019)), and presented in Figure 6.4.

Figure 6.2: The locations of the boreholes employed for the analysis in this chapter (Google Earth, 2018). The tunnel centreline is shown using a red line.

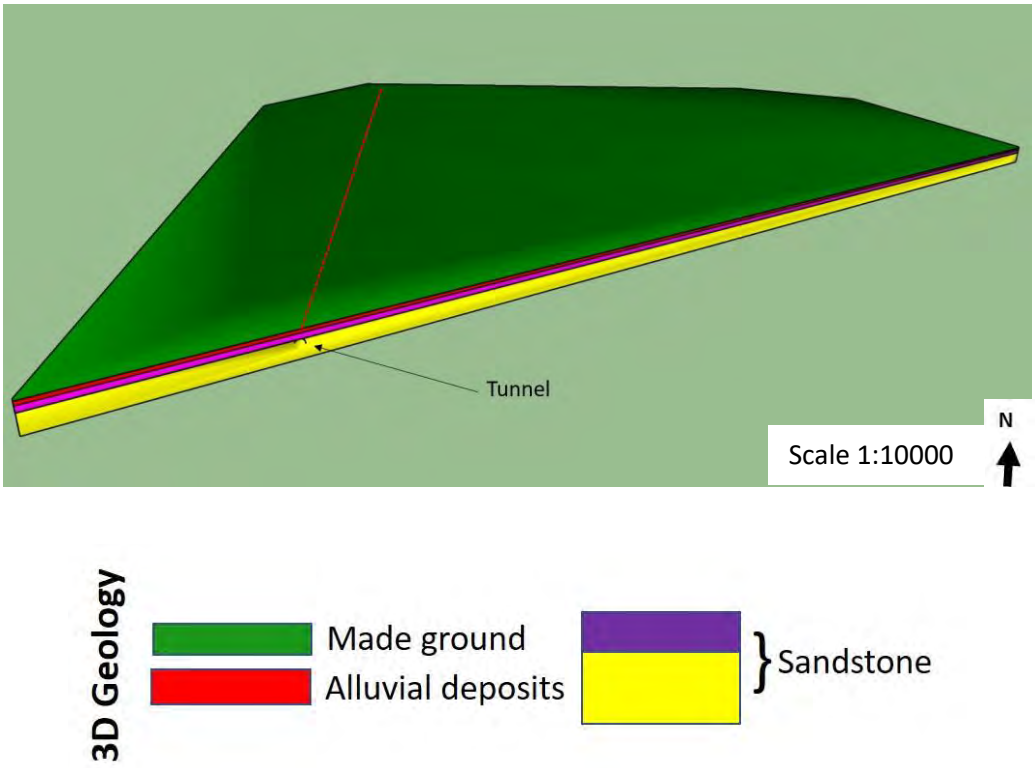

Figure 6.3: The 3D geological and tunnel models' visualisation using SketchUp (Trimble Inc., 2019), from the method proposed by Providakis et al. (2019). The tunnel alignment is also presented by a dotted red line.

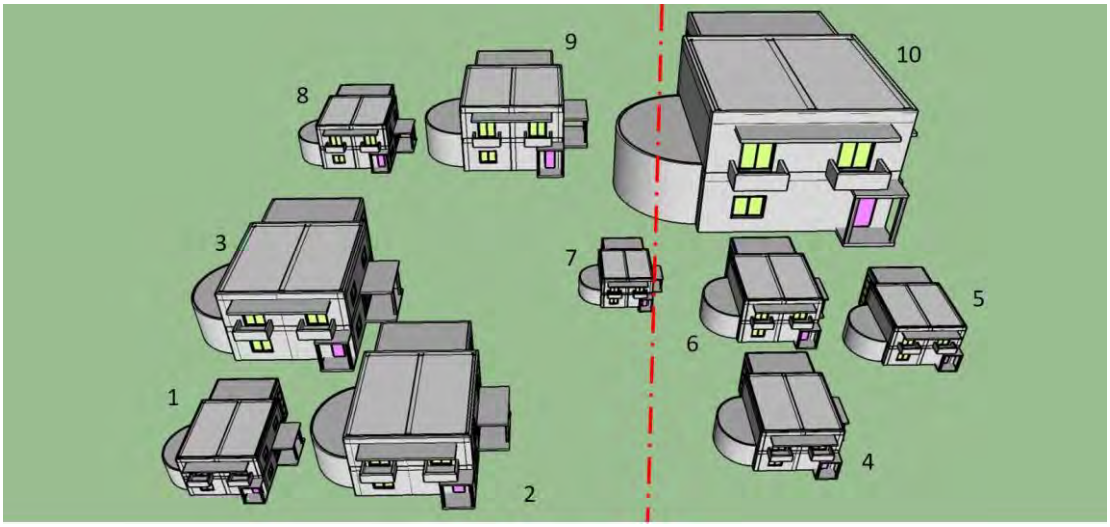

Figure 6.4: The position of the buildings (with their numbers) taken from SketchUp (Trimble Inc., 2016; SUPodium, 2018; Graphisoft, 2018). The tunnel centreline is marked with a dotted red line.

6.3 Utilising Analytical methods to estimate the Settlement Hazard

To provide the tunnelling-induced settlement risk analysis, empirical/analytical models using a resulting settlement trough have been used (Peck, 1969). Similar to the previous chapters, this aligns with a settlement trough (curve), created below the ground surface in the ground among the buildings. There have been many methods to estimate the settlement due to tunnelling in soft ground. The analytical method adopted here uses Equation (4.5) from Loganathan and Poulos (1998) and Loganathan (2011), presented in Chapter 4.

To provide the spatial distribution at the ground surface, the ground (volume) loss, Poisson's ratio of the soil and the soil friction angle were needed, as demonstrated in Table 6.1. These are geotechnical factors, which are characterised by a related uncertainty. Hence, representative estimations to evaluate this uncertainty throughout the construction, were required. These

estimations were based on a combination of knowledge and understanding of local geological conditions, previous experience and statistics.

Evaluation of uncertainties in geological/geotechnical analyses have been important for providing effective resultants (Zhang et al., 2012; Wang et al., 2016; Phoon and Tang, 2019). Ground characteristics could be considered, based on actual data records and geological expertise and knowledge (Phoon and Kulhawy, 1999; Zhang et al., 2012; Phoon and Tang, 2019).

In this chapter, the concept of the problem changes from a geomechanical (correlating deterministic information based on specific values of the ground (volume) loss, Poisson's ratio and friction angle) to a multidisciplinary (including (randomly) distributed uncertainty estimations within predefined ranges of values). Hence, each uncertain geotechnical factor X, i.e. ground loss, Poisson's ratio and friction angle, could be estimated, using Equation (6.1).

$$X = \mu \pm \sigma Y \quad (6.1)$$

where μ is the mean and σ the standard deviation (square root of variance) of factor X, and Y is a standardised random variate, which is assumed here to be normally distributed within a range of [-3, +3].

Table 6.1: The mean and standard deviation values of the geotechnical factors used.

Factor (X)	**Mean (μ)**	**Standard Deviation (σ)**
Ground loss	0.175	0.04
Soil Poisson's ratio	0.25	0.03
Soil friction angle	35	4

6.3.1 Damage extent and severity of the settlement hazard

Among various approaches for assessing building damage due to tunnel-induced settlements, the proposed approach (to provide a representative example) implemented the Building Damage Assessment from the Risk Categories shown in Table 4.4 (Rankin, 1988; CIRIA, 1996), using Equation (4.5) (Chapter 4). These were employed to provide the Damage Extent due to the settlement hazard. The analysis is conducted using MATLAB (as shown in Appendix B), and BIM is used to collect all the information on the maximum settlement and ground slope from building footprints locations.

To provide the Damage Severity of a building due to the settlement hazard, the Building Damage Assessment criteria, which were adapted from Burland (1995) and Mair et al. (1996), were also employed using Table 4.5. The Limiting Tensile Strain Method (LTSM) was utilised to assign the settlement-induced building damage through the critical tensile strains (Burland and Wroth, 1974; Boscardin and Cording, 1989). It should be noted again that LTSM does not emphasise on detailed interactions associated with the foundations. The critical strain (ε_{crit}) was obtained using Equation (4.12) (Burland and Wroth, 1974; Boscardin and Cording, 1989; Burland 1995). To provide the critical strain, ε_{crit}, for every building in the area investigated, their detailed material and geometrical information (such as building length, width and height, sagging/hogging areas and the construction material). This information was collected employing BIM from the IFC building models used (SUPodium, 2018; Graphisoft, 2018), as introduced by Providakis et al. (2019). Hence, the building damage for every building is then obtained using Equation (4.12) and was categorised using the damage categories of Table 4.5 (Burland, 1995; Mair et al., 1996). A maximum difference normalisation was also employed here to correlate factors and values that initially have completely different ranges, with factors estimated to have a (0, 1) frame (Wang et al., 2017).

The ratio of Young's modulus and shear modulus (E/G) of the buildings was a challenging factor, which was used in this type of assessment. This is often heterogeneous due to the diversity of the building materials used within a construction. It varies from E/G=2.6, in the case of masonry structures, to E/G=12.5, for concrete structures. The severity of the settlement damage does not only depend on the settlement magnitude and extent, but also on the material sensitivity within the construction. Masonry buildings can be more susceptible to damage when compared to buildings from reinforced concrete (for example, in the case of shear stiffness of a masonry building is low). Here, the masonry buildings have been selected as an example to explore the proposed methodology. The mean and standard deviation values used (E/G range within 2.6 and 2.8), are shown in Table 6.2. Hence, the current method considers the uncertainty estimation of E/G in addition to the geotechnical factors. This estimation is shown in Equation (6.2).

$$X_{E/G} = \mu_{E/G} \pm \sigma_{E/G} Y_{E/G} \quad (6.2)$$

where the uncertainty factor, $X_{E/G}$, can be estimated here using the mean value, $\mu_{E/G}$, and the standard deviation, $\sigma_{E/G}$; the random variate (standardised) is $Y_{E/G}$, which is assumed to be normally distributed in the range of [-3, +3].

Table 6.2: The mean and standard deviation values of E/G ratio used in the present analysis.

Factor ($X_{E/G}$)	**Mean ($\mu_{E/G}$)**	**Standard Deviation ($\sigma_{E/G}$)**
E/G	2.7	0.03

6.4 Uncertainty analysis for estimating the Settlement Economic Risk

In the case of a model that includes many inputs with uncertainties, a stochastic analysis could be employed to provide subsequent uncertainty evaluations, i.e. how the input uncertainty affects the characteristics of this model (Wittwer, 2005). This type of analysis has been commonly used in geotechnical analyses (Cheung and Tang, 2005; Zhang et al., 2009; Peng et al., 2017; Cao et al, 2019).

Monte Carlo simulation is a method of stochastic modelling, in which the output probability distribution is provided by repeated random-sampling tests of inputs (Zhang, et al., 2012). It has been widely utilised in similar geotechnical problems to perform uncertainty analyses (Rowe and Fraser, 1995; Wang et al., 2010; Zhang, et al., 2012; Cao et al., 2017). A large number of those simulations assures that a random variation of the inputs used, is reflected (Vose, 1996). In the present analysis, using Monte Carlo simulations, the uncertainties of the adopted geotechnical factors (Equation (6.1)) or of the E/G value (Equation (6.2)), had an impact on each other. The overall idea of the Monte Carlo analysis used, is shown in Figure 6.5. The building damage in this analysis was a function of the critical tensile strain (ε_{crit}), as shown in Table 4.5 (Chapter 4). The steps of the Monte Carlo simulations employed in the analysis of this chapter were:

1. Define the probability distributions of possible inputs (factors): ground (volume) loss, Poisson's ratio, friction angle and E/G ratio. In this case, it is assumed that these factors vary according to a normal probability distribution.
2. Generate the random (representative) inputs from the probability distribution over the domain, using Equations (6.1) and (6.2).
3. Calculate the resultants of building Damage Categories (outputs) according to Table 4.5 using Equations (4.5) and (4.12) and the generated inputs.

4. Repeat the steps 1–3, using 1000 simulations.
5. Aggregate the results.

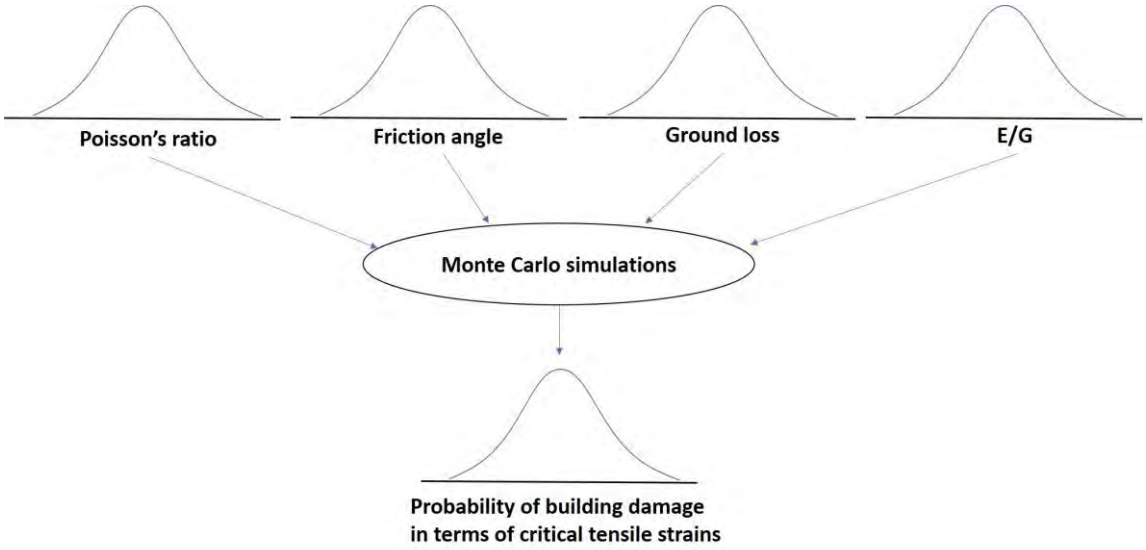

Figure 6.5: The overall approach of the Monte Carlo simulations used in this analysis.

6.4.1 Probability distribution of building damage

Each of the ten buildings within the area investigated was analysed using the adopted approach. To provide robust probability estimations, these Monte Carlo simulations were run 1000 times in MATLAB, which is a reasonable number, as suggested by Vose (1996). Thus, for every building a probability for any Damage Category to occur, was provided. The detailed MATLAB scripts used, are provided in Appendix D.

The resulting probability distributions for the damage of each building examined, is presented in Figures 6.6-6.10, as bar graphs of the Damage Categories (1-5). The probability values were then used to develop the settlement economic risk of this damage.

a)

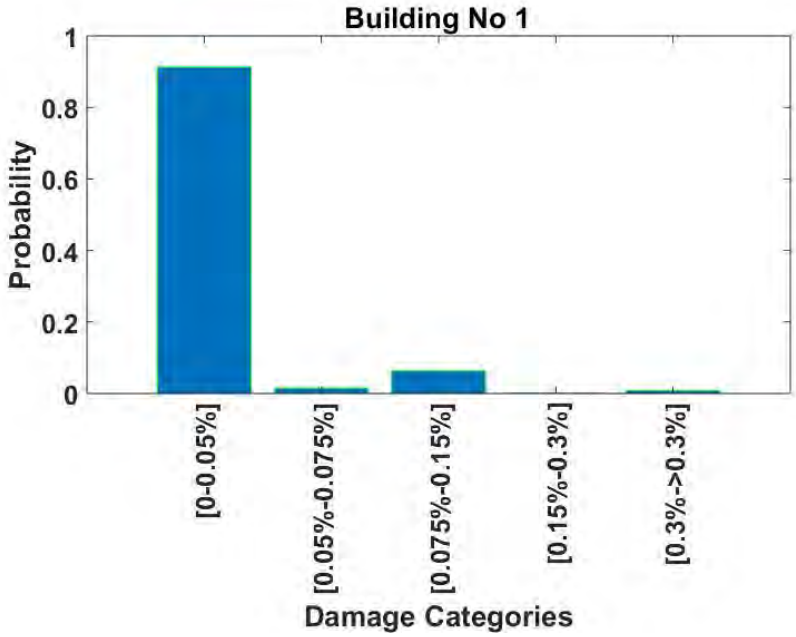

b)

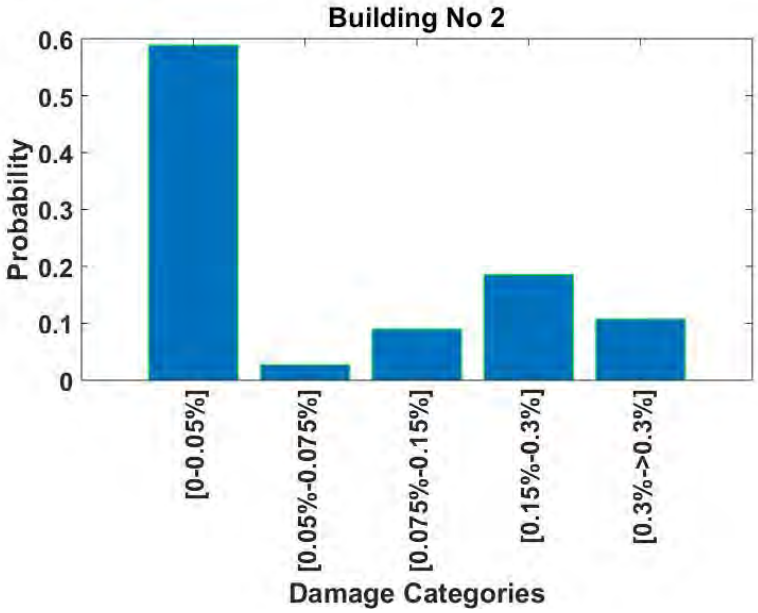

Figure 6.6: The bar graphs demonstrating the probability of a Damage Category to occur for building (a) No. 1 and (b) No. 2.

a)

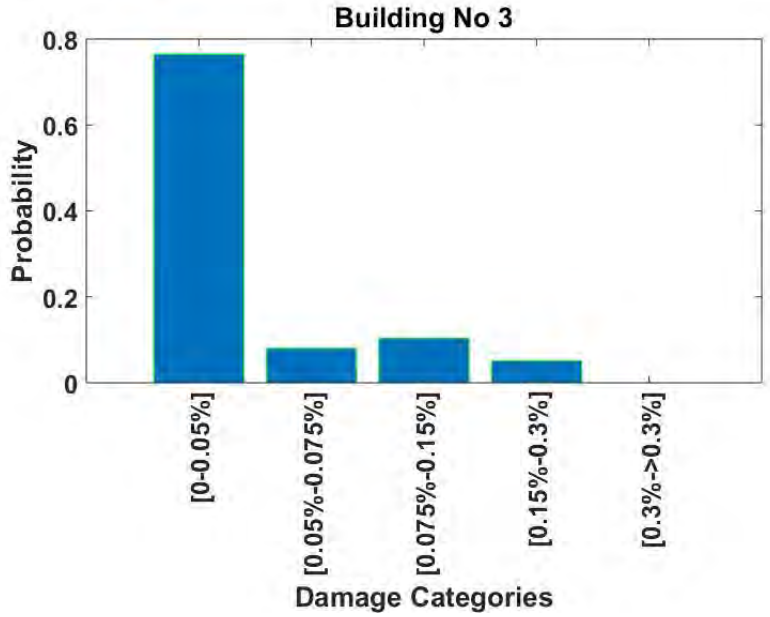

b)

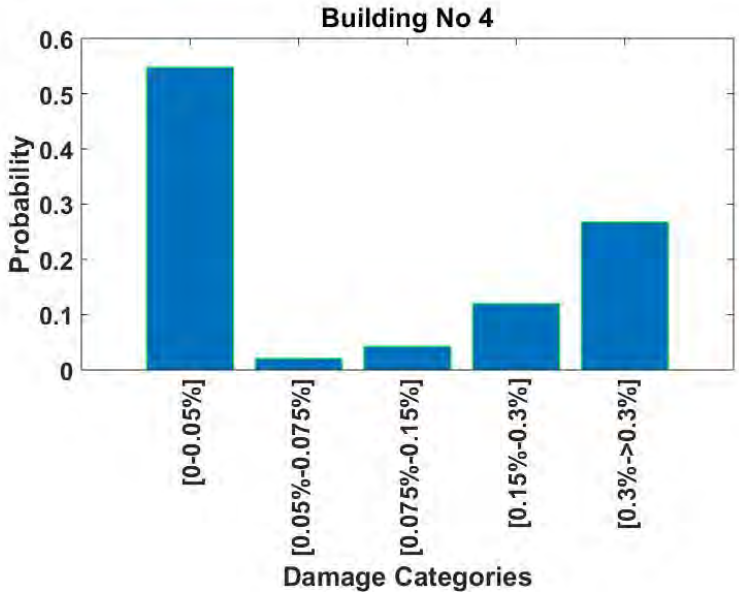

Figure 6.7: The bar graphs demonstrating the probability of a Damage Category to occur for building (a) No. 3 and (b) No. 4.

a)

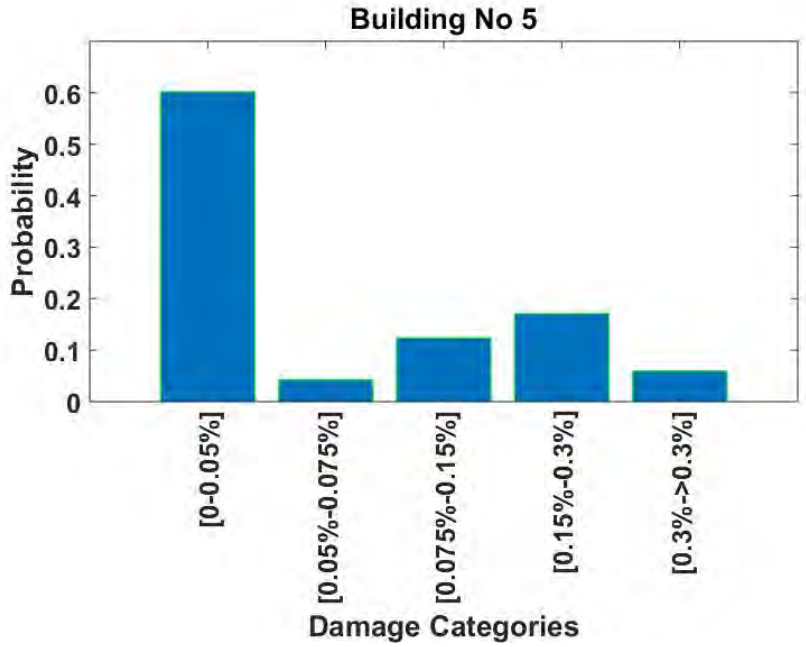

b)

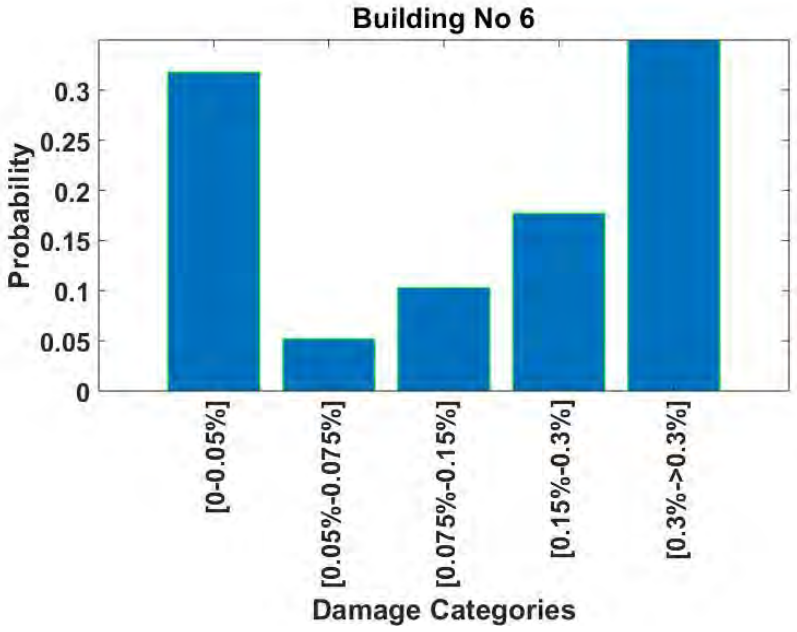

Figure 6.8: The bar graphs demonstrating the probability of a Damage Category to occur for building (a) No. 5 and (b) No. 6.

a)

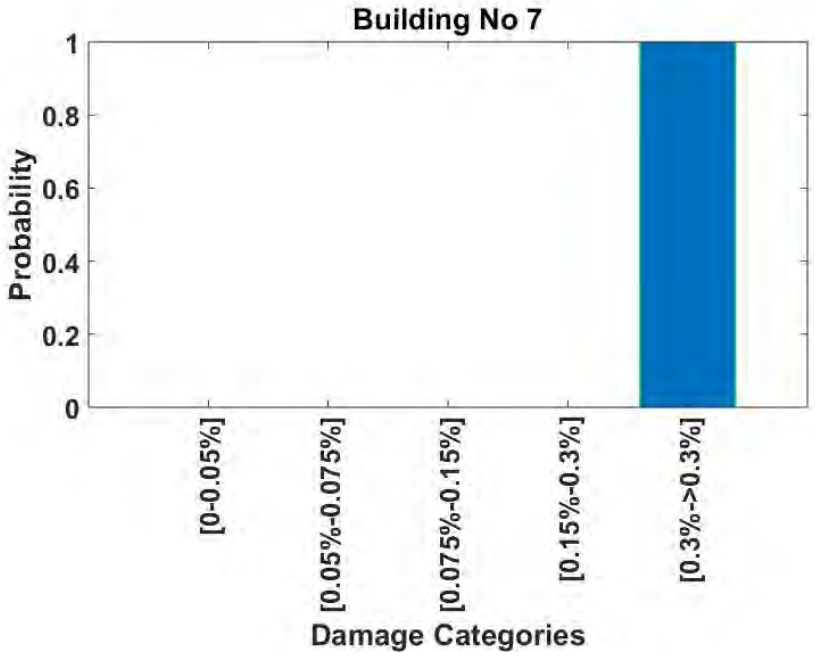

b)

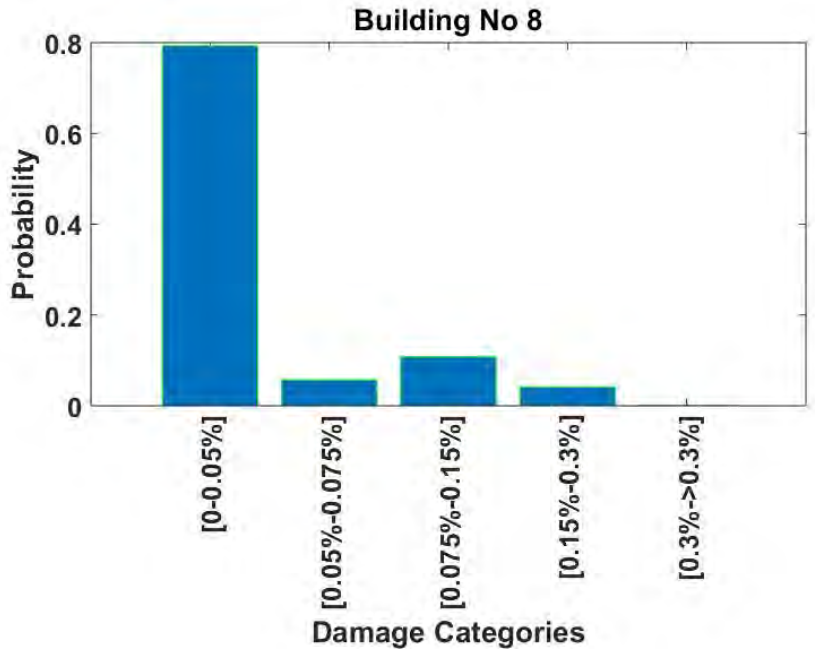

Figure 6.9: The bar graphs demonstrating the probability of a Damage Category to occur for building (a) No. 7 and (b) No. 8.

a)

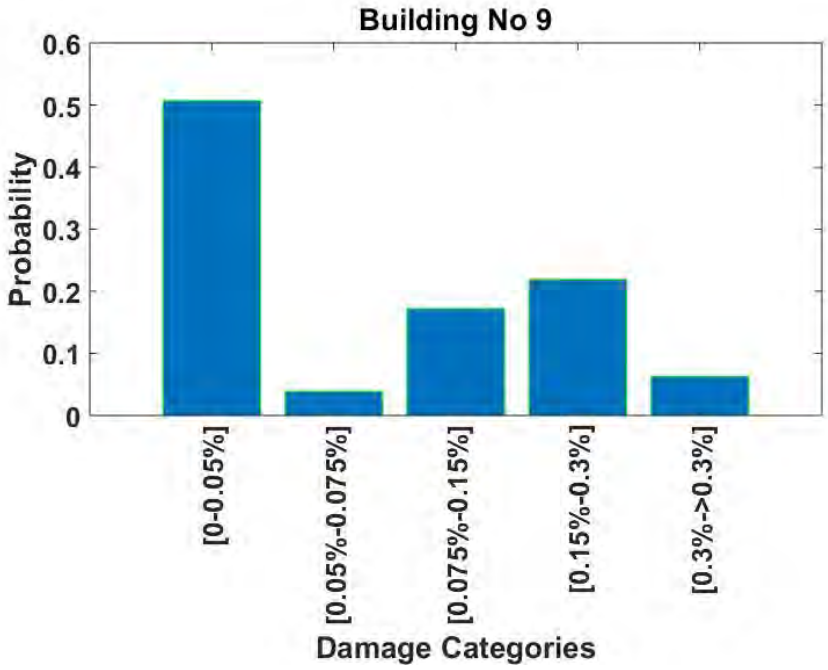

b)

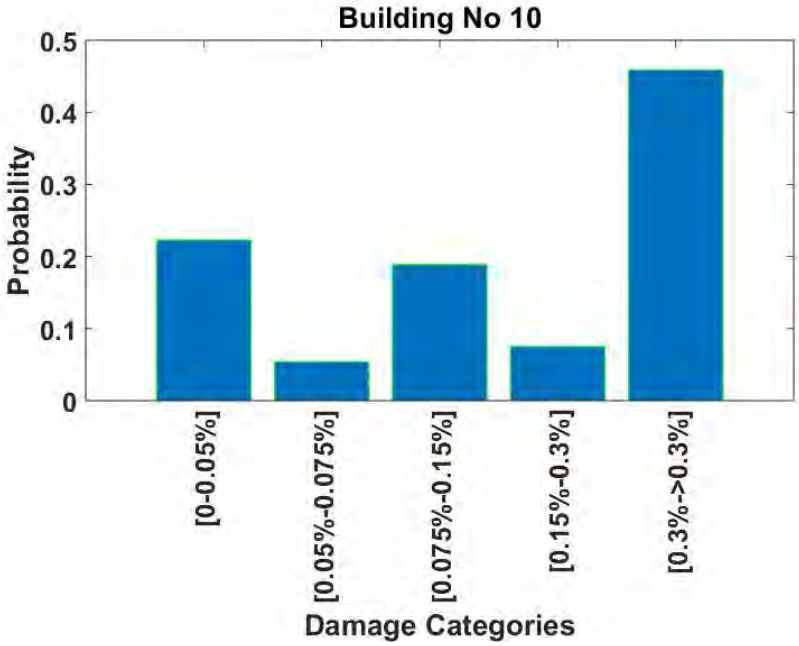

Figure 6.10: The bar graphs demonstrating the probability of a Damage Category to occur for building (a) No. 9 and (b) No. 10.

6.4.2 Building damage cost analysis using Probability Density Functions

The probabilistic methods adopted here, utilised Probability Density Functions (PDFs), which have provided an effective approach for such problems previously (Zhang, 2009). In the proposed approach, these were combined with the Monte Carlo method to provide a robust (building-damage) cost analysis. In terms of economic costs, among the many cost analyses available, one that successfully related costs with geotechnical elements, was provided by Sundell et al. (2019). An efficient cost analysis for a geotechnical risk assessment would be related to repair costs. Hence, in the current example, (low-rise) building-damage costs, due to tunnel-induced settlements, were utilised.

As already noted, in the proposed settlement-induced building-damage scheme, the critical tensile strain (ε_{crit}) levels were associated with this damage. Minor critical strains were related to negligible damage, and hence small repair-costs, whereas larger critical strains had an effect on the function or the main structure of a building, and result in reasonable damage and costs. The consequences of this damage are described by a continuous function, providing the Settlement Economic risk (Rs) for each building, as presented in Equation (6.3) (Sundell et al., 2019).

$$R_s = \int C_s f_s ds \tag{6.3}$$

where Rs is the Settlement Economic Risk due to tunnelling given by a combination of the economic cost, Cs, caused by settlements and the Probability Density Function (PDF) of damage occurred, fs.

The Settlement Economic Risk, Rs, was initially estimated for every building. The sum of the Rs for all the buildings included in the study area provided the total economic risk for a specific

settlement hazard for this area. Economic costs (Cs) consisted of direct costs (i.e. costs of repairing of settlement damage) as well as indirect costs (e.g. related to project delay, a reduced market value of damaged buildings and tenant issues) (Sundell et al., 2019). The direct costs were only considered here, focusing on demonstrating the adopted approach. The economic cost valuation was based on previous research and is not directly related to tunnelling-induced settlement damage, because no efficient database for related damage exists for the UK. Thus, in this chapter, the 'Damage Index' adopted by Blong (2003) was used that enables the damage evaluation due to any hazard and any type of building to be provided. This was employed to provide the settlement damage, in terms of complete replacement costs, for any examined building or building at risk. This was expressed in units of average gross charge (cost) for a new property (house) in metre squared of floor area. The average gross charge for a new construction in England and Wales in the year 2016 was 2,400£/m^2, and the highest reasonable gross charge reached 6,600£/m^2 in the wider London area (Office for National Statistics, 2017). The average property area in England and Wales in the year 2016 was 90.1m^2 (Office for National Statistics, 2017).

To estimate the damage costs from a particular hazard, the full scale of potential values from 0 to 1 corresponded to the complete range of the observed damage, i.e. from negligible damage to the total collapse of the building. Blong (2003), after reviewing studies of natural hazard damage, indicated five different damage categories as: light, moderate, heavy, severe and collapse; and then added a relative description for the nature of this damage. The summary of those categories is presented in Table 6.3, adapted from Blong (2003). Each Damage Category has a corresponding range of values of damage, where for estimation purposes, Blong (2003) has taken the central value and called this the 'Central Damage Value (CDV)' (Table 6.3).

Table 6.3: The Central Damage Value (CDV) categories, as adapted from Blong (2003).

Damage	**CDV**	**Range**	**Geohazard**
Light	0.02	0.01-0.05	Hairline cracks (<0.1mm)
Moderate	0.10	0.05-0.20	Minor foundation settlement
Heavy	0.40	0.20-0.60	Walls out of perpendicular by several degrees; floors inclined/heaved; open cracks in walls
Severe	0.75	0.60-0.90	Structure grossly distorted; partition walls and brick infill at least partly collapsed; footings lose bearing; service pipes disrupted
Collapse	1.00	0.90-1.00	Partial/total collapse

In the present method, the five damage categories adopted from Blong (2003) were correlated with the building Damage Categories (No. 1-5), based on the critical tensile strains, taken from Chapter 4 Table 4.5 (Burland, 1995; Mair et al., 1996), which was caused by tunnel-induced settlements, which were created within the footprints of the buildings. Hence, the cost of the settlement damage for each of the five Damage Categories was estimated from Equation (6.4).

$$Average\ damage\ cost\ per\ m^2\ floor\ area\ (£/m^2) = Central\ Damage\ Value(CDV) \times Average\ cost\ of\ a\ new\ property\ in\ England\ and\ Wales(£/m^2) \quad (6.4)$$

Using Equation (6.4) and Table 6.3, the average damage cost per m^2 (gross) floor area was estimated for each corresponding Damage Category, as shown in Table 6.4. As the Probability Density Functions (PDFs) were not directly defined using a number, the highest reasonable damage cost for a respective category is estimated by combining the author's expertise in this field. The resulting highest value would then represent the 95% percentile in the respective category. The values of the 95% percentile cost per m^2 floor area for each Damage Category are summarised in Table 6.4. To provide these values, the prices used have been adapted, using the study of Sundell et al. (2019) in combination with the author's expertise, in addition to the highest gross charge (cost) in the wider London area, taken from the Office for National Statistics (2017). It should be noted that the focus here was to present the framework of the method rather than providing exact (detailed) values for those costs, which would then depend on specific costs related to a country/region or city.

Table 6.4: Average and 95% percentile damage costs for each Damage Category adapted from Burland (1995), Mair et al. (1996), Blong (2003), Office for National Statistics (2017) and Sundell et al. (2019).

Damage Category (No)	Damage severity	Critical tensile strain (%)	Average damage cost per m^2 floor area	95% percentile damage cost per m^2 floor area
1	Negligible	0-0.05	0.02×2400 £/m^2 = 48 £/m^2	110 £/m^2
2	Very slight	0.05-0.075	0.10×2400 £/m^2 = 240 £/m^2	900 £/m^2
3	Slight	0.075-0.15	0.40×2400 £/m^2 = 960£/m^2	3300 £/m^2
4	Moderate	0.15-0.3	0.75×2400 £/m^2 = 1800 £/m^2	5000 £/m^2
5	Severe to very severe	> 0.3	1.00×2400 £/m^2 = 2400 £/m^2	6600 £/m^2

The damage from several hazards often follows a skewed probability distribution (Hansen and Singleton, 1983). A lognormal distribution is commonly used in analysing the positive skewed damage distributions of PDF (Hansen and Singleton, 1983). By definition, a PDF of damage is 'lognormally' distributed when the log-transformed PDF of the damage is normally distributed. This can be described as a function: $Y = \ln(X)$ that is normally distributed with a mean, μ, and

a variance, σ^2. Then, X is lognormally distributed with parameters, mean (μ) and variance (σ^2). It should be noted that μ and σ^2 are not the mean and variance of the lognormal random variable, X, but are the mean and variance of the log-transformed random variable, Y, and the lognormal distribution is commonly referred to, as $LN(\mu, \sigma^2)$. The lognormal PDF was chosen in the current analysis, in this chapter to obtain positive (damage) costs, Cs, and represent larger uncertainties in the correct part (branch) of the curve (Hansen and Singleton, 1983). If the average cost per m^2 is the expected value m and the 95% percentile is the variable q for each Damage Category, the Equations (6.5)-(6.8) can be used to evaluate the parameters μ, and variance, σ^2, of the log-normal PDF for damage cost, Cs, for each Damage Category (Singh, 1997). The value from the lognormal distribution, m, and the 95% percentile, q, are given by Equations (6.5) and (6.6), respectively (Singh, 1997).

$$m = \exp(\mu + 0.5\sigma^2) \quad (6.5)$$

$$q = \exp(\mu + z_{0.95}\sigma) \quad (6.6)$$

where $z_{0.95}$ is the 95% percentile of the standard normal distribution profile (approximately equal to 1.645).

Then taking the logarithms of m and q, are given by Equations (6.7) and (6.8) (Singh, 1997).

$$\log(m) = \mu + 0.5\sigma^2 \quad (6.7)$$

$$\log(q) = \mu + z_{0.95}\sigma \quad (6.8)$$

Using Equations (6.5)-(6.8), the Equations (6.9) and (6.10) (Singh, 1997) are finally derived.

$$\sigma = z_{0.95} \pm \sqrt{{z_{0.95}}^2 + 2\log\left(\frac{m}{q}\right)} \quad (6.9)$$

$$\mu = \log(q) - z_{0.95}\sigma \quad (6.10)$$

The equation with the positive solution for σ and μ is selected (unless q > m). Table 6.5 shows the resulting mean (μ) and variance (σ^2) for the lognormal PDF, $LN(\mu, \sigma^2)$, for the building damage costs for each Damage Category. Using these values, a lognormal PDF (fs), describing the variation in the corresponding (repair) cost (Cs) for each Damage Category, is demonstrated in Figures 6.11-6.13 (using MATLAB). The MATLAB codes used are provided in Appendix D.

Table 6.5: The computed mean and variance for every Damage Category (Sundell et al., 2019).

Damage category	Mean (μ)	Variance (σ^2)	LN(μ, σ^2)
1	3.6780	0.3863	LN(3.6780, 0.3863)
2	4.5077	1.9460	LN(4.5077, 1.9460)
3	6.1957	1.3426	LN(6.1957, 1.3426)
4	7.1503	0.6904	LN(7.1503, 0.6904)
5	7.4481	0.6703	LN(7.4481, 0.6703)

a)

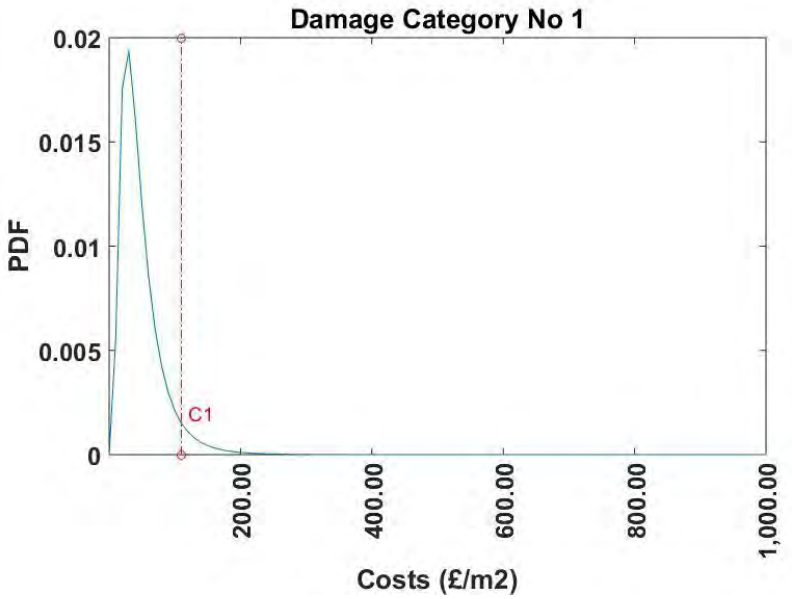

b)

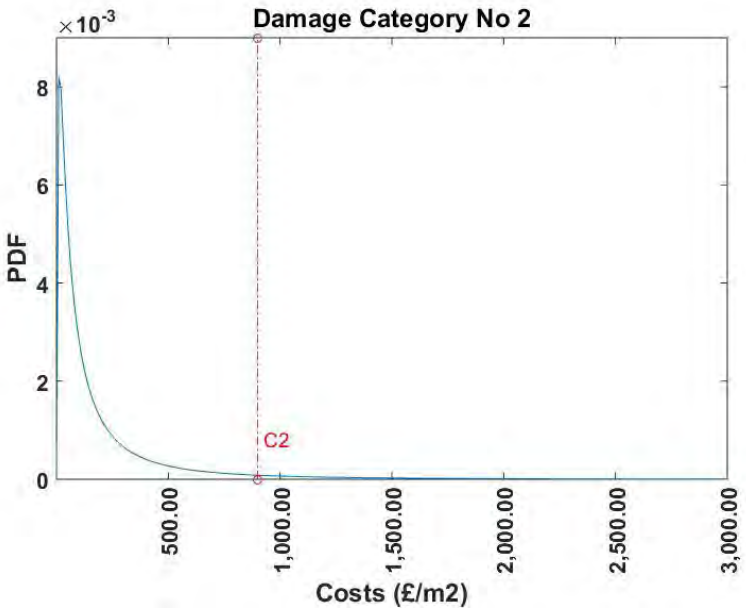

Figure 6.11: The variation in repair costs of buildings due to settlement using the PDF, for (a) Damage Category No. 1 (negligible) and (b) Damage Category No. 2 (very slight). The red dotted line shows the 95% percentile cost.

a)

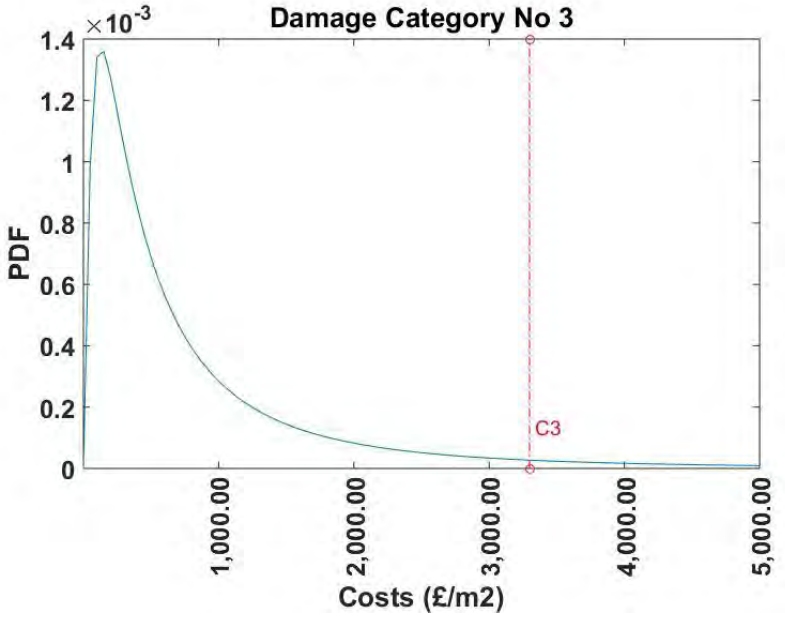

b)

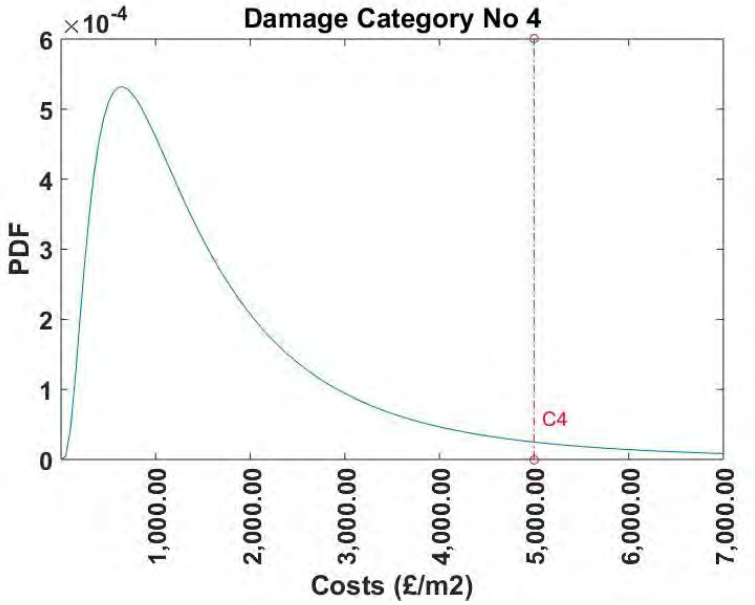

Figure 6.12: The variation in repair costs of buildings due to settlement using the PDF, for (a) Damage Category No. 3 for the (slight) and (b) Damage Category No. 4 the (moderate). The red dotted line shows the 95% percentile cost.

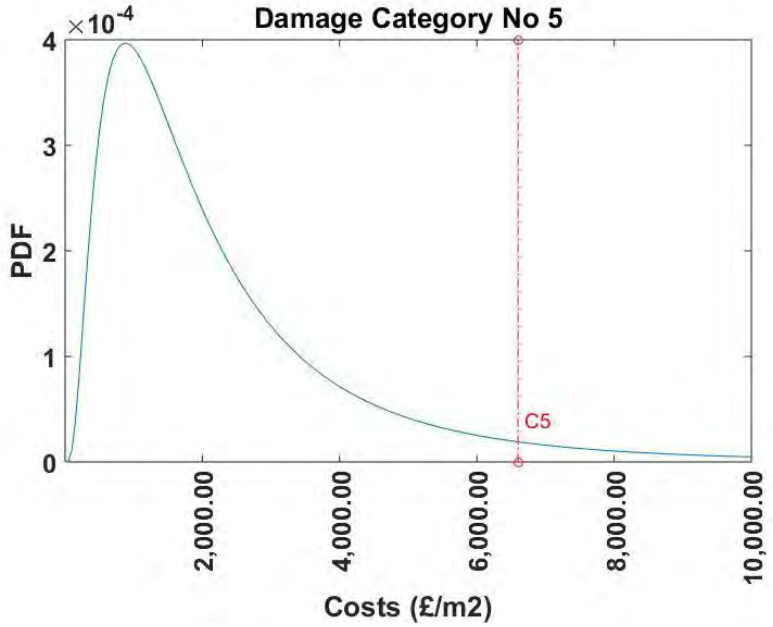

Figure 6.13: The variation in repair costs of buildings due to settlement using the PDF, for damage category (No. 5) (severe). The red dotted line shows the 95% percentile cost.

Finally, the Settlement Economic Risk was provided for a building in relation to the probability of damage within one of the Damage Categories. This was estimated through Equation (6.3), using the integral indicated by the area bounded by the PDF curve for a Damage category and by the repair costs up to the point of the cost corresponding to the probability for this Damage Category. By way of example, as shown in Figure 6.14, the Settlement Economic Risk for the Damage Category No. 5 (severe), was provided using the grid-area created by the PDF curve and the repair costs up to the cost corresponding in this case to the 95% percentile probability of damage (Damage Category No. 5). The same was done for the other Damage Categories. Their summation then provides the Settlement Economic Risk to a particular building. These can then be presented in the multidimensional visualisations of this chapter, as shown in the following section.

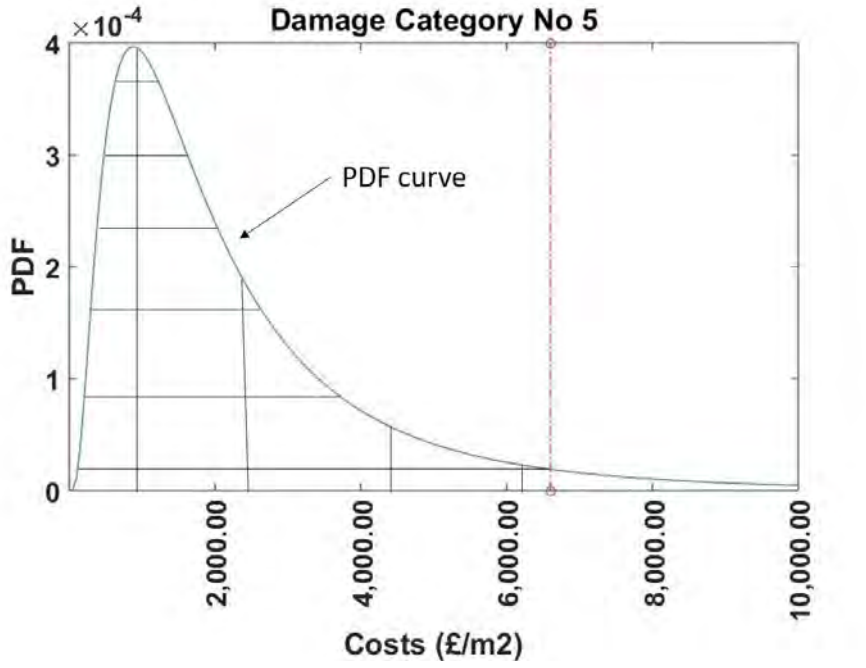

Figure 6.14: Example of the PDF curve for the Damage Category No.5 (severe) with a gridded area embedded to estimate the Settlement Economic Risk. A red dotted line indicates the cost for the probability of damage, in this case the 95% percentile (Damage Category No. 5).

6.5 Settlement Economic Risk assessment visualisations

The 3D visualisations using BIM of the resulting Settlement Economic Risk for the buildings caused by the tunnelling-induced settlements, using the proposed analysis, are presented in Figure 6.15. Risk-based colours of the buildings were generated within those visualisations, which presented the probability of this risk to occur (using Equation (6.3) and Monte Carlo simulations). In addition, these visualisations contain the Damage Extent due to the tunnelling-induced settlements. This is shown by the surface settlement risk, using Table 4.4 (Rankin, 1988; CIRIA, 1996) and Equation (4.5) (in Chapter 4), to provide the whole picture of this assessment.

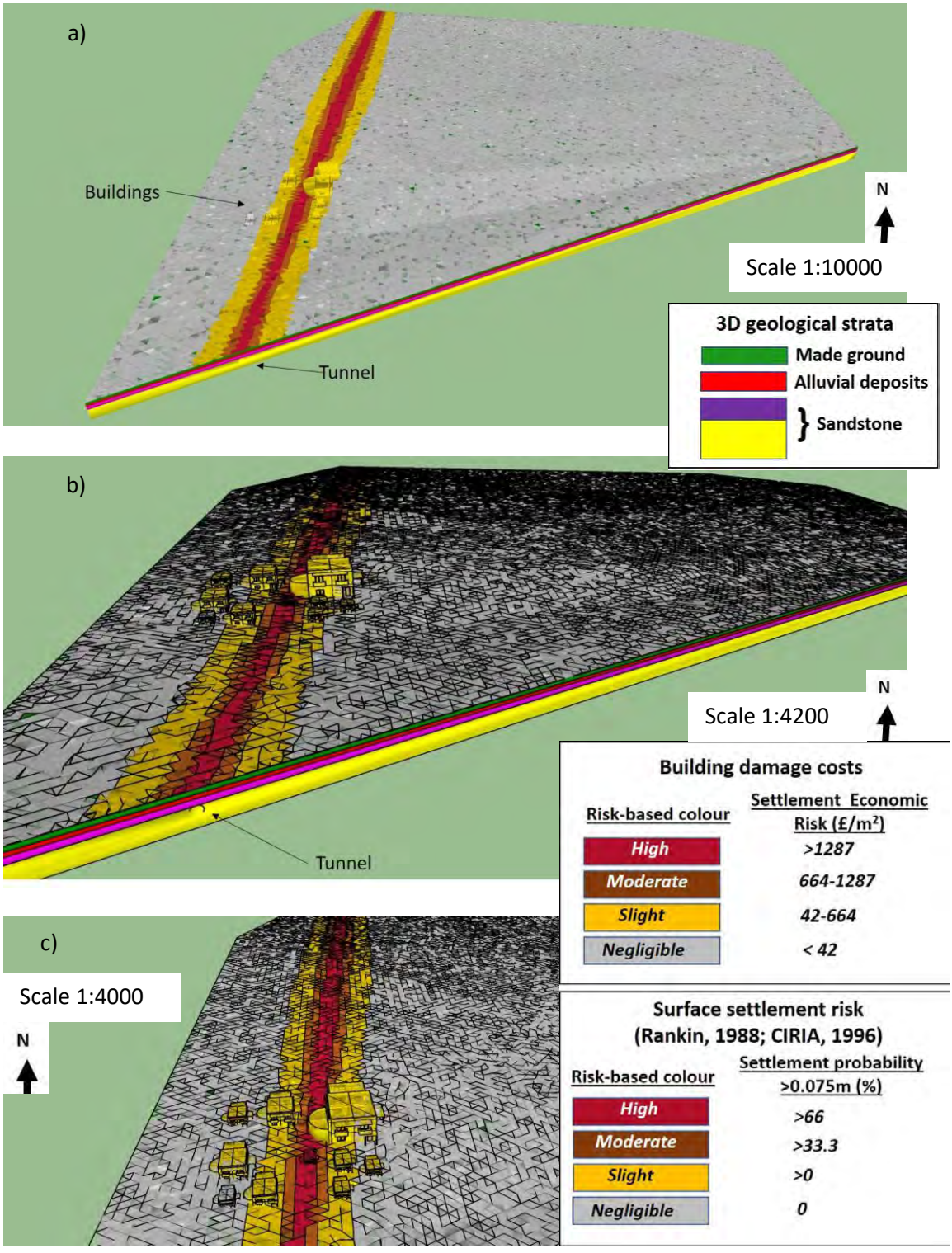

Figure 6.15: 3D visualisations of the resulting Settlement Economic Risk caused by ground settlement due to tunnelling (with a diameter of 10m), via a (a) wide, (b) close and (c) closer view in SketchUp (Trimble Inc., 2016).

To demonstrate the power of this tool and present the 'sensitivity' of the proposed method, alternative visualisation examples of Settlement Economic Risk due to ground settlements caused by tunnelling, were developed. These were based on changing the diameter and the location of the tunnel centreline, as shown in Figures 6.16-6.19. The corresponding graphs for the building-damage and cost analyses were performed to provide the resulting visualisations of Settlement Economic Risk in Figures 6.16-6.19, and are presented in Appendix D, i.e. the probability of a Damage Category to occur for each building is presented in Figures D.1-D.20 and the variation in repair costs of buildings due to settlement using PDF for each Damage Category is presented in Figures D.21-D.32. Additional 3D visualisations (BIM), presenting extra views of each assessment are also presented in Figures D.33-D.35 (Appendix D).

Initially, the diameter of the tunnel centreline diameter was reduced to 8m, and the resulting visualisations (risk-based coloured buildings) were presented in Figure 6.16. To provide even more detailed resultants and confirm the proposed analysis, the location of the tunnel centreline was also changed. In this case, it was placed approximately 200m away from the closest building of the built-up area, as shown in Figure 6.17. The Damage Extent is also included again in these visualisations, presenting the settlement risk on the ground surface (surface settlement risk), using Table 4.4 (Rankin, 1988; CIRIA, 1996) and Equation (4.5).

The same process was carried out again for a tunnel with a 10.5m diameter, with a centreline initially below and then away from the built-up area, as shown in the resulting visualisations of Settlement Economic Risk in Figures 6.18 and 6.19.

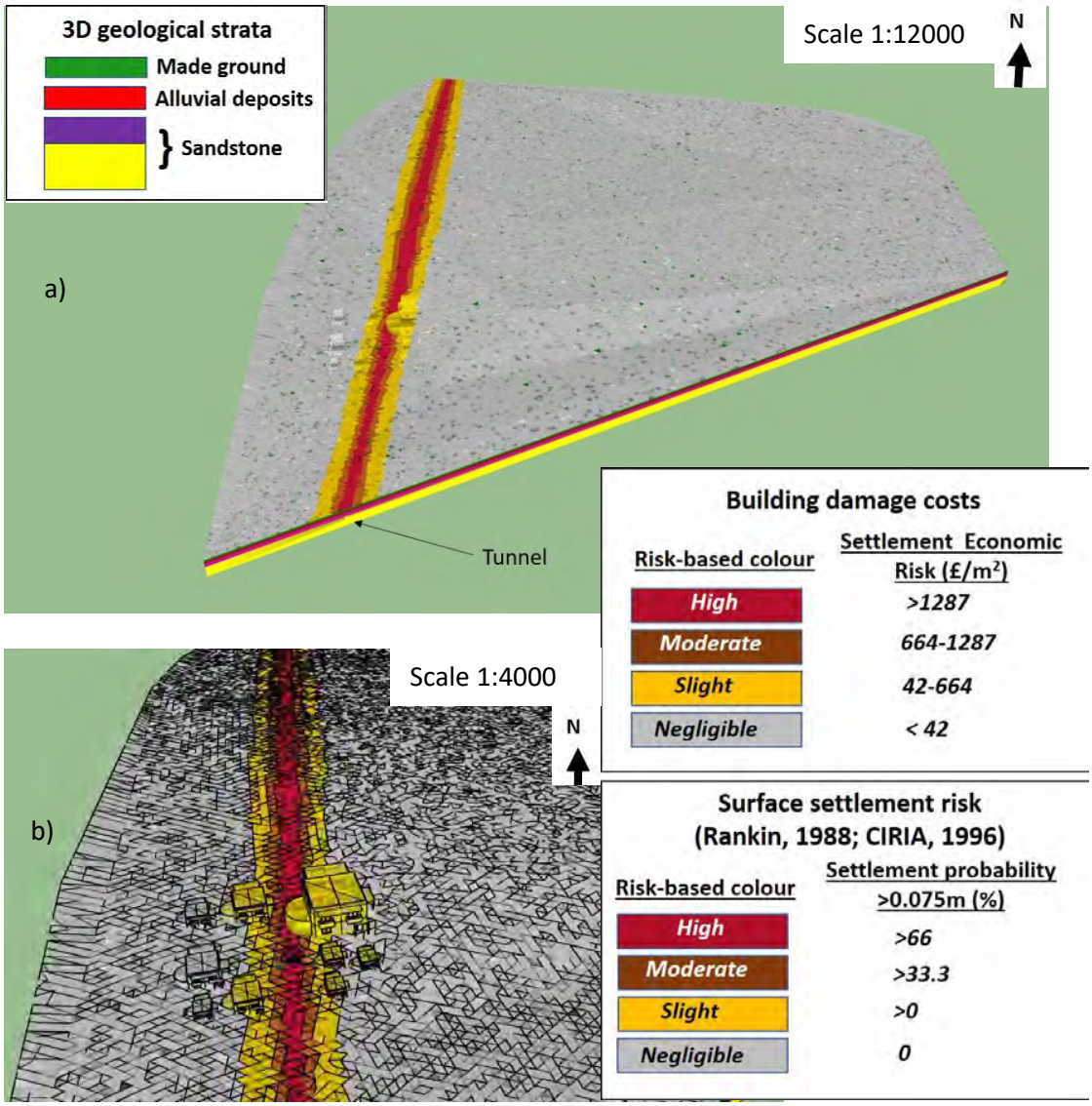

Figure 6.16: 3D visualisations of the resulting Settlement Economic Risk caused by ground settlements due to a tunnel construction below the built-up area. The tunnel generated here had with a diameter of 8m and is presented via a (a) wide and (b) close view in SketchUp (Trimble Inc., 2016).

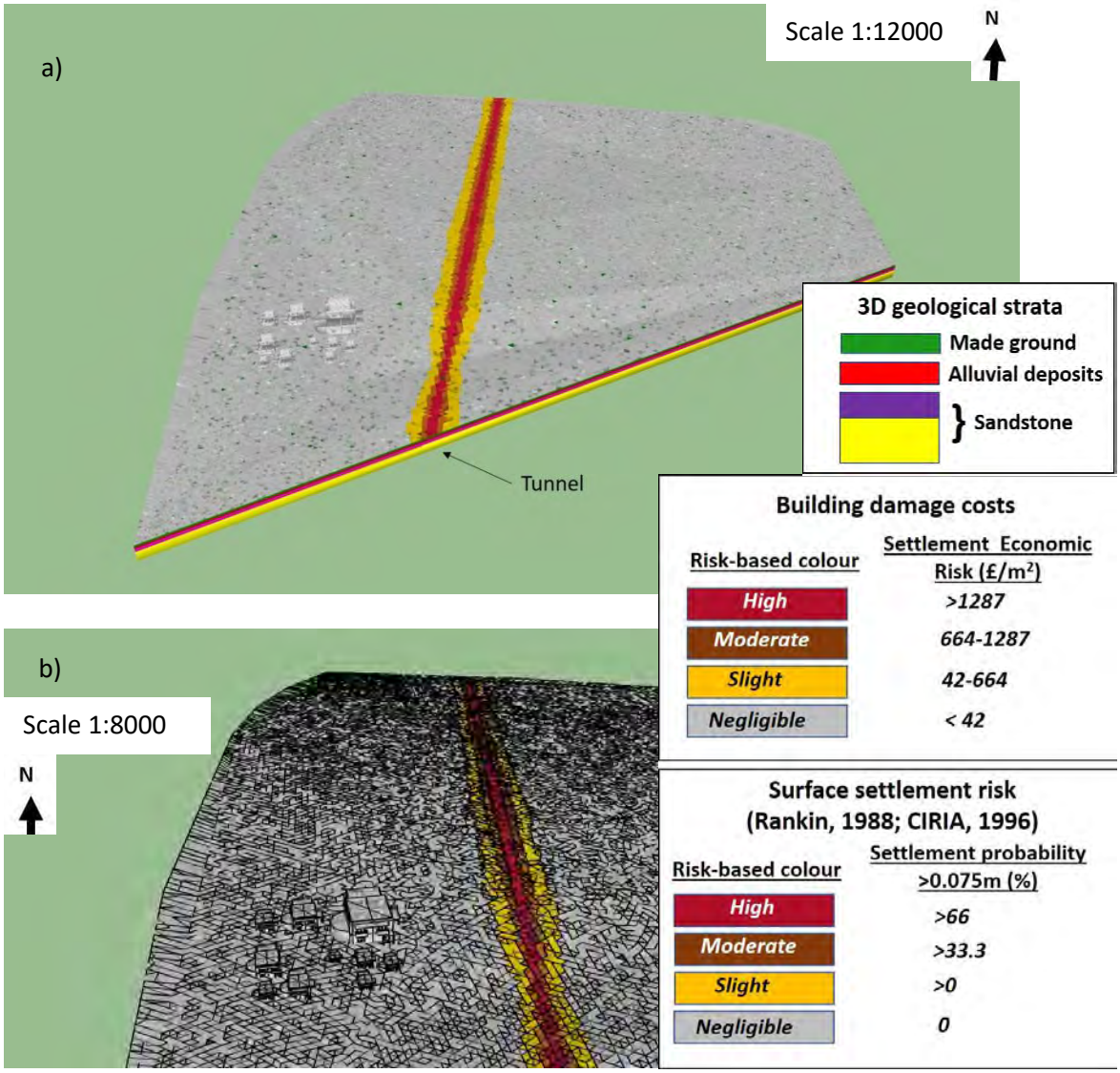

Figure 6.17:3D visualisations of the resulting Settlement Economic Risk caused by ground settlements due to a tunnel construction approximately 200m away from the built-up area. The tunnel generated here had a diameter of 8m and is presented using a (a) wide and (b) close view in SketchUp (Trimble Inc., 2016).

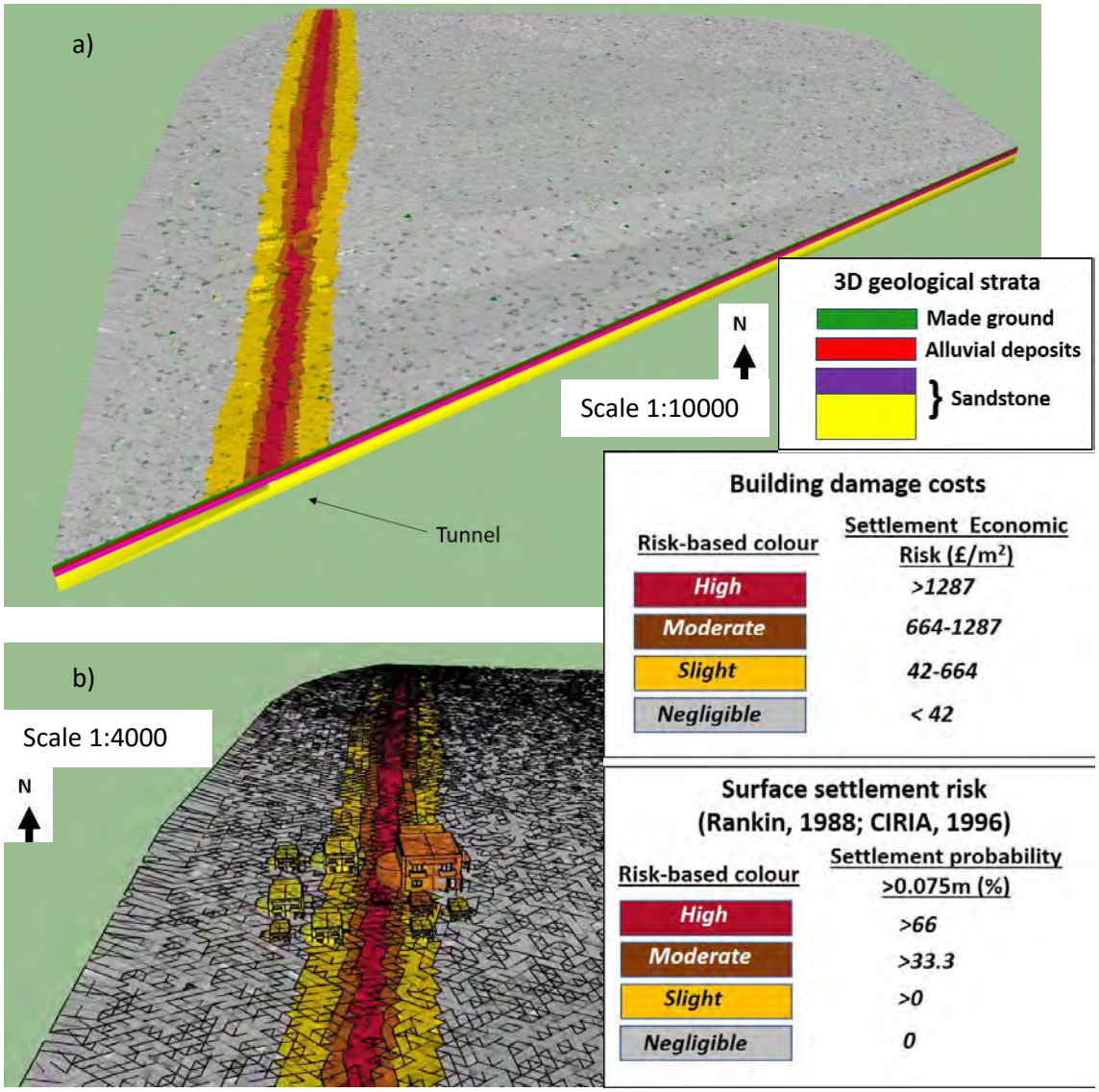

Figure 6.18: 3D visualisations of the resulting Settlement Economic Risk caused by ground settlements due to a tunnel construction below the built-up area. The tunnel used here had a diameter of 10.5m and is presented using a (a) wide and (b) close view in SketchUp (Trimble Inc., 2016).

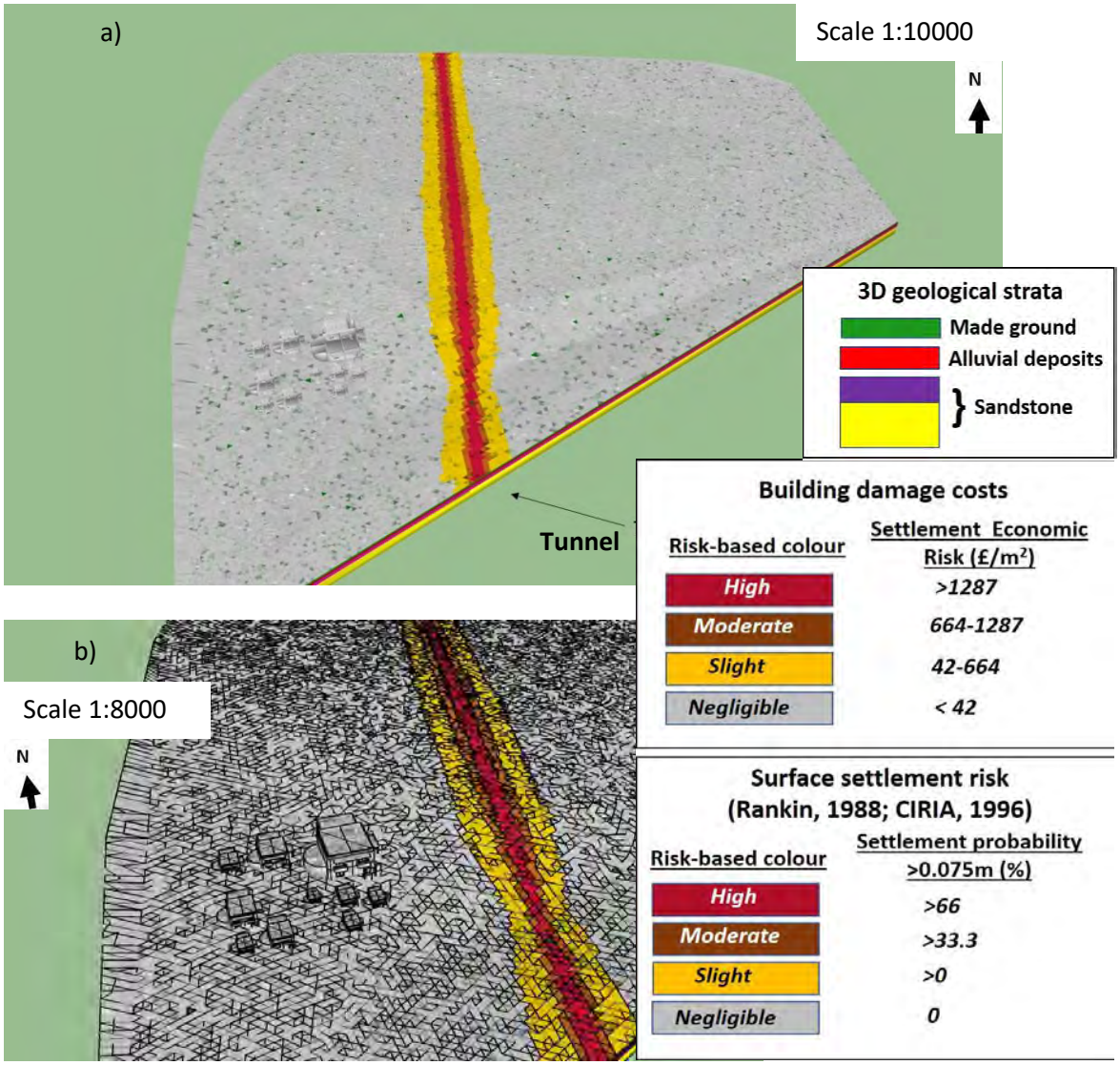

Figure 6.19: 3D visualisations of the resulting Settlement Economic Risk caused by ground settlements due to a tunnel construction around 200m away from the built-up area. The tunnel used in this case had a diameter of 10.5m and is presented via a (a) wide and (b) close view in SketchUp (Trimble Inc., 2016).

6.6 Discussion of the results

The 3D visualisations provided the Settlement Economic Risk for buildings due to settlements. The probability of the risk using Equation (6.3) and the Monte Carlo simulations, is shown by corresponding risk-based colours. The resulting multidimensional risk assessment visualisations were provided using the proposed analysis, which was presented by the corresponding building-damage and cost analysis graphs.

Figure 6.15 demonstrated the 3D visualisations (in SketchUp) of the Settlement Economic Risk and the Damage Extent. Risk-based colours were employed in the visualisations representing various levels of risk for the buildings and the ground surface. This was formed due to the resulting settlement, generating a subsequent settlement trough in the area. These visualisations demonstrated a higher risk along the tunnel centreline, where risk increased towards the tunnel centreline. As a result, buildings closer to the tunnel centreline showed a probability of higher settlement economic risk. However, it is important to note that areas of sagging and hogging are significant in indicating potential building damage. The buildings that lie within higher-risk areas caused by surface settlements showed a higher Settlement Economic Risk, as illustrated in Figure 6.15c. On the contrary, those that lied away from this zone showed a lower economic risk, presented with slight or negligible risk-based colours, as shown in Figure 6.15. Therefore, buildings having a brown and red colour, i.e. with a moderate to high settlement economic risk would need a more detailed investigation concerning potential damage. Because of the power of BIM to capture all the detailed information regarding a building, it was evident that the building characteristics, such as building dimensions, would have an effect on the assessment analysis resultants and resulting visualisations. Hence, larger buildings would be prone to a higher risk, due to a larger corresponding area extending over the settlement trough, and hence, the potential for differential settlement and cost in £/m^2, as demonstrated in Figure 6.15.

To provide a more detailed demonstration of the resulting visualisations in Figure 6.15, the Settlement Economic Risk to individual buildings was indicated. To present this, representative Building Nos. 1, 2, 3, 7 and 10 were employed, and their locations were demonstrated in Figure 6.4 and their corresponding visualisations are shown in Figure 6.15. Building Nos. 1, 2 and 7 fell directly above the negligible, slight and high-risk zones of settlement, respectively, and indicated a corresponding negligible, slight and high Settlement Economic Risk, respectively (Figure 6.15). However, the building dimensions would be the determining factor in the case of the resulting risk visualisation for Building No. 3, since it is larger than Building No. 1 (Figure 6.15). In this case, the dimensions of this building had a strong effect on its resulting slight risk, even though it is located outside the settlement impact zone of the trough (negligible surface settlement risk). The Building No. 10 was located across all zones of the surface settlement risk, yet with a larger proportion located within the slight risk zone, as shown in Figure 6.15. This, in combination with its large dimensions resulted in a slight Settlement Economic Risk for this building. The previous (resulting) visualisations aligned with the graphs of the building-damage categories in Figures 6.6-6.10. Buildings with a moderate risk or above, i.e. shown in brown to red colours, could be investigated further, as required.

To demonstrate the power and the accuracy of the proposed method, alternative representative visualisations were provided. The alterations of the resulting Settlement Economic Risk based on particular representative changes of criteria within the model, follow.

Figure 6.16 was produced to demonstrate the Settlement Economic risk, using a different diameter of the tunnel centreline, which was changed to a diameter of 8m. This is because the diameter was considered an important property of the tunnel, as shown in Equation (4.5). This provided risk assessment visualisations where the risk exhibited slight changes from the previous in Figure 6.15, as expected due to slightly reducing the tunnel diameter. The settlement

trough was presented with higher surface settlement risk (on the ground surface) along the tunnel centreline. Settlement risk was shown to increase towards the centreline (Figure 6.16). Buildings closer to the tunnel centreline showed a probability of higher economic risk caused by settlements. These built within zones of higher surface settlement risk demonstrate a higher economic risk, than those built outside of these zones (Figure 6.16). The building dimensions (which were adopted from BIM) played again an important role, in which larger buildings, in general, were shown to be more prone to this risk.

In the same visualisation in Figure 6.16, most of the buildings exhibited a similar Settlement Economic Risk to Figure 6.15, as expected. However, as shown in Figure 6.16, Buildings No. 3 and 8 (their locations were demonstrated in Figure 6.4), exhibited a negligible risk (lower than the previous assessment shown in Figure 6.15), as expected, due to the smaller diameter employed. The rest of the buildings responded to this tunnel construction similarly to (a diameter of 10m assessed in) Figure 6.15.

Apart from changing the diameter, the tunnelling proximity to the buildings was used to demonstrate the sensitivity of this method. Figure 6.17 was produced using the proposed analysis, having again a tunnel centreline with a diameter of 8m. However, in this case, the tunnel centreline was placed approximately 200m away from the first building of the built-up area found. The resulting Settlement Economic Risk visualisations caused by tunnelling here, were demonstrated in Figure 6.17. The resulting changes in the demonstrations for this risk, which were caused by the change of the location of the tunnel (away from the built-up area), were compared with the previous Figures 6.16 (and Figure 6.15). These visualisations presented again a higher Surface settlement risk along the tunnel centreline. This could be explained by the development of the resulting settlement trough, which in this case was away from the built-up area. The settlement risk was then increasing towards the centreline, providing areas of

settlement risk. In this visualisation, as no buildings were located within or close to these impact zones, the Settlement Economic Risk to buildings was expected to change (decrease), comparing to the previous Figure 6.16. This was confirmed by the resulting visualisations of Figure 6.17, which exhibited a negligible Settlement Economic Risk (grey risk-based colours) for all the buildings, as expected. This was found due to the distance of the tunnel from the buildings, which produced a negligible settlement effect by being off the settlement trough's impact-zones.

Similarly to the previous examples (of Figures 6.15, 6.16 and 6.17), Figures 6.18 and 6.19 were provided to demonstrate the sensitivity of the proposed method and confirm the accuracy of its resultants.

More specifically, via changing the tunnel diameter to 10.5m in Figure 6.18, again a higher settlement risk along the tunnel centreline was demonstrated, which was becoming higher towards the centre of this tunnel centreline. The risk-based colours on the ground surface again were slightly different, as expected, due to the larger diameter of the tunnel used (than in Figure 6.16). The buildings closer to the tunnel centreline would indicate a greater damage risk, and hence a higher Settlement Economic Risk. Thus, the main difference in Figure 6.18 from the previous visualisations (in Figures 6.15 and 6.16) is associated with the buildings.

Figure 6.18 demonstrated changes of risk levels when comparing with Figure 6.15. Building No 1 changed to a slight Settlement Economic Risk (from grey to yellow colour). Settlement Economic Risk was also increased in Building Nos 6 and 10 to a moderate level (in orange colour). Then, when comparing Figure 6.18 with Figure 6.16, the resulting visualisations using a (even larger) diameter of 10.5m also gave an increased (higher) Settlement Economic Risk, as expected. In particular, Building Nos 1, 3 and 8 were now shown in Figure 6.18 to have a

slight risk. The resulting Settlement Economic Risk shown on Building Nos 6 and 10 was also now changed to a moderate level, as demonstrated in Figure 6.18. The previous changes in the resulting visualisations of the Settlement Economic Risk for buildings occurred due to the larger diameter of the tunnel centreline used, and hence they confirmed the accuracy of the proposed analysis method. In addition, the dimensions of a building played a role in the previous changes (increased/reduced risk) of the resulting visualisations of risk, by way of example, as presented by the change of the risk-based colours of Building No 10.

Figure 6.19 showed the resulting visualisations, when the tunnel centreline of a diameter of 10.5m (as shown in Figure 6.18) was placed at approximately 200m away from (the first building of) the built-up area. These provided a higher settlement risk along the tunnel centreline, and towards its centre. Similarly to the visualisation example shown in Figure 6.17, the buildings were not enough close to be affected by the resulting settlement (trough), as presented in Figure 6.19. Therefore, the resulting Settlement Economic Risk assessment visualisations gave a negligible risk, with grey faces of all the buildings investigated.

The resulting 3D visualisations of the Settlement Economic Risk for buildings (Figures 6.16-6.19) also aligned with the graphs of the probability for a building-damage category and variation in repair costs of buildings due to settlement (which are demonstrated in detail in Figures D.1-D.20 and Figures D.21-D.32 (Appendix D), respectively). Those buildings which were demonstrated with a moderate risk or above, i.e. in brown and red colours, could be investigated/analysed further, as required.

These 3D visualisations produced a robust tool for assessing Settlement Economic Risk in relation to building damage by exploring the tunnelling-induced Settlement Hazard. This could be important information for improving the understanding, as required in this field. These

visualisations could support geotechnical cost-benefit analyses, involving such 'real-life' applications, as the one explored here, which could advance sustainable decision-making. The analysis could also be expanded to incorporate the (Settlement) Vulnerability aspects in a future analysis.

6.7 Summary

In this chapter, a framework was generated to support urban planning and relevant decision-making associated with geohazard risk through a robust and integrated information modelling system. 3D ground modelling was again used through utilising BIM and its data integration power. This used again the same 3D models used in the previous chapter (Chapter 5). However, the aim here was to develop an urban geohazard risk assessment tool, based on the integration of the BIM framework with an uncertainty analysis to build a thorough geohazard information platform. In particular, to obtain comprehensive and useful outcomes for an urban area, the focus was on the resulting economic costs. The relevant interactions and integrations of BIM with the analytical and modelling tools used were described. Integrated 3D risk-based visualisations of economic costs caused by the geohazard, were produced, which could support ground investigations and sustainable urban planning.

7 DISCUSSION

7.1 Overview

In this research, an integrated information system for urban geohazard risk, in this case using the example of the tunnelling-induced settlement risk (soft ground), was provided. This system was based on a BIM-based framework for a preliminary assessment tool. The integrated outcomes of the proposed tool were presented by advanced risk assessment analyses and visualisations (SketchUp) using BIM. A discussion of the results combined follows, to provide a clear understanding of the findings of the proposed approach.

7.2 Discussion of all the results combined

As cities expand, urban geohazards and their effects have been affecting human lives and the built environment, and causing economic impact for many decades. These aspects have been widely considered in relevant urban planning and sustainable decision-making by a range of (modelling) tools and approaches which predict (assess) the corresponding risk, such as in Culshaw et al. (2006), Kim et al. (2015) and Bathrellos et al. (2017). The robust knowledge and understanding of the ground conditions and interactions were key aspects in assessing urban geohazard risk (Aldiss et al., 2012, Price et al., 2016). In addition, due to the nature of the ground (Griffiths, 2016), a method that could be applied to various types of geohazards is found to be suitable and align with sustainable thinking. Therefore, the need for providing a framework using advanced methods to 'inform' about the urban geohazard risk via an integrated system was evident (Bridge et al., 2005). Subsequent methods using maps (Culshaw et al., 2006; Papaioannou et al., 2015; Bathrellos et al., 2017) and 3D ground models (Entwisle et al., 2008; Thornton et al., 2018) were produced from several analyses. However, they lacked in demonstrating a corresponding modelling 'system', which could provide integrated (risk assessment) information while considering the complexity of the ground and ground-building

interactions. In this research, it was found that BIM could be key in supporting a framework for such an information system, by extending BIM's previous use and thinking, which focused on structural and geotechnical information, such as in Ladenhauf et al. (2016) and Zou et al. (2017), and Svensson (2016) and Wang et al. (2019), respectively, to provide advanced aspects associated with geohazard risk assessment information. Therefore, an integrated information modelling system for assessing geohazards in urban areas was developed, using the proposed BIM-based methodology. Key aspects to build this integrated system were the development of a complete risk assessment and a framework to establish and process the information where this assessment would be based.

The proposed integrated system provided the information using a comprehensive or a 'package' of geohazard risk assessment for an urban area. This was based on a framework that could explore basic components constituting a geohazard risk assessment (Fedeski and Gwilliam, 2007), such as the hazard and vulnerability, which are enhanced by cost-related estimations that are critical for sustainable decision-making (Price et al., 2016). A comprehensive geohazard risk assessment tool was developed by exploring these components, using advanced (geohazard risk assessment) analyses and the power of BIM (to support this tool).

The framework for this tool was successfully presented using the example of assessing ground settlement risk due to a tunnel construction. However, due to the variability of the ground (Griffiths, 2016), the aim (of this tool) was to be capable for assessing any type of urban geohazard, using the power of BIM. This key strength has provided an advance on relevant tools to date, which tended to focus on assessing specific geohazards (Kazakis et al., 2015; Papaioannou et al., 2015). More specifically, a framework was developed that was based on correlating information of several important criteria (for example the tunnel-induced settlement factors, using data taken from borehole records) to produce advanced geohazard risk assessment

analyses, which expanded on prior research (as noted earlier) by utilising BIM to process (and then visualise) this information. As presented in this research, this framework provided an integrated tool for the rigorous investigation of urban geohazard risk, where the criteria used could be adjusted to support any associated geohazard, as required. Hence, the proposed tool could also advance the fields of ground investigation and sustainable urban planning.

In addition, the knowledge and understanding of the ground and ground-building interactions are important for the geohazard decision-making in urban areas (Aldiss et al., 2012, Price et al., 2016). The proposed modelling system demonstrated that it could be used to obtain rigorous information on such geohazard decision-making. More specifically, the information for ground and ground-building interaction was based on the strength of BIM to combine geotechnical and structural information, using the proposed methodology. This integrated information improved previous relevant practice (applications) and research (such as in Jørgensen et al. (2015) and Vatcher et al. (2016)), which were lacking in providing a system to integrate this information. Hence, the proposed system allows the user to assess with time the geohazard effect on the area and buildings (and the impact of a new infrastructure construction on existing constructions), using advanced geohazard risk assessment analyses and integrated building damage assessments. As presented in the outcomes of this research, the integrated (geotechnical-structural) information was important to provide the advanced analyses used. This aspect improved the current geohazard risk assessment analyses (for example in Papaioannou et al., 2015 and Kim et al., 2019) by a powerful with a low computational cost analysis, which could be used, for example, at early construction stages. In addition, this was extended in the proposed approach by providing an economic risk assessment, which directly exhibited the relevant (damage) cost risk caused by a geohazard. Areas and buildings with (potential) higher costs of damage due to geohazard were shown. This could provide a useful ‘real-life’ application for

decision-makers by implementing a cost analysis within the proposed geohazard information system, enhancing previous assessments (Sundell et al., 2019). It is important to note that the integrated information that was used in the proposed system was provided by a unique method for integrating BIM building information with geohazard risk assessment analysis information, which enhanced relevant geotechnical applications associated with BIM (Svensson, 2016; Zhang et al., 2018). BIM supported this data integration, which is crucial for solving geohazard and ground-building problems. This integration could enhance urban geohazard assessments by including important BIM (structural) information and processing it to provide a corresponding analysis. In this case, for example, the ground-building interaction aspects (outcomes) in relation to geohazard risk were successfully provided using available BIM-building data, which was implemented in the corresponding building damage assessments.

In terms of the role of BIM specifically, this was principal in providing this system. The proposed BIM-based assessment enhanced risk assessments, which were previously conducted using 2D maps and 3D ground models (Gakis et al., 2016; Bathrellos et al, 2017). This was achieved by BIM's data integration (interaction) strengths of storing, managing, processing, linking together and multidimensionally visualising the data to build an information modelling system, as demonstrated in the proposed approach. These aspects extended the computer-aided geohazard risk assessment approaches available to date, by introducing an 'interactive and automated' framework to process the information (data). As demonstrated in the methodology, this framework could produce robust urban geohazard risk assessment outcomes, which is confirmed by the 3D visualisations of this research.

More specifically, the integrated 3D visualisations using BIM (SketchUp) was a major strength provided by the data advances of this system. The integrated 3D geological, buildings and underground structures model was developed by an automated process using BIM, as described

in the methodology of this research (Chapter 3), which adds to previous modelling such as in Svensson (2016). The visualisations of the 3D models including the risk/costs assessments were presented successfully using the proposed approach to clearly exhibit potential construction areas or buildings at risk and at economic cost risk. These integrated visualisations were achieved by the data advances of the proposed framework, using the power of BIM. BIM processed the data needed to provide the risk assessment analysis, which was then employed in the multidimensional visualisations (on SketchUp). This improves the previous risk assessments using 3D ground models (Thornton et al., 2018) and previous BIM models (for example, from Kim et al. (2015)) by including integrated BIM-based risk assessment (i.e. attributed) information within the 3D (geology-buildings) models developed, while incorporating the advantages of BIM. This information advances geohazard and ground-related risk-based modelling visualisations. As a result, they reduced geological uncertainty and improved knowledge and understanding of the subsurface, because the 3D ground (geological) modelling is enhanced with 'interactive' (and dynamic) risk assessment predictions. The integrated 3D visualisations also demonstrated the importance of the impact factors, and their severity and alterations with time and tunnel location, broadening the previous findings (such as in Kim et al. (2015)). By way of example, 3D visualisations could then be used as 'thematic' 3D maps of combinations of geohazards, which could affect an urban area, if required. Hence, this supports complex decision-making. In addition, the proposed approach could support the 'discussion' of (complex) outcomes of geohazard risk (effects) and building response in relation to a corresponding risk assessment analysis between scientists/engineers, and clients, asset owners and authorities.

An integration with other modelling tools (software) of the 3D models (including the risk-based assessment visualisations) is also provided using the data advantages of this system, which

could extend the power of the risk assessment developed. This was provided here using integrated tools that utilised, for example, spatial modelling tools, and hence extended the available 3D ground models to date, such as in Gakis et al. (2016). As a result, integration with applications that could support and enhance or be used in further investigation, is supported using the proposed framework. Hence, these aspects make this framework useful as a sustainable tool to support ground investigation, which is based on its compatibility advantages.

An advantage of the proposed methodology is that it extended data sharing/integration aspects, which makes the model capable of handling different types of information (data) to produce successful outcomes. Therefore, key in the proposed framework was to efficiently model different scales of data. The scale of the different data used, such as the values of vulnerability factors, is provided via a normalisation method, as presented in Chapter 5. This makes the proposed system capable of processing any type of relevant data (such as geological/geotechnical data) required for the assessment analysis, and then presenting the resulting 3D models through BIM. It should be noted that the 3D visualisations presented outcomes of assessing geohazard risk, in this case of settlement risk, with a consequent building damage assessment, which focuses on exploring the settlement risk (i.e. the area and buildings at risk), and not on providing a detailed assessment of building damage and its components (for example, building cracks, damaged elements/parts of a building). Such a detailed assessment could be examined at a later stage, using the proposed approach (presented in the Future Work). However, the proposed model could be adjusted to be used in a wider or city scale due to the power of BIM and its data integration advantages. More specifically, this could be provided by employing specific analysis criteria and data (records) for a larger area in the 3D modelling. In terms of computational power, which is required for use in a city scale, this is generally increasing with the size of the area examined and the ‘detail’ of the assessment required, i.e.

the complexity of the ground and parameters investigated. The city-scale use and the relevant computing resources needed could be studied in detail in a future work, which is based on the current framework.

In addition, the scarcity and distribution of (borehole) data is important for the relevant modelling (Wu et al., 2005). The proposed methodology considers the issues associated with data scarcity and different density of data in the model in a similar fashion with typical modelling in the field, i.e. the detail of the resulting 3D risk-based visualisations using BIM is decreasing with decreasing density of data. However, the proposed tool employs the BIM-based approach to easily share the data and handle this problem.

In terms of the data uncertainty of the model, this has been considered via providing a method for estimating the cost of building damage due tunnel-induced settlements (geohazard). This provided more accurate outcomes through 3D visualisations. The uncertainty of data was explored through the actual probability of building-damage cost risk. More specifically, the resulting BIM-based models presented detailed risk outcomes, using probabilistic analyses and the Monte Carlo simulations. These analyses explored the probability for each category of risk to occur through a number of (possible) scenarios or runs, i.e. the proposed method used 1000 scenarios. Hence, the increased number of simulated scenarios, which then provided increased estimates of risk, was key in the proposed approach. Therefore, a method for better knowledge and understanding of geohazard impact was presented (through assessing the economic risk), which could be extended in a future work that is based on the current framework.

The proposed framework could help planners, engineers and scientists, clients, asset owners, local communities and authorities, and other people involved in decision-making via providing a tool for better the knowledge and understanding of the geohazards. More specifically, it could

be used as a 'preliminary' assessment tool, in early (design) phases of construction projects to show susceptible areas or buildings to urban geohazards. These have been presented in this research (in Figures 4.7-4.9, Figures 5.14-5.15 and Figures 6.15-6.19), using integrated risk-based 3D visualisations of geological, structural and geohazard risk assessment (using risk-based visualisations) models.

These models could allow engineers/scientists to utilise this geohazard information and more easily identify risk-prone areas, and, for example, plan alternative tunnelling routes or construction, or focus on problematic areas with a higher risk for further assessment, if required. Likewise, in the case of an adjacent critical infrastructure to tunnelling, the effects of potential ground settlement that could make (a part of) it inaccessible or useless, could be avoided by utilising this tool. In addition, (building damage) cost risk indications (using integrated risk-based 3D visualisations) would also be useful for decision-making. Essentially, these would mean knowing in real-time of subsequent geohazard risk or damage (and costs), which adds to current relevant thinking. This system could advice on the need for further or more detailed investigation or a 'secondary' assessment analysis (such as a FEM analysis) to be targeted at higher-risk areas, as presented in the results of this research. Therefore, a further or more detailed analysis could then be based on this system or could be based as part of a broader relevant monitoring regime. In addition, this tool enables easy and rapid use with low computational power needs and adjustable (to any urban geohazard) utilisation, which could expand current ground investigation, and decision-making to advance sustainability. Local communities and authorities could also use this information, as 'urban geohazard risk maps' to support decision-making in relation to various urban developments. Hence, such an information system could, for example, assist for planning wider (city) scale development schemes, or provide 'safe' areas for potential construction and sustainable urban expansion.

Finally, these aspects are achieved by an integrated system, where data integration/interactions are provided and linked together (using BIM), and advancing 3D models, such as the models developed by Gakis et al. (2016) and Thornton et al. (2018). Hence, complex decision-making is supported by allowing the information to be more directly accessible and comprehensible, as described in the proposed methodology and demonstrated in the model outcomes (3D visualisations). This system improves knowledge and understanding in relation to ground investigation and underground construction. Therefore, the proposed geohazard information modelling system supports relevant decision-making by advancing sustainable urban planning.

8 CONCLUSIONS AND FUTURE WORK

8.1 Conclusions

A critical review of previous research demonstrated the need for sustainable urban planning tools which focus on the efficient access to knowledge and understanding of the subsurface. Hence, the information for (assessing) geohazard risk in an urban area would be important in relevant decision-making. However, a geohazard risk assessment tool that could provide this information efficiently does not exist. Hence, an integrated modelling system that could provide information for decision-making in relation to the subsurface needed to be developed, based on advanced (digital) data integration and 3D modelling visualisations. Such an integrated tool would be capable of assessing urban geohazards and supporting sustainable urban planning successfully.

The aim of this research for creating an integrated modelling information system for urban geohazard risk assessment has been achieved. This system was based on developing a framework for a preliminary assessment tool to support geohazard decision-making and ground investigations. This tool used a tunnelling-induced settlement risk assessment, as a representative urban geohazard risk assessment to demonstrate the proposed methodology. More specifically, it employed a basic (geohazard) risk assessment to process the analysis of the geotechnical/geological information. The risk assessment analysis was based on exploring the subsequent risk assessment components, i.e. the Settlement Hazard and Vulnerability, and evaluating the uncertainty using probabilities. This allowed a complete risk assessment package, which could support any urban geohazard required and provide robust ground-structure interaction information using building-damage and cost assessments. To provide this package, the idea was to integrate BIM with a (dynamic) geohazard risk assessment analysis, in this case for tunnel-induced settlements. BIM played an important role as the main

integration/interaction and visualisation 'platform'. More specifically, beyond clearly visualising the 3D geology-tunnel-building model of the area investigated, the use of BIM enhanced 3D ground modelling by storing, managing, sharing and visualising in 3D the resulting tunnel-induced settlement risk assessment information (data). This information was provided using BIM-building data combined with geotechnical data.

The tunnelling-induced settlement risk assessment analyses were undertaken in MATLAB. They combined analytical methods and building damage assessments, and advanced spatiotemporal analyses (using AHP and ARX) and probabilistic analyses/distributions using Monte Carlo simulations, using (factor) data taken from boreholes. The georeferenced 3D geology-tunnel-building model from the example study area in Birmingham, UK, was developed by integrated data processes (and conversions) using SketchUp (BIM). In addition, the resulting 3D visualisations of settlement risk and settlement economic risk assessments, confirmed the successful integration of the analysis and data processes used within the methodology adopted.

Initially, the tunnel-induced settlement risk assessment was provided by exploring the settlement hazard via 3D visualisations using BIM. This was repeated for several tunnel locations to confirm the accuracy of the method adopted. Ground surface areas and buildings at risk were provided with corresponding risk-based colours successfully. The ones with high risk could be taken to further investigation or more detailed analysis. Further understanding was obtained by individual building damage assessments.

The vulnerability of the study area due to tunnel-induced settlement was then explored, which was combined with the settlement hazard to provide a robust settlement risk assessment. This was produced by a spatiotemporal analysis which incorporated more criteria, i.e. geotechnical

and structural factors, to the settlement risk assessment using BIM. The risk assessment was successfully presented by multidimensional BIM visualisations and exhibited risk-prone areas and building damage. The proposed approach, which is adjustable to any urban geohazard, enhanced the relevant knowledge and understanding for sustainable decision-making by including a number of (settlement) vulnerability factors.

A Settlement Economic Risk assessment due to a potential tunnel construction using BIM was finally generated to complete the present risk assessment. This was based on an uncertainty analysis, which was successfully undertaken by an integrated probabilistic approach (using Monte Carlo simulations). In this way, the building-damage costs risk was rigorously assessed and visualised in 3D using BIM, generating an efficient application for ground-structure interactions. The proposed approach provided useful outcomes for decision-making by exploring different tunnel diameter and location examples, which demonstrated the relation of the tunnel diameter and location from the built-up area. The accuracy of the proposed approach was also confirmed.

The proposed integrated modelling system provided ‘real-time’ urban geohazard information with efficient outcomes, in this case of an advanced settlement risk assessment analysis due to tunnel construction. This system provided an advance on current geohazard risk assessments and knowledge and understanding of the subsurface, aligning with a sustainable urban planning tool. It is based on a framework which enhanced previous research and applications by:

- providing a ‘preliminary’ assessment tool that could advance geohazard decision-making and ground investigations;
- involving an integrated ‘package’ of a geohazard risk assessment to be based, using the power of BIM;

- using advanced risk assessment analyses (including an uncertainty analysis), which was integrated with BIM;
- enhancing relevant (geohazard) decision-making methods, i.e. the 3D ground models by integrating, visualising and linking together all aspects of a geohazard risk assessment (analysis), using BIM for the geohazard data storage, management (processes) and 3D visualisations.

More specifically, this system involved a complete and integrated risk assessment tool, which could be used to assess any urban geohazard easily and rapidly by considering the ground variability. This could be used as a preliminary assessment tool, and hence enhance sustainable ground investigation and decision-making. It also combined BIM (building data) and geohazard risk assessment (data), which enhances geotechnical applications.

This system was based on a framework for an advanced risk assessment 'package'. This comprehensive framework explored important aspects of an urban geohazard risk assessment, such as hazard, vulnerability and associated costs (probability). These 'components' were estimated by advanced risk assessment analyses, using various criteria and their combinations, uncertainty and probability analyses and Building Damage Assessments including risk of building-damage costs. This integrated system of analyses provided efficient information for geohazard risk and ground-building interactions, using borehole data, and hence enhanced the relevant knowledge and understanding. An important aspect of this system which expanded on previous analyses was based on the data integration and communication that used the power of BIM. The integration of BIM with the risk assessment analysis was developed, which advanced the urban geohazard risk assessments.

BIM successfully collected, processed, managed and visualised the data needed in this research. It supported the (data) integration with the (time-dependent) risk assessment to form this system. This integration extended 3D ground modelling and computer-aided methods, by introducing a system that could effectively manage the data of this assessment and visualise it in 3D. The efficient 3D visualisations of 3D geology-tunnel-building models including complete geohazard risk assessment visualisations demonstrated the effect of specific criteria (factors) with time. These aspects successfully formed a framework for a preliminary assessment tool, which allows engineers/scientists to identify risk-prone 'areas', easily, early, with low computational power needs, and then advice for further or more detailed investigation or analysis. Therefore, this 'multi-purpose' tool improved knowledge and understanding of the underground associated with ground investigation and supported decision-making for sustainable urban land-use planning.

The aim of this research was to create an integrated framework for an information system for assessing geohazard risk in an urban area. A framework for a 'package' which is capable of advancing relevant risk assessment and supporting decision-making in deterministic and uncertain conditions was provided, using a comprehensive geohazard risk assessment tool. To obtain such a complete tool, several important geohazard criteria and their effects, i.e. economic costs, were considered within advanced geohazard risk assessment analyses. This was carried out by a process of integrating BIM with these analyses. BIM played a key role in supporting this process. An integration of these 'components' was produced to extend 3D (geological) modelling aspects, using (conventional) borehole data, as a preliminary assessment tool. These provided important ground-building interactions information using 3D visualisations, which could enhance ground investigation. The user could easily identify hazardous areas and risk for building damage and costs, associated with any urban geohazard. Finally, important indications

were drawn for sustainable urban planning, using the resulting ground-related information taken from this BIM-based integrated system to advise for avoiding areas, which are susceptible to geohazards.

8.2 Future work

An integrated geohazard information system for assessing the risk in urban areas was developed. This provided a complete framework for an advanced risk assessment analysis tool using integrated data processes and three-dimensional visualisations for an urban geohazard. However, extensions based on the present framework could be made in future work to enhance it further.

Initially, a new version of the reported framework in the future could use more or other geotechnical and/or structural factors in the corresponding geohazard risk assessment analysis, if required. In addition, other tunnelling-induced ground movements (such as subsurface settlements) could also be investigated using the proposed tool. This could also be extended to explore hard rocks. A questionnaire made by experts, which could indicate important factors to be selected, could also accompany a future (multi-criteria decision) geohazard risk assessment analysis (AHP) based on the proposed approach. A geohazard risk assessment analysis using Artificial Neural Networks (ANN), based on the proposed framework, could also be undertaken to obtain further results and test the use of ANN within the proposed methodology.

In addition, an important aspect of the present framework is that it could work with the any other geohazard. Thus, in future work it could provide a risk assessment for different geohazards. For example, flood or contaminated land risk could be adopted, based on the current approach. However, the present system is designed to work with multiple geohazards,

and hence a comprehensive risk assessment that investigates the effect of a combination of a number of geohazards (Equation 3.2) could be explored.

In a future version of the proposed methodology for the Settlement Economic Risk assessment, the particular geometrical parameters of BIM-based building element data (i.e. columns, beams, walls, doors and windows) could be integrated also within a subsequent ground-building interaction analysis due to (for example) settlements. Then, using the proposed approach (combination of the extracted probabilistic distributions of ground settlements and the particular building-damage cost probability curves) any given damage scenario (i.e. Damage Category) could be modelled. These extended models could then enable the prediction of damage costs per element, element-group, storey and building, using various Damage Categories. Additionally, regarding the economic value employed in the uncertainty analysis, in future work a comprehensive cost distribution rather than a mean value could be estimated. In addition, a potential integration with ground improvement techniques could also be based on the current framework, targeted in the higher-risk areas shown in the 3D visualisations. This is closely related to the corresponding Settlement Economic Risk (and the Settlement Risk) assessment visualisations, which could demonstrate if it is required.

The level of detail of the proposed tool could also be adapted in the future with respect to the geohazard (geotechnics) and the features of the urban area (structures) investigated. Hence, a higher level of detail, such as the mesh grid analysis or using more complex structural components, could be adopted in the present models. As a result, future risk assessment visualisations based on the present framework could be extended, although a higher computational power would be needed. In addition, further use of more 3D models, i.e. buildings structures and/or other surface/ground features and alternative underground structures, such as pipes or extra tunnels, could be also adopted in the future. These applications

would be based on the current 3D modelling framework. More complex 3D geology (including more strata or other features) could also be explored in future work based on the current modelling. Further work based on the proposed system, could also be conducted on an enhanced version of the current model applied to a larger scale, i.e. a city (or regional) scale. This could allow more comprehensive investigations and relevant knowledge and understanding for a wider area.

It should be noted that the proposed preliminary assessment tool for assessing urban geohazard risk is capable of being integrated with other more detailed analysis/modelling tools, if required. Therefore, for example, a FEM analysis could be adopted as a 'secondary' assessment tool, using the risk assessment information (data) required from the present tool. This information could focus (more) on high-risk areas to be further investigated. This integration is based on the mesh generated in the current framework. Likewise, an integration with other modelling tools/software is provided by the current framework using BIM, by the data processes and communication advantages of this concept. Additional integrated visualisation could be also integrated with the present framework to enhance knowledge and understanding of the underground. By way of example, the contourmaps used could be extended to include more/other factors. Likewise, the integrated visualisations of borehole locations could provide useful information for other applications.

REFERENCES

3D systems (2018) STL File (website: https://uk.3dsystems.com/) [Accessed 5 March 2018].

Abanda, F.H., Vidalakis, C., Oti, A.H. and Tah, J.H. (2015) A critical analysis of Building Information Modelling systems used in construction projects. *Advances in Engineering Software*, *90*, pp.183-201.

Admiraal, H. and Cornaro, A. (2016) Why underground space should be included in urban planning policy–And how this will enhance an urban underground future. *Tunnelling and Underground Space Technology*, *55*, pp.214-220.

AGS (2019) Association of Geotechnical & Geoenvironmental Specialists (AGS) (website: https://www.ags.org.uk/) [Accessed 15 October 2019].

Akbarnezhad, A., Ong, K.C.G. and Chandra, L.R. (2014) Economic and environmental assessment of deconstruction strategies using building information modeling. *Automation in Construction*, *37*, pp.131-144.

Al-Bittar, T., Soubra, A. H. and Thajeel, J. (2018). Kriging-based reliability analysis of strip footings resting on spatially varying soils. *Journal of Geotechnical and Geoenvironmental Engineering*, *144*(10), 04018071.

Aldiss, D. T., Black, M. G., Entwisle, D. C., Page, D. P. and Terrington, R. L. (2012) Benefits of a 3D geological model for major tunnelling works: an example from Farringdon, east–central London, UK. *Quarterly Journal of Engineering Geology and Hydrogeology,* 45, pp. 405 –414.

Alwan, Z., Jones, P. and Holgate, P. (2016). Strategic sustainable development in the UK construction industry, through the framework for strategic sustainable development, using Building Information Modelling. *Journal of Cleaner Production*.

Amirebrahimi, S., Rajabifard, A., Mendis, P. and Ngo, T. (2016). A BIM-GIS integration method in support of the assessment and 3D visualisation of flood damage to a building. *Journal of Spatial Science*, pp.1-34.

Amorosi, A., Boldini, D., de Felice, G., Lasciarrea, W. G. and Malena, M. (2019) Three-dimensional numerical modelling of historical masonry structures affected by tunnelling-induced settlements. In *Structural Analysis of Historical Constructions* (pp. 947-956). Springer, Cham.

Atkinson, J.H., Potts, D.M. (1979) Subsidence above shallow tunnels in soft ground. J. Geotech. Geoenviron. Eng. (ASCE) 103 (4), 307–325.

Attewell, P.B, Yeats, J, and Selby, A.R, (1986) Soil Movements Induced by Tunneling and Their Effects on Pipelines and Structures. Glasgow: Blackie.

Attewell, P.B. and Woodman, J.P. (1982) Predicting the dynamics of ground settlement and its derivatives caused by tunnelling in soil. *Ground Engineering 15* (7), PP.13–22 & 36.

Autodesk Inc. (2018) Revit (website: https://www.autodesk.co.uk) [Accessed 10 March 2018]

Avgerinos, V., Potts, D. M., Standing, J. R. and Wan, M. S. P. (2018) Predicting tunnelling-induced ground movements and interpreting field measurements using numerical analysis: Crossrail case study at Hyde Park. *Géotechnique*, *68*(1), 31-49.

Ayalew, L., Yamagishi, H., Marui, H. and Kanno, T. (2005) Landslides in Sado Island of Japan: Part II. GIS-based susceptibility mapping with comparisons of results from two methods and verifications. *Engineering geology*, *81*(4), pp.432-445.

Bartolomey, A.A., Makovetsky, O.A., Ponomaryov, A.B. and Ofrikhter, V.G. (2003) Geotechnical trends in urban terrains evolution, *Proc. XIII ECSMGE Conference*, pp.573-578, Prague.

Bathrellos, G. D., Skilodimou, H. D., Chousianitis, K., Youssef, A. M. and Pradhan, B. (2017). Suitability estimation for urban development using multi-hazard assessment map. *Science of the total environment*, *575*, 119-134.

Bathrellos, G., Skilodimou, H. and Crysanthaki, I. (2007) Building and constructive materials as an urban geological resource in Trikala Prefecture. *Bulletin of Geological Society of Greece, Proceedings of the 11th Intern. Congress, Athens, May, 2007*.

Bathrellos, G.D., Gaki-Papanastassiou, K., Skilodimou, H.D., Papanastassiou, D. and Chousianitis, K.G. (2012) Potential suitability for urban planning and industry development using natural hazard maps and geological–geomorphological parameters. *Environmental earth sciences*, *66*(2), pp.537-548.

Bathrellos, G.D., Kalivas, D.P. and Skilodimou, H.D. (2009) GIS-based landslide susceptibility mapping models applied to natural and urban planning in Trikala, Central Greece. *Estud Geol*, *65*(1), pp.49-65.

Bathrellos, G.D., Skilodimou, H.D., Chousianitis, K., Youssef, A.M. and Pradhan, B. (2017) Suitability estimation for urban development using multi-hazard assessment map. *Science of the Total Environment*, *575*, pp.119-134.

Bauduin, C. (2003) Uncertainties and their relevance for the design of deep excavations near existing structures. *Proceedings of the XIII ECSMGE Conference*, Prague, pp. 445-449.

Baynes, F. (2010). Sources of geotechnical risk. *Quarterly Journal of Engineering Geology and Hydrogeology*, 43(3), pp.321-331.

BCA (2012) Singapore BIM Guide. Building and Construction Authority. Singapore.

Bello-Dambatta, A., Farmani, R., Javadi, A.A. and Evans, B.M. (2009). The Analytical Hierarchy Process for contaminated land management. *Advanced Engineering Informatics*, *23*(4), pp.433-441.

Benardos, A.G. and Kaliampakos, D.C. (2004) A methodology for assessing geotechnical hazards for TBM tunnelling—illustrated by the Athens Metro, Greece. International Journal of Rock Mechanics and Mining Sciences, 41(6), 987-999.

Berendrecht, W.L. and van Geer, F.C. (2016). A dynamic factor modeling framework for analyzing multiple groundwater head series simultaneously. *Journal of Hydrology*, *536*, pp.50-60.

Berhane, G. and Walraevens, K. (2013). Geological and geotechnical constraints for urban planning and natural environment protection: a case study from Mekelle City, Northern Ethiopia. *Environmental earth sciences*, *69*(3), pp.783-798.

BGS (2018) Groundwater data and information of Heathlanes, UK (website: https://www.bgs.ac.uk/research/groundwater/datainfo/levels/sites/Heathlanes.html) British Geological Survey (BGS), NERC, UK [Accessed 05.05.2018].

Bhatt, B.P., Awasthi, K.D., Heyojoo, B.P., Silwal, T. and Kafle, G. (2013) Using geographic information system and analytical hierarchy process in landslide hazard zonation. *Applied Ecology and Environmental Sciences*, *1*(2), pp.14-22.

Bierkens, M.F., Knotters, M. and Hoogland, T. (2001) Space-time modeling of water table depth using a regionalized time series model and the Kalman Filter. Water Resources Research, 37(5), 1277-1290.

Blong, R. (2003). A new damage index. *Natural hazards*, *30*(1), 1-23.

Borrmann, A., Kolbe, T., Donaubauer, A., Steuer, H., Jubierre, J. and Flurl, M. (2014). Multi-Scale Geometric-Semantic Modeling of Shield Tunnels for GIS and BIM Applications. *Computer-Aided Civil and Infrastructure Engineering, 30* (4), pp.263-281.

Boscardin, M. D. and Cording, E. J. (1989) Building response to excavation–induced settlement. *Journal of Geotechnical Engineering 115*(1), 1–21.

Bottero, M. and Peila, D. (2005) The use of the Analytic Hierarchy Process for the comparison between microtunnelling and trench excavation. *Tunnelling and underground space technology*, 20(6), 501-513.

Bowyer, A. (1981) “Computing dirichlet tessellations,” The Computer Journal, vol.24, no.2, pp.162–166.

Breunig, M. and Zlatanova, S. (2011) 3D geo-database research: Retrospective and future directions. *Computers & Geosciences*, 37(7), pp.791-803.

Bridge, D., Hough, E., Kessler, H., Price, S. and Reeves, H. (2005) Urban geology: integrating surface and sub-surface geoscientific information for development needs. In *The Current Role of Geological Mapping in Geosciences*, pp.129-134. Springer, Dordrecht.

Brundtland, G.H. (1987) Our Common Future. United Nations Report of the World Commission on Environment and Development.

Bryde, D., Broquetas, M. and Volm, J.M. (2013) The project benefits of building information modelling (BIM). *International journal of project management*, *31*(7), pp.971-980.

buildingSMART (2017) Industry Foundation Classes Edition 3 (website: http://www.buildingsmart.org).

Burke, H. F., Ford, J. R., Hughes, L., Thorpe, S. and Lee, J. R. (2017). A 3D geological model of the superficial deposits in the Selby area.

Burland, J. and Wroth, C. (1974) Settlement of buildings and associated damage. In *Proceedings of the conference on settlement of structures,* 611–654. London, UK: Pentech Press.

Burland, J. B. (1995) Assessment of risk of damage to buildings due to tunnelling and excavation. Invited Special Lecture. *In: 1st Int. Conf. on Earthquake Geotech. Engineering, IS Tokyo '95*.

Burland, J. B., Standing, J. R., Jardine, F. M. (2001) Building response to tunnelling - Case studies from construction of the Jubilee Line Extension, Volume 1: Projects and Methods. London: T. Telford.

Burland, J.B., Broms, J.B. and de Mello, V.F.B. (1977) Behavior of foundations and structures on soft ground. *Proceedings of the 9th International Conference on Soil Mechanics and Foundation Engineering (SMFE), Tokyo, Japan, July 10- 15, 1977,* pp.495-546.

Busby, J.P., Entwisle, D., Hobbs, P., Jackson, P., Johnson, N., Lawley, R., Linley, K., Mayr, T., Palmer, R., Raines, M. and Reeves, H. (2012). A GIS for the planning of electrical earthing. *Quarterly Journal of Engineering Geology and Hydrogeology*, *45*(3), pp.379-390.

Calcagno, P., Baujard, C., Guillou-Frottier, L., Dagallier, A. and Genter, A. (2014) Estimation of the deep geothermal potential within the Tertiary Limagne basin (French Massif Central): An integrated 3D geological and thermal approach. *Geothermics*, *51*, 496-508.

CanBIM AEC (CAN) Designers Committee (2012) AEC (CAN) BIM Protocol: Implementing Canadian BIM Standards for the Architectural, Engineering and Construction industry based on international collaboration, Version 1.0.

Cao, Z. J., Peng, X., Li, D. Q. and Tang, X. S. (2019). Full probabilistic geotechnical design under various design scenarios using direct Monte Carlo simulation and sample reweighting. *Engineering geology*, *248*, 207-219.

Cao, Z., Wang, Y. and Li, D. (2017) Practical reliability analysis of slope stability by advanced Monte Carlo simulations in a spreadsheet. In Probabilistic Approaches for Geotechnical Site Characterization and Slope Stability Analysis, pp. 147-167. Springer, Berlin, Heidelberg.

Cardona, O.D., van Aalst, M.K., Birkmann, J., Fordham, M., McGregor, G., Perez, R., Pulwarty, R.S., Schipper, E.L.F. and Sinh, B.T. (2012) Determinants of risk: exposure and vulnerability. *In: Managing the Risks of Extreme Events and Disasters to Advance Climate Change Adaptation [Field, C.B., V. Barros, T.F. Stocker, D. Qin, D.J. Dokken, K.L. Ebi, M.D. Mastrandrea, K.J. Mach, G.-K. Plattner, S.K. Allen, M. Tignor, and P.M. Midgley (eds.)]. A Special Report of Working Groups I and II of the Intergovernmental Panel on Climate Change (IPCC).* Cambridge University Press, Cambridge, UK, and New York, NY, USA, pp. 65-108.

Castelletti, A., Antenucci, J. P., Limosani, D., Quach Thi, X. and Soncini-Sensa, R. (2011). Interactive response surface approaches using computationally intensive models for multiobjective planning of lake water quality remediation, *Water Resour. Res., (47), W09534, doi:10.1029/2011WR010552.*

Chakeri, H., Ozcelik, Y. and Unver, B. (2013) Effects of important factors on surface settlement prediction for metro tunnel excavated by EPB. Tunnelling and Underground Space Technology, 36, 14-23.

Chandler, R., J., McGregor, I., D. and Morin, G., R. (2012) The role of geotechnical data in building information modelling. In: Australian–New Zealand Conference on Geomechanics (ANZ 2012)

Chandler, R., McGregor, I. and Morin, G. (2011) The role of geotechnical data in building information modelling, [website accessed 01 Sept 2016] from: http://www.keynetix.com/wpcontent/uploads/2013/07/chandlermcgregormorinfinal.pdf.

Chang, J. and Lin, H. (2016) Underground Pipeline Management Based on Road Information Modeling to Assist in Road Management. *J. Perform. Constr. Facil.*, 30(1), p.C4014001.

Chapman, D., Providakis, S. and Rogers, C. (2019) BIM for the Underground–An enabler of trenchless construction. *Underground Space*. https://doi.org/10.1016/j.undsp.2019.08.001.

Chapman, D.N., Metje, N. and Stark, A. (2017) Introduction to tunnel construction. Crc Press, London.

Chen, Y., Zhou, H., Zhang, H., Du, G. and Zhou, J. (2015) Urban flood risk warning under rapid urbanization. *Environmental Research*, 139, pp.3-10.

Chetouani, Y. (2008) Using ARX and NARX approaches for modeling and prediction of the process behavior: Application to a reactor-exchanger. Asia-Pacific Journal of Chemical Engineering, 3(6), 597-605.

Cheung, R.W.M. and Tang, W.H. (2005) Realistic assessment of slope reliability for effective landslide hazard mangement. Geotechnique, 55(1), pp.85-94.

Chew, L.P. (1989) Constrained Delaunay triangulations. Algorithmica, vol.4, no.1–4, pp.97–108.

Chi, H.L., Wang, X. and Jiao, Y. (2015) BIM-enabled structural design: impacts and future developments in structural modelling, analysis and optimisation processes. *Archives of computational methods in engineering*, *22*(1), pp.135-151.

Chien Kuo-Feng, Wu Zong-Han, Huang Shyh-Chang (2014) Identifying and assessing critical risk factors for BIM projects: Empirical study. Automation in Construction, (45), pp.1–15.

Chiles, J. P., and Delfiner, P. (2009) Geostatistics: modeling spatial uncertainty (Vol. 497). John Wiley & Sons, London, UK.

Chiu, W.K. and Tan, S.T. (2000) Multiple material objects: from CAD representation to data format for rapid prototyping. *Computer-aided design, 32*(12), pp.707-717.

CIRIA (1996) Prediction and effects of ground movements caused by tunnelling in soft ground beneath urban areas. Construction Industry Research and Information Association (CIRIA). Project Report 30.

Clarke, J. A. and Laefer, D. F. (2014). Evaluation of risk assessment procedures for buildings adjacent to tunnelling works. *Tunnelling and Underground Space Technology*, *40*, 333-342.

Clayton, C. (2002) Managing geotechnical risk: time for change? *Geotechnical Engineering*, 155(1), pp.79-80.

Clough, G.W. and Schmidt, B. (1981) Design and performance of excavations and tunnels in soft clay. Developments in Geotechnical Engineering, 20, pp.567-634.

Cooper, A.H. (2008) The GIS approach to evaporite-karst geohazards in Great Britain. *Environmental Geology*, *53*(5), pp.981-992.

Cording, E.J. and Hansmire, W.H. (1975) Displacements around soft ground tunnels. *Proceedings of the 5th Pan-American Conference on Soil Mechanics and Foundation Engineering, Buenos Aires, Argentina, October 27-31, 1975,* pp.571-633.

Corvalan, C., Hales, S., McMichael, A.J., Butler, C. and McMichael, A. (2005) *Ecosystems and human well-being: health synthesis*. World Health Organization, Geneva, Switzerland.

Costalago Meruelo, A., Simpson, D., Veres, S. and Newland, P. (2016) Improved system identification using artificial neural networks and analysis of individual differences in responses of an identified neuron. *Neural Networks*, 75, pp.56-65.

Coutinho-Rodrigues, J., Simão, A. and Antunes, C.H. (2011) A GIS-based multicriteria spatial decision support system for planning urban infrastructures. *Decision Support Systems*, *51*(3), pp.720-726.

Culshaw, M., Nathanail, C., Leeks, G., Alker, S., Bridge, D., Duffy, T., Fowler, D., Packman, J., Swetnam, R., Wadsworth, R. and Wyatt, B. (2006) The role of web-based environmental information in urban planning—the environmental information system for planners. *Science of The Total Environment*, 360(1-3), pp.233-245.

Culshaw, M.G. (2005) From concept towards reality, developing the attributed 3D geological model of the shallow subsurface. *Quarterly Journal of Engineering Geology and Hydrogeology* 38, 231–284.

Culshaw, M.G. and Price, S.J. (2011) The 2010 Hans Cloos lecture: the contribution of urban geology to the development, regeneration and conservation of cities. *Bulletin of Engineering Geology and Environment*, *70*(3), pp.333-376.

Dai, F.C., Lee, C.F. and Zhang, X.H. (2001) GIS-based geo-environmental evaluation for urban land-use planning: a case study. *Engineering geology*, *61*(4), pp.257-271.

Daliakopoulos, I.N., Coulibaly, P. and Tsanis, I.K. (2005) Groundwater level forecasting using artificial neural networks. *Journal of hydrology*, *309*(1-4), pp.229-240.

DCLG (2012) National Planning Policy Framework, Department for Communities and Local Government. ISBN: 978-1-4098-3413-7

de Rienzo, F., Oreste, P. and Pelizza, S. (2008) Subsurface geological-geotechnical modelling to sustain underground civil planning. *Engineering Geology*, 96(3-4), pp.187-204.

Delatte, N.J. (2008) Beyond Failure: Forensic Case Studies for Civil Engineers. ASCE.

Delaunay, B. (1934) Sur la sphere vide. IzvestIa AkademII Nauk SSSR, vol.6, pp. 793–800.

Deng, Y., Cheng, J.C. and Anumba, C. (2016). A framework for 3D traffic noise mapping using data from BIM and GIS integration. *Structure and Infrastructure Engineering*, *12*(10), pp.1267-1280.

Devleeschouwer, X. and Pouriel, F. (2006) Brussels Urban Geology (BUG): a 2D and 3D model of the underground by means of GIS. *IAEG2006*.

Devriendt, M. (2006) Tunnel induced ground movements and control instrumentation. Course Notes. British Tunnelling Society, Course on Tunnel Design and Construction, University of Surrey, Guildford, UK.

Dijkstra, T.A., Reeves, H.J., Dashwood, C., Pennington, C., Freeborough, K., Mackay, J.D., Uhlemann, S.S., Chambers, J.E. and Wilkinson, P.B. (2015) Development of models to inform a national Daily Landslide Hazard Assessment for Great Britain. In *EGU General Assembly Conference Abstracts* (Vol. 17).

Dindarloo, S.R. and Siami-Irdemoosa, E. (2015) Maximum surface settlement based classification of shallow tunnels in soft ground. *Tunnelling and Underground Space Technology*, 49, pp.320-327.

Ding, Z., Ji, X., Li, X. and Wen, J. (2019) Numerical Investigation of 3D deformations of existing buildings induced by tunnelling. *Geotechnical and Geological Engineering*, *37*(4), 2611-2623.

Dirichlet, G.L. (1850) Uber die Reduktion der positiven quadratischen formen mit drei unbes-timmten ganzen Zahlen. Journal fur die Reine und Angewandte Mathematik, vol.40, pp. 209–227.

Djamaluddin, I., Mitani, Y. and Ikemi, H. (2012) GIS-Based Computational Method for Simulating the Components of 3D Dynamic Ground Subsidence during the Process of Undermining. *Int. J. Geomech.*, 12(1), pp.43-53.

Dong, M., Neukum, C., Hu, H. and Azzam, R. (2014) Real 3D geotechnical modeling in engineering geology: a case study from the inner city of Aachen, Germany. *Bull Eng Geol Environ*, 74(2), pp.281-300.

Eadie, R., Browne, M., Odeyinka, H., McKeown, C. and McNiff, S. (2013) BIM implementation throughout the UK construction project lifecycle: An analysis. *Automation in Construction*, 36, pp.145-151.

Eastman, C., Teicholz, P., Sacks, R. and Liston, K. (2011) BIM Handbook (2nd Edition). A Guide to Building Information Modeling for Owners, Managers, Designers, Engineers and Contractors, John Wiley & Sons, New Jersey.

El May, M., Dlala, M. and Chenini, I. (2010) Urban geological mapping: Geotechnical data analysis for rational development planning. *Engineering Geology*, 116(1-2), pp.129-138.

Eleftheriadis, S., Mumovic, D., Greening, P. and Chronis, A. (2015) BIM enabled optimisation framework for environmentally responsible and structurally efficient design systems. In *32nd International Symposium on Automation and Robotics in Construction and Mining: Connected to the Future, Proceedings* (Vol. 32, pp. 1-9). International Symposium on Automation and Robotics in Construction (ISARC).

Entwisle, D., Wildman, G., Campbell, S., Merritt, J., Self, S., Monaghan, A. and Reeves, H. (2008) 3D geological modelling and geotechnical GIS for planning and development: an example from Glasgow, UK.

Entwisle, D.C., Culshaw, M.G., Hulbert, A.G., Shelley, W.A., Self, S.J. and Dobbs, M.R. (2016) The Glasgow (Scotland) geotechnical GIS: a desk study tool. *Geological Society, London, Engineering Geology Special Publications*, *27*(1), pp.63-80.

Ersoy, H., Bulut, F. and Berkün, M. (2013) Landfill site requirements on the rock environment: a case study. *Engineering Geology*, *154*, pp.20-35.

Fang, Q. and Boas, D. (2009) Tetrahedral mesh generation from volumetric binary and gray-scale images, Proceedings of IEEE International Symposium on Biomedical Imaging (ISBI 2009), pp. 1142-1145.

Fedeski M. and Gwilliam J. (2007) Urban sustainability in the presence of flood and geological hazards: The development of a GIS-based vulnerability and risk assessment methodology. Landscape and Urban Planning (83), pp 50–61.

Fernández, D.S. and Lutz, M.A. (2010) Urban flood hazard zoning in Tucumán Province, Argentina, using GIS and multicriteria decision analysis. *Engineering Geology*, *111*(1-4), pp.90-98.

Ferrario, M., Bonadeo, L., Brunamonte, F., Livio, F., Martinelli, E., Michetti, A., Censi Neri, P., Chiessi, V., Comerci, V. and Höbig, N. (2015). Late Quaternary environmental evolution of the Como urban area (Northern Italy): A multidisciplinary tool for risk management and urban planning. *Engineering Geology*, 193, pp.384-401.

Fisonga, M., Wang, F. and Mutambo, V. (2018) The estimation of sampling density in improving geostatistical prediction for geotechnical characterization. *International Journal of Geotechnical Engineering*, 1-8.

Fookes, P.G. (1997). Geology for engineers: the geological model, prediction and performance. Quarterly Journal of Engineering Geology, 30, 293–424.

Fordyce, F.M., Brown, S.E., Ander, E.L., Rawlins, B.G., O'Donnell, K.E., Lister, T.R., Breward, N. and Johnson, C.C. (2005) GSUE: urban geochemical mapping in Great Britain. *Geochemistry: Exploration, Environment, Analysis*, *5*(4), pp.325-336.

Freeborough, K., Dashwood, C., Doce, D.D., Jessamy, G., Brooks, S., Reeves, H. and Abbott, S. (2019) A national assessment of landslide hazard from Outside Party Slopes to the rail network of Great Britain. *Quarterly Journal of Engineering Geology and Hydrogeology*, *52*(3), pp.312-319.

Gakis, A., Cabrero, P., Entwisle, D. and Kessler, H. (2016). 3D geological model of the completed Farringdon underground railway station. In *Crossrail Project: Infrastructure design and construction* (pp. 431-446). ICE Publishing.

Georgiadou, M.C. (2016) Building Information Modelling in UK Construction Projects: A State of the Art Review. *RICS COBRA 2016*.

Geuzaine, C. and Remacle J.-F. (2009) Gmsh: a three-dimensional finite element mesh generator with built-in pre- and post-processing facilities. International Journal for Numerical Methods in Engineering 79(11), pp. 1309-1331.

Ghorbani, M., Sharifzadeh, M., Yasrobi, S. and Daiyan, M. (2012) Geotechnical, structural and geodetic measurements for conventional tunnelling hazards in urban areas – The case of Niayesh road tunnel project. *Tunnelling and Underground Space Technology,* (31), pp.1-8.

Giardina, G., DeJong, M. J., Chalmers, B., Ormond, B., and Mair, R. J. (2018). A comparison of current analytical methods for predicting soil-structure interaction due to tunnelling. *Tunnelling and Underground Space Technology*, *79*, 319-335.

Giardina, G., Ritter, S., DeJong, M. J. and Mair, R. J. (2017) Influence of building geometry on bending and shear deformations of buildings subject to tunnelling subsidence: numerical modelling. In *EURO: TUN 2017: IV International Conference on Computational Methods in Tunneling and Subsurface Engineering*.

Gibson, A.D. and Chowdhury, R. (2009). Planning and geohazards From: CULSHAW, M. G., REEVES, H. J., JEFFERSON, I. & SPINK, T. W. (eds) Engineering Geology for Tomorrow's Cities. Geological Society, London, Engineering Geology Special Publications, The Geological Society of London. (22), pp. 113–123.

Giddings, B., Hopwood, B. and O'brien, G. (2002) Environment, economy and society: fitting them together into sustainable development. *Sustainable development*, *10*(4), pp.187-196.

Glaser, S.D., Baise, L.G (2000). System identification estimation of soil properties at the Lotung site. *Soil Dynamics and Earthquake Engineering,* (19), pp.521-531.

Golias, N.A. and Dutton, R.W. (1997) Delaunay triangulation and 3D adaptive mesh generation. Finite Elements in Analysis and Design, 25(3-4), pp.331-341.

González-Garcia, J. and Jessell, M. (2016). A 3D geological model for the Ruiz-Tolima Volcanic Massif (Colombia): Assessment of geological uncertainty using a stochastic approach based on Bézier curve design. *Tectonophysics*, *687*, 139-157.

Google Earth (2018) Birmingham, UK; (from website: http://www.google.com/earth/index.html) [Viewed 15 March 2018].

Google Inc. (2015) Google Earth Pro (website: https://earth.google.com/download-earth.html) [Accessed 15 June 2017].

Google Inc. (2018) Google Earth (website: https://www.google.com/earth/) [Accessed 3 Mar 2018].

Graphisoft (2018) Archicad 22 (http://www.graphisoft.com/archicad/) [Accessed 15 January 2018].

Griffiths, J.S. (2016) Incorporating geomorphology in engineering geological ground models. *Geological Society, London, Engineering Geology Special Publications*, *27*(1), pp.159-168.

Griffiths, J.S., Stokes, M., Stead, D. and Giles, D. (2012) Landscape evolution and engineering geology: results from IAEG Commission 22. *Bull Eng Geol Environ* (71), pp 605–636.

Grimm, N.B., Faeth, S.H., Golubiewski, N.E., Redman, C.L., Wu, J., Bai, X. and Briggs, J.M. (2008) Global change and the ecology of cities. S*cience*, *319*(5864), 756-760.

Guillard, C. and Zezere, J. (2012) Landslide susceptibility assessment and validation in the framework of municipal planning in Portugal: the case of Loures municipality. *Environmental management*, *50*(4), pp.721-735.

Guzzetti, F., Reichenbach, P. and Ghigi, S. (2004). Rockfall hazard and risk assessment along a transportation corridor in the Nera Valley, Central Italy. *Environmental management*, *34*(2), pp.191-208.

Hack, R., Orlic, B., Ozmutlu, S., Zhu, S. and Rengers, N. (2005). Three and more dimensional modelling in geo-engineering. *Bull Eng Geol Environ*, 65(2), pp.143-153.

Hall, J.W., Henriques, J.J., Hickford, A.J., Nicholls, R.J., Baruah, P., Birkin, M., Chaudry, M., Curtis, T.P., Eyre, N., Jones, C. and Kilsby, C.G. (2014) Assessing the long-term performance of cross-sectoral strategies for national infrastructure. *Journal of Infrastructure Systems*, *20*(3), p.04014014.

Hammond, C.J., Prellwitz, R.W. and Miller, S.M. (1992) Landslide hazard assessment using Monte Carlo simulation. In Proceedings of 6th international symposium on landslides, Christchurch, New Zealand, Balk

Hansen, L.P. and Singleton, K.J. (1983) Stochastic consumption, risk aversion, and the temporal behavior of asset returns. Journal of political economy, 91(2), pp.249-265.

Harding, C. (2004) Site investigation and site conceptual models. The link between geology and engineering. In: Jardine RJ, Potts DM, Higgins KG (eds) Advances in geotechnical engineering: the Skempton conference, vol 2. Thomas Telford. London, pp 1304–1315.

He, Y., Fu, D., Zhao, Z., Su, J. and Lü, G. (2008) Analysis of spatial interpolation methods to precipitation based on GIS in Xinjiang. Research of Soil and Water Conservation, 15(6), 35-37.

Hojjati, A., Jefferson, I., Metje, N. and Rogers, C.D.F. (2017) Embedding sustainability criteria into pre-appraisal of underground utility for future cities. *Proceedings of the Institution of Civil Engineers-Urban Design and Planning*, *170*(6), 258-271.

Howard, A., Hatton, B., Reitsma, F. and Lawrie, K. (2009) Developing a geoscience knowledge framework for a national geological survey organisation. *Computers & Geosciences*, 35(4), pp.820-835.

HSE (2017) ALARP "at a glance", website accessed 10 September 2017 (address: http://www.hse.gov.uk/risk/theory/alarpglance.htm).

Hu, J., and Wan, N. (2010) Mine Information System Based on 3D Geological Modeling. In *2010 Third International Symposium on Information Science and Engineering* (pp. 405-408). IEEE.

Huang, X., Chen, G. and Li, Z. (2012) Research on Constructing 3D Geological Model of the Construction Layers in Daxing New City Area of Beijing. *AMR*, 594-597, pp.2897-2901.

Huber, M., Marconi, F. and Moscatelli, M. (2015). Risk-based characterisation of an urban building site. *Georisk: Assessment and Management of Risk for Engineered Systems and Geohazards*, 9(1), pp.49-56.

Hunt, D.V. and Rogers, C.D. (2005) Barriers to sustainable infrastructure in urban regeneration. In *Proceedings of the Institution of Civil Engineers-Engineering Sustainability* (Vol. 158, No. 2, pp. 67-81). Thomas Telford Ltd.

Hunt, D.V., Jefferson, I., Gaterell, M.R. and Rogers, C.D. (2009) Planning for sustainable utility infrastructure. *Proceedings of the Institution of Civil Engineers-Urban Design and Planning*, *162*(4), pp.187-201.

Hunt, D.V., Lombardi, D.R., Rogers, C.D. and Jefferson, I. (2008) Application of sustainability indicators in decision-making processes for urban regeneration projects. In *Proceedings* –

Institution of Civil Engineers. Engineering Sustainability (Vol. 161, No. 1, p. 77). Institution of Civil Engineers (ICE), London, UK.

Hunt, D.V.L., Makana, L.O., Jefferson, I. and Rogers, C.D.F. (2016) Liveable cities and urban underground space. *Tunnelling and Underground Space Technology*, *55*, 8-20.

Hyun, K.C., Min, S., Choi, H., Park, J. and Lee, I.M. (2015) Risk analysis using fault-tree analysis (FTA) and analytic hierarchy process (AHP) applicable to shield TBM tunnels. *Tunnelling and Underground Space Technology*, 49, 121-129.

ICE (2009) The State of the Nation: Defending Critical Infrastructure. Institution of Civil Engineers (ICE), London, UK.

Imseeh, W.H. and Alshibli, K.A. (2018) 3D finite element modelling of force transmission and particle fracture of sand. *Computers and Geotechnics,* Volume 94, Pages 184-195, Institute of British Architects, London.

ITA/AITES (2007) Settlements induced by tunnelling in soft ground. *Tunnelling and Underground Space Technology*, 22(2), pp 119-149.

Jarna, A., Bang-Kittilsen, A., Haase, C., Henderson, I., Høgaas, F., Iversen, S. and Seither, A. (2015). 3-Dimensional Geological mapping and modeling activities at the Geological Survey of Norway. *Int. Arch. Photogramm. Remote Sens. Spatial Inf. Sci.*, XL-2/W4, pp.11-16.

Jørgensen, F., Høyer, A. S., Sandersen, P. B., He, X., and Foged, N. (2015). Combining 3D geological modelling techniques to address variations in geology, data type and density–An example from Southern Denmark. *Computers & geosciences*, *81*, 53-63.

Juang, C.H., Yang, S.H. and Yuan, H. (2005) Model uncertainty of shear wave velocity-based method for liquefaction potential evaluation. *Journal of geotechnical and geoenvironmental engineering,* 131(10), pp.1274-1282.

Kang, T.W. and Hong, C.H. (2015) A study on software architecture for effective BIM/GIS-based facility management data integration. *Automation in Construction*, *54*, pp.25-38.

Kayastha, P., Dhital, M.R. and De Smedt, F. (2013) Application of the analytical hierarchy process (AHP) for landslide susceptibility mapping: A case study from the Tinau watershed, west Nepal. *Computers & Geosciences*, 52, 398-408.

Kazakis, N., Kougias, I. and Patsialis, T. (2015) Assessment of flood hazard areas at a regional scale using an index-based approach and Analytical Hierarchy Process: Application in Rhodope–Evros region, Greece. *Science of the Total Environment*, 538, 555-563.

Kessler H., Turner, A. K., Culshaw, M. and Royse, K. (2008) Unlocking the potential of digital 3D geological subsurface models for geotechnical engineers. In: *European econference of the International Association for Engineering geology, Madrid, Spain, 15-20 Sept 2008*.

Kessler, H., Wood, B., Morin, G., Gakis, A., McArdle, G., Rabson, O., Fitzgerald, R. and Dearden, R. (2015) Building Information Modelling (BIM) – A Route for Geological Models to Have Real World Impact. Special Report. AER/AGS, 13-18.

Khakestar, M. S., Hassani, H., Moarefvand, P., and Madani, H. (2016). Prediction of the collapsing risk of mining slopes based on geostatistical interpretation of geotechnical parameters. *Journal of the Geological Society of India*, *87*(1), 97-104.

Kim, C., Kim, B. and Kim, H. (2013) 4D CAD model updating using image processing-based construction progress monitoring. *Automation in Construction*, *35*, pp.44-52.

Kim, H. J., Dinoy, P. R. T., Choi, H. S., Lee, K. B., and Mission, J. L. C. (2019). Spatial interpolation of SPT data and prediction of consolidation of clay by ANN method. *Coupled systems mechanics*, *8*(6), 523-535.

Kim, J.I., Kim, J., Fischer, M. and Orr, R. (2015) BIM-based decision-support method for master planning of sustainable large-scale developments. *Automation in Construction*, *58*, pp.95-108.

Kim, S., Kim, J., Jung, J. and Heo, J. (2015). Development of a 3D Underground Cadastral System with Indoor Mapping for As-Built BIM: The Case Study of Gangnam Subway Station in Korea. *Sensors*, 15(12), pp.30870-30893.

Knotters, M. and Bierkens, M.F. (2001) Predicting water table depths in space and time using a regionalised time series model. Geoderma, 103(1-2), 51-77.

Kolat, C., Ulusay, R. and Suzen, M.L. (2012) Development of geotechnical microzonation model for Yenisehir (Bursa, Turkey) located at a seismically active region. *Engineering geology*, *127*, pp.36-53.

Krige, D.G. (1951) A statistical approach to some basic mine valuation problems on the witwatersrand, Journal of the Chemical, Metallurgical and Mining Society of South Africa, vol.52, no.6, pp. 119–139.

Lacroix, P. and Helmstetter, A. (2011) Location of seismic signals associated with microearthquakes and rockfalls on the Séchilienne landslide, French Alps. *Bulletin of the Seismological Society of America*, *101*(1), pp.341-353.

Ladenhauf, D., Battisti, K., Berndt, R., Eggeling, E., Fellner, D.W., Gratzl-Michlmair, M. and Ullrich, T. (2016) Computational geometry in the context of building information modeling. *Energy and buildings*, *115*, pp.78-84.

Lawson, C.L. (1977) Software for $C1$ surface interpolation. In Mathematical Software III, Academic Press, New York, NY, USA.

Lázaro, J. M., Navarro, J. Á. S., Gil, A. G., & Romero, V. E. (2014). 3D-geological structures with digital elevation models using GPU programming. *Computers & geosciences*, *70*, 138-146.

Lee, D.T. and Lin, A.K. (1986) Generalized Delaunay triangulation for planar graphs. Discrete & Computational Geometry, vol.1, no. 1, pp. 201–217.

Lee, E. M. and Jones, D. K. C. (2004) Landslide risk assessment. Thomas Telford, London.

Lee, G.K. and Chan, E.H. (2008) The analytic hierarchy process (AHP) approach for assessment of urban renewal proposals. Social indicators research, 89(1), 155-168.

Lee, H.W., Oh, H., Kim, Y. and Choi, K. (2015) Quantitative analysis of warnings in building information modeling (BIM). *Automation in Construction*, *51*, pp.23-31.

Legat, K. (2006) Approximate direct georeferencing in national coordinates. ISPRS Journal of Photogrammetry and Remote Sensing, 60(4), pp.239-255.

Li, L., Wu, K. and Zhou, D. (2014). AutoCAD-based prediction of 3D dynamic ground movement for underground coal mining. *International Journal of Rock Mechanics and Mining Sciences*, 71, pp.194-203.

Li, Y. and Briggs, R. (2008) Scalable and error tolerant automated georeferencing under affine transformations. In IGARSS 2008-2008 IEEE International Geoscience and Remote Sensing Symposium (Vol. 5, pp. V-232). IEEE.

Li, Y., Wang, H., Zhao, X. and Zhang, J. (2013) Research on BIM Technology Application in the Construction of a Subway Station. *AMM*, 405-408, pp.3396-3400.

Liu, R. and Issa, R.R.A. (2012) 3D visualization of sub-surface pipelines in connection with the building utilities: Integrating GIS and BIM for facility management. In *Computing in Civil Engineering (2012)*, pp. 341-348.

Liu, S., Meng, X. and Tam, C. (2015) Building information modeling based building design optimization for sustainability. *Energy and Buildings*, *105*, pp.139-153.

Liu, Y., Van Nederveen, S. and Hertogh, M. (2017) Understanding effects of BIM on collaborative design and construction: An empirical study in China. *International Journal of Project Management*, *35*(4), pp.686-698.

Liu, Y.C. and Chen, C.S. (2007) A new approach for application of rock mass classification on rock slope stability assessment. *Engineering geology*, *89*(1-2), pp.129-143.

Lo, S., Wu, J., Lin, F. and Hsu, C. (2015). Visual Sensing for Urban Flood Monitoring. *Sensors*, 15(8), pp.20006-20029.

Loganathan, N. (2011) An innovative method for assessing tunnelling-induced risks to adjacent structures. Parsons Brinckerhoff Inc., New York, NY, USA.

Loganathan, N. and Poulos, H. (1998) Analytical Prediction for Tunneling-Induced Ground Movements in Clays. *Journal of Geotechnical and Geoenvironmental Engineering, 124*(9), pp.846-856.

Lu, S., Wu, I. and Hsiung, B. (2012) Applying building information modelling in environmental impact assessment for urban deep excavation projects. *Gerontechnology*, 11(2).

Luo, Q. (2014) Design and Implementation of Information System of 3D City of Geotechnical Engineering. *AMM*, 716-717, pp.521-524.

MacLeamy, P. (2010) Effort Curve, *HOK, (*http://www.hok.com/thought-leadership/patrick-macleamy-on-thefuture-of-the-building-industry/) [Accessed 25.08.2016].

Maesano, F. E. and D'Ambrogi, C. (2017). Vel-IO 3D: A tool for 3D velocity model construction, optimization and time-depth conversion in 3D geological modeling workflow. *Computers & geosciences*, *99*, 171-182.

Mair, R. J. (1993) The Unwin memorial lecture 1992: Developments in geotechnical engineering research: application to tunnels and deep excavations. *Proc. Instn. Civ. Engrs. Civil Engineering, 97*, pp. 27-41.

Mair, R. J., Taylor, R. N. and Burland, J. B. (1996) Prediction of ground movements and assessment of risk of building damage due to bored tunnelling. *In Geotechnical Aspects of Underground Construction in Soft Ground,* 713–718. Rotterdam: Balkema.

Mair, R., J. and Taylor, R.N. (1997) Bored tunneling in the urban environment. Proceedings of the 14th International Conference on Soil Mechanics and Foundation Engineering (ICSMFE), Hamburg, Germany, September 6- 12, 1997, 2353-2385.

Marache, A., Dubost, J., Breysse, D., Denis, A. and Dominique, S. (2009) Understanding subsurface geological and geotechnical complexity at various scales in urban soils using a 3D model. *Georisk: Assessment and Management of Risk for Engineered Systems and Geohazards,* 3(4), pp.192-205.

Marinoni O. (2004) Implementation of the analytical hierarchy process with VBA in ArcGIS. Computer and Geosciences, 30, 637–646.

Marker, B.R. (1998) Incorporation of information on geohazards into the planning process. *Geological Society, London, Engineering Geology Special Publications*, *15*(1), pp.385-389.

Mashhadian, M., Abedi, S. and Noshadravan, A. (2018) Probabilistic multiscale characterization and modeling of organic-rich shale poroelastic properties. *Acta Geotechnica,* 13(4), pp.781-800.

Masoud, A.A. (2015) Geotechnical evaluation of the alluvial soils for urban land management zonation in Gharbiya governorate, Egypt. *Journal of African Earth Sciences*, *101*, pp.360-374.

Matheron, G. (1963) Principles of geostatistics. *Economic Geology,* vol.58, no.8, pp. 1246–1266.

Mathworks Inc. (2016) Matlab R2016a (from website: https://uk.mathworks.com/products/matlab.html) [Accessed 12 December 2016].

Mathworks Inc. (2017) MATLAB File Exchange. (from website: https://uk.mathworks.com/matlabcentral/fileexchange) [Accessed 15 January 2017].

McCall, G.J.H. (1998) Geohazards and the urban environment. *Geological Society, London, Engineering Geology Special Publications*, *15*(1), pp.309-318.

Mei, G. (2014) Summary on several key techniques in 3D geological modeling. The Scientific World Journal, 2014.

Mercado, V., El-Sekelly, W., Zeghal, M. and Abdoun, T., (2015). Identification of soil dynamic properties through an optimization analysis. *Computers and Geotechnics*, *65*, pp.175-186.

Merz, B., Kreibich, H., Schwarze, R. and Thieken, A. (2010). Review article" Assessment of economic flood damage". Natural Hazards and Earth System Sciences, 10(8), 1697-1724.

Metje, N., Atkins, P.R., Brennan, M.J., Chapman, D.N., Lim, H.M., Machell, J., Muggleton, J.M., Pennock, S., Ratcliffe, J., Redfern, M. and Rogers, C.D.F. (2007) Mapping the Underworld–State-of-the-art review. *Tunnelling and underground space technology*, *22*(5-6), pp.568-586.

Mielby, S., Eriksson, I., Diarmad, S., Campbell, G. and Lawrence, D. (2017). Opening up the subsurface for the cities of tomorrow. The subsurface in the planning process. Procedia Engineering, 209, pp.12-25.

Miettinen, R. and Paavola, S. (2014) Beyond the BIM utopia: Approaches to the development and implementation of building information modeling. *Automation in construction*, *43*, pp.84-91.

Migilinskas, D., Popov, V., Juocevicius, V. and Ustinovichius, L. (2013). The Benefits, Obstacles and Problems of Practical Bim Implementation. *Procedia Engineering*, 57, pp.767-774.

Morelli, S., Segoni, S., Manzo, G., Ermini, L. and Catani, F. (2012). Urban planning, flood risk and public policy: The case of the Arno River, Firenze, Italy. *Applied Geography*, 34, pp.205-218.

Morin G., Hassall, S., Chandler, R. (2014). Case study - The real life benefits of Geotechnical Building Information Modelling. Information Technology in Geo-Engineering D.G. Toll et al. (Eds.), IOS Press, 2014; pp 95-102.

Nathanail, C. P. (2013). The Tenth Glossop Lecture Engineering geology of sustainable risk-based contaminated land management. Quarterly Journal of Engineering Geology and Hydrogeology, 46, 6 –29

NBS (2014) *NBS National BIM Report 2014*. National Building Specification, Royal Institute of British Architects, London.

Neaupane, K.M. and Adhikari, N.R. (2006) Prediction of tunneling-induced ground movement with the multi-layer perceptron. *Tunnelling and Underground Space Technology,* 21(2), 151-159.

NERC UKCEH (2018) National River Flow Archive (website: https://nrfa.ceh.ac.uk), Wallingford, UK [Accessed 05.05.2018].

Nezarat, H., Sereshki, F. and Ataei, M., (2015) Ranking of geological risks in mechanized tunneling by using Fuzzy Analytical Hierarchy Process (FAHP). Tunnelling and Underground Space Technology, 50, 358-364.

Nguyen, V.U. and Chowdhury, R.N., 1985. Simulation for risk analysis with correlated variables. *Geotechnique*, *35*(1), pp.47-58.

O'Reilly, M.P. and New, B.M. (1982) Settlements above tunnels in the United Kingdom – their magnitude and prediction. *Tunnelling'82*. The Institution of Mining and Metallurgy, London, pp. 55–64.

Office for National Statistics (2017) House price per square metre and house price per room, England and Wales: 2004 to 2016 (from website: https://www.ons.gov.uk/releases/housepricepersquaremeterandhousepriceperroomenglandandwales2004to2016) [Accessed 15 April 2019].

olde Scholtenhuis, L.L., Hartmann, T. and Dorée, A.G. (2016) 4D CAD based method for supporting coordination of urban subsurface utility projects. *Automation in construction,* 62, 66-77.

Oliver, M.A. and Webster, R. (1990) Kriging: a method of interpolation for geographical information systems. International Journal of Geographical Information Systems, vol. 4, no. 3, pp. 313– 332.

Oskay, C. and Zeghal, M. (2011) A survey of geotechnical system identification techniques. Soil Dynamics and Earthquake Engineering, 31(4), 568-582.

Owens, S. and Cowell, R. (2011) Land and limits: interpreting sustainability in the planning process. Routledge.

Pacheco-Martínez J., Hernandez-Marín, M., Burbey, T. J., González-Cervantes, N., Ortíz-Lozano, J. Á., Zermeño-De-Leon, M. E. and Solís-Pinto, A. (2013) Land subsidence and ground failure

associated to groundwater exploitation in the Aguascalientes Valley, México. *Engineering Geology* (164) pp 172–186.

Papadopoulou-Vrynioti, K., Bathrellos, G., Skilodimou, H., Kaviris, G. and Makropoulos, K. (2013). Karst collapse susceptibility mapping considering peak ground acceleration in a rapidly growing urban area. *Engineering Geology*, 158, pp.77-88.

Papaioannou, G., Vasiliades, L. and Loukas, A. (2015) Multi-Criteria Analysis Framework for Potential Flood Prone Areas Mapping. Water Resources Management, 29(2), pp.399-418.

Parry, S., Baynes, F. J., Culshaw, M. G., Eggers, M., Keaton, J. F., Lentfer, K., Novotny, J. and Paul, D. (2014) Engineering geological models: an introduction: IAEG commission 25. *Bull Eng Geol Environ,* 73, pp 689-706.

Peck, R.B. (1969) Deep excavations and tunnelling in soft ground. *In: Proceedings of the 7th International Conference on Soil Mechanics and Foundation Engineering, State of the Art Volume, vol. 3.* Mexican Society of Soil Mechanics, Mexico, pp. 225–290.

Peduto, D., Nicodemo, G., Maccabiani, J. and Ferlisi, S. (2017) Multi-scale analysis of settlement-induced building damage using damage surveys and DInSAR data: A case study in The Netherlands. *Engineering geology*, *218*, pp.117-133.

Peng, X., Li, D. Q., Cao, Z. J., Gong, W. and Juang, C. H. (2017). Reliability-based robust geotechnical design using Monte Carlo simulation. *Bulletin of Engineering Geology and the Environment*, *76*(3), 1217-1227.

Phoon, K. K. and Tang, C. (2019). Characterisation of geotechnical model uncertainty. *Georisk: Assessment and Management of Risk for Engineered Systems and Geohazards*, *13*(2), 101-130.

Phoon, K.K. and Kulhawy, F.H. (1999) Evaluation of geotechnical property variability. *Canadian Geotechnical Journal,* 36(4), pp.625-639.

Pinheiro, M., Emery, X., Miranda, T., Lamas, L. and Espada, M. (2018). Modelling geotechnical heterogeneities using geostatistical simulation and finite differences analysis. *Minerals*, *8*(2), 52.

Potts, D. M., Zdravkovic, L., Addenbrooke, T. I., Higgins, K. G., and Kovacevic, N. (2001). Finite element analysis in geotechnical engineering: Application (Vol. 2). Thomas Telford, London, UK.

Price, D.G., (1971) Engineering geology in the urban environment. *Quarterly Journal of Engineering Geology and Hydrogeology*, *4*(3), pp.191-208.

Price, S., Ford, J., Campbell, S. and Jefferson, I. (2016). Urban Futures: the sustainable management of the ground beneath cities. *Geological Society, London, Engineering Geology Special Publications*, 27(1), pp.19-33.

Providakis, S., Rogers, C.D.F and Chapman, D.N. (2019) Predictions of settlement risk induced by tunnelling using BIM and 3D visualization tools. *Tunnelling and Underground Space Technology,* 92, https://doi.org/10.1016/j.tust.2019.103049.

Qi, X. H., and Liu, H. X. (2019). An improved global zonation method for geotechnical parameters. *Engineering geology*, *248*, 185-196.

Rafiee, A., Dias, E., Fruijtier, S. and Scholten, H. (2014). From BIM to Geo-analysis: View Coverage and Shadow Analysis by BIM/GIS Integration. *Procedia Environmental Sciences*, 22, pp.397-402.

Rahimi, M., Shafieezadeh, A., Wood, D., Kubatko, E. J., and Dormady, N. C. (2019). Bayesian calibration of multi-response systems via multivariate Kriging: Methodology and geological and geotechnical case studies. *Engineering Geology*, *260*, 105248.

Rajan, V.T. (1994) Optimality of the Delaunay triangulation in R d. *Discrete & Computational Geometry,* 12(2), pp.189-202.

Rankin, W. (1988) Ground movements resulting from urban tunnelling: predictions and effects. Geological Society, London, *Engineering Geology Special Publications, 5*(1), pp.79-92.

Rawlins, B.G., Harris, J., Price, S., Bartlett, M., (2013) A review of climate change impacts on urban soil functions with examples and policy insights from England, UK. Soil Use and Management, 31, pp. 46-61, http://doi.org/10.1111/sum.12079

Roberts, N., Nadim, F. and Kalsnes, B. (2009) Quantification of vulnerability to natural hazards. *Georisk: Assessment and Management of Risk for Engineered Systems and Geohazards,* 3(3), pp.164-173.

Roberts, N.J., Nadim, F. and Kalsnes, B. (2009) Quantification of vulnerability to natural hazards. *Georisk: Assessment and Management of Risk for Engineered Systems and Geohazards*, *3*(3), pp.164-173.

Rogers, C.D., Lombardi, D.R., Leach, J.M. and Cooper, R.F. (2012) The urban futures methodology applied to urban regeneration. In *Proceedings of the Institution of Civil Engineers-Engineering Sustainability* (Vol. 165, No. 1, pp. 5-20), Thomas Telford Ltd.

Rogers, C.D.F. (2009) Substructures, underground space and sustainable urban environments. Geol. Soc., London, *Eng. Geol. Spec. Publ. 22* (1), 177–188.

Rosenbaum, M. (2003) Characterisation of the shallow subsurface: implications for urban infrastructure and environmental assessment. In: Rosenbaum, M.S., Turner, A.K. (Eds.), New Paradigms in Subsurface Prediction. Springer, Berlin, Heidelberg, Lecture Notes in Earth Sciences, vol. 99, pp. 3–6.

Rowe, R. K., and Fraser, M. J. (1995) Effect of uncertainty in the assessment of the potential impact of waste disposal facilities. Geoenvironment 2000, Geotech. Spec. Publ. 46, ASCE, New York, 270–284.

Rozos, D., Bathrellos, G.D. and Skillodimou, H.D. (2011) Comparison of the implementation of rock engineering system and analytic hierarchy process methods, upon landslide susceptibility mapping, using GIS: a case study from the Eastern Achaia County of Peloponnesus, Greece. *Environmental Earth Sciences,* 63(1), 49-63.

Ruby (2017) Ruby 2.4 (website: https://www.ruby-lang.org/en/) [Accessed 10 June 2017].

Saaty, T.L. (1977) A scaling method for priorities in hierarchical structures. Journal of Mathematical Psychology, 15, 234–281.

Saaty, T.L. (1980). The analytic hierarchy process: planning, priority setting, resource allocation. McGraw-Hill Book Co, New York, NY, USA.

Saaty, T.L. and Vargas, L.G. (1990) The Analytic Hierarchy Process series. University of Pittsburg.

Sagaseta, C. (1987) Analysis of undrained soil deformation due to ground loss. *Geotechnique*, London, England, 37, 301-320.

Santos, O.J. Jr. and Celestino, T.B. (2008) Artificial neural networks analysis of Sao Paulo subway tunnel settlement data. Tunnelling and Underground Space Technology, 23(5), 481-491.

Schindler, S., Hegemann, F., Koch, C., König, M. and Mark, P. (2016) Radar interferometry based settlement monitoring in tunnelling: Visualisation and accuracy analyses. *Visualization in Engineering* pp.4-7.

Sengezer, B. and Koç, E., (2005) A critical analysis of earthquakes and urban planning in Turkey. *Disasters*, *29*(2), pp.171-194.

Shahin M. A., Maier H. R., and Jaksa M. B. (2004) Data division for developing neural networks applied to geotechnical engineering, *Journal of Computing in Civil Engineering*, vol. 18, no. 2, pp. 105–114.

Shahin, M., Jaksa, M. and Maier, H. (2009) Recent Advances and Future Challenges for Artificial Neural Systems in Geotechnical Engineering Applications. *Advances in Artificial Neural Systems*, pp.1-9.

Shewchuk, J.R., (2002) Delaunay refinement algorithms for triangular mesh generation. Computational geometry, 22(1-3), pp.21-74.

Shin, H.S., Kwon, Y.C., Jung, Y.S., Bae, G.J. and Kim, Y.G., (2009) Methodology for quantitative hazard assessment for tunnel collapses based on case histories in Korea. International Journal of Rock Mechanics and Mining Sciences, 46(6), 1072-1087.

Sigtryggsdóttir, F., Snæbjörnsson, J., Grande, L. and Sigbjörnsson, R. (2015) Interrelations in multi-source geohazard monitoring for safety management of infrastructure systems. Structure and Infrastructure Engineering, 12(3), pp.327-355.

Silva, M., Salvado, F., Couto, P. and Azevedo, Á. (2016) Roadmap Proposal for Implementing Building Information Modelling (BIM) in Portugal. *OJCE*, 06(03), pp.475-481.

Simons, N., Menzies, B. and Matthews, M. (2002) *A short course in geotechnical site investigation*. London: Thomas Telford.

Singh, A. K. (1997) Technology Support Center Issue: Lognormal Distribution in Environmental Applications. US Environmental Protection Agency, National Exposure Research Laboratory.

Skilodimou, H., Livaditis, G., Bathrellos, G. and Verikiou-Papaspiridakou, E., (2003). Investigating the Flooding Events of the Urban Regions of Glyfada and Voula, Attica, Greece: A Contribution to Urban Geomorphology. *Geografiska Annaler, Series A: Physical Geography*, 85(2), pp.197-204.

Smallman, C. (2000) Crisis and risk management. Lecture presentation, NIMBAS-Bradford MBA Programme, September 2000. Utrecht: NIMBAS University.

Steel, J., Drogemuller, R. and Toth, B. (2012) Model interoperability in building information modelling. Softw Syst Model (11) pp. 99–109.

Succar, B., 2009. Building information modelling framework: A research and delivery foundation for industry stakeholders. *Automation in construction*, *18*(3), pp.357-375.

Sun, C. G. and Kim, H. S. (2017). GIS-based regional assessment of seismic site effects considering the spatial uncertainty of site-specific geotechnical characteristics in coastal and inland urban areas. *Geomatics, Natural Hazards and Risk*, *8*(2), 1592-1621.

Sun, C. G., and Kim, H. S. (2016). Geostatistical assessment for the regional zonation of seismic site effects in a coastal urban area using a GIS framework. *Bulletin of Earthquake Engineering*, *14*(8), 2161-2183.

Sun, C.G., 2012. Applications of a GIS-based geotechnical tool to assess spatial earthquake hazards in an urban area. *Environmental Earth Sciences*, *65*(7), pp.1987-2001.

Sundell, J., Haaf, E., Tornborg, J. and Rosén, L. (2019) Comprehensive risk assessment of groundwater drawdown induced subsidence. Stochastic Environmental Research and Risk Assessment, 33(2), pp.427-449.

SUPodium (2018) SUPlugins (website: http://www.SUplugins.com/ifc2skp.php) [viewed on 3 June 2018].

Suwansawat, S. and Einstein, H.H. (2006) Artificial neural networks for predicting the maximum surface settlement caused by EPB shield tunneling. Tunnelling and underground space technology, 21(2), 133-150.

Svensson, M. (2016) GeoBIM for optimal use of geotechnical data. In: Proceedings of the 17th Nordic Geotechnical Meeting: Challenges in Nordic Geotechnic. Reykjavik: IGS, pp. 605-611.

Taheri, K., Gutiérrez, F., Mohseni, H., Raeisi, E. and Taheri, M. (2015) Sinkhole susceptibility mapping using the analytical hierarchy process (AHP) and magnitude–frequency relationships: a case study in Hamadan province, Iran. Geomorphology, 234, 64-79.

Tame, C., Cundy, A., Royse, K., Smith, M. and Moles, N. (2013) Three-dimensional geological modelling of anthropogenic deposits at small urban sites: A case study from Sheepcote Valley, Brighton, UK. *Journal of Environmental Management*, 129, pp.628-634.

Tang, W.H. (1984) Principles of probabilistic characterization of soil properties. *Geotechnical Safety and Reliability*, pp. 39-39.

Tawelian, L. and Mickovski, S. (2016) The Implementation of Geotechnical Data into the BIM Process. *Procedia Engineering*, 143, pp.734-741.

Tegtmeier, W., Zlatanova, S., van Oosterom, P. and Hack, H. (2014) 3D-GEM: Geo-technical extension towards an integrated 3D information model for infrastructural development. *Computers & Geosciences*, 64, pp.126-135

Tengborg, P. and Sturk, R. (2016) Development of the use of underground space in Sweden. *Tunnelling and Underground Space Technology*, *55*, pp.339-341.

Terzaghi, K. (1950) Geologic aspects of soft ground tunnelling. In: Trask, J. (Ed.), Applied Sedimentation (Chapter 11). John Wiley, New York.

Thierry, P., Prunier-Leparmentier, A.M., Lembezat, C., Vanoudheusden, E. and Vernoux, J.F. (2009) 3D geological modelling at urban scale and mapping of ground movement susceptibility from gypsum dissolution: The Paris example (France). *Engineering Geology*, 105(1-2), 51-64.

Thornton, J. M., Mariethoz, G. and Brunner, P. (2018). A 3D geological model of a structurally complex Alpine region as a basis for interdisciplinary research. *Scientific data*, *5*(1), 1-20.

Touch, S., Likitlersuang, S. and Pipatpongsa, T. (2014) 3D geological modelling and geotechnical characteristics of Phnom Penh subsoils in Cambodia. *Engineering geology*, *178*, 58-69.

Trimble Inc. (2016) Sketchup Pro 2016. (https://www.sketchup.com/) [Accessed 3 November 2016].

Turner, A. (2005) Challenges and trends for geological modelling and visualisation. Bulletin of Engineering Geology and the Environment, 65(2), pp.109-127.

Turner, A.K. (2000) Geoscientific modeling: past, present, and future. *Geographic information systems in petroleum exploration and development. AAPG Computer Applications in Geology*, *4*, pp.27-36.

UK National Ecosystem Assessment (2011) The UK National Ecosystem Assessment. Understanding Nature's value to Society: Synthesis of the Key Findings. NEP-WCMC, Cambridge, UK.

UKRI NERC (2018a) BGS Geoindex. (from website: https://www.bgs.ac.uk/geoindex/) [Accessed 10.06.2018].

UKRI NERC (2018b) BGS Geology of Britain viewer. (from website: https://www.bgs.ac.uk/discoveringGeology/geologyOfBritain/viewer.html) [Accessed 10.06.2018].

UNDHA (1992) Internationally agreed glossary of basic terms related to disaster management. United Nations, Department of Humanitarian Affairs, DNA/93/36, Geneva.

UNISDR (2009) 2009 UNISDR Terminology on Disaster Risk Reduction (website: https://www.undrr.org/publication/2009-unisdr-terminology-disaster-risk-reduction) United Nations International Strategy for Disaster Reduction (UNISDR). United Nations, Geneva, Switzerland [Accessed 15.09.2019].

UNISDR (2011) Global Assessment Report on Disaster Risk Reduction: Revealing Risk, Redefining Development. United Nations International Strategy for Disaster Reduction (UNISDR). United Nations, Geneva, Switzerland [Accessed 15.09.2019].

United Nations (2015) The UN Sustainable Development Goals (website: http://www.un.org/sustainabledevelopment/summit/) United Nations, New York [Accessed 15 Jul 2018].

van Staveren, M.T. (2009) Extending to geotechnical risk management, *Georisk: Assessment and Management of Risk for Engineered Systems and Geohazards,* 3:3,174-183.

Vanneschi, C., Salvini, R., Massa, G., Riccucci, S. and Borsani, A. (2014) Geological 3D modeling for excavation activity in an underground marble quarry in the Apuan Alps (Italy). *Computers & geosciences*, *69*, 41-54.

Varouchakis, E.A. (2017) Modeling of temporal groundwater level variations based on a Kalman filter adaptation algorithm with exogenous inputs. Journal of Hydroinformatics, 19(2), 191-206.

Vatcher, J., McKinnon, S. D. and Sjöberg, J. (2016) Developing 3-D mine-scale geomechanical models in complex geological environments, as applied to the Kiirunavaara Mine. *Engineering geology*, *203*, 140-150.

Vázquez-Suñé, E., Sánchez-Vila, X. and Carrera, J. (2004) Introductory review of specific factors influencing urban groundwater, an emerging branch of hydrogeology, with reference to Barcelona, Spain. *Hydrogeology Journal*, 13(3), pp.522-533.

Velasco, V., Gogu, R., Vázquez-Suñè, E., Garriga, A., Ramos, E., Riera, J. and Alcaraz, M. (2013). The use of GIS-based 3D geological tools to improve hydrogeological models of sedimentary media in an urban environment. *Environmental earth sciences*, *68*(8), 2145-2162.

Verruijt, A., and Booker, J. R. (1996) Surface settlements due to deformation of a tunnel in an elastic half plane." *Geotechnique,* London, England, 46(4), 753-756.

Voronoi, G. (1908) Nouvelles applications des parametres continus a la theorie des formes quadratiques. Deuxieme memoire. Recherches sur les parallelloedres primitifs. *Journal fur die Reine und Angewandte Mathematik,* vol.1908, no.134, pp. 198– 287.

Vose, D. (1996) Quantitative risk analysis: a guide to Monte Carlo simulation modelling. John Wiley & Sons.

Wang, J., Zhang, S. and Teizer, J. (2015) Geotechnical and safety protective equipment planning using range point cloud data and rule checking in building information modeling. *Automation in Construction*, 49, pp.250-261.

Wang, M., Deng, Y., Won, J. and Cheng, J.C., (2019) An integrated underground utility management and decision support based on BIM and GIS. *Automation in Construction*, *107*, p.102931.

Wang, X., Lu, K., Wang, S., Huang, X. and Kang, L. (2017) Spatiotemporal assessment of rainstorm hazard risk in Qinling mountains of China. Human and Ecological Risk Assessment: An International Journal, 23(2), 257-275.

Wang, Y., Cao, Z. and Au, S.K. (2010) Efficient Monte Carlo simulation of parameter sensitivity in probabilistic slope stability analysis. Computers and Geotechnics, 37(7-8), pp.1015-1022.

Wang, Y., Cao, Z., and Li, D. (2016). Bayesian perspective on geotechnical variability and site characterization. *Engineering Geology*, *203*, 117-125.

Watson, D.F. (1981) Computing the n-dimensional Delaunay tessellation with application to Voronoi polytopes. The Computer Journal, vol.24, no.2, pp. 167–172.

Weber, C. (2003) Interaction model application for urban planning. *Landscape and Urban Planning*, *63*(1), pp.49-60.

Weidman, L., Maloney, J. M. and Rockwell, T. K. (2019). Geotechnical data synthesis for GIS-based analysis of fault zone geometry and hazard in an urban environment. *Geosphere*, *15*(6), 1999-2017.

Whitebread, K., Dick, G. and Campbell, D. (2016). *The subsurface and urban planning in the City of Glasgow*. City of Glasgow Case Report. Glasgow: Glasgow City Council and British Geological Survey, p.3.

Whitman, R.V. (2000) Organizing and evaluating uncertainty in geotechnical engineering. Journal of Geotechnical and Geoenvironmental Engineering, 126(7), pp.583-593.

Wittwer, J.W. (2005) Simulation-based design under uncertainty for compliant microelectromechanical systems.

Wongsaroj, J., Soga, K., and Mair, R. J. (2013) Tunnelling-induced consolidation settlements in London Clay. Géotechnique, 63(13), 1103-1115.

Wu, Q., Xu, H. and Zou, X. (2005) An effective method for 3D geological modeling with multi-source data integration. *Computers & Geosciences*, *31*(1), 35-43.

Wycisk, P., Hubert, T., Gossel, W., and Neumann, C. (2009) High-resolution 3D spatial modelling of complex geological structures for an environmental risk assessment of abundant mining and industrial megasites. *Computers & Geosciences* (35), pp. 165–182.

Xiaodong, T., Xueyu, R. and Yuexian, W. (2002) Mesh simplification based on super-face and genetic algorithm in reverse engineering. *The International Journal of Advanced Manufacturing Technology*, *20*(4), pp.303-312.

Xie, X., Yang, Y. and Ji, M. (2016) Analysis of ground surface settlement induced by the construction of a largXIe-diameter shield-driven tunnel in Shanghai, China. *Tunnelling and Underground Space Technology*, *51*, 120-132.

Xie, X.Y. and Xie, T.C. (2015) Research for framework of bim-based platform on facility maintenance management on the operating stage in metro station. In *Applied Mechanics and Materials* (Vol. 743, pp. 702-710). Trans Tech Publications.

Yalcin, A. and Bulut, F. (2007) Landslide susceptibility mapping using GIS and digital photogrammetric techniques: a case study from Ardesen (NE-Turkey). Nat Hazards 41, 201–226, doi:10.1007/ s11069-006-9030-0.

Yang, H., Cao, S., Wang, S., Fan, Y., Wang, S. and Chen, X. (2016) Adaptation assessment of gob-side entry retaining based on geological factors. *Engineering geology*, *209*, pp.143-151.

Yoshimatsu, H. and Abe, S. (2006) A review of landslide hazards in Japan and assessment of their susceptibility using analytical hierarchy process (AHP) method. Landslides 3, 149–158. doi:10.1007/ s10346-005-0031-y.

Youssef, A.M., Pradhan, B., Sefry, S.A. and Abdullah, M.M.A. (2015) Use of geological and geomorphological parameters in potential suitability assessment for urban planning development at Wadi Al-Asla basin, Jeddah, Kingdom of Saudi Arabia. *Arabian Journal of Geosciences*, *8*(8), pp.5617-5630.

Yu, L., Pan, Y. and Wu, Y. (2009) Research on data normalization methods in multi-attribute evaluation. In 2009 International Conference on Computational Intelligence and Software Engineering, Wuhan, China, 11-13 Dec. 2009, 1-5, IEEE, doi: 10.1109/CISE.2009.5362721.

Yun, H.-B. and Reddi, L.N. (2011). Nonparametric Monitoring for Geotechnical Structures Subject to Long-Term Environmental Change. *Advances in Civil Engineering*. Article ID 275270, doi:10.1155/2011/275270

Zhang, J., Tang, W.H., Zhang, L.M. and Huang, H.W. (2012) Characterising geotechnical model uncertainty by hybrid Markov Chain Monte Carlo simulation. Computers and Geotechnics, 43, pp.26-36.

Zhang, J., Wu, C., Wang, L., Mao, X. and Wu, Y. (2016) The Work Flow and Operational Model for Geotechnical Investigation Based on BIM. *IEEE Access*, *4*, pp.7500-7508.

Zhang, J., Wu, C., Wang, Y., Ma, Y., Wu, Y. and Mao, X. (2018). The BIM-enabled geotechnical information management of a construction project. *Computing*, *100*(1), 47-63.

Zhang, J., Zhang, L.M. and Tang, W.H. (2009) Bayesian framework for characterizing geotechnical model uncertainty. Journal of Geotechnical and Geoenvironmental Engineering, 135(7), pp.932-940.

Zhu, L. F., Li, M. J., Li, C. L., Shang, J. G., Chen, G. L., Zhang, B., and Wang, X. F. (2013). Coupled modeling between geological structure fields and property parameter fields in 3D engineering geological space. *Engineering geology*, *167*, 105-116.

Zhu, L., Zhang, C., Li, M., Pan, X., & Sun, J. (2012). Building 3D solid models of sedimentary stratigraphic systems from borehole data: An automatic method and case studies. *Engineering Geology*, *127*, 1-13.

Zou, Y., Kiviniemi, A. and Jones, S.W. (2017) A review of risk management through BIM and BIM-related technologies. *Safety science*, *97*, pp.88-98.

APPENDICES

Appendix A: Data integration (input/output) and management used throughout the research

A.1 Utilising MATLAB

MATLAB (Mathworks Inc., 2016) was employed throughout this study to provide the analysis (and the related aspects) and the set-up for the 3D modelling. The use of MATLAB was based on implementing custom-made scripts. To demonstrate its use in this research, the scripts (codes) developed are presented throughout the Appendices, with respect to the corresponding approach they were utilised for (using a stepwise approach). The corresponding comments of the scripts are written in boldface.

A.2 API and Ruby API integration

Ruby-based command lines (codes) defined the characteristics, such as the geometry and post-analysis assessment features of the integrated 3D geology-tunnel-building models, which followed the steps (pattern) of:

- extraction of the assessment resultant data;
- categorising the previous data;
- setting (generating) the model defined with this data.

This code was produced for each corresponding ‘part’ of the 3D model, in MATLAB to align with an automated approach. By way of example, the following Ruby programming language script for setting a specific 3D object was typically used in this research:

```
$group = Sketchup.active_model.entities.add_group
$group.entities.add_faces_from_mesh(mesh)
$group.material = "LightGrey"
$group.material.alpha = 0.8
```

```
$mesh = Geom::PolygonMesh.new
```

A.3 Creation of the 3D models

In this section, the MATLAB custom-made scripts used to create the 3D geology-tunnel-building models, are described in detail. In addition, MATLAB's Iso2mesh toolbox by Qianqian Fang (Fang and Boas, 2009; Mathworks Inc., 2017) was adapted to generate the mesh of the 3D models used. Geom3d toolbox (Mathworks Inc., 2017) was also adapted, to visualise (and manage) 3D geometries and their mesh in MATLAB.

A.3.1 Topography (ground surface)

To generate the ground surface mesh, an interpolation process was used (with the corresponding comment text in bold):

```
ntopo=200; The number of interpolation points in the
longitude(LONG)-direction.
mtopo=200; The number of interpolation points in the latitude(LAT)-
direction.
xmin1=floor(min(Atopo1(:,1))); where Atopo1(:,1) is the array of
ground surface (points) Ordnance Survey's (OS)LONG-coordinates.
xmax1=ceil(max(Atopo1(:,1)));
ymin1=floor(min(Atopo1(:,2))); where Atopo1(:,2) is the array of
ground surface (points) OS LAT-coordinates.
ymax1=ceil(max(Atopo1(:,2)));
F2=scatteredInterpolant(Atopo1(:,1),Atopo1(:,2), Atopo1(:,3),
'linear','nearest');
[xq,yq] = meshgrid(xmin1:(xmax1-xmin1)/ntopo:xmax1,ymin1:(ymax1-
ymin1)/mtopo:ymax1);
ztopo=F2(xq,yq);
figure;plot3(Atopo1(:,1),Atopo1(:,2),Atopo1(:,3),'*'); The 3D plot
of the ground surface.
hold on
mesh(xq,yq,ztopo); The 3D plot of ground surface mesh.
```

A.3.2 3D geology model

Each geological layer is obtained by deriving the borehole (data) logs in different depths (in m Above Ordnance Datum (mAOD). To demonstrate how the 3D geological strata were created, the following MATLAB script of an example of a 3D stratum developed, is provided for the geological layer No.3 (weathered to clay sandstone layer), as shown in Figure A.1:

```
VarName13=Atopo3(:,1); where Atopo3(:,1) is the array of layer No.3 OS LONG-coordinates as extracted from the borehole log data.

VarName14=Atopo3(:,2); where Atopo3(:,2) is the array of layer No.3 OS LAT-coordinates as extracted from the borehole log data.

VarName15=Atopo3(:,3); where Atopo3(:,1) is the array of layer No.3 altitude(ALT)(in mAOD)-coordinates along its thickness direction as extracted from the borehole log data.

Thick3=Atopo3(:,3)-Atopo4(:,3); The thickness of layer No.3.

[faces_grdl_12,
vertices_grdl_12]=surf2solid(VarName13,VarName14,VarName15,'thicknes
s',-Thick3'); The conversion of 3D surface geological object layer No.3 to a 3D volume geological solid object layer No.3.
```

A.3.3 3D tunnel model

```
p0=[404600 282900 120]; LONG – LAT – Tunnel DEPTH coordinates of the Tunnel starting point.

p1=[405000 285300 120]; LONG – LAT – Tunnel DEPTH coordinates of the Tunnel ending point.

DIAMt=10; The tunnel diameter used in this example.

[Vcyl, Fcyl] = cylinderMesh([p0 p1 0.5*DIAMt]); Creation of 3D tunnel surface object and extraction of its 3D cell vertices coordinates (Vcyl) and interconnected 3D 4-noded cell faces (Fcyl).

Tes120 = delaunayTriangulation(Vcyl(:,1),Vcyl(:,2),Vcyl(:,3));
Delaunay Triangulation of 3D cell vertices coordinates of the tunnel to 3D 3-noded cells as shown in Figure A.2.

[K200,v200] = convexHull(Tes120); Convex hull creation of the extracted 3-noded 3D cells.

vertg(:,1)=vertices_grdl_13(:,1); LONG-Coordinates of the specific geological layer which is the layer through which the tunnel is excavated.
```

`vertg(:,2)=vertices_grdl_13(:,2);` **LAT-Coordinates of the specific geological layer which is the layer through which the tunnel is excavated.**

`vertg(:,3)=vertices_grdl_13(:,3);` **ALT-Coordinates of the specific geological layer which is the layer through which the tunnel is excavated.**

`[newnode802,newface801]=surfboolean(vertg,faces_grdl_131,'diff',Tes120.Points,K200);` **Boolean difference operation to create 3D cells as a simulation of space that was previously occupied by the geological layers, along the excavation, as shown in Figures A.1a and A.3.**

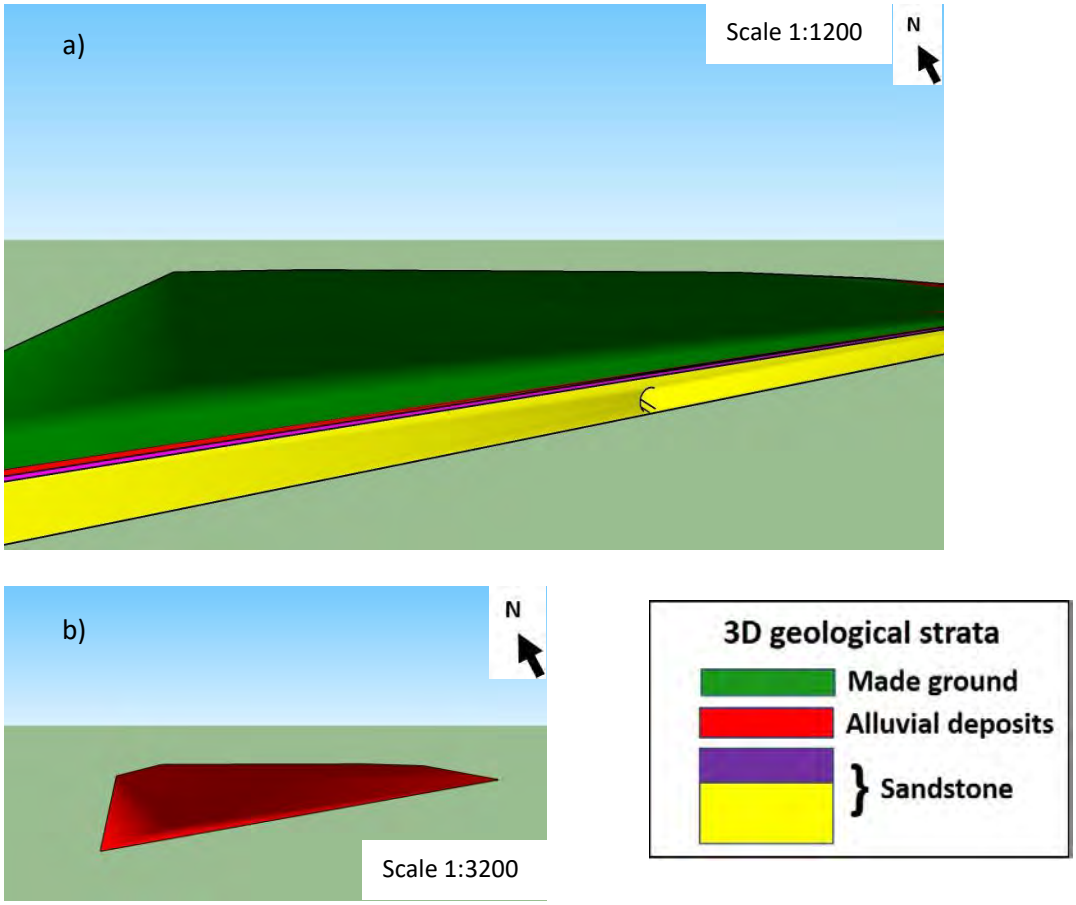

Figure A.1: A visualisation example of the (a) whole 3D geology model generated (including the tunnel) and (b) the alluvial stratum only, using BIM (SketchUp) (Chapter 4).

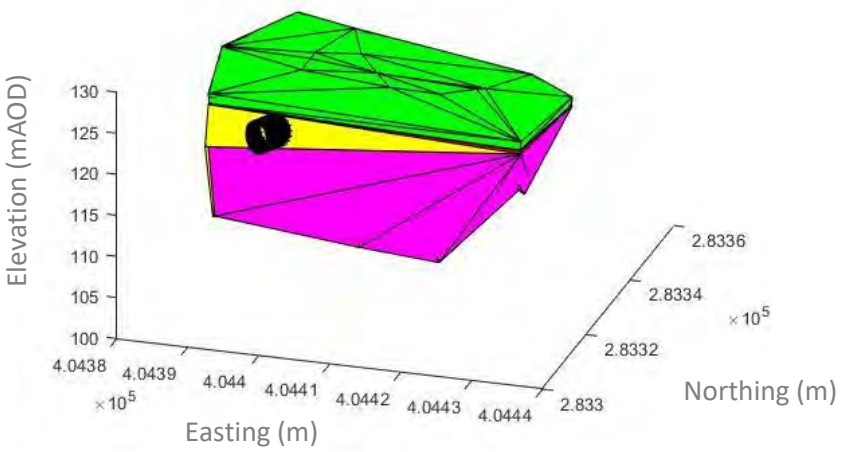

Figure A.2: An initial visualisation example using MATLAB, showing the tunnel (extracted) within the 3D geology model.

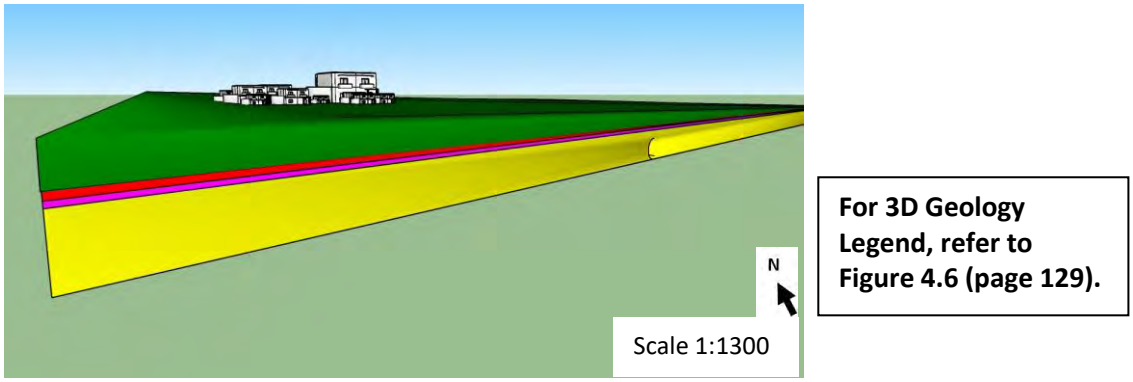

Figure A.3: A resulting visualisation of the 3D geology-tunnel-building model using BIM (SketchUp) (Chapter 4).

A.4 Integrated visualisations using geospatial tools

An integration with spatial tools has been made to provide further visualisations. This mainly utilised Google Earth (Google Inc., 2018), using its advantages for further or more detailed

integrated visualisations. Custom-made MATLAB scripts were also used. In addition, GoogleEarth toolbox by Scott L. Davis (Mathworks Inc., 2017) was adapted to provide the Google Earth integrated (3D) visualisations. The data integration that took place developed the:

- points within the study area;
- contourlines within the study area (from the present analysis), and
- locations of the borehole cylinders (and colourbars),

extracted using Keyhole Markup Language (KML) (format), which is employed for visualising data in Google Earth Pro (Google Earth, 2015). In this way, the resulting visualisations/maps using Google Earth could be generated in the current study. An initial example of the approach used, presents a satellite image integrated with the 3D geology-building model and an initial settlement risk assessment, as shown in Figure A.4. This example demonstrates the power of the current framework to provide integrated visualisations (of assessments).

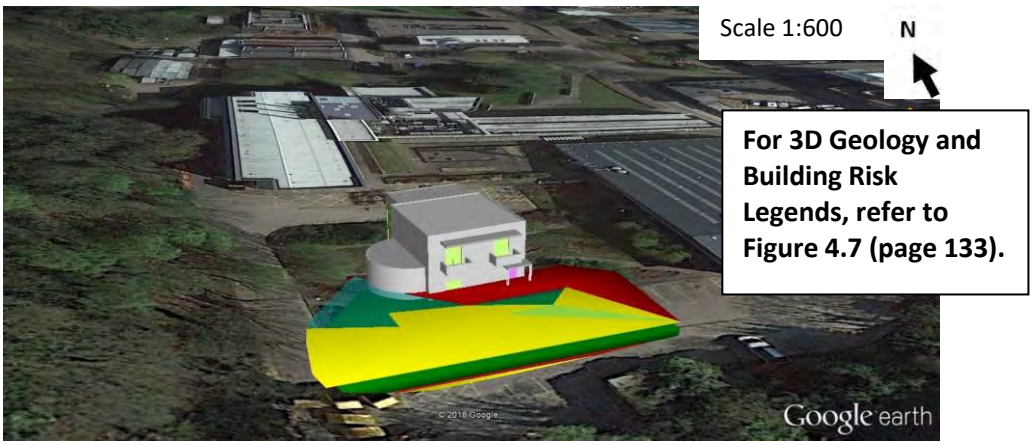

Figure A.4: An extra 3D application of a risk assessment conducted using Google Earth Pro (Google Inc., 2015) in this research.

The information taken from borehole data can be derived and simulated into the Google Earth Pro (Google Earth, 2015) environment, by using 3D long thin cylinders, adjusted to the actual latitude and longitude (spatial) locations of the boreholes. To provide the cylinders and the contourmaps within the visualisations in Google Earth Pro (Google Earth, 2015), the process starts with the indication of the actual location x1, y1 of the boreholes. An example script for the creation of a cylinder taken from the current analysis follows:

```
kmlStr11 = ge_cylinder(x1,y1,0.55,3*40, 'divisions',3, 'name','
Cylinder number 2, less divisions.','lineWidth',5.0,
'lineColor','FFFFFF00','polyColor','FFFFFF00'); where 0.55 and 3*40
are the horizontal and vertical scale factors, respectively, to
adjust the geometrical size of each cylindrical model.
```

Likewise, to locate and provide in Google Earth Pro (Google Earth, 2016) each borehole point:

```
tmp =
ge_point(Long,Latg,t*1e6,'iconURL',[iconStrBase,'/icon31.png'],'msgT
oScreen',true,'name','')
```

To provide the contourlines (along which the same value of borehole data is shown):

```
kmlStr =
ge_contour(Lon1,flipud(Lat1),flipud(Largezii),'colorMap','jet','line
Values',lineValues,
'cLimLow',cLimLow,'cLimHigh',cLimHigh,'lineWidth',3);
```

An example presenting the process described and the integration of the 3D model with Google Earth (Google Inc., 2018) is provided in Figure A.5.

Figure A.5: An integrated visualisation using Google Earth (Google Inc., 2018), showing the borehole locations (cylinders) including their logs.

A.5 Georeferencing

An example process that was used, which provided georeferenced locations of features is described through the next scripts. A georeference transformation was conducted using these scripts, by providing the BIM local x/y coordinates, the OS longitude/latitude coordinates and the STL file information (for each building), then executing series of affine transformations from one coordinate system to the other, and extracting the information to STL:

```
A=[107.013,69.188,-0; 17.529,87.207,-0; -38.504, 93.979, -0; -
41.325, -52.093, -0; -0.525, -48.146, -0]; The BIM local x/y
coordinates of 5 specific control points at the investigated site.

B=[404593.783845, 283422.14795, 0; 404487.244773, 283466.434606, 0;
404425.192069, 283468.826924, 0; 404415.396708, 283323.434586, 0;
404461.820388, 283319.693471, 0]; The OS LONG/LAT coordinates at the
same 5 (as above) specific control points at the investigated site.

[regParams,Bfit,ErrorStats]=absor(A',B','doScale','TRUE'); To find
the rotation and also the scaling and translation affine
transformation factors that best maps BIM Local coordinate system of
control point coordinates to OS LONG/LAT coordinate system.
```

```
fv = stlread('STL_test_pollaIFC_campus_refined_house_bin.stl'); To import an STL mesh for each building in the site, returning a PATCH-compatible face-vertex structure.

patch(fv1,'FaceColor',[0.8 0.8 1.0], 'EdgeColor','none', 'FaceLighting','gouraud','AmbientStrength', 0.15); Provides the patch-compatible face vertex structure for each building.

regParams.R(3,3)=1./regParams.s;
TRANS=regParams.R*regParams.s;
TRANS(:,4)=regParams.t; Computes the affine transformation matrix using the previously evaluated transformation factors that best maps the two coordinated systems.

PT = transformPoint3d(fv.vertices(:,1), fv.vertices(:,2), fv.vertices(:,3), TRANS); Estimates the actual OS LONG/LAT coordinates of all points that draw each building.

stlwrite('testres1.stl', fv.faces,PT); To save the resulting OS LONG/LAT coordinates for subsequent analysis.
```

Resulting 3D geology-tunnel-building models and risk assessments were properly located using the previous MATLAB scripts, as shown in the initial example in Figures A.3, A.4 and A.6.

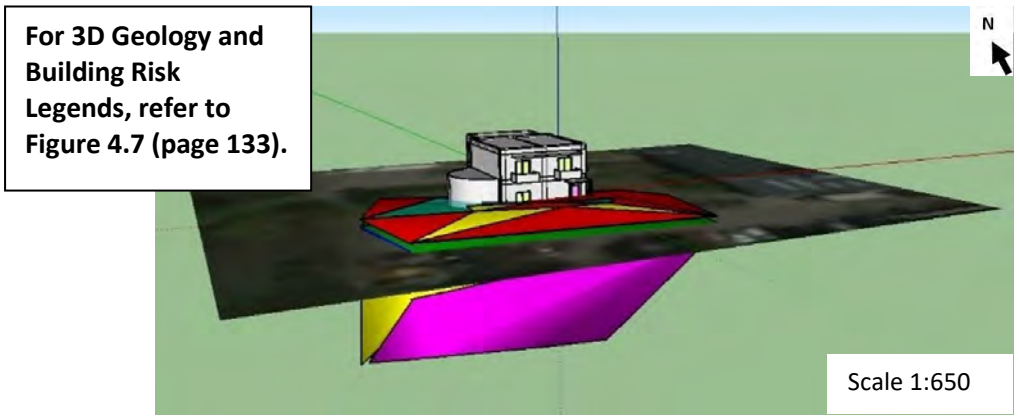

Figure A.6: An integrated visualisation including an initial settlement assessment used, which demonstrates the integration capabilities of the adopted framework using BIM (SketchUp).

Appendix B: Estimation of the tunnelling-induced settlement hazard using analytical models and BIM

B.1 3D tunnelling-induced settlement risk: Building damage assessments

By way of example, a script to present the damage assessment for a particular building, is described next. Initially, the mesh should be extracted from the STL model:

```
Tes120yyy =
delaunayTriangulation(fv.vertices(:,1),fv.vertices(:,2),fv.vertices(:,3)); Creates the Delaunay triangulations for each building model transformed to the actual OS LONG/LAT coordinate system.
C201=polyhedronCentroid(Tes120yyy.Points, Tes120yyy.convexHull);
Computes the OS LONG/LAT coordinates for the centroid of the volume of each building model.
```

Considering the actual location of each centroid of each building, the damage is investigated by two planes (which cut perpendicularly each building) for each building. The first plane is parallel to the length (longest building dimension) and passes through its centroid, while the second is perpendicular to the previous (first) plane (and extending along the width). Thus, for the first building:

```
px1 = sliceDelaunay(Tes120yyy, [1.0707 -0.1103 0], [C201(1,1) C201(1,2) C201(1,3)]); Returns the cross-section points of a plane cutting the Delaunay triangulated building model with normal [1.0707, -0.1103, 0].

px2 = sliceDelaunay(Tes120yyy, [0.1103 1.0707 0], [C201(1,1) C201(1,2) C201(1,3)]); Returns the cross-section points of a plane cutting the Delaunay triangulated building model with normal [0.1103, 1.0707, 0]. This plane is vertical to the previously defined plane with normal [1.0707, -0.1103, 0].

px3 = sliceDelaunay(Tes120yyy, [0 0 1], [C201(1,1) C201(1,2) C201(1,3)]);
```

To check the damage along px1 plane:

```
d = px1(1,:).^2 + px1(2,:).^2 + px1(3,:).^2;
[dmax, maxidx] = max(d);
```

```
[dmin, minidx] = min(d);
xmin = px1(1,minidx); ymin = px1(2,minidx); zmin = px1(3,minidx);
xmax = px1(1,maxidx); ymax = px1(2,maxidx); zmax = px1(3,maxidx);
d1 = (px1(1,:)-xmax).^2 + (px1(2,:)-ymax).^2 + (px1(3,:)-zmax).^2;
[dmax1, maxidx1] = max(d1);
[dmin1, minidx1] = min(d1);
xmin1 = px1(1,minidx1); ymin1 = px1(2,minidx1); zmin1 =
px1(3,minidx1);
xmax1 = px1(1,maxidx1); ymax1 = px1(2,maxidx1); zmax1 =
px1(3,maxidx1);
```

The results were obtained as points generated across the whole px1 plane, parameterised by a variable t. To provide more points the spacing of t was required to be reduced.

```
point1=[xmax1 ymax1 zmax1];
point2=[xmin1 ymin1 zmin1];
tseg=0:0.1:1;
Cseg=repmat(point1,length(tseg),1)'+(point2-point1)'*tseg;
dCseg = sqrt((Cseg(1,:)-Cseg(1,1)).^2 + (Cseg(2,:)-Cseg(2,1)).^2 +
(Cseg(3,:)-Cseg(3,1)).^2);
Lengthbuild=0;
for i=1:length(Cseg(1,:));
    iminus1=i-1;
    if i==1
        iminus1=1;
    end
        Lengthbuild=Lengthbuild+(dCseg(1,i)-dCseg(1,iminus1)); To
search for the longest distance between points generated across the
whole px1 plane.
    End
```

To register the OS LONG/LAT coordinates for each point of the px1 cutting plane:

```
zcentros1=Fdepth1(Cseg(1,:),Cseg(2,:));
Pcentros1(:,1)=Cseg(1,:);
Pcentros1(:,2)=Cseg(2,:);
Pcentros1(:,3)=Cseg(3,:)'+zcentros1';
```

To create a plane (planep) which contains the tunnel centreline starting from the point (p1x0) and ending to the point (p1y0), and has a third point (p1z0) located at the cross section of the vertical plane which passes through the tunnel centreline and the ground surface. DEPTHt is the altitude (in mAOD) of the tunnel centreline.

```
ztopop1=Fdepth1(405000, 285300);
p1x0=[404400, 282900, DEPTHt];
p1y0=[405000, 285300, DEPTHt];
p1z0=[405000, 285300, ztopop1];
planep=createPlane(p1x0, p1y0, p1z0);
```

For each point located in the previously defined plane px1 of each building, its distance to the plane (planep) is estimated (which is the distance to the tunnel centreline). Thus, by applying this distance within closed-form equations for estimating ground settlements (Equations (4.5) and (4.6)), these ground movements can be provided for every point on a plane px1:

```
POINTP1P=projPointOnPlane(Pcentros1,planep);The altitude in mAOD of
surface points.
DISTP1P=(distancePoints3d(Pcentros1,POINTP1P));
DIAM=DIAMt;
```

The closed-form Equation (4.5) was used to estimate the ground (surface) settlements:

```
SURF200P=Fdepth1(POINTP1P(:,1),POINTP1P(:,2))-DEPTHt; To provide the
depth H of tunnel axis from ground surface.
SURFC0P=VL*0.5*DIAM*0.5*DIAM*(4*SURF200P.*(1-pois));
SURFC2P=(1./(SURF200P.^2+DISTP1P.^2));
SURFC02P=SURFC0P.*SURFC2P;
SURFC03P=1./(SURF200P.*cot(45+0.5*phiB)+0.5*DIAM).^2;
SURFC1P=exp(-1.38*SURFC03P.*DISTP1P.^2);
SURFC01P=SURFC02P.*SURFC1P; To estimate the ground surface
settlements.
```

In addition, the closed-form Equation (4.6) was employed to estimate the horizontal ground movement (Δ_h) (on the ground surface), and is described as:

```
SURFC0PZ=-VL*0.5*DIAM*0.5*DIAM*(1+(3-4*pois)).*DISTP1P;
SURFC2PZ=(1./(SURF200P.^2+DISTP1P.^2));
SURFC02PZ=SURFC0PZ.*SURFC2PZ;
SURFC03PZ=1./(SURF200P.*cot(45+0.5*phiB)+0.5*DIAM).^2;
SURFC1P=exp(-1.38*SURFC03PZ.*DISTP1P.^2);
SURFC01PZ=SURFC02PZ.*SURFC1P; To provide the horizontal ground
movement.
DIFF_HOR=abs(SURFC01PZ(1)-SURFC01PZ(length(Cseg))); To estimate the
relative settlement at different spans between the points of the
cutting plane px1.
```

Then, to search for the location of inflection point across the settlement curve of px1 cutting plane and compute the length of hogging and sagging zone at cutting plane px1:

```
ysetl=-SURFC01P(:,1)';
xx=log10(dCseg(1,:));
df1=gradient(ysetl,xx);
df2=gradient(df1,xx);
id=sign(df2);
idx=strfind(id,[-1 1]);
inflexionP=xx(idx+1); To find the inflection point.
LengthHog=0;
LengthSag=0;
setlhog=0;
setlsag=0;
for i=1:length(Cseg(1,:));
    iminus1=i-1;
    if i==1
        iminus1=1;
    end
    if id(i) <= 0
        LengthHog=LengthHog+(dCseg(1,i)-dCseg(1,iminus1));
        setlhog(i)=SURFC01P(i,1);To obtain the hogging zone length.
    else
        LengthSag=LengthSag+(dCseg(1,i)-dCseg(1,iminus1));
        setlsag(i)=SURFC01P(i,1);To find the length of sagging zone.
    end
```

```
end
```

Then, the estimation of the maximum bending strain (strbH), diagonal strain (diagstrH), horizontal strain (horstrH), the total bending strain (strbsH) and critical strain (strcritH) for the hogging zone below each building follows:

```
Height=max(px1(3,:)); The height of the building used.

pois=(Emod-2)/2; The Poisson's ratio.

MOM=Height^3/3; The section moment of area of the equivalent beam
height of the building at the hogging zone.

TAU=Height; The furthest distance from the neutral axis to the edge
of the equivalent beam for the hogging zone.

strbH=((max(setlhog)-
min(setlhog))/LengthHog)/(LengthHog/(12*TAU)+...

    (3*MOM*Emod/(2*TAU*LengthHog*Height))); To provide the max
bending strain at the hogging zone.

diagstrH=((max(setlhog)-
min(setlhog))/LengthHog)/((Height*LengthHog*LengthHog)/(18*MOM*Emod)
+1); To provide the diagonal strain at the hogging part.

horstrH=DIFF_HOR/(LengthHog+LengthSag); To provide the horizontal
strain at the hogging part, taking into account the maximum of
relative settlements under each building across the plane px1.

strbsH=strbH+horstrH; To provide the total bending strain at the
hogging part.

strdsH=horstrH*(1-pois)*0.5+sqrt(horstrH*horstrH*0.5*(1-
pois)*0.5*(1-pois)+diagstrH*diagstrH); To provide the total diagonal
strain at the hogging part.

strcritH=max(strbsH,strdsH); To provide the critical strain at the
hogging part.
```

In addition, the maximum bending strain (strbS), the diagonal strain (diagstrS), horizontal strain (horstrS), the total bending strain (strbsS) and the critical strain (strcritS) for the sagging zone below each building are estimated by:

```
MOM=Height^3/12; The section moment of area of the equivalent beam
height of the building at the sagging zone

TAU=Height/2; The longest distance from the neutral axis to the edge
of the equivalent beam for the sagging zone.

strbS=((max(setlsag)-
min(setlsag))/LengthSag)/(LengthSag/(12*TAU)+...
```

```
    (3*MOM*Emod/(2*TAU*LengthSag*Height))); To estimate the maximum
bending strain at the sagging zone.

diagstrS=((max(setlsag)-
min(setlsag))/LengthSag)/((Height*LengthSag*LengthSag)/(18*MOM*Emod)
+1); To estimate the diagonal strain at the sagging part.

end

horstrS=DIFF_HOR/(LengthHog+LengthSag); To estimate the horizontal
strain at the sagging part considering the maximum of relative
settlements under each building across the plane px1.

strbsS=strbS+horstrS; To provide the total bending strain at the
sagging part.

strdsS=horstrS*(1-pois)*0.5+sqrt(horstrS*horstrS*0.5*(1-
pois)*0.5*(1-pois)+diagstrS*diagstrS); To provide the total diagonal
strain at the sagging part.

strcritS=max(strbsS,strdsS); To provide the critical strain at the
sagging part.
```

The estimated maximum critical strains for the hogging and sagging zone are correlated with the appropriate damage criterion, using Table 4.5 (Burland, 1995; Mair et al., 1996):

```
    if max(strcritH,strcritS) < 0.0005; To indicate if maximum
tensile strain is less than 0.05% damage category exists.

    hold on;
plotmesh(fv01.vertices,fv01.faces,'FaceAlpha',0.3,'FaceColor','b');
To colour the building in blue if max tensile strain <0.05%.

    end

    if max(strcritH, strcritS) >=0.0005 && max(strcritH, strcritS) <
0.00075; To indicate if maximum tensile strain is less than 0.075%
and greater than 0.05% damage category exists.

    hold on;
plotmesh(fv01.vertices,fv01.faces,'FaceAlpha',0.3,'FaceColor','c');
To colour the building cyan if max tensile strain <0.075% or >0.05%

    end

    if max(strcritH, strcritS) >=0.00075 && max(strcritH, strcritS)
< 0.0015; To indicate if maximum tensile strain is less than 0.15%
and greater than 0.0075% damage category exists.

    hold on;
plotmesh(fv01.vertices,fv01.faces,'FaceAlpha',0.3,'FaceColor','m');
Colour of the building in magenta if max tensile strain <0.15% or
>0.0075%

    end
```

```
    if max(strcritH, strcritS) >=0.0015 && max(strcritH, strcritS) <
0.003; Indicates if maximum tensile strain less than 0.3% and
greater than 0.15% damage category exists.

    hold on;
plotmesh(fv01.vertices,fv01.faces,'FaceAlpha',0.3,'FaceColor','y');
Colours the building yellow if max tensile strain <0.3% or >0.15%

    end

    if max(strcritH, strcritS) >=0.003; To indicate if maximum
tensile strain is greater than 0.15% damage category exists.

    hold on;
plotmesh(fv01.vertices,fv01.faces,'FaceAlpha',0.3,'FaceColor','r');
To colour the building red if maximum tensile strain >0.3%.

    end
```

The same process is done for the plane px2. Finally, using the previous MATLAB codes the 3D visualisations could then be provided, as shown in sections B.1.1 and B.1.2.

B.1.1 Phase 1 Building Damage Assessment visualisations

Further visualisations showing a wider view of the (Phase 1) damage extent are provided in Figures B.1, B2 and B.3.

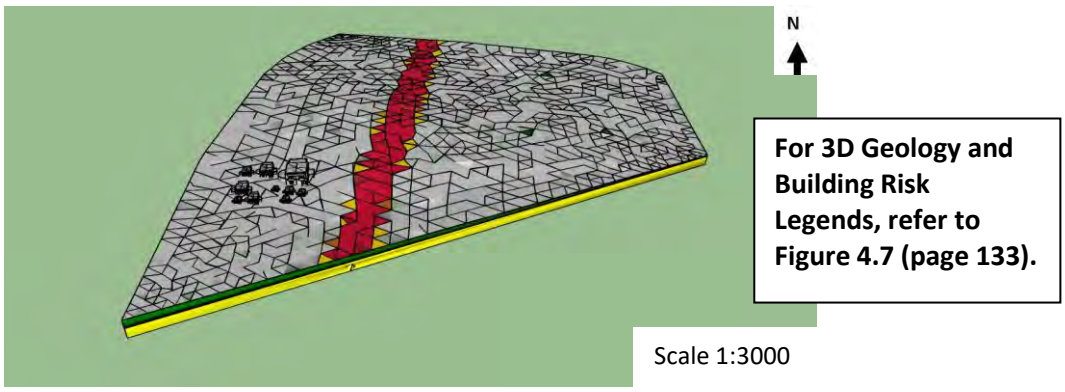

Figure B.1: Settlement risk assessment for a tunnel 30m away (Providakis et al., 2019).

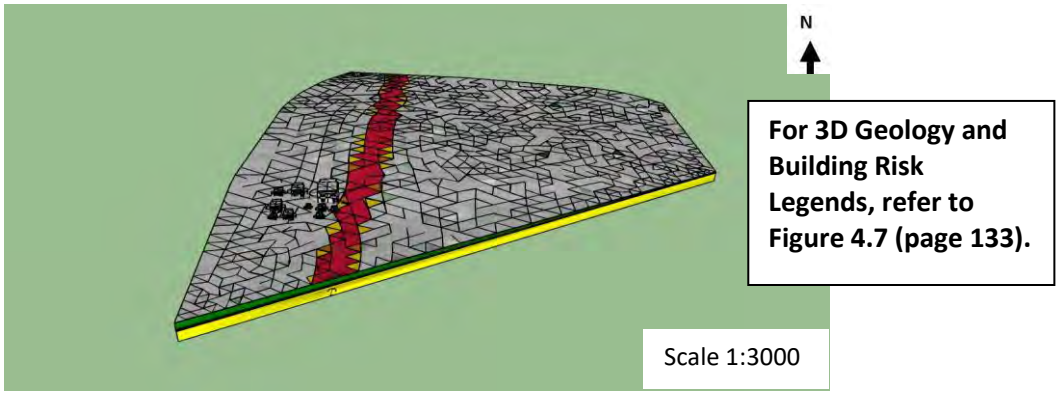

Figure B.2: Settlement risk assessment for a tunnel 10m away (Providakis et al., 2019).

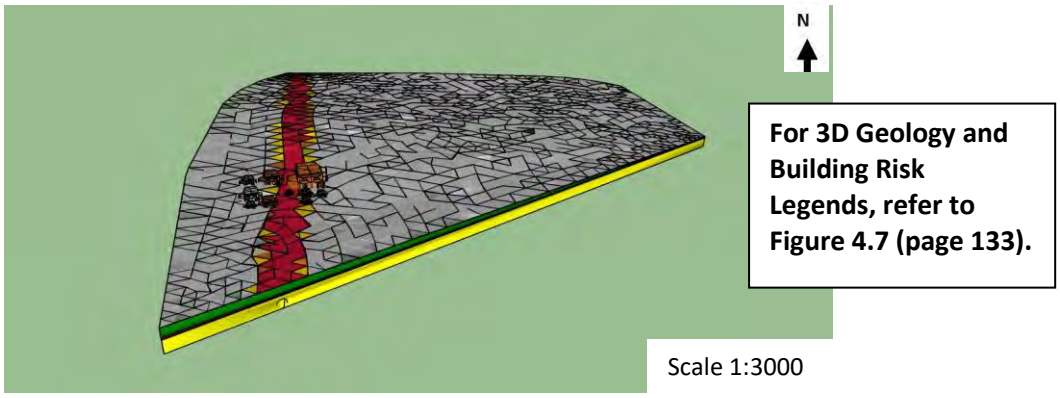

Figure B.3: Settlement risk assessment for a tunnel below the building block (Providakis et al., 2019).

B.1.2 Phase 2 Building Damage Assessment visualisations

Results were demonstrated in Figures 4.13 to 4.16 in Chapter 4.

Appendix C: Estimation of the tunnelling-induced settlement vulnerability using a 3D spatiotemporal analysis and BIM

C.1 Spatial analysis using the Analytical Hierarchy Process (AHP)

Initially, the settlement vulnerability factors are extracted in the MATLAB analysis. These are given an appropriate corresponding range, as shown in Table 5.1. An algorithm to test each one of them was produced. Table 5.1 also shows the weights of the vulnerability factors used. Then the Settlement Vulnerability Index could be obtained by Equation (5.9), using the values adopted from the previous script. Then the Building Damage Assessments could be conducted similarly to the previous Chapter 4, using the analytical methods in combination with the Damage extent and severity. Details of the previous steps of the MATLAB analysis follow.

C.1.1 Estimation of the risk ranges/ratings of the settlement vulnerability factors (AHP) and the Settlement Vulnerability Index

The settlement vulnerability factors taken from each borehole measurements (logs) are estimated in a predefined grid of points distributed in the investigated area, as in the following scripts using MATLAB:

```
for i=1:length(Atopo1(:,1))
    iop=iop+1;
```

To set the risk ranges and ratings of the undrained shear strength factor (newE111) by:

```
    if( newE111(iop) <=50 )
        P111(iop)=3;
    end
    if( newE111(iop) <=100 && newE111(iop) > 50 )
        P111(iop)=2;
    end
    if( newE111(iop) <=150 && newE111(iop) > 100 )
        P111(iop)=1;
    end
```

```
if( newE111(iop) > 150 )
    P111(iop)=0;
end
```

To set the risk ranges and ratings of the soil density factor (newE222):

```
if( newE222(iop) <=1800 )
    P222(iop)=3;
end
if( newE222(iop) <=2000 && newE222(iop) > 1800 )
    P222(iop)=2;
end
if( newE222(iop) <=2100 && newE222(iop) > 2000 )
    P222(iop)=1;
end
if( newE222(iop) > 2100 )
    P222(iop)=0;
End
```

To set the risk ranges and ratings of the unit weight factor (newE333):

```
if( newE333(iop) <=18 )
    P333(iop)=3;
end
if( newE333(iop) <=20 && newE333(iop) > 18 )
    P333(iop)=2;
end
if( newE333(iop) <=24 && newE333(iop) > 20 )
    P333(iop)=1;
end
if( newE333(iop) > 24 )
    P333(iop)=0;
End
```

To set the risk ranges and ratings of groundwater table fluctuation (ratio) factor (newE444):

```
if( newE444(iop) <0 )
    P444(iop)=0;
end
if( newE444(iop) < 1 && newE444(iop) >= 0 )
    P444(iop)=2;
end
if( newE444(iop) < 5 && newE444(iop) >= 1 )
    P444(iop)=4;
end
if( newE444(iop) < 10 && newE444(iop) >= 5 )
    P444(iop)=6;
end
if( newE444(iop) < 20 && newE444(iop) >= 10 )
    P444(iop)=8;
end
```

```
    if( newE444(iop) > 20 )
        P444(iop)=10;
    End
```

To set the risk ranges and ratings of the Young's modulus factor (newE555):

```
    if( newE555(iop) <=10 )
        P555(iop)=3;
    end
    if( newE555(iop) <=100 && newE555(iop) > 10 )
        P555(iop)=2;
    end
    if( newE555(iop) <=200 && newE555(iop) > 100 )
        P555(iop)=1;
    end
    if( newE555(iop) > 200 )
        P555(iop)=0;
    End
```

To set the risk ranges and ratings of the hydraulic conductivity factor (newE777):

```
    if( newE777(i) <=10e-8 )
        P777a(i)=0;
    end
    if( newE777(i) <=1e-4 && newE777(i) > 10e-8 )
        P777a(i)=1;
    end
    if( newE777(i) <=10e-2 && newE777(i) > 1e-4 )
        P777a(iop)=2;
    end
    if( newE777(i) > 10e-2 )
        P777a(iop)=3;
    End
```

Then, to use a normalisation process for (between) these settlement vulnerability factors:

```
for ikl=1:length(Atopo1(:,1))
    iop1=iop1+1;
VIA1(iop1)=P111(iop1)/3;
VIA2(iop1)=P222(iop1)/3;
VIA3(iop1)=P333(iop1)/3;
VIA4(iop1)=P444(iop1)/10;
VIA5(iop1)=P555(iop1)/3;
VIA7(iop1)=P777a(iop1)/3;
end
```

To provide the Damage Severity Index of the buildings and set their ranges as a function of critical strain, which is extracted for each building from the LTSM approach:

```
    if max(strcritH,strcritS) < 0.0005
    B11(1)=0.01;
    end
    if max(strcritH, strcritS) >=0.0005 && max(strcritH, strcritS) <
0.00075
    B11(1)=1;
    end
    if max(strcritH, strcritS) >=0.00075 && max(strcritH, strcritS)
< 0.0015
    B11(1)=2;
    end
    if max(strcritH, strcritS) >=0.0015 && max(strcritH, strcritS) <
0.003
    B11(1)=3;
    end
    if max(strcritH, strcritS) >=0.003
    B11(1)=4;
    End
```

To implement a normalisation process for the Damage Severity Index:

```
    iop=0;
for i=1:length(B11)
    iop=iop+1;
    VIB(iop)=B11(iop)/4;
end
```

To use interpolation for each settlement (geotechnical) vulnerability factor, to provide their values at the specified borehole locations:

```
FVIA1=scatteredInterpolant(Atopo1(:,1),Atopo1(:,2),VIA1',
'linear','nearest');
```

Then, to use interpolation for each building's Damage Severity Index to provide their values at the borehole locations:

```
FVIB=scatteredInterpolant(AtopoB(:,1),AtopoB(:,2),VIB', 'linear',
'nearest');
```

To set a predefined grid of points to provide the Settlement Vulnerability Index, considering both settlement vulnerability factors and the Damage Severity Index of the buildings:

```
    mtopo=50;
    ntopo=50;
```

```
      xmin1A=floor(min(Atopo1(:,1)));
      xmin1B=floor(min(AtopoB(:,1)));
      xmin1=min(xmin1A,xmin1B);
% xmax1=4.05e5;
      xmax1A=ceil(max(Atopo1(:,1)));
      xmax1B=ceil(max(AtopoB(:,1)));
      xmax1=max(xmax1A,xmax1B);
      ymin1A=floor(min(Atopo1(:,2)));
      ymin1B=floor(min(AtopoB(:,2)));
      ymin1=min(ymin1A,ymin1B);
% ymax1=2.84e5;
      ymax1A=ceil(max(Atopo1(:,2)));
      ymax1B=ceil(max(AtopoB(:,2)));
      ymax1=max(ymax1A,ymax1B);
      [xval,yval] = meshgrid(xmin1:(xmax1-
xmin1)/ntopo:xmax1,ymin1:(ymax1-ymin1)/mtopo:ymax1);
      xval1=xmin1:(xmax1-xmin1)/ntopo:xmax1;
      yval1=ymin1:(ymax1-ymin1)/ntopo:ymax1;
```

For each point of the predefined grid, a kriging (interpolation) approach is adopted to evaluate the distribution of each settlement vulnerability factor in the investigated area. The evaluation of undrained shear strength factor (here as Zhat1) is adopted as follows:

```
    x=Atopo1(:,1);
    y=Atopo1(:,2);
    z=VIA1';
    v = variogram([x y],z,'plotit',false);
    [dum,dum,dum,vstruct1] =
variogramfit(v.distance,v.val,[],[],[],'model','stable','plotit',fal
se);
    [Zhat1,Zvar1] = kriging(vstruct1,x,y,z,xval,yval);
```

The same method is adopted for the rest of the settlement vulnerability factors. Hence, to provide the (distribution of the) Damage Extent Index within the area investigated:

```
szset=size(settl1103);
iko1=0;
for iko=1:szset
    iko1=iko1+1;
    if( settl1103(iko1,1) <=0.01 && settl1103(iko1,1) >= 0 )
        Psz(iko1)=0;
    end
    if( settl1103(iko1,1) <=0.05 && settl1103(iko1,1) > 0.01 )
        Psz(iko1)=1;
    end
    if( settl1103(iko1,1) <=0.075 && settl1103(iko,1) > 0.05 )
```

```
        Psz(iko1)=2;
    end
    if( settl1103(iko1,1) <=100 && settl1103(iko1,1) > 0.075 )
        Psz(iko1)=3;
    End
```

To implement a normalisation process for the Damage Extent Index (as a factor):

```
    VIA1103m(iko1)=Psz(iko1)/3;
End
```

For every point of the predefined grid, a kriging approach is adopted to provide the (distribution of the) Damage Extent Index as an impact factor (here as Zhat99) causing ground settlements in the study area. This is carried out using the following lines:

```
    zm=VIA1103m';
    v103m = variogram([centros103(:,1)
centros103(:,2)],zm,'plotit',false);
    [dum,dum,dum,vstruct1103m] =
variogramfit(v103m.distance,v103m.val,[],[],[],'model','stable','plo
tit',false);
    [Zhat99,Zvar99] =
kriging(vstruct1103m,centros103(:,1),centros103(:,2),zm,xval,yval);
```

For every point of the predefined grid, the Settlement Vulnerability Index (ZhatAll) is obtained by the sum of the weighted effects of each settlement vulnerability factors in the study area – here to provide the settlement distributions, the building Damage Extent Index (acting as a factor) was multiplied by the Settlement Vulnerability Index, as described in the following:

```
for iok=1:mtopo+1
    for jok=1:ntopo+1
ZhatAll(iok,jok)=(24.49*(Zhat1(iok,jok)-newZhat1min)/(newZhat1max-
newZhat1min)+...
    13.2*(Zhat2(iok,jok)-newZhat2min)/(newZhat2max-newZhat2min)+...
    8.2*(Zhat3(iok,jok)-newZhat3min)/(newZhat3max-newZhat3min)+...
    24.5*(Zhat4(iok,jok)-newZhat4min)/(newZhat4max-newZhat4min)+...
    24.5*(Zhat5(iok,jok)-newZhat5min)/(newZhat5max-newZhat5min)+...
    5.2*(Zhat7(iok,jok)-newZhat7min)/(newZhat7max-newZhat7min))*...
    (Zhat99(iok,jok)-newZhat99min)/(newZhat99max-newZhat99min);
    end
end
close all;
delete(findall(0));
end
```

C.2 Temporal analysis using ARX

The temporal analysis of the tunnel-induced settlement is based on using the System Identification process (using MATLAB) with an output analysis of groundwater table level time-variation using the ARX modelling (using MATLAB). Initially, the OS coordinates (LONG/LAT/ALT) of 16 borehole (well) locations are imported from spreadsheet (data) files:

```
 [Atopo1w_old(:,1),Atopo1w_old(:,2),Atopo1w_old(:,3)] =
importfile7('wde_16topo_and_9wells_bham_LatLonmeters_OS_2_startingva
lues_geosmooth.xlsx','path_over_landf',2,17);
F2topow=scatteredInterpolant(Atopo1(:,1),Atopo1(:,2),Atopo1(:,3));
Atopo1w_new(:,3)=F2topow(Atopo1w_old(:,1),Atopo1w_old(:,2));
Atopo1w_new(:,2)=Atopo1w_old(:,2);
Atopo1w_new(:,1)=Atopo1w_old(:,1);
```

The time-history of the depths of the groundwater head are imported using a spreadsheet file with 2 columns. The first column is the monitoring time-step, and the second is the groundwater head value monitored at this specific time for each of the 16 borehole (well) locations:

```
GWmat1 = importfile('GW_WS_R03_t.xlsx','Sheet1','A2:B36');
GWmat2 = importfile('GW_WS_R04_t.xlsx','Sheet1','A2:B36');
GWmat3 = importfile('GW_BHR_100_t.xlsx','Sheet1','A2:B36');
GWmat4 = importfile('GW_BHR_101_t.xlsx','Sheet1','A2:B36');
GWmat5 = importfile('GW_BHR_102_t.xlsx','Sheet1','A2:B36');
GWmat6 = importfile('GW_BHR_103_t.xlsx','Sheet1','A2:B36');
GWmat7 = importfile('GW_BHR_104_t.xlsx','Sheet1','A2:B36');
GWmat8 = importfile('GW_BHR_105_t.xlsx','Sheet1','A2:B36');
GWmat9 = importfile('GW_BHR_106_t.xlsx','Sheet1','A2:B36');
GWmat10 = importfile('GW_WS_01_t.xlsx','Sheet1','A2:B36');
GWmat11 = importfile('GW_WS_02_t.xlsx','Sheet1','A2:B36');
GWmat12 = importfile('GW_OP_01_t.xlsx','Sheet1','A2:B36');
GWmat13 = importfile('GW_OP_02_t.xlsx','Sheet1','A2:B36');
GWmat14 = importfile('GW_TP_01_t.xlsx','Sheet1','A2:B36');
GWmat15 = importfile('GW_TP_02_t.xlsx','Sheet1','A2:B36');
GWmat16 = importfile('GW_TP_03_t.xlsx','Sheet1','A2:B36');
```

A fitting process was then applied between the discrete monitoring time-steps, to generate continuous time series of data for each of the 16 borehole (well) locations:

```
GWafx1=createFit(GWmat1(:,1),GWmat1(:,2));
GWafx2=createFit(GWmat2(:,1),GWmat2(:,2));
GWafx3=createFit(GWmat3(:,1),GWmat3(:,2));
GWafx4=createFit(GWmat4(:,1),GWmat4(:,2));
```

```
GWafx5=createFit(GWmat5(:,1),GWmat5(:,2));
GWafx6=createFit(GWmat6(:,1),GWmat6(:,2));
GWafx7=createFit(GWmat7(:,1),GWmat7(:,2));
GWafx8=createFit(GWmat8(:,1),GWmat8(:,2));
GWafx9=createFit(GWmat9(:,1),GWmat9(:,2));
GWafx10=createFit(GWmat10(:,1),GWmat10(:,2));
GWafx11=createFit(GWmat11(:,1),GWmat11(:,2));
GWafx12=createFit(GWmat12(:,1),GWmat12(:,2));
GWafx13=createFit(GWmat13(:,1),GWmat13(:,2));
GWafx14=createFit(GWmat14(:,1),GWmat14(:,2));
GWafx15=createFit(GWmat15(:,1),GWmat15(:,2));
GWafx16=createFit(GWmat16(:,1),GWmat16(:,2));
```

To provide a time window for estimating the time variation of groundwater level depth, using the previously produced fitting curve, i.e. between 23-April-2017 and 02-February-2019:

```
Datestring1 = '23-April-2017 10:00:00';
Datestring2 = '02-February-2019 10:00:00';
formatIn = 'dd-mmm-yyyy';
datenumber1=datenum(Datestring1,formatIn);
datenumber2=datenum(Datestring2,formatIn);
Askdate=[datenumber1:0.5:datenumber2];
```

To evaluate the time-history of the groundwater level depths (e.g. GRDL1) at the time window used:

```
GRDL1=feval(GWafx1,Askdate);
GRDL2=feval(GWafx2,Askdate);
GRDL3=feval(GWafx3,Askdate);
GRDL4=feval(GWafx4,Askdate);
GRDL5=feval(GWafx5,Askdate);
GRDL6=feval(GWafx6,Askdate);
GRDL7=feval(GWafx7,Askdate);
GRDL8=feval(GWafx8,Askdate);
GRDL9=feval(GWafx9,Askdate);
GRDL10=feval(GWafx10,Askdate);
GRDL11=feval(GWafx11,Askdate);
GRDL12=feval(GWafx12,Askdate);
GRDL13=feval(GWafx13,Askdate);
GRDL14=feval(GWafx14,Askdate);
GRDL15=feval(GWafx15,Askdate);
GRDL16=feval(GWafx16,Askdate);
```

To create the ARX models, GWMeasuredData1 to GWMeasureddata16 was used as the object data produced for the values of groundwater head arrays, using the following:

```
GWMeasuredData1 = iddata(GRDL1, [], 0.5, 'Tstart', datenumber1);
GWMeasuredData2 = iddata(GRDL2, [], 0.5, 'Tstart', datenumber1);
GWMeasuredData3 = iddata(GRDL3, [], 0.5, 'Tstart', datenumber1);
```

```
GWMeasuredData4 = iddata(GRDL4, [], 0.5, 'Tstart', datenumber1);
GWMeasuredData5 = iddata(GRDL5, [], 0.5, 'Tstart', datenumber1);
GWMeasuredData6 = iddata(GRDL6, [], 0.5, 'Tstart', datenumber1);
GWMeasuredData7 = iddata(GRDL7, [], 0.5, 'Tstart', datenumber1);
GWMeasuredData8 = iddata(GRDL8, [], 0.5, 'Tstart', datenumber1);
GWMeasuredData9 = iddata(GRDL9, [], 0.5, 'Tstart', datenumber1);
GWMeasuredData10 = iddata(GRDL10, [], 0.5, 'Tstart', datenumber1);
GWMeasuredData11 = iddata(GRDL11, [], 0.5, 'Tstart', datenumber1);
GWMeasuredData12 = iddata(GRDL12, [], 0.5, 'Tstart', datenumber1);
GWMeasuredData13 = iddata(GRDL13, [], 0.5, 'Tstart', datenumber1);
GWMeasuredData14 = iddata(GRDL14, [], 0.5, 'Tstart', datenumber1);
GWMeasuredData15 = iddata(GRDL15, [], 0.5, 'Tstart', datenumber1);
GWMeasuredData16 = iddata(GRDL16, [], 0.5, 'Tstart', datenumber1);
```

To estimate the time (date) sampling instants (GWt1) according to the time windows used:

```
GWt1 = GWMeasuredData1.SamplingInstants;
```

Then, to apply the ARX modelling:

```
GWm1=arx(GWMeasuredData1,[5], 'InitialState', 'Estimate');
GWm2=arx(GWMeasuredData2,[5], 'InitialState', 'Estimate');
GWm3=arx(GWMeasuredData3,[5], 'InitialState', 'Estimate');
GWm4=arx(GWMeasuredData4,[5], 'InitialState', 'Estimate');
GWm5=arx(GWMeasuredData5,[5], 'InitialState', 'Estimate');
GWm6=arx(GWMeasuredData6,[5], 'InitialState', 'Estimate');
GWm7=arx(GWMeasuredData7,[5], 'InitialState', 'Estimate');
GWm8=arx(GWMeasuredData8,[5], 'InitialState', 'Estimate');
GWm9=arx(GWMeasuredData9,[5], 'InitialState', 'Estimate');
GWm10=arx(GWMeasuredData10,[5], 'InitialState', 'Estimate');
GWm11=arx(GWMeasuredData11,[5], 'InitialState', 'Estimate');
GWm12=arx(GWMeasuredData12,[5], 'InitialState', 'Estimate');
GWm13=arx(GWMeasuredData13,[5], 'InitialState', 'Estimate');
GWm14=arx(GWMeasuredData14,[5], 'InitialState', 'Estimate');
GWm15=arx(GWMeasuredData15,[5], 'InitialState', 'Estimate');
GWm16=arx(GWMeasuredData16,[5], 'InitialState', 'Estimate');
```

To predict the groundwater level time-history for the specified time window steps:

```
GWyF1 = predict(GWm1, GWMeasuredData1, Horizon);
GWyF2 = predict(GWm2, GWMeasuredData2, Horizon);
GWyF3 = predict(GWm3, GWMeasuredData3, Horizon);
GWyF4 = predict(GWm4, GWMeasuredData4, Horizon);
GWyF5 = predict(GWm5, GWMeasuredData5, Horizon);
GWyF6 = predict(GWm6, GWMeasuredData6, Horizon);
GWyF7 = predict(GWm7, GWMeasuredData7, Horizon);
GWyF8 = predict(GWm8, GWMeasuredData8, Horizon);
GWyF9 = predict(GWm9, GWMeasuredData9, Horizon);
GWyF10 = predict(GWm10, GWMeasuredData10, Horizon);
GWyF11 = predict(GWm11, GWMeasuredData11, Horizon);
GWyF12 = predict(GWm12, GWMeasuredData12, Horizon);
GWyF13 = predict(GWm13, GWMeasuredData13, Horizon);
GWyF14 = predict(GWm14, GWMeasuredData14, Horizon);
```

```
GWyF15 = predict(GWm15, GWMeasuredData15, Horizon);
GWyF16 = predict(GWm16, GWMeasuredData16, Horizon);
```

To extract the groundwater (GW) head level time response at 16 predefined borehole (well) locations as an output vector of the predicted values:

```
GWyFData1 = GWyF1.OutputData;      % extracts GW head response of
monitoring well number 1
GWyFData2 = GWyF2.OutputData;      % extracts GW head response of
monitoring well number 2
GWyFData3 = GWyF3.OutputData;      % extracts GW head response of
monitoring well number 3
GWyFData4 = GWyF4.OutputData;      % extracts GW head response of
monitoring well number 4
GWyFData5 = GWyF5.OutputData;      % extracts GW head response of
monitoring well number 5
GWyFData6 = GWyF6.OutputData;      % extracts GW head response of
monitoring well number 6
GWyFData7 = GWyF7.OutputData;      % extracts GW head response of
monitoring well number 7
GWyFData8 = GWyF8.OutputData;      % extracts GW head response of
monitoring well number 8
GWyFData9 = GWyF9.OutputData;      % extracts GW head response of
monitoring well number 9
GWyFData10 = GWyF10.OutputData;      % extracts GW head response of
monitoring well number 10
GWyFData11 = GWyF11.OutputData;      % extracts GW head response of
monitoring well number 11
GWyFData12 = GWyF12.OutputData;      % extracts GW head response of
monitoring well number 12
GWyFData13 = GWyF13.OutputData;      % extracts GW head response of
monitoring well number 13
GWyFData14 = GWyF14.OutputData;      % extracts GW head response of
monitoring well number 14
GWyFData15 = GWyF15.OutputData;      % extracts GW head response of
monitoring well number 15
GWyFData16 = GWyF16.OutputData;      % extracts GW head response of
monitoring well number 16
```

To provide the groundwater table level response of for example the WS-R03 well over the time window steps of the predefined data (example Figure C.1a):

```
plot(GWt1, GWyFData1, 'r.-')
title('Predicted GW response for WS-R03 monitoring well over a
data's time span')
```

The following lines provided the groundwater table contourmap (of the groundwater head data), and it also called the function gridfit to model the scattered data with a smooth surface of the form z=f(x,y):

```
n=200; m=200; % n+1 and m+1 nodes of the x and y grid respectively.

 [Atopo1w_old(:,1),Atopo1w_old(:,2),Atopo1w_old(:,3)] =
importfile7('wde_16topo_and_9wells_bham_LatLonmeters_OS_2_startingva
lues_geosmooth.xlsx','path_over_landf',2,17);
F2topow=scatteredInterpolant(Atopo1(:,1),Atopo1(:,2),Atopo1(:,3));
Atopo1w_new(:,3)=F2topow(Atopo1w_old(:,1),Atopo1w_old(:,2));
Atopo1w_new(:,2)=Atopo1w_old(:,2);
Atopo1w_new(:,1)=Atopo1w_old(:,1);
```

To set the spatial grid:

```
A=Atopo1w_new(1:9,:);
xmin=floor(min(A(:,1)));
xmax=ceil(max(A(:,1)));
ymin=floor(min(A(:,2)));
ymax=ceil(max(A(:,2)));
xi=linspace(xmin,xmax,n+1); % n+1 x-nodes
yi=linspace(ymin,ymax,m+1); % m+1 y-nodes
```

The 3rd column of an array, A, contains the values of GW head depth at a chosen time step (date) of monitoring, e.g. 09 February 2018, as described in the following:

```
DateString = '09-February-2018';
formatIn = 'dd-mmm-yyyy';
datenumber=datenum(DateString,formatIn);

datestr(datenumber,1)
inx=min(find(GWt1(:,1)>=datenumber));
A(1,3)=GWyFData1(inx);
A(2,3)=GWyFData2(inx);
A(3,3)=GWyFData3(inx);
A(4,3)=GWyFData4(inx);
A(5,3)=GWyFData5(inx);
A(6,3)=GWyFData6(inx);
A(7,3)=GWyFData7(inx);
A(8,3)=GWyFData8(inx);
A(9,3)=GWyFData9(inx);
```

To fit a smooth surface to the scattered data of the 16 borehole (wells) using the vectors A(:,1), A(:,2) and A(:,3), an interpolation is employed, which significantly reduces the error (estimations), as described in the following lines in MATLAB:

```
xmin2=floor(min(A2(:,1)));
xmax2=ceil(max(A2(:,1)));
ymin2=floor(min(A2(:,2)));
ymax2=ceil(max(A2(:,2)));
xi=linspace(xmin2,xmax2,n+1);
yi=linspace(ymin2,ymax2,m+1);
ziii =
gridfit(A2(:,1),A2(:,2),A2(:,3),xi,yi,'smoothness',5,'interp','neare
st');
```

To make the contours for the groundwater head values at specific time-steps:

```
[C3,h3]=contour(xi,yi,ziii,6);
    set(h3,'ShowText','on','TextStep',get(h3,'LevelStep')*2,
'LineWidth', 4);
hold on
    colormap bone
    colormap(flipud(colormap))
xlim([xmin2-.01*(xmax2-xmin2) xmax2+.01*(xmax2-xmin2)]);
ylim([ymin2-.01*(ymax2-ymin2) ymax2+.01*(ymax2-ymin2)]);
hold on
hold on
for mm=1:length(A2(:,1))
nx=min(find(xi>=A2(mm,1)));
ny=min(find(yi>=A2(mm,2)));
xi(nx);
yi(ny);
ziii(ny,nx);
[delx dely]=gradient(-ziii,0.2,0.2);
delx(ny,nx);
dely(ny,nx);
G=sqrt(delx(ny,nx)^2+dely(ny,nx)^2);
A=atan(abs(dely(ny,nx)/delx(ny,nx)));
hold on
quiver(xi(nx),yi(ny),delx(ny,nx),dely(ny,nx),'LineWidth',
2,'AutoScaleFactor',15,'MaxHeadSize',0.8, 'Color','r')
```

An example of an initial ARX analysis of groundwater table level fluctuation is provided, to show how steps of this framework were developed and demonstrate its efficiency. This application focused on a particular area in the campus of the University of Birmingham (Southwestern part), providing the corresponding groundwater table fluctuations. Figure C.1a shows these fluctuations, taken from a specified borehole of the groundwater with time. Then,

a contourmap of the area is demonstrated in Figure C.1b, showing the fluctuations of the groundwater table within the area and the borehole spots used. In the same figure the potential move of the groundwater is demonstrated using arrows. This was extended to the integrated visualisation of Figure C.2, which shows the contours within a Google Earth (Google Inc., 2018) environment. This was included to extend the relevant understanding and show the potential for integrated applications using the current framework. By way of example, this framework could also work with contamination aspects, as the move of the groundwater could be indicative for contaminant move, which could provide further support for land contamination and decision-making.

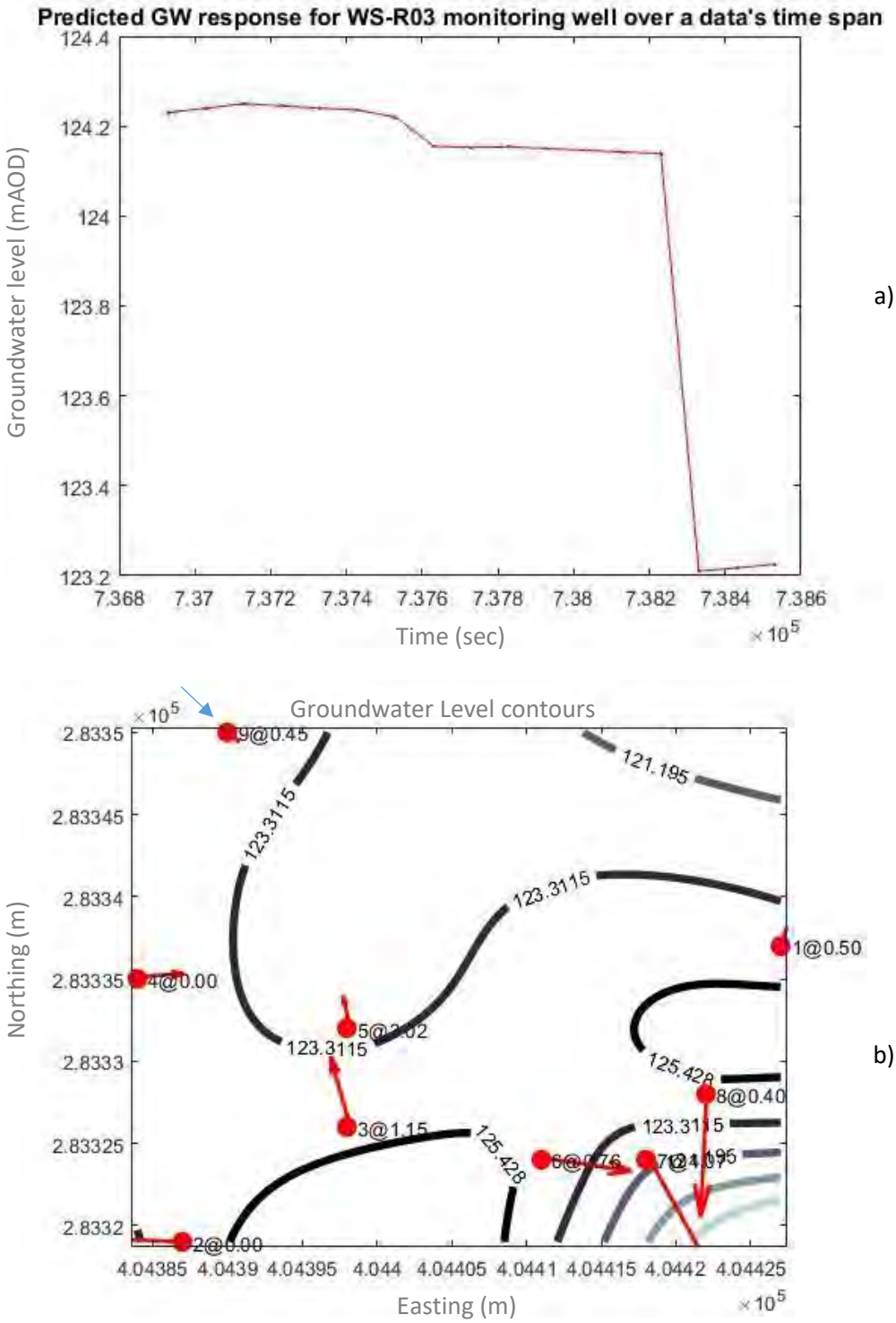

Figure C.1: The resulting groundwater head (GW) (a) fluctuation (graph) and (b) contourlines, using ARX in MATLAB. WS-R03 well is marked with a blue arrow.

Figure C.2: An integrated contourmap (Figure C.1b) using Google Earth (Google Inc., 2018).

C.3 Settlement Risk Assessment visualisations

C.3.1 Settlement risk distributions

The settlement risk distributions were produced by kriging interpolation using (MATLAB):

```
[Zhat2,Zvar2] = kriging(vstruct2,x,y,z,xval,yval);
```

C.3.2 Settlement risk assessment using BIM

The settlement risk assessment using the Settlement Vulnerability Index estimated by the process described (using AHP and ARX) is shown in Figure C.3.

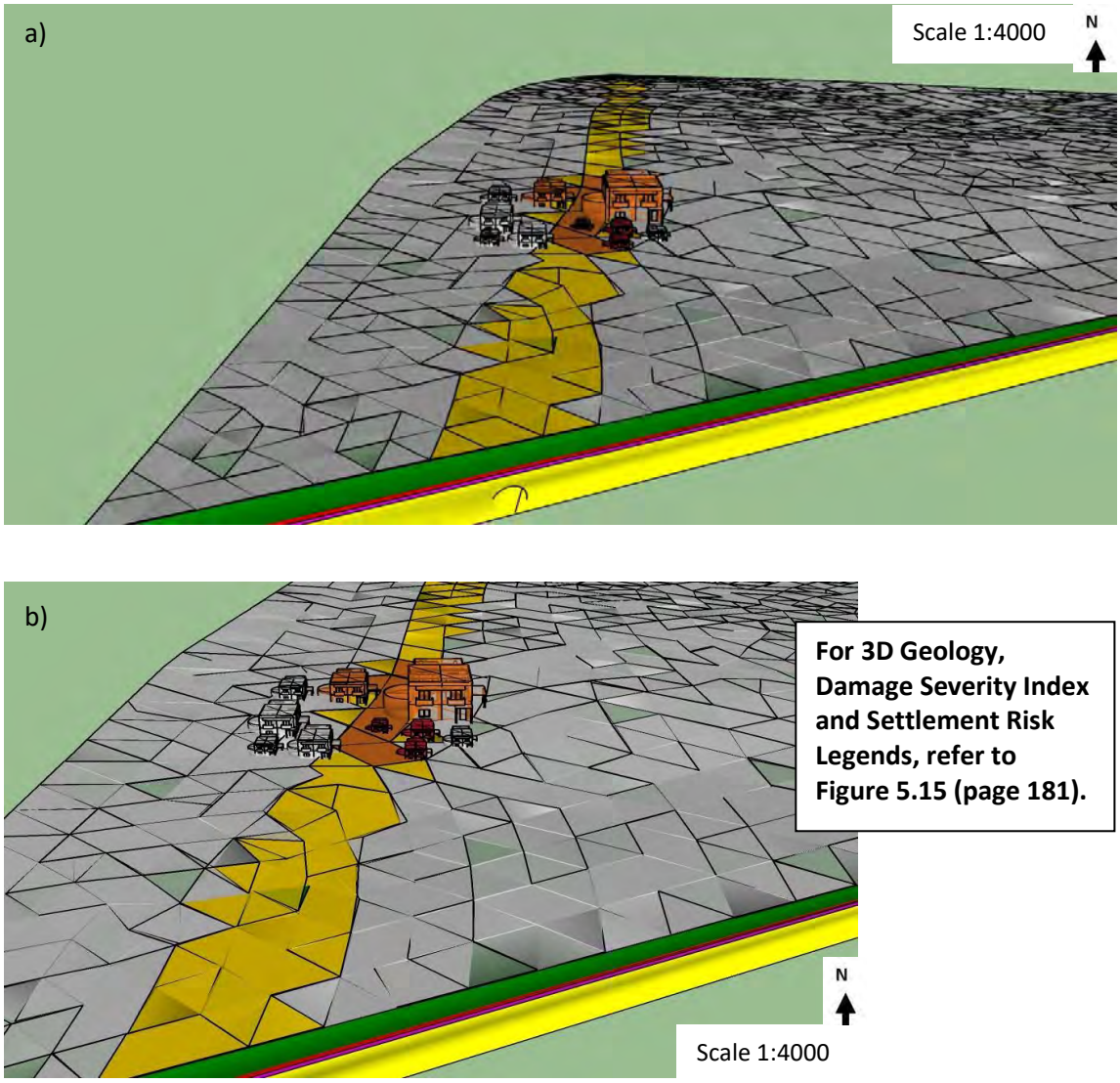

Figure C.3: 3D visualisations of the temporal changes using BIM of the settlement risk assessment, estimated at times (a) at t1: 25.08.2017, and (b) t2: 15.10.2017.

Appendix D: Estimation of the tunnelling-induced settlement economic risk of building damage through an uncertainty analysis using BIM

D.1 Probability distribution of building damage

For each uncertain factor the following MATLAB scripts were used to return randomly distributed values (new_E111, new_E333, new_E444), by considering their mean values and standard deviations, and keeping them within appropriate limits (mean value ± 3 * standard deviation values).

```
function [new_E111] = elasticmodulusrng_1_2_eco(); To provide the
values of ground loss (mean=0.175 and standard deviation: std=0.04).
  mean11 = 0.175;
  stdv11 = 0.04;
```

To estimate the values:

```
  new_E11 = normRandLimit(mean11, stdv11, [-3 3]);
function rr = normRandLimit(m, s, b)
  while true
    rr = randn(1);
    if( rr > b(1) && rr < b(2) )
      break;
    end
  end
```

and to apply the limits:

```
  rr = rr * s + m;

function [new_E333, new_E444] = elasticmodulusrng_3_4_eco(); To
estimate the values of the (soil's) Poisson's ratio (mean=0.25 and
std=0.03).
  mean33 = 0.25;
  stdv33 = 0.03;
```

To provide the values of friction angle (mean=35 and std=4):

```
  Mean44 = 35;
  Stdv44 = 4;
```

To provide the values:

```
  new_E333 = normRandLimit(mean333, stdv333, [-3 3]);
  new_E444 = normRandLimit(mean444, stdv444, [-3 3]);
 function rr = normRandLimit(m, s, b)
  while true
```

```
    rr = randn(1);
    if( rr > b(1) && rr < b(2) )
      break;
    end
  end
  % now apply the limits:
  rr = rr * s + m;

function [new_E555] = elasticmodulusrng_5_6_eco(); To provide the
values of E/G ratio (mean=2.7 and std=0.03) for building No. 1.
  mean11 = 2.7;
  stdv11 = 0.03;
```

To provide the values:

```
  new_E11 = normRandLimit(mean11, stdv11, [-3 3]);
function rr = normRandLimit(m, s, b)
  while true
    rr = randn(1);
    if( rr > b(1) && rr < b(2) )
      break;
    end
  end
```

To apply the limits:

```
  rr = rr * s + m;
```

To execute the Monte Carlo simulations, the randomly distributed values of the selected uncertain factors were applied for 100 runs (i.e. nmonte=1000) to provide the statistical distribution of ground settlements and the subsequent economic risk for each building investigated (adjacent to the tunnel). This is carried out using the following (MATLAB):

```
nmonte=1000;
for imonte=1:nmonte;
[newE111(imonte)]=elasticmodulusrng_1_2_eco();
newE111max=0;
newE111min=1e50;
iop=0;
for i=1:length(Atopo1(:,1))
    iop=iop+1;
    [newE333(i) newE444(i)]=elasticmodulusrng_3_4_eco();
if newE333(iop) >= newE333max
    newE333max=newE333(iop);
end
if newE444(iop) >= newE444max
    newE444max=newE444(iop);
end
```

```
if newE333(iop) <= newE333min
    newE333min=newE333(iop);
end
if newE444(iop) <= newE444min
    newE444min=newE444(iop);
end
end
iop1=0;
iop2=0;
for ikl=1:length(Atopo1(:,1))
    iop1=iop1+1;
    iop2=iop2+1;
VIA3(iop1)=newE333(iop1);
VIA4(iop1)=newE444(iop1);
End

VL=newE111(imonte); The first uncertain factor (ground loss) used.
    x3001=Atopo1(:,1);
    y3001=Atopo1(:,2);
    z3001=VIA3';
    v3001 = variogram([x3001 y3001],z3001,'plotit',false);
    [dum,dum,dum,vstruct3001] =
variogramfit(v3001.distance,v3001.val,[],[],[],'model','blinear','pl
otit',false);
    [Zhat3001,Zvar3001] =
kriging(vstruct3001,x3001,y3001,z3001,centros103(:,1),centros103(:,2
));
pois=Zhat3001; The second uncertain factor (soil Poisson's ratio)
used.
    x3002=Atopo1(:,1);
    y3002=Atopo1(:,2);
    z3002=VIA4';
    v3002 = variogram([x3001 y3001],z3001,'plotit',false);
    [dum,dum,dum,vstruct3002] =
variogramfit(v3002.distance,v3002.val,[],[],[],'model','blinear','pl
otit',false);
    [Zhat3002,Zvar3002] =
kriging(vstruct3002,x3002,y3002,z3002,centros103(:,1),centros103(:,2
));
toc;
phiB=Zhat3002; The third uncertain factor (friction angle) used.

DISTP1P103=DISTP103;
SURF200P103=Fdepth1(POINTP103(:,1),POINTP103(:,2))-DEPTHt;
SURFC0P103=VL*0.5*DIAM*0.5*DIAM*(4*SURF200P103.*(1-pois));
SURFC2P103=(1./(SURF200P103.^2+DISTP1P103.^2));
SURFC02P103=SURFC0P103.*SURFC2P103;
SURFC03P103=1./(SURF200P103.*cot(45+0.5*phiB)+0.5*DIAM).^2;
SURFC1P103=exp(-1.38*SURFC03P103.*DISTP1P103.^2);
SURFC01P103=SURFC02P103.*SURFC1P103;
settl1103=SURFC01P103;
vq21risk103=settl1103;
```

```
Emod=newE555(imonte); The fourth uncertain factor (E/G ratio) for
Building No.1.
GG1(imonte,1)=Emod;
Building_damage_assessment_Stage2_b1_muchcloser_eco3
AtopoB(1,1)=C201(1,1);
AtopoB(1,2)=C201(1,2);
AtopoB(1,3)=C201(1,3);
px3b1(1,:)=px3(1,:);
px3b1(2,:)=px3(2,:);
    if max(strcritH,strcritS) < 0.0005
    B11(1,imonte)=0;
    end
    if max(strcritH, strcritS) >=0.0005 && max(strcritH, strcritS) <
0.00075
    B11(1,imonte)=1;
    end
    if max(strcritH, strcritS) >=0.00075 && max(strcritH, strcritS)
< 0.0015
    B11(1,imonte)=2;
    end
    if max(strcritH, strcritS) >=0.0015 && max(strcritH, strcritS) <
0.003
    B11(1)=3;
    end
    if max(strcritH, strcritS) >=0.003
    B11(1,imonte)=4;
    End
Emod=newE666(imonte); The fourth uncertain factor (E/G ratio) for
Building No.2.
GG1(imonte,2)=Emod;
Building_damage_assessment_Stage2_b2_muchcloser_eco3
AtopoB(2,1)=C201(1,1);
AtopoB(2,2)=C201(1,2);
AtopoB(2,3)=C201(1,3);
px3b2(1,:)=px3(1,:);
px3b2(2,:)=px3(2,:);
    if max(strcritH,strcritS) < 0.0005
    B11(2,imonte)=0;
    end
    if max(strcritH, strcritS) >=0.0005 && max(strcritH, strcritS) <
0.00075
    B11(2,imonte)=1;
    end
    if max(strcritH, strcritS) >=0.00075 && max(strcritH, strcritS)
< 0.0015
    B11(2,imonte)=2;
    end
    if max(strcritH, strcritS) >=0.0015 && max(strcritH, strcritS) <
0.003
    B11(2,imonte)=3;
    end
    if max(strcritH, strcritS) >=0.003
    B11(2,imonte)=4;
```

```
    end
Emod=newE777(imonte); The fourth uncertain factor (E/G ratio) for
Building No.3.
    GG1(imonte,3)=Emod;
    Building_damage_assessment_Stage2_b3_muchcloser_eco3
    AtopoB(3,1)=C201(1,1);
    AtopoB(3,2)=C201(1,2);
    AtopoB(3,3)=C201(1,3);
    px3b3(1,:)=px3(1,:);
    px3b3(2,:)=px3(2,:);
    if max(strcritH,strcritS) < 0.0005
    B11(3,imonte)=0;
    end
    if max(strcritH, strcritS) >=0.0005 && max(strcritH, strcritS) <
0.00075
    B11(3,imonte)=1;
    end
    if max(strcritH, strcritS) >=0.00075 && max(strcritH, strcritS)
< 0.0015
    B11(3,imonte)=2;
    end
    if max(strcritH, strcritS) >=0.0015 && max(strcritH, strcritS) <
0.003
    B11(3,imonte)=3;
    end
    if max(strcritH, strcritS) >=0.003
    B11(3,imonte)=4;
    end
Emod=newE888(imonte); The fourth uncertain factor (E/G ratio) for
Building No.4.
GG1(imonte,4)=Emod;
Building_damage_assessment_Stage2_b4_muchcloser_eco3
AtopoB(4,1)=C201(1,1);
AtopoB(4,2)=C201(1,2);
AtopoB(4,3)=C201(1,3);
px3b4(1,:)=px3(1,:);
px3b4(2,:)=px3(2,:);
    if max(strcritH,strcritS) < 0.0005
    B11(4,imonte)=0;
    end
    if max(strcritH, strcritS) >=0.0005 && max(strcritH, strcritS) <
0.00075
    B11(4,imonte)=1;
    end
    if max(strcritH, strcritS) >=0.00075 && max(strcritH, strcritS)
< 0.0015
    B11(4,imonte)=2;
    end
    if max(strcritH, strcritS) >=0.0015 && max(strcritH, strcritS) <
0.003
    B11(4,imonte)=3;
    end
    if max(strcritH, strcritS) >=0.003
```

```
    B11(4,imonte)=4;
    end
Emod=newE999(imonte); The fourth uncertain factor (E/G ratio) for
Building No.5.
GG1(imonte,5)=Emod;
Building_damage_assessment_Stage2_b5_muchcloser_eco3
AtopoB(5,1)=C201(1,1);
AtopoB(5,2)=C201(1,2);
AtopoB(5,3)=C201(1,3);
px3b5(1,:)=px3(1,:);
px3b5(2,:)=px3(2,:);
    if max(strcritH,strcritS) < 0.0005
    B11(5,imonte)=0;
    end
    if max(strcritH, strcritS) >=0.0005 && max(strcritH, strcritS) <
0.00075
    B11(5,imonte)=1;
    end
    if max(strcritH, strcritS) >=0.00075 && max(strcritH, strcritS)
< 0.0015
    B11(5,imonte)=2;
    end
    if max(strcritH, strcritS) >=0.0015 && max(strcritH, strcritS) <
0.003
    B11(5,imonte)=3;
    end
    if max(strcritH, strcritS) >=0.003
    B11(5,imonte)=4;
    end
Emod=newE101010(imonte); The fourth uncertain factor (E/G ratio) for
Building No.6.
GG1(imonte,6)=Emod;
Building_damage_assessment_Stage2_b6_muchcloser_eco3
AtopoB(6,1)=C201(1,1);
AtopoB(6,2)=C201(1,2);
AtopoB(6,3)=C201(1,3);
px3b6(1,:)=px3(1,:);
px3b6(2,:)=px3(2,:);
    if max(strcritH,strcritS) < 0.0005
    B11(6,imonte)=0;
    end
    if max(strcritH, strcritS) >=0.0005 && max(strcritH, strcritS) <
0.00075
    B11(6,imonte)=1;
    end
    if max(strcritH, strcritS) >=0.00075 && max(strcritH, strcritS)
< 0.0015
    B11(6,imonte)=2;
    end
    if max(strcritH, strcritS) >=0.0015 && max(strcritH, strcritS) <
0.003
    B11(6,imonte)=3;
    end
```

```
    if max(strcritH, strcritS) >=0.003
    B11(6,imonte)=4;
    end
Emod=newE111111(imonte); The fourth uncertain factor (E/G ratio) for
Building No.7.
GG1(imonte,7)=Emod;
Building_damage_assessment_Stage2_b7_muchcloser_eco3
AtopoB(7,1)=C201(1,1);
AtopoB(7,2)=C201(1,2);
AtopoB(7,3)=C201(1,3);
px3b7(1,:)=px3(1,:);
px3b7(2,:)=px3(2,:);
    if max(strcritH,strcritS) < 0.0005
    B11(7,imonte)=0;
    end
    if max(strcritH, strcritS) >=0.0005 && max(strcritH, strcritS) <
0.00075
    B11(7,imonte)=1;
    end
    if max(strcritH, strcritS) >=0.00075 && max(strcritH, strcritS)
< 0.0015
    B11(7,imonte)=2;
    end
    if max(strcritH, strcritS) >=0.0015 && max(strcritH, strcritS) <
0.003
    B11(7,imonte)=3;
    end
    if max(strcritH, strcritS) >=0.003
    B11(7,imonte)=4;
    end
Emod=newE121212(imonte); The fourth uncertain factor (E/G ratio) for
Building No.8.
GG1(imonte,8)=Emod;
Building_damage_assessment_Stage2_b8_muchcloser_eco3
AtopoB(8,1)=C201(1,1);
AtopoB(8,2)=C201(1,2);
AtopoB(8,3)=C201(1,3);
px3b8(1,:)=px3(1,:);
px3b8(2,:)=px3(2,:);
    if max(strcritH,strcritS) < 0.0005
    B11(8,imonte)=0;
    end
    if max(strcritH, strcritS) >=0.0005 && max(strcritH, strcritS) <
0.00075
    B11(8,imonte)=1;
    end
    if max(strcritH, strcritS) >=0.00075 && max(strcritH, strcritS)
< 0.0015
    B11(8,imonte)=2;
    end
    if max(strcritH, strcritS) >=0.0015 && max(strcritH, strcritS) <
0.003
    B11(8,imonte)=3;
```

```
    end
    if max(strcritH, strcritS) >=0.003
    B11(8,imonte)=4;
    end
Emod=newE131313(imonte); The fourth uncertain factor (E/G ratio) for
Building No.9.
GG1(imonte,9)=Emod;
Building_damage_assment_Stage2_b9_muchcloser_eco3
AtopoB(9,1)=C201(1,1);
AtopoB(9,2)=C201(1,2);
AtopoB(9,3)=C201(1,3);
px3b9(1,:)=px3(1,:);
px3b9(2,:)=px3(2,:);
    if max(strcritH,strcritS) < 0.0005
    B11(9,imonte)=0;
    end
    if max(strcritH, strcritS) >=0.0005 && max(strcritH, strcritS) <
0.00075
    B11(9,imonte)=1;
    end
    if max(strcritH, strcritS) >=0.00075 && max(strcritH, strcritS)
< 0.0015
    B11(9,imonte)=2;
    end
    if max(strcritH, strcritS) >=0.0015 && max(strcritH, strcritS) <
0.003
    B11(9,imonte)=3;
    end
    if max(strcritH, strcritS) >=0.003
    B11(9,imonte)=4;
    end
Emod=newE141414(imonte); The fourth uncertain factor (E/G ratio) for
Building No.10.
GG1(imonte,10)=Emod;
Building_damage_assessment_Stage2_b10_muchcloser_eco3
AtopoB(10,1)=C201(1,1);
AtopoB(10,2)=C201(1,2);
AtopoB(10,3)=C201(1,3);
px3b10(1,:)=px3(1,:);
px3b10(2,:)=px3(2,:);
    if max(strcritH,strcritS) < 0.0005
    B11(10,imonte)=0;
    end
    if max(strcritH, strcritS) >=0.0005 && max(strcritH, strcritS) <
0.00075
    B11(10,imonte)=1;
    end
    if max(strcritH, strcritS) >=0.00075 && max(strcritH, strcritS)
< 0.0015
    B11(10,imonte)=2;
    end
    if max(strcritH, strcritS) >=0.0015 && max(strcritH, strcritS) <
0.003
```

```
    B11(10,imonte)=3;
    end
    if max(strcritH, strcritS) >=0.003
    B11(10,imonte)=4;
    end
iko1=0;
for iko=1:szset
    iko1=iko1+1;
    if( settl1103(iko1,1) <=0.01 && settl1103(iko1,1) >= 0 )
        Psz(iko1)=0;
    end
    if( settl1103(iko1,1) <=0.05 && settl1103(iko1,1) > 0.01 )
        Psz(iko1)=1;
    end
    if( settl1103(iko1,1) <=0.075 && settl1103(iko,1) > 0.05 )
        Psz(iko1)=2;
    end
    if( settl1103(iko1,1) <=100 && settl1103(iko1,1) > 0.075 )
        Psz(iko1)=3;
    end
    VIA1103mc(iko1,imonte)=Psz(iko1);
end
clear ZhatAll;
clear ZvarAll;
for iok=1:length(B11(:,imonte))
ZhatAll(iok,imonte)=B11(iok,imonte);
VImc(iok,imonte)=ZhatAll(iok,imonte);
end
close all;
delete(findall(0));
end
for ijol=1:szset
    z1111(ijol,1)=sum(VIA1103mc(ijol,:)==0,2);
    z1111(ijol,2)=sum(VIA1103mc(ijol,:)==1,2);
    z1111(ijol,3)=sum(VIA1103mc(ijol,:)==2,2);
    z1111(ijol,4)=sum(VIA1103mc(ijol,:)==3,2);
end
y1111(1,1) = sum(VImc(1,:)==0,2);
y1111(1,2) = sum(VImc(1,:)==1,2);
y1111(1,3) = sum(VImc(1,:)==2,2);
y1111(1,4) = sum(VImc(1,:)==3,2);
y1111(1,5) = sum(VImc(1,:)==4,2);
y1111(2,1) = sum(VImc(2,:)==0,2);
y1111(2,2) = sum(VImc(2,:)==1,2);
y1111(2,3) = sum(VImc(2,:)==2,2);
y1111(2,4) = sum(VImc(2,:)==3,2);
y1111(2,5) = sum(VImc(2,:)==4,2);
y1111(3,1) = sum(VImc(3,:)==0,2);
y1111(3,2) = sum(VImc(3,:)==1,2);
y1111(3,3) = sum(VImc(3,:)==2,2);
y1111(3,4) = sum(VImc(3,:)==3,2);
y1111(3,5) = sum(VImc(3,:)==4,2);
y1111(4,1) = sum(VImc(4,:)==0,2);
```

```
y1111(4,2) = sum(VImc(4,:)==1,2);
y1111(4,3) = sum(VImc(4,:)==2,2);
y1111(4,4) = sum(VImc(4,:)==3,2);
y1111(4,5) = sum(VImc(4,:)==4,2);
y1111(5,1) = sum(VImc(5,:)==0,2);
y1111(5,2) = sum(VImc(5,:)==1,2);
y1111(5,3) = sum(VImc(5,:)==2,2);
y1111(5,4) = sum(VImc(5,:)==3,2);
y1111(5,5) = sum(VImc(5,:)==4,2);
y1111(6,1) = sum(VImc(6,:)==0,2);
y1111(6,2) = sum(VImc(6,:)==1,2);
y1111(6,3) = sum(VImc(6,:)==2,2);
y1111(6,4) = sum(VImc(6,:)==3,2);
y1111(6,5) = sum(VImc(6,:)==4,2);
y1111(7,1) = sum(VImc(7,:)==0,2);
y1111(7,2) = sum(VImc(7,:)==1,2);
y1111(7,3) = sum(VImc(7,:)==2,2);
y1111(7,4) = sum(VImc(7,:)==3,2);
y1111(7,5) = sum(VImc(7,:)==4,2);
y1111(8,1) = sum(VImc(8,:)==0,2);
y1111(8,2) = sum(VImc(8,:)==1,2);
y1111(8,3) = sum(VImc(8,:)==2,2);
y1111(8,4) = sum(VImc(8,:)==3,2);
y1111(8,5) = sum(VImc(8,:)==4,2);
y1111(9,1) = sum(VImc(9,:)==0,2);
y1111(9,2) = sum(VImc(9,:)==1,2);
y1111(9,3) = sum(VImc(9,:)==2,2);
y1111(9,4) = sum(VImc(9,:)==3,2);
y1111(9,5) = sum(VImc(9,:)==4,2);
y1111(10,1) = sum(VImc(10,:)==0,2);
y1111(10,2) = sum(VImc(10,:)==1,2);
y1111(10,3) = sum(VImc(10,:)==2,2);
y1111(10,4) = sum(VImc(10,:)==3,2);
y1111(10,5) = sum(VImc(10,:)==4,2);
for lol=1:szset
    count_nums=z1111(lol,:);
    adds(lol,:,1)=count_nums./sum(count_nums);
end
count_num1=y1111(1,:);
add1(:,1)=count_num1(1,1:5)./sum(count_num1(1,1:5));
count_num2=y1111(2,:);
add2(:,1)=count_num2(1,1:5)./sum(count_num2(1,1:5));
count_num3=y1111(3,:);
add3(:,1)=count_num3(1,1:5)./sum(count_num3(1,1:5));
count_num4=y1111(4,:);
add4(:,1)=count_num4(1,1:5)./sum(count_num4(1,1:5));
count_num5=y1111(5,:);
add5(:,1)=count_num5(1,1:5)./sum(count_num5(1,1:5));
count_num6=y1111(6,:);
add6(:,1)=count_num6(1,1:5)./sum(count_num6(1,1:5));
count_num7=y1111(7,:);
add7(:,1)=count_num7(1,1:5)./sum(count_num7(1,1:5));
count_num8=y1111(8,:);
```

```
add8(:,1)=count_num8(1,1:5)./sum(count_num8(1,1:5));
count_num9=y1111(9,:);
add9(:,1)=count_num9(1,1:5)./sum(count_num9(1,1:5));
count_num10=y1111(10,:);
add10(:,1)=count_num10(1,1:5)./sum(count_num10(1,1:5));
str = {'[0 0.05%]'; '[0.05% 0.075%]';'[0.075% 0.15%]'; '[0.15%
0.3%]';'[0.3% >0.3%]';};
str1 = {'[0 0.01]'; '[0.01 0.05]'; '[0.05 0.075]'; '[0.075
>0.075]'};

h0=figure;
ino=1;
bar(adds(ino,:,1),'EdgeColor','g') To plot the probability histogram
for the soil vulnerability.
set(gca, 'XTickLabel',str1, 'XTick',1:numel(str1))
xticklabel_rotate([],90,str1);
saveas(h0, 'probability0.png');
h1=figure;
bar(add1,'EdgeColor','g') To plot the probability histogram for
Building No. 1.
set(gca, 'XTickLabel',str, 'XTick',1:numel(str))
xticklabel_rotate([],90,str);
saveas(h1, 'probability1.png');
h2=figure;
bar(add2,'EdgeColor','g') To plot the probability histogram for
Building No. 2.
set(gca, 'XTickLabel',str, 'XTick',1:numel(str))
xticklabel_rotate([],90,str);
saveas(h2, 'probability2.png');
h3=figure;
bar(add3,'EdgeColor','g') To plot the probability histogram for
Building No. 3.
set(gca, 'XTickLabel',str, 'XTick',1:numel(str))
xticklabel_rotate([],90,str);
saveas(h3, 'probability3.png');
h4=figure;
bar(add4,'EdgeColor','g') To plot the probability histogram for
Building No. 4.
set(gca, 'XTickLabel',str, 'XTick',1:numel(str))
xticklabel_rotate([],90,str);
saveas(h4, 'probability4.png');
h5=figure;
bar(add5,'EdgeColor','g') To plot the probability histogram for
Building No. 5.
set(gca, 'XTickLabel',str, 'XTick',1:numel(str))
xticklabel_rotate([],90,str);
saveas(h5, 'probability5.png');
h6=figure;
bar(add6,'EdgeColor','g') To plot the probability histogram for
Building No. 6.
set(gca, 'XTickLabel',str, 'XTick',1:numel(str))
xticklabel_rotate([],90,str);
saveas(h6, 'probability6.png');
```

```
h7=figure;
bar(add7,'EdgeColor','g') To plot the probability histogram for
Building No. 7.
set(gca, 'XTickLabel',str, 'XTick',1:numel(str))
xticklabel_rotate([],90,str);
saveas(h7, 'probability7.png');
h8=figure;
bar(add8,'EdgeColor','g') Plots the probability histogram for
Building No. 8.
set(gca, 'XTickLabel',str, 'XTick',1:numel(str))
xticklabel_rotate([],90,str);
saveas(h8, 'probability8.png');
h9=figure;
bar(add9,'EdgeColor','g') Plots the probability histogram for
Building No. 9.
set(gca, 'XTickLabel',str, 'XTick',1:numel(str))
xticklabel_rotate([],90,str);
saveas(h9, 'probability9.png');
h10=figure;
bar(add10,'EdgeColor','g') Plots the probability histogram for
Building No.10.
set(gca, 'XTickLabel',str, 'XTick',1:numel(str))
xticklabel_rotate([],90,str);
saveas(h10, 'probability10.png');
```

The resulting MATLAB histograms showing the probability of a Damage Category to occur, for each building, follow.

Initially, a tunnel with a diameter of 8m placed below the built-up area was used (corresponding to the BIM visualisations in Chapter 6), as shown in Figures D.1 – D.5:

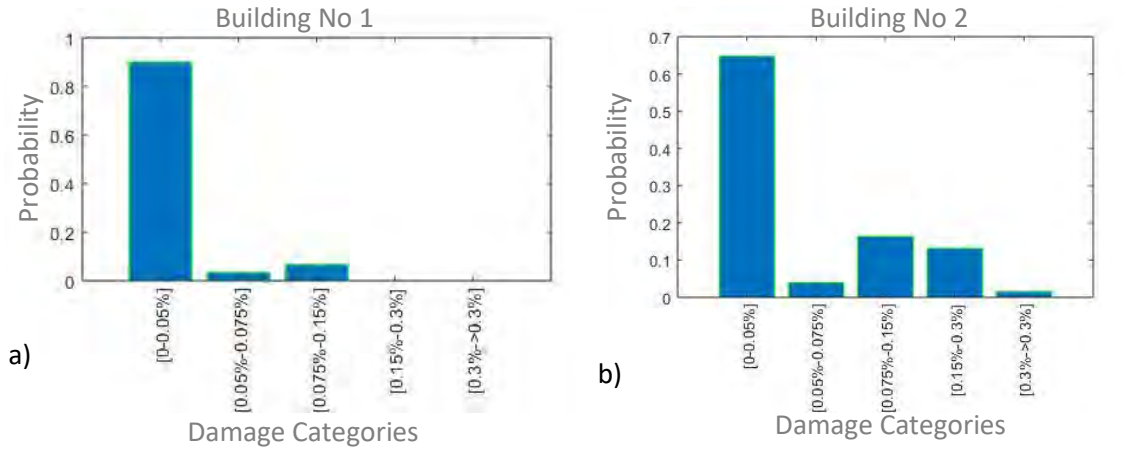

Figure D.1: The graphs showing the probability of a Damage Category to occur for building (a) No. 1 and (b) No. 2.

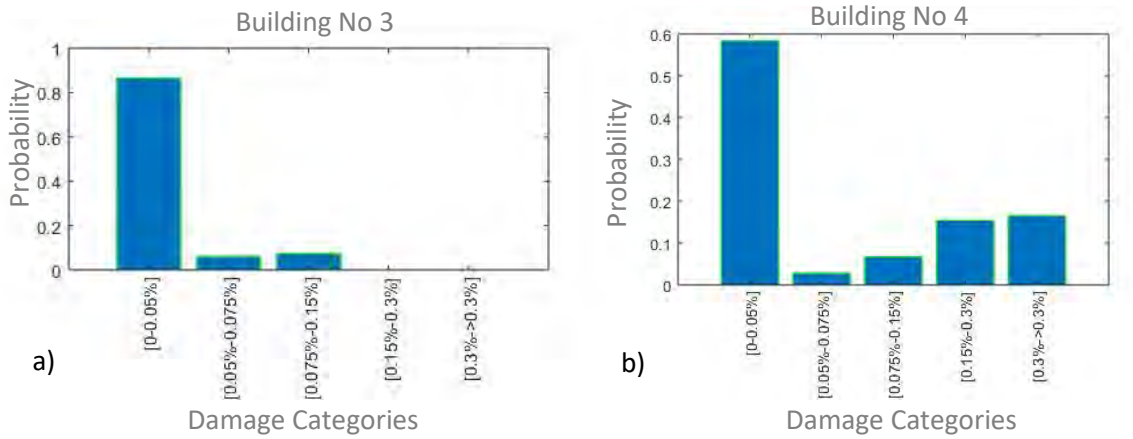

Figure D.2: The graphs showing the probability of a Damage Category to occur for building (a) No. 3 and (b) No. 4.

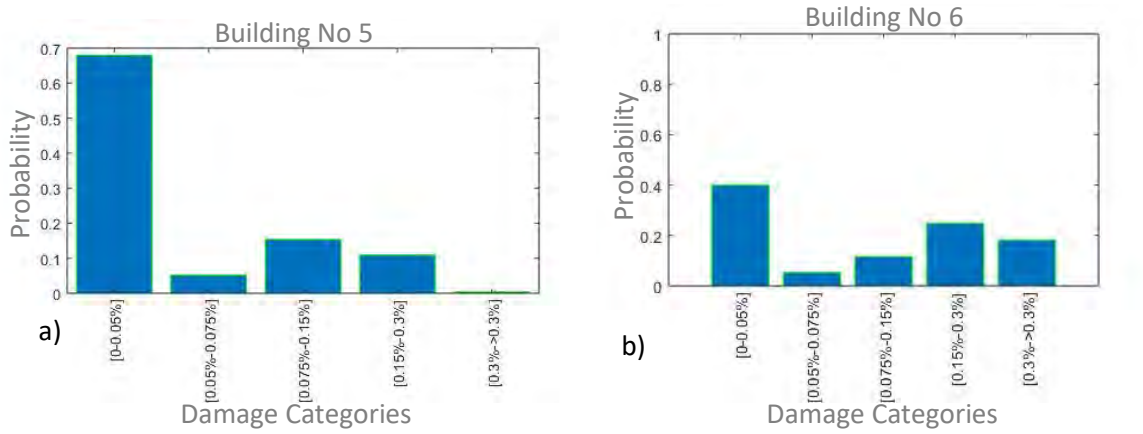

Figure D.3: The graphs showing the probability of a Damage Category to occur for building (a) No. 5 and (b) No. 6.

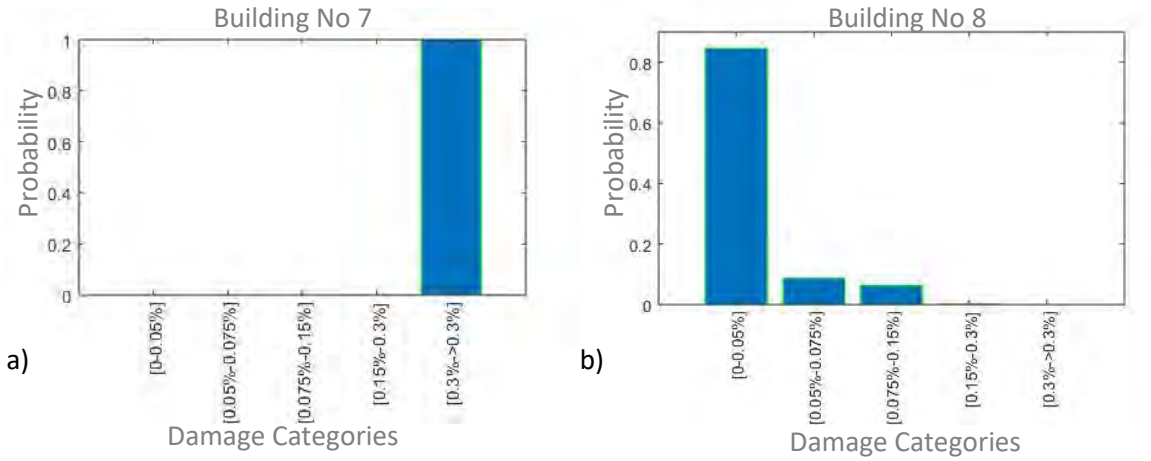

Figure D.4: The graphs showing the probability of a Damage Category to occur for building (a) No. 7 and (b) No. 8.

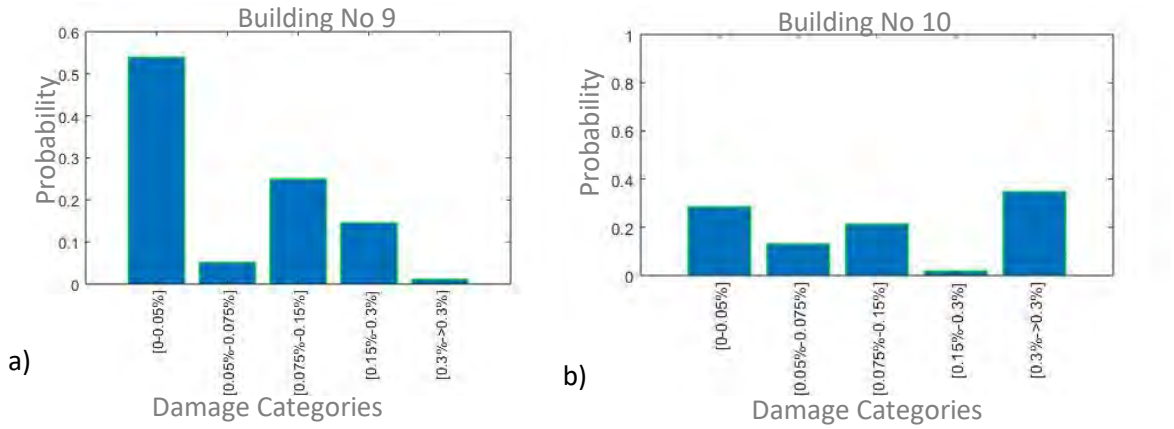

Figure D.5: The graphs showing the probability of a Damage Category to occur for building (a) No. 9 and (b) No. 10.

Then, in the case of a tunnel with an 8m diameter placed at approximately 200m away from the built-up area, the graphs are shown in Figures D.6 – D.10:

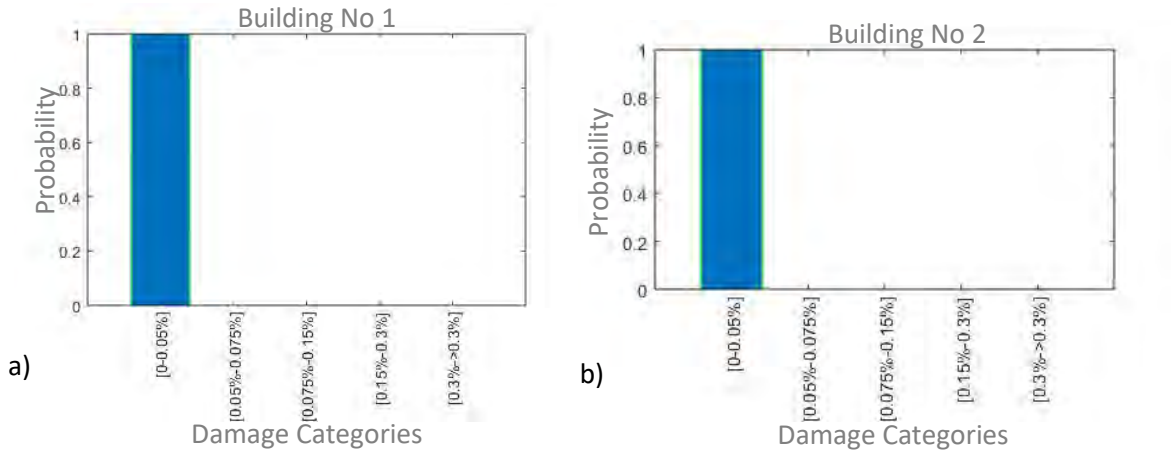

Figure D.6: The graphs showing the probability of a Damage Category to occur for building (a) No. 1 and (b) No. 2.

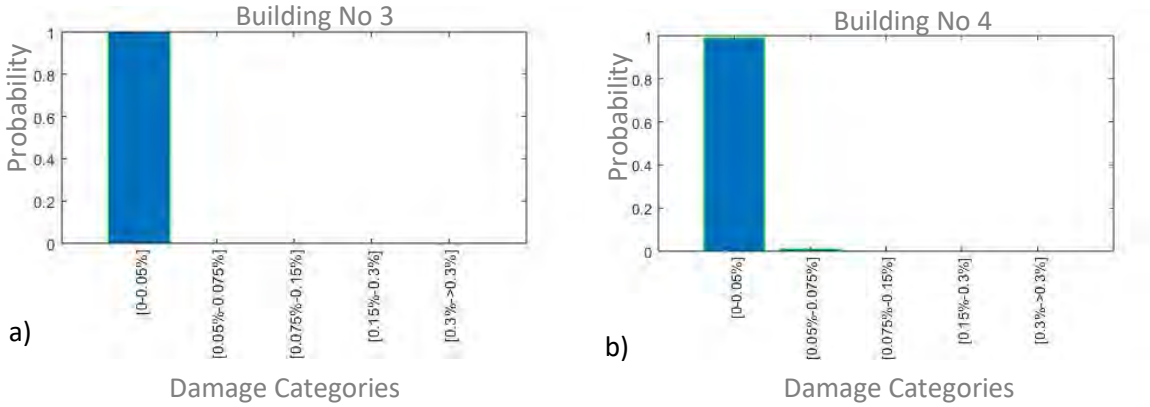

Figure D.7: The graphs showing the probability of a Damage Category to occur for building (a) No. 3 and (b) No. 4.

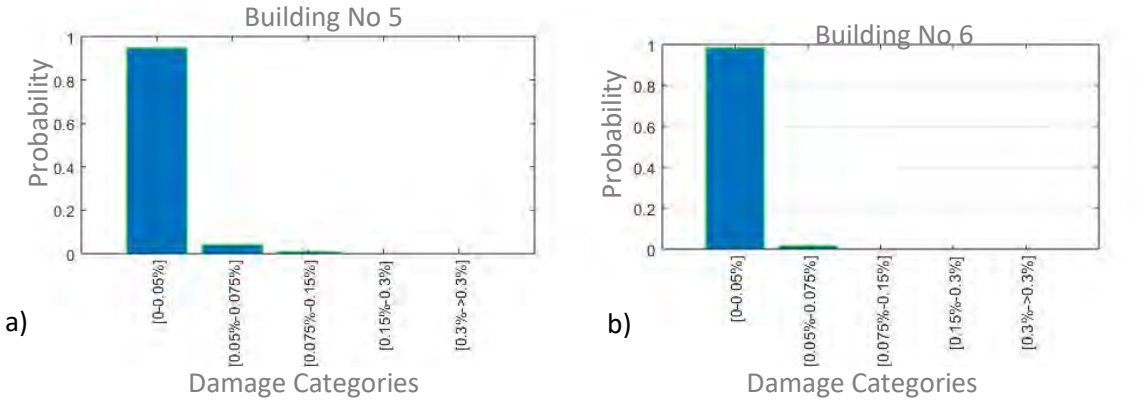

Figure D.8: The graphs showing the probability of a Damage Category to occur for building (a) No. 5 and (b) No. 6.

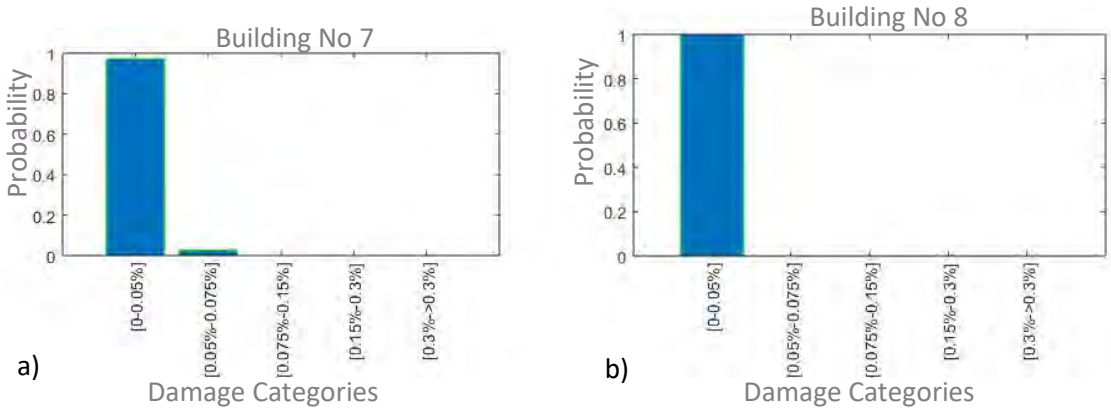

Figure D.9: The graphs showing the probability of a Damage Category to occur for building (a) No. 7 and (b) No. 8.

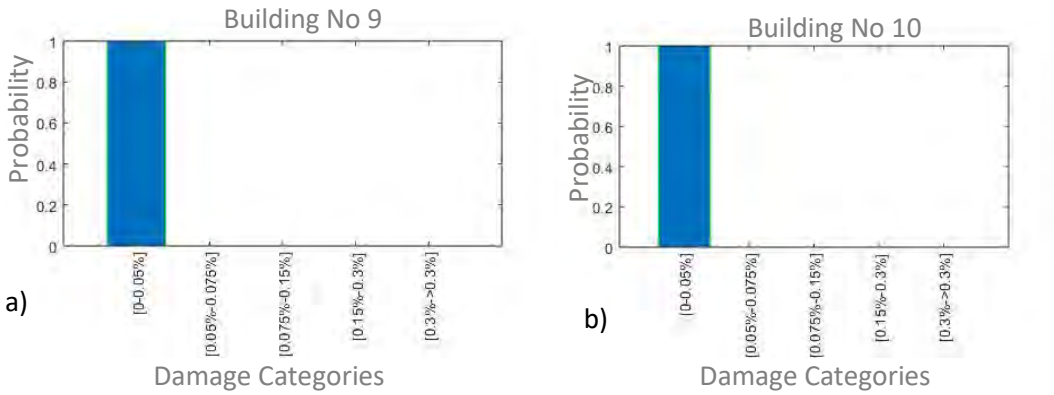

Figure D.10: The graphs showing the probability of a Damage Category to occur for building (a) No. 9 and (b) No. 10.

For a tunnel with a diameter of 10.5m, placed below the built-up area, the graphs are shown in Figures D.11 – D.15:

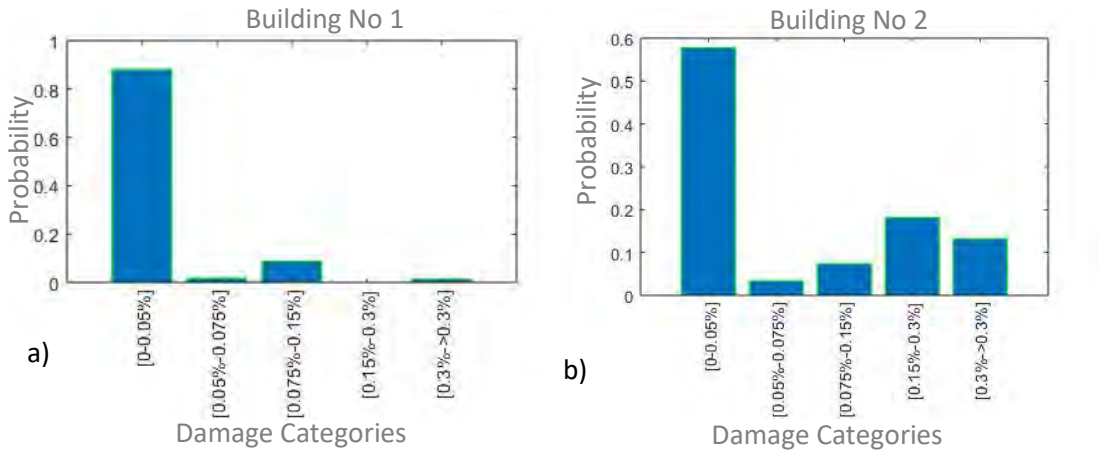

Figure D.11: The graphs showing the probability of a Damage Category to occur for building (a) No. 1 and (b) No. 2.

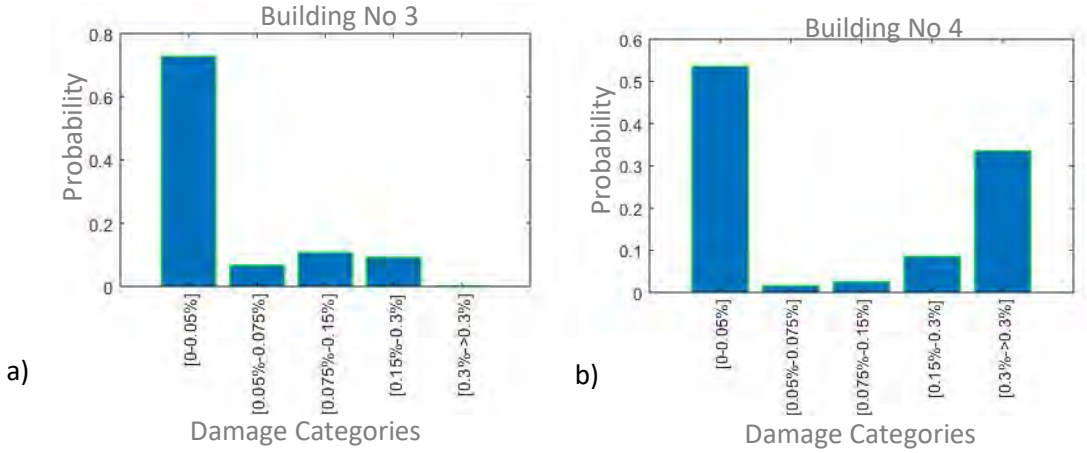

Figure D.12: The graphs showing the probability of a Damage Category to occur for building (a) No. 3 and (b) No. 4.

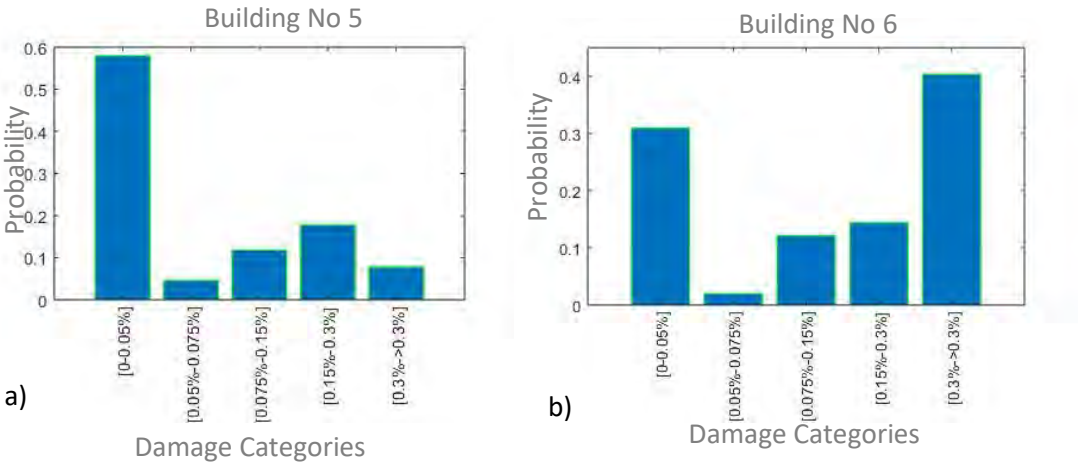

Figure D.13: The graphs showing the probability of a Damage Category to occur for building (a) No. 5 and (b) No. 6.

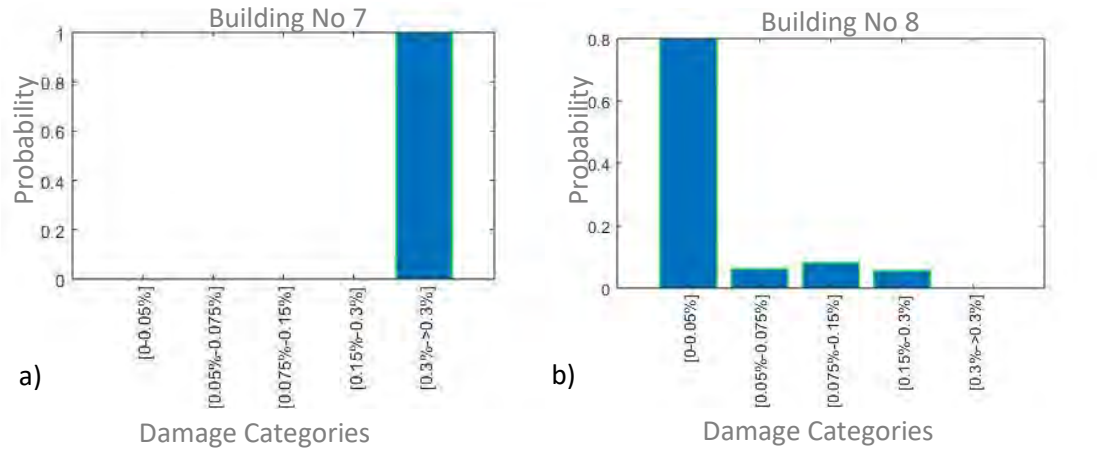

Figure D.14: The graphs showing the probability of a Damage Category to occur for building (a) No. 7 and (b) No. 8.

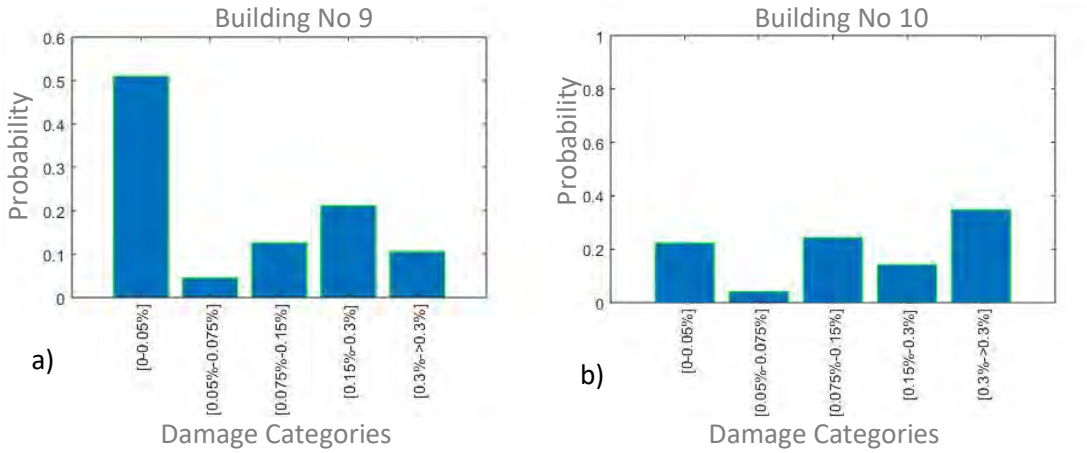

Figure D.15: The graphs showing the probability of a Damage Category to occur for building (a) No. 9 and (b) No. 10.

In the case of a tunnel with a diameter of 10.5m, placed around 200m away from the built-up area, the graphs are shown in Figures D.16 – D.20:

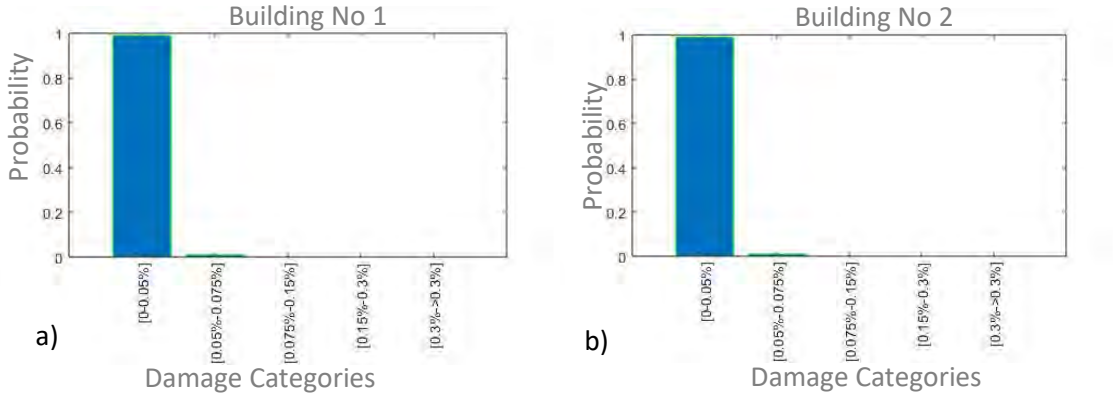

Figure D.16: The graphs showing the probability of a Damage Category to occur for building (a) No. 1 and (b) No. 2.

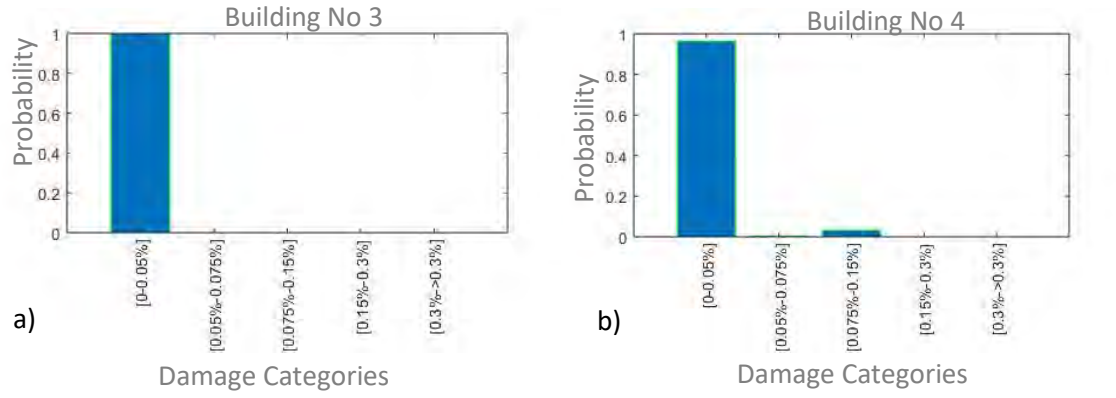

Figure D.17: The graphs showing the probability of a Damage Category to occur for building (a) No. 3 and (b) No. 4.

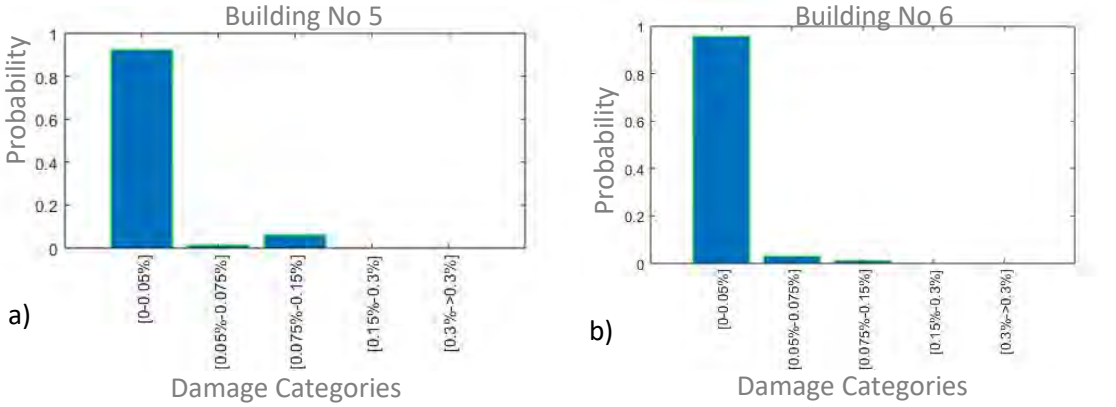

Figure D.18: The graphs showing the probability of a Damage Category to occur for building (a) No. 5 and (b) No. 6.

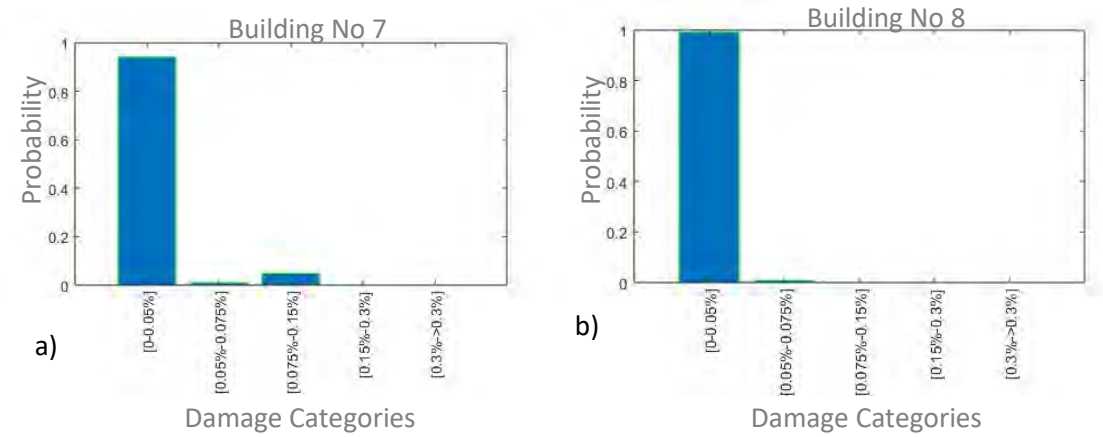

Figure D.19: The graphs showing the probability of a Damage Category to occur for building (a) No. 7 and (b) No. 8.

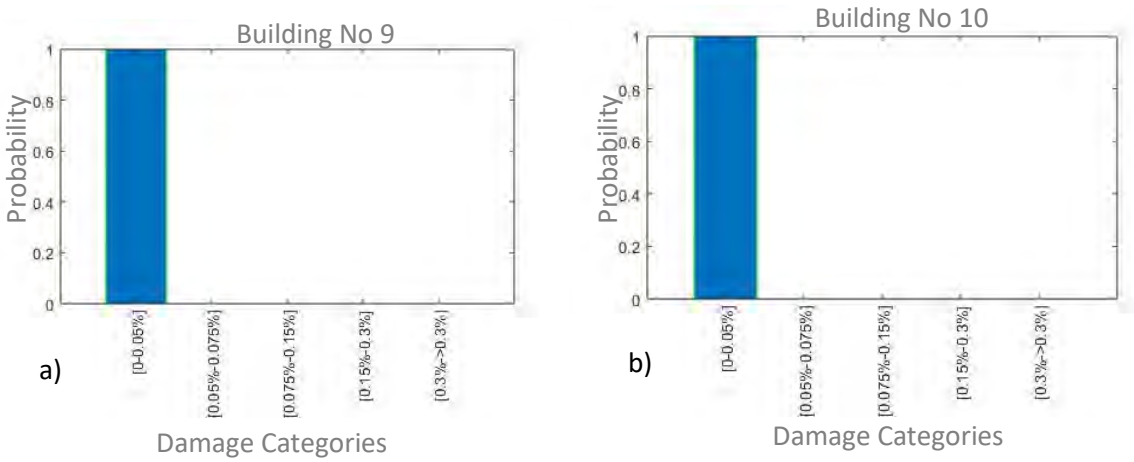

Figure D.20: The graphs showing the probability of a Damage Category to occur for building (a) No. 9 and (b) No. 10.

D.2 Building damage cost analysis using Probability Density Functions

The PDF and 95% percentile costs are produced for each Damage Category for each building. The adopted mean (mu_test1…mu_test5) and maximum (xa_test1…xa_test5) (economic) cost in £ per m^2 of each building for each Damage Category would be:

```
mu_test1=30;
mu_test2=300;
mu_test3=900;
mu_test4=1500;
```

```
mu_test5=2400;
xa_test1=70;
xa_test2=900;
xa_test3=2000;
xa_test4=2300;
xa_test5=4000;
sigma1_test1=1.645-sqrt(1.645^2+2*log(mu_test1/xa_test1)); To
extract the first solution of lognormal sigma for Damage Category
No.1.
sigma2_test1=1.645+sqrt(1.645^2+2*log(mu_test1/xa_test1)); To
extract the second solution of lognormal sigma for Damage Category
No.1.
mu1_test1=log(xa_test1)-1.645*sigma1_test1; To extract the first
lognormal mu (z0.95=1.645) for Damage Category No.1.
mu2_test1=log(xa_test1)-1.645*sigma2_test1; To extract the second
lognormal mu for Damage Category No.1.
```

The same is carried out for the rest of building Damage Categories.

To consider then the probability of each Damage Category to occur, for each building:

```
prob1=add1(1,1);
prob2=add1(2,1);
prob3=add1(3,1);
prob4=add1(4,1);
prob5=add1(5,1);

mu1=mu1_test1;
mu2=mu1_test2;
mu3=mu1_test3;
mu4=mu1_test4;
mu5=mu1_test5;
sigma1=sigma1_test1;
sigma2=sigma1_test2;
sigma3=sigma1_test3;
sigma4=sigma1_test4;
sigma5=sigma1_test5;
```

To provide the PDF of damage costs due to tunnel-induced settlements for Damage Category

No.1 (negligible), in the case of Building No.1:

```
pd1 = makedist('Lognormal','mu',mu1,'sigma',sigma1);
ytxt=currSym('GBP');
x = (0:10:1000)';
y = pdf(pd1,x);
pctvala = prctile(y,95);
xa = logninv(0.95,mu1,sigma1); where xa is the 0.95 quantile of
lognormal distribution for Damage Category No.1.
xa1 = logninv(prob1,mu1,sigma1); where xa1 is the prob1*100%
quantile of lognormal distribution for Damage Category No.1.
ya1 = pdf(pd1,xa1);
y1= cdf(pd1,xa);
```

```
plot(x,y)
h = gca;
h.XTick = [0 500 1000 1500 2000];
h.XTickLabel = {'0',['1.000,00' num2str(ytxt)],['2.000,00'
num2str(ytxt)],...
['3.000,00' num2str(ytxt)],['4.000,00' num2str(ytxt)]};
vline(xa,'-.or','C1')
```

Likewise, for the Damage Category No.2 (very slight) of Building No. 1:

```
pd2= makedist('Lognormal','mu',mu2,'sigma',sigma2);
x = (0:10:3000)';
y = pdf(pd2,x);
pctvalb = prctile(y,95);
xb = logninv(0.95,mu2,sigma2); where xb is the 0.95 quantile of
lognormal distribution for Damage Category No.2.
y2= cdf(pd2,xb);
xa2 = logninv(prob2,mu2,sigma2); where xa2 is the prob1*100%
quantile of lognormal distribution for Damage Category No.2.
ya2 = pdf(pd2,xa2);
figure; plot(x,y)
h = gca;
h.XTick = [0 1000 2000 3000 4000];
h.XTickLabel = {'0',['1.000' num2str(ytxt)],['2.000'
num2str(ytxt)],...
['3.000' num2str(ytxt)],['4.000' num2str(ytxt)]};
vline(xb,'-.or','C2')
```

Likewise, for Damage Category No. 3 (slight) of building No. 1:

```
pd3 = makedist('Lognormal','mu',mu3,'sigma',sigma3);
x = (0:50:5000)';
y = pdf(pd3,x);
pctvalc = prctile(y,95);
xc = logninv(0.95,mu3,sigma3); where xc is the 0.95 quantile of
lognormal distribution for Damage Category No.3.
y3= cdf(pd3,xc);
xa3 = logninv(prob3,mu3,sigma3); where xa3 is the prob1*100%
quantile of lognormal distribution for Damage Category No.3.
ya3 = pdf(pd3,xa3);
figure; plot(x,y)

h = gca;
h.XTick = [0 1000 2000 3000 4000];
h.XTickLabel = {'0',['1.000' num2str(ytxt)],['2.000'
num2str(ytxt)],...
['3.000' num2str(ytxt)],['4.000' num2str(ytxt)]};
vline(xc,'-.or','C3')
pctval = prctile(y,95);
```

Likewise, for Damage Category No.4 (moderate) of Building No. 1:

```
pd4 = makedist('Lognormal','mu',mu4,'sigma',sigma4);
```

```
x = (0:50:5000)';
y = pdf(pd4,x);
pctvalc = prctile(y,95);
xd = logninv(0.95,mu4,sigma4); where xd is the 0.95 quantile of
lognormal distribution for Damage Category No.4.
y4= cdf(pd4,xd);
xa4 = logninv(prob4,mu4,sigma4); where xa4 is the prob1*100%
quantile of lognormal distribution for Damage Category No 4.
ya4 = pdf(pd4,xa4);
figure; plot(x,y)
h = gca;
h.XTick = [0 1000 2000 3000 4000];
h.XTickLabel = {'0',['1.000' num2str(ytxt)],['2.000'
num2str(ytxt)],...
['3.000' num2str(ytxt)],['4.000' num2str(ytxt)]};
vline(xd,'-.or','C4')
pctval = prctile(y,95);
```

Likewise, for Damage Category No.5 of Building No. 1:

```
pd5 = makedist('Lognormal','mu',mu5,'sigma',sigma5);
x = (0:50:5000)';
y = pdf(pd5,x);
pctvalc = prctile(y,95);
xe = logninv(0.95,mu5,sigma5); where xe is the 0.95 quantile of
lognormal distribution for Damage Category No.5.
xmue=logninv(0.5,mu5,sigma5);
y5= cdf(pd5,xe);
xa5 = logninv(prob5,mu5,sigma5); where xa5 is the prob1*100%
quantile of lognormal distribution for Damage Category No.5.
ya5 = pdf(pd5,xa5);
figure; plot(x,y)
h = gca;
h.XTick = [0 1000 2000 3000 4000];
h.XTickLabel = {'0',['1.000' num2str(ytxt)],['2.000'
num2str(ytxt)],...
['3.000' num2str(ytxt)],['4.000' num2str(ytxt)]};
vline(xe,'-.or','C5')
vline(xmue,'-.or','C4')
figure
pctval = prctile(y,95);
```

Finally, the Settlement Economic Risk per m^2 (TRisk1) for the Building No.1, considering the probability for all the Damage Categories to occur, can then be estimated using the following:

```
prob1=add1(1,1);
prob2=add1(2,1);
prob3=add1(3,1);
prob4=add1(4,1);
prob5=add1(5,1);
xa1 = logninv(prob1,mu1,sigma1); %% xa is the 0.95 quantile of
lognormal distribution
```

```
ya1 = pdf(pd1,xa1);
xa2 = logninv(prob2,mu2,sigma2); %% xa is the 0.95 quantile of
lognormal distribution
ya2 = pdf(pd2,xa2);
xa3 = logninv(prob3,mu3,sigma3); %% xa is the 0.95 quantile of
lognormal distribution
ya3 = pdf(pd3,xa3);
xa4 = logninv(prob4,mu4,sigma4); %% xa is the 0.95 quantile of
lognormal distribution
ya4 = pdf(pd4,xa4);
xa5 = logninv(prob5,mu5,sigma5); %% xa is the 0.95 quantile of
lognormal distribution
ya5 = pdf(pd5,xa5);
yProb=[ya1; ya1; ya2; ya2; ya3; ya3; ya4; ya4; ya5; ya5; 0];
xCost=[0; xa; xa; xb; xb; xc; xc; xd; xd; xe; xe];
plot(xCost,yProb);
yProb=[prob1; prob1; prob2; prob2; prob3; prob3; prob4; prob4;
prob5; prob5; 0];
xCost=[0; xa; xa; xb; xb; xc; xc; xd; xd; xe; xe];
ERisk1(1)=0;
ERisk1(2)=0;
ERisk1(3)=0;
ERisk1(4)=0;
ERisk1(5)=0;
if(prob1~=1) xCost1_interval=(0:1:xa1)'; end;
if(prob1==1) xCost1_interval=(0:1:70)';end;
yPDF1_interval=pdf(pd1,xCost1_interval);
yPDF1p=yPDF1_interval.*xCost1_interval;
if(prob1~=0) ERisk1(1)=trapz(xCost1_interval,yPDF1p); end;
xCost2_interval=(0:1:xa2)';
yPDF2_interval=pdf(pd2,xCost2_interval);
yPDF2p=yPDF2_interval.*xCost2_interval;
if(prob2~=0) ERisk1(2)=trapz(xCost2_interval,yPDF2p); end;
xCost3_interval=(0:1:xa3)';
yPDF3_interval=pdf(pd3,xCost3_interval);
yPDF3p=yPDF3_interval.*xCost3_interval;
if(prob3~=0) ERisk1(3)=trapz(xCost3_interval,yPDF3p); end;
xCost4_interval=(0:1:xa4)';
yPDF4_interval=pdf(pd4,xCost4_interval);
yPDF4p=yPDF4_interval.*xCost4_interval;
if(prob4~=0) ERisk1(4)=trapz(xCost4_interval,yPDF4p); end;
xCost5_interval=(0:1:xa5)';
yPDF5_interval=pdf(pd5,xCost5_interval);
yPDF5p=yPDF5_interval.*xCost5_interval;
if(prob5~=0) ERisk1(5)=trapz(xCost5_interval,yPDF5p); end;
ERiskTotal1=ERisk1(1)+ERisk1(2)+ERisk1(3)+ERisk1(4)+ERisk1(5);
TRisk1=ERiskTotal1*2*polyarea(px3b1(1,:),px3b1(2,:));
hold on
yProbb1=[ya2+(ya1-ya2)/2; ya3+(ya2-ya3)/2; ya4+(ya3-ya4)/2;
ya5+(ya4-ya5)/2; ya5/2];
xCostb1=[xa; xb; xc; xd; xe];
yProbb11=[ya1; ya2; ya3; ya4; ya5];
```

```
xCostb11=[xa/2; xa+(xb-xa)/2; xb+(xc-xb)/2; xc+(xd-xc)/2; xd+(xe-
xd)/2];
Area1=2*polyarea(px3b1(1,:),px3b1(2,:));
Economic_Risk_b1=trapz(xCost,yProb);
Economic_Total_b1=Economic_Risk_b1*Area1; The Settlement Economic
Risk (per m²).
```

The Settlement Economic Risk (per m^2) is provided similarly for each building.

The graphs of the cost variations of the buildings due to settlements for each damage category, follow. Hence, for a tunnel with an 8m diameter, placed below the built-up area, the graphs are shown in Figures D.21 – D.23:

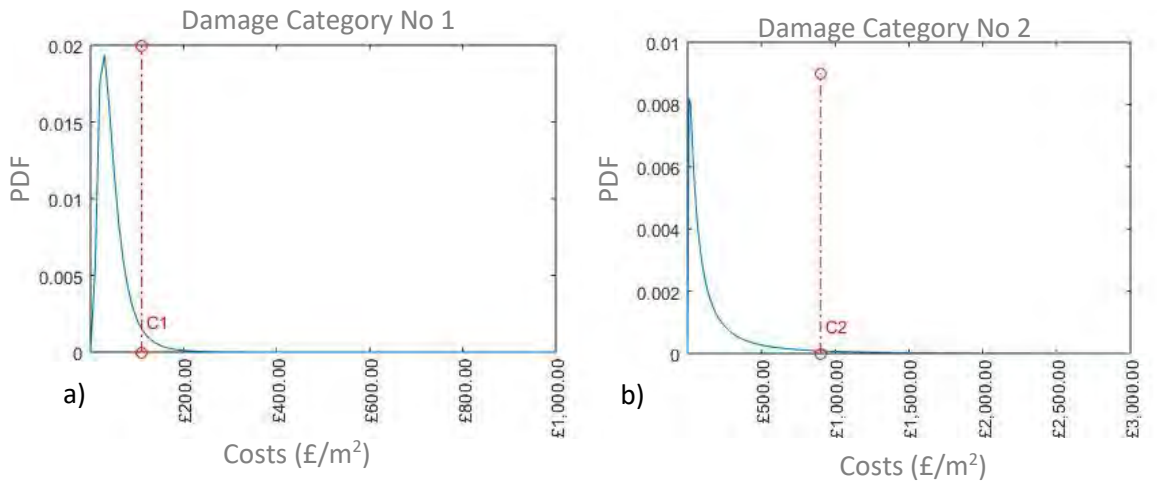

Figure D.21: The PDFs of building damage costs, for (a) Damage Category No. 1 (negligible) and (b) Damage Category No. 2 (very slight). The red dotted line shows the 95% percentile cost.

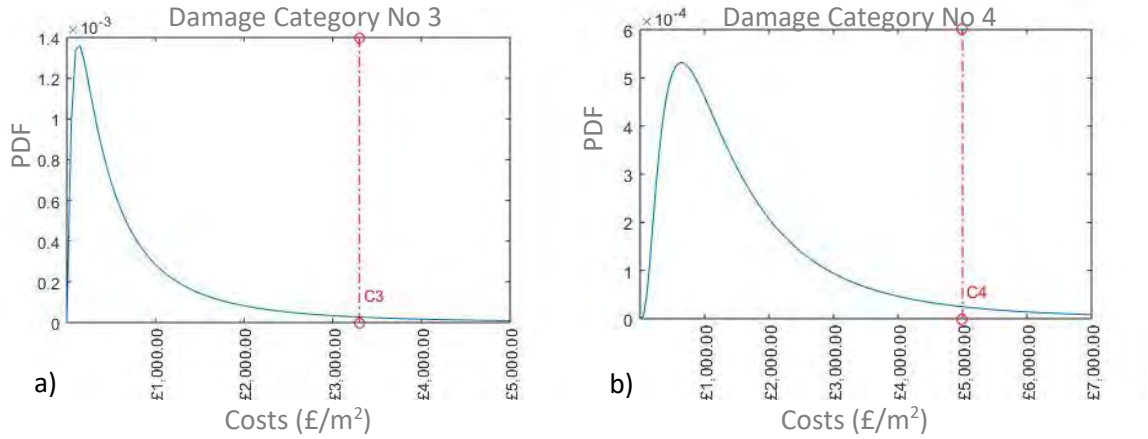

Figure D.22: The PDFs of building damage costs, for (a) Damage Category No. 3 (slight) and (b) Damage Category No. 4 (moderate). The red dotted line shows the 95% percentile cost.

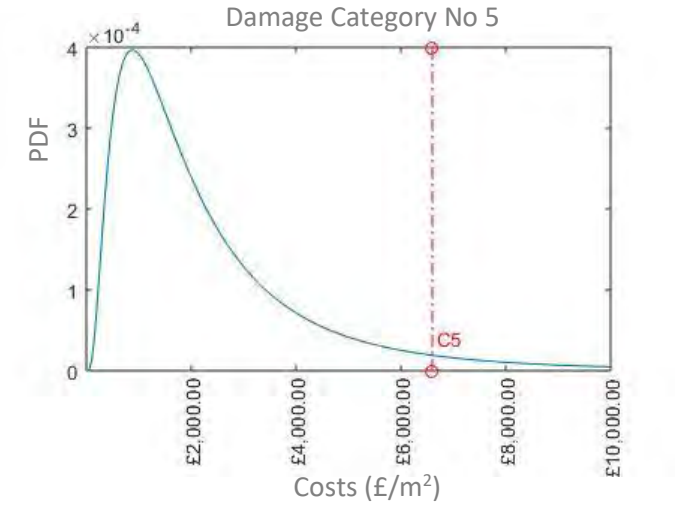

Figure D.23: The PDF of building damage costs, for Damage Category No. 5 (severe). The red dotted line shows the 95% percentile cost.

Then, for a tunnel with an 8m diameter placed approximately 200m away from the built-up area, the graphs are shown in Figures D.24–D.26:

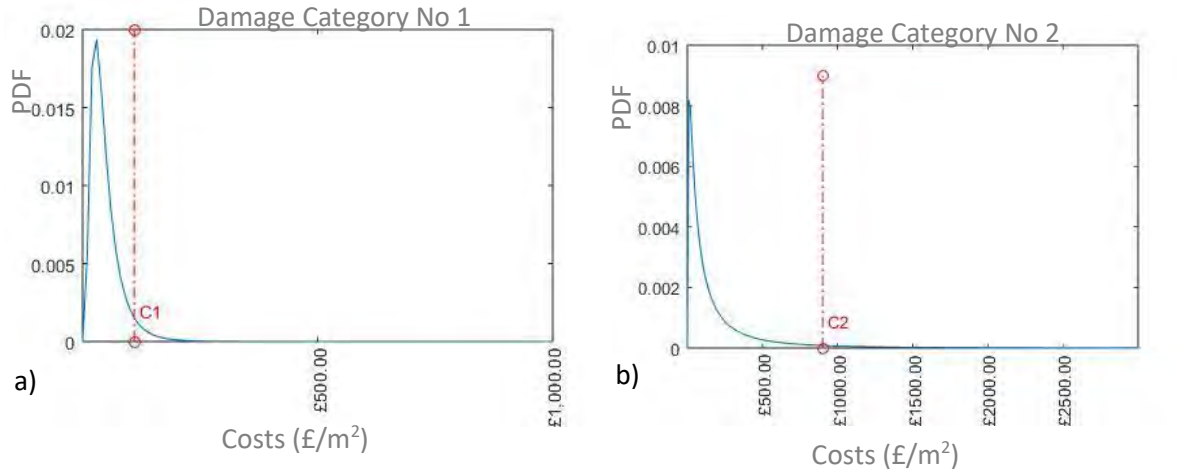

Figure D.24: The PDFs of building damage costs, for (a) Damage Category No. 1 (negligible) and (b) Damage Category No. 2 (very slight). The red dotted line shows the 95% percentile cost.

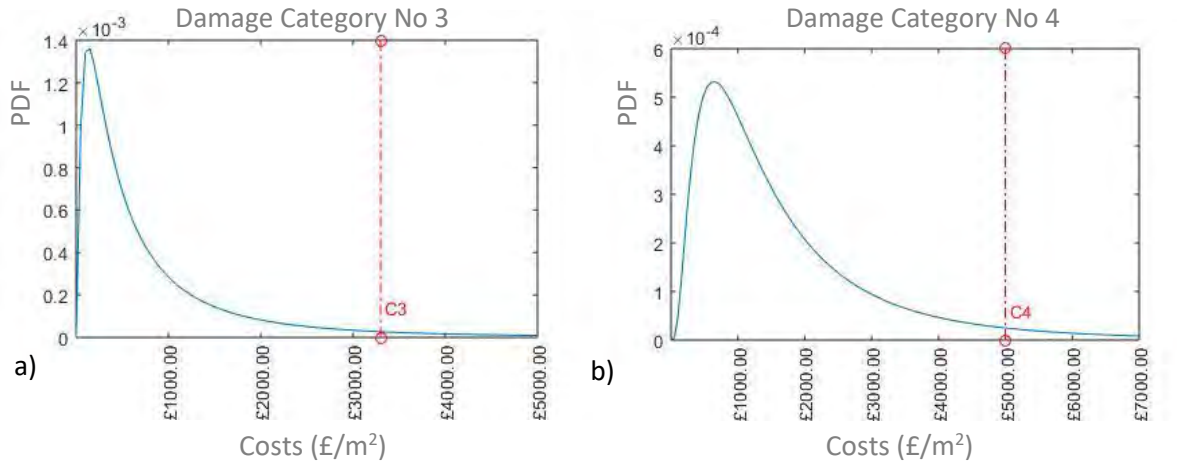

Figure D.25: The PDFs of building damage costs, for (a) Damage Category No. 3 (slight) and (b) Damage Category No. 4 (moderate). The red dotted line shows the 95% percentile cost.

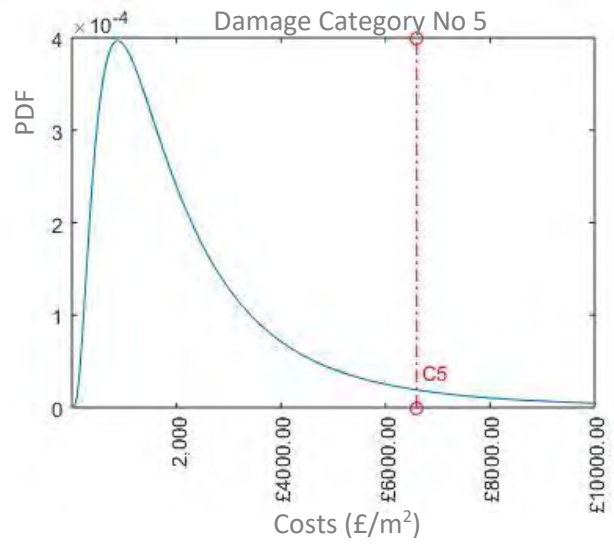

Figure D.26: The PDF of building damage costs, for Damage Category No. 5 (severe). The red dotted line shows the 95% percentile cost.

For a tunnel with a diameter of 10.5m, placed below the built-up area, the graphs are shown in Figures D.27 – D.29:

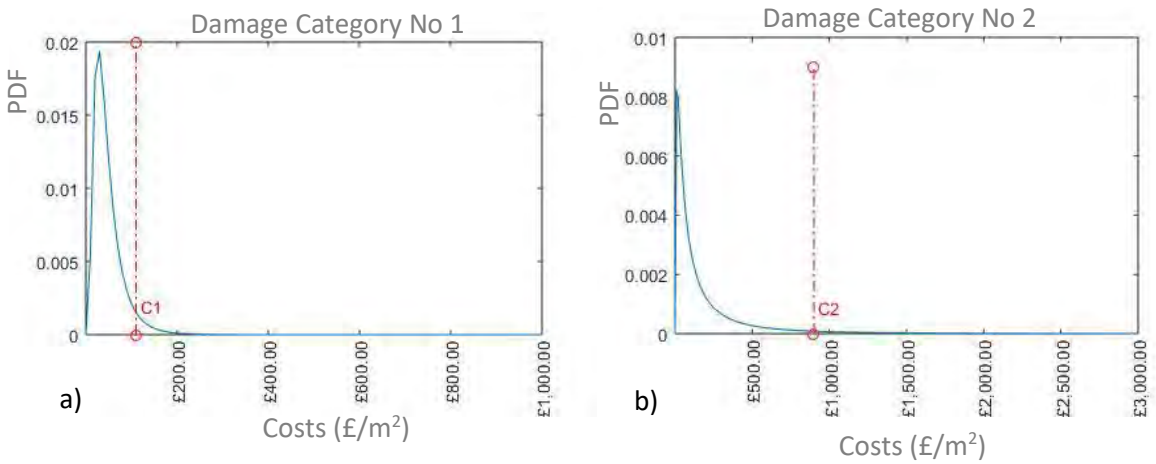

Figure D.27: The PDFs of building damage costs, for (a) Damage Category No. 1 (negligible) and (b) Damage Category No. 2 (very slight). The red dotted line shows the 95% percentile cost.

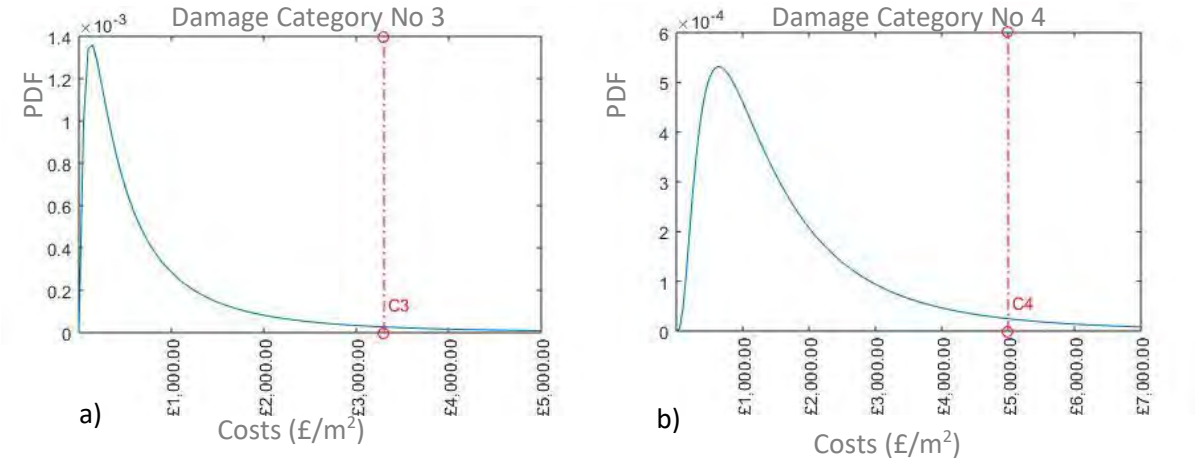

Figure D.28: The PDFs of building damage costs, for (a) Damage Category No. 3 (slight) and (b) Damage Category No. 4 (moderate). The red dotted line shows the 95% percentile cost.

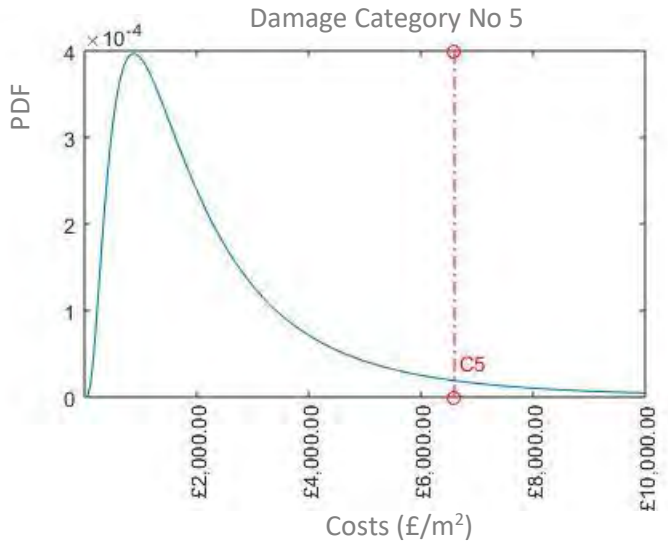

Figure D.29: The PDF of building damage costs, for Damage Category No. 5 (severe). The red dotted line shows the 95% percentile cost.

Finally, in the case of a tunnel with a diameter of 10.5m, placed around 200m away from the built-up area, the graphs are shown in Figures D.30 – D.32:

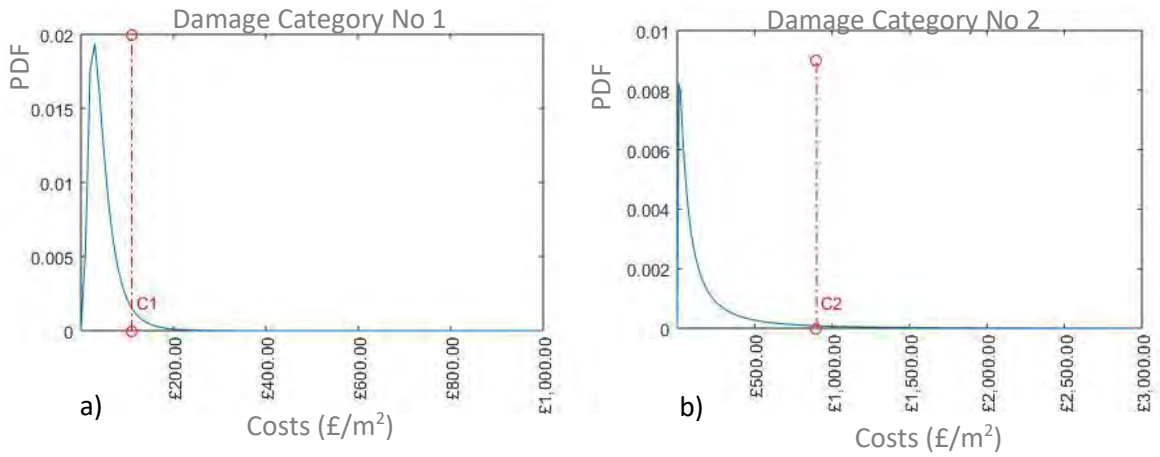

Figure D.30: The PDFs of building damage costs, for (a) Damage Category No. 1 (negligible) and (b) Damage Category No. 2 (very slight). The red dotted line shows the 95% percentile cost.

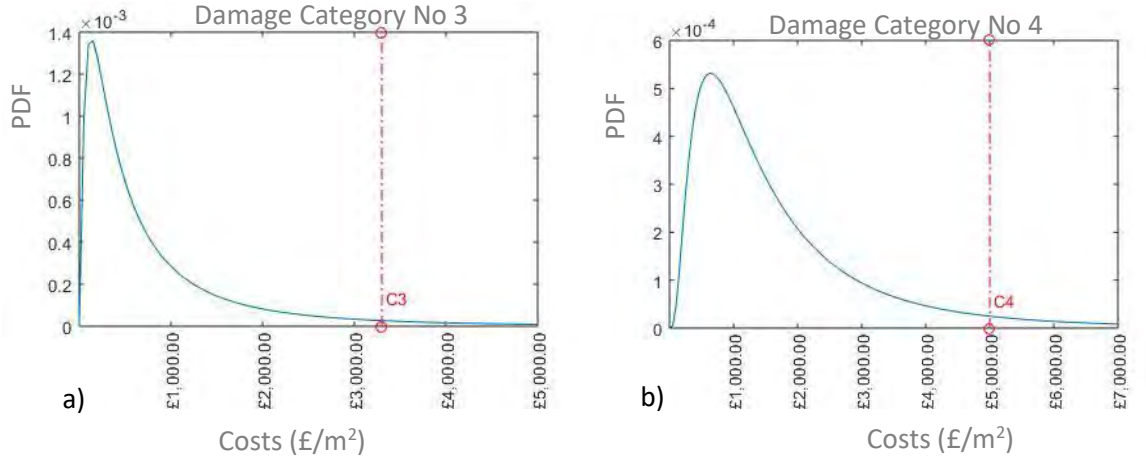

Figure D.31: The PDFs of building damage costs, for (a) Damage Category No. 3 (slight) and (b) Damage Category No. 4 (moderate). The red dotted line shows the 95% percentile cost.

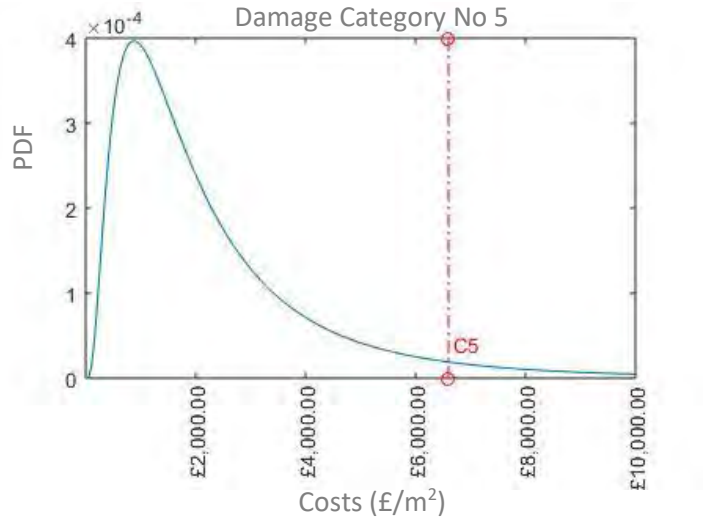

Figure D.32: The PDF of building damage costs, for Damage Category No. 5 (severe). The red dotted line shows the 95% percentile cost.

D.3 Settlement Economic Risk assessment visualisations using BIM.

Further resulting visualisations of the Settlement Economic Risk are presented in the Figures D.33, D34 and D.35, for a diameter of 10m, 8m and 10.5m, respectively.

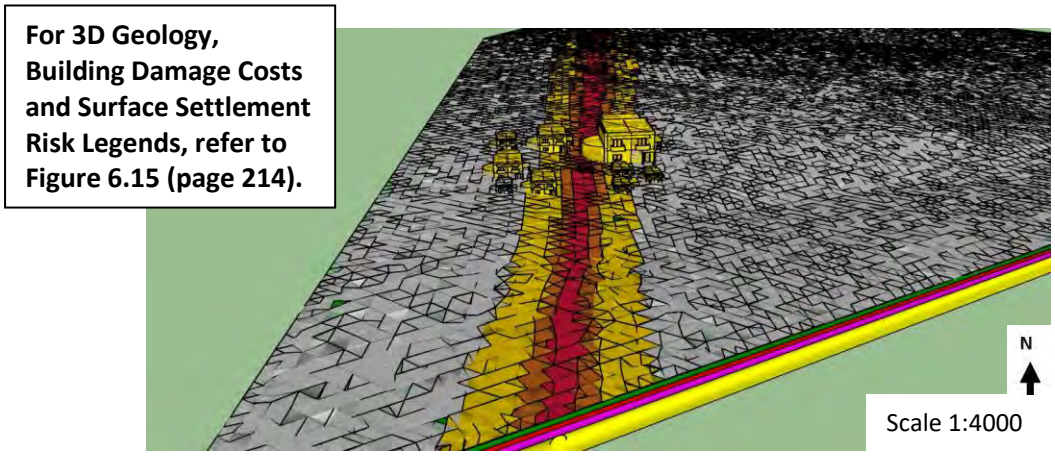

Figure D.33: 3D visualisations (SketchUp) of the resulting Settlement Economic Risk caused by ground settlement due to tunnelling (with a diameter of 10m).

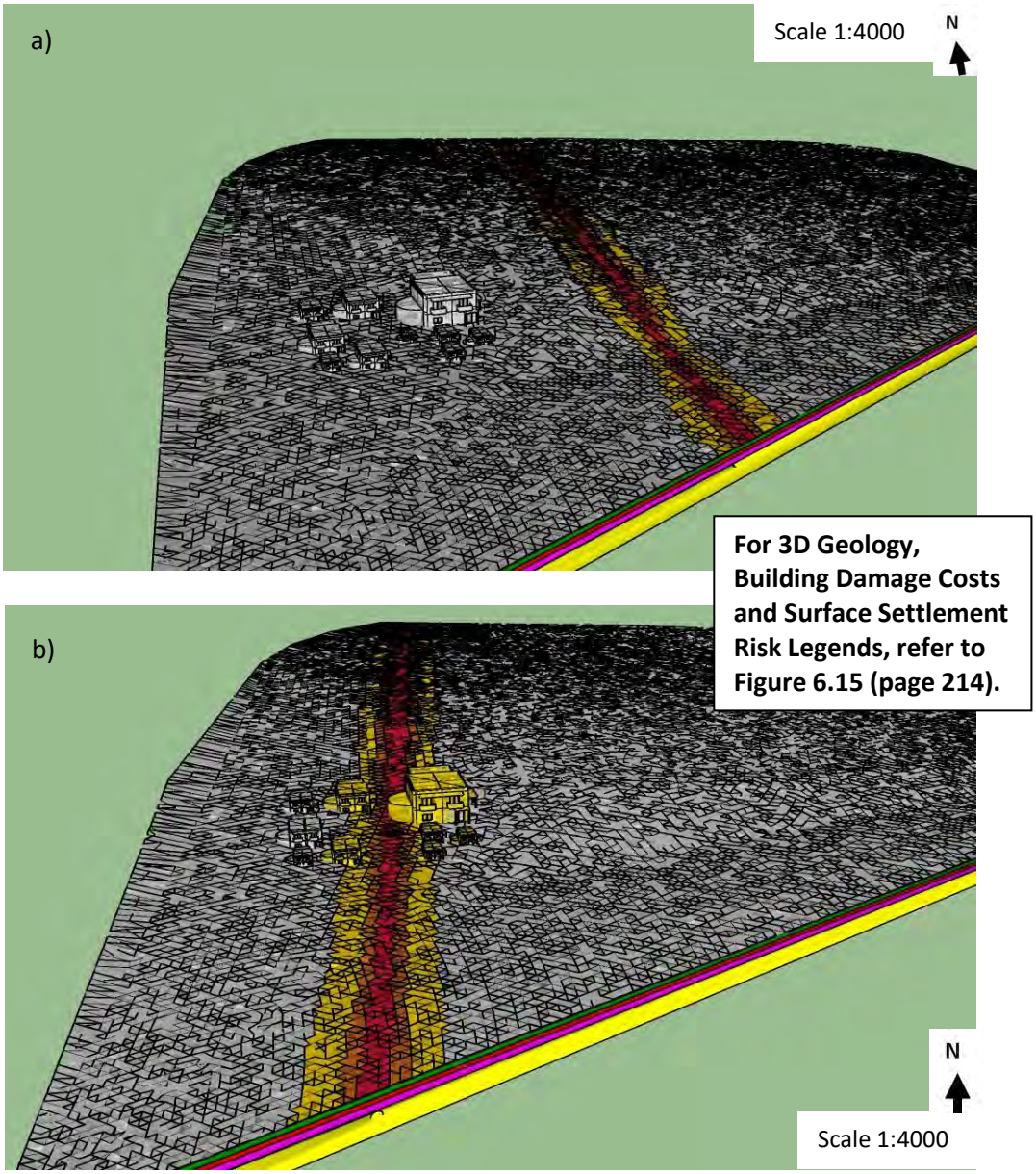

Figure D.34: 3D visualisations (SketchUp) of the resulting Settlement Economic Risk caused by ground settlements due to a tunnel construction with a diameter of 8m, (a) below the built-up area and (b) 200m away from the built-up area.

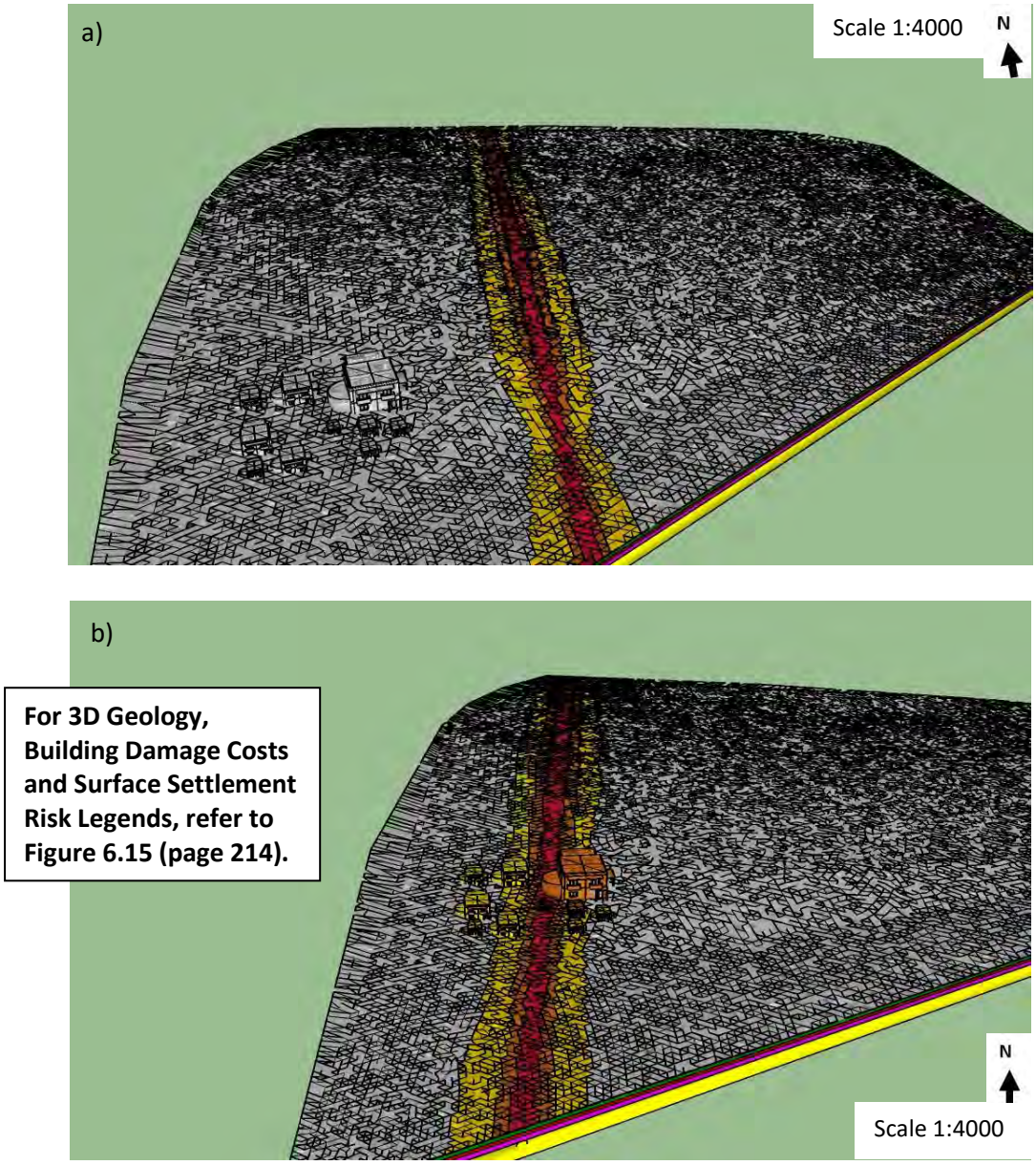

Figure D.35: 3D visualisations (SketchUp) of the resulting Settlement Economic Risk caused by ground settlements due to a tunnel construction with a diameter of 10.5m, (a) below the built-up area and (b) 200m away from the built-up area.